

https://dspace.org/

Foreign atoms on the three low index diamond surfaces

Makau, Nicolas W

2008-04-08T10:18:20Z
http://hdl.handle.net/10539/4742

Downloaded from a DSpace repository. https://dspace.org/

FOREIGN ATOMS ON THE THREE LOW INDEX DIAMOND SURFACES

By

Nicholas W. Makau

A thesis submitted to the Faculty of Science, University of the Witwatersrand, Johannesburg, in fulfilment of the requirements for the degree of Doctor of Philosophy.

Johannesburg, 2006.

Declaration

I declare that this thesis is my own unaided work. It is being submitted for the degree of Doctor of Philosophy in the University of the Witwatersrand, Johannesburg. It has not been submitted before for any degree or examination in any other university.

_____

(Signature of candidate)

_____day of_____2006

VOLUME II

This volume presents results of the first principles theoretical calculations of oxygen atoms and hydroxyl groups adsorbed on the bulk terminated (1×1) diamond (111) surfaces as well as on the (2×1) reconstructed surfaces. The work is treated here separate from the experimental investigations discussed in volume I since its approach is fundamentally different.

To my wife Rosemary M. Muange and our children
Mercy Mueni and Stacy Ngenyi.

Contents

Declaration **i**

ii

List of Figures **vi**

List of Tables **xiv**

1 *ab initio* Density Functional Theory (DFT) study of the adsorption of oxygen atoms and hydroxyl groups on the (111) diamond surfaces **1**

1.1 Outline of the Chapter 1
1.1.1 General introduction 2
1.1.2 Theoretical Background 3
1.2 The Hartree-Fock (HF) Theory 5
1.3 Density functional theory (DFT) 7
1.3.1 Hohenberg-Kohn Theorems 10
1.3.2 Kohn-Sham (K-S) Theorems 11
1.3.3 Local Density Approximation (LDA) and Local Spin Density (LSDA) for the exchange-correlation energy. 14
1.3.4 Generalized Gradient Approximation (GGA) and Functionals of the electron density. 16
1.3.5 The PBE functional 18
1.4 Basis set 20
1.5 The diamond (111) surface 23
1.6 The Computational procedure 29
1.7 Calculations of the bulk parameters of the free carbon, oxygen and diamond-carbon atoms, as well as those of the oxygen molecule and the hydroxyl groups. 30
1.8 Surface modelling 41
1.9 Results 46
1.9.1 Structural diagrams of the relaxed geometries of the (1×1) bulk terminated (111) diamond surfaces. 48

1.9.2 Relaxed geometries for the (2×1) reconstructed (111) diamond surfaces 55
1.10 Structural and bond-length changes within the bulk and near surface regions of (1×1) bulk terminated (111) diamond surfaces, together with those of the C-O, C-OH and O-H bonds. 58
1.10.1 Bulk and near surface C-C bond lengths 66
1.10.2 Bond lengths and their % changes within the topmost C-C surface bilayer of bulk terminated (1×1) C(111) surfaces. 69
1.11 Bond angles within the bulk and near surface regions of a bulk terminated (1×1) diamond (111) surface. 76
1.12 C-O and C-OH bond lengths and their orientations from the (1×1) bulk terminated (111) diamond surface. 77
1.13 Bulk and near surface C-C bond lengths of (2×1) reconstructed diamond (111) surfaces; for clean and O or OH-terminated surfaces. 85
1.14 C-C bond lengths and their % changes in the lower and upper π-bonded chains of (2×1) reconstructed diamond (111) surfaces. 91
1.15 C-O, C=O, C-OH and O-H bonds on the (2×1) reconstructed diamond (111) surfaces. 95
1.15.1 Changes in the work function of the bulk terminated (1×1) diamond (111) surface due to the adsorbed O atoms and/or OH groups. 99
1.15.2 Changes in the work function of (2×1) reconstructed diamond (111) surfaces terminated with O and OH adsorbates compared to that of a clean one. 108
1.16 Total and adsorption energies of oxygen atoms and hydroxyl groups, adsorbed at different sites and coverages on bulk terminated C(111) surface. 112
1.16.1 Adsorption energies of O atoms and OH groups on a (2×1) reconstructed diamond (111) surface: the most and least preferred bonding sites. 132
1.17 Density of states(Dos) for bulk and surface carbon atoms of (1×1) bulk terminated C(111) surfaces, as well as those of the adsorbed oxygen atoms. 138
1.17.1 Dos for the bulk-like carbon atoms 147
1.17.2 Dos for surface carbon atoms from C(111)-(1×1) surfaces. 149
1.17.3 Density of states for the adsorbed oxygen atoms on a (1×1) bulk terminated diamond (111) surface. 154
1.17.4 Density of states for the bulk and surface carbon atoms of (2×1) reconstructed diamond (111) surfaces as well as those of the adsorbed oxygen atoms. 158
1.18 Conclusions 169
1.19 Recommendation 178

A **180**

A.1 Less stable structures for oxygen atoms and hydroxyl groups on the C(111)-(1×1) surface. 180

A.2 Less stable structures for oxygen atoms and hydroxyl groups on the C(111)-(2×1) surface. 191

A.3 Work function for C(111) surfaces terminated with oxygen atoms and hydroxyl groups on the C(111)-(1×1) surface. 193

A.4 Density of states for the less stable structures for oxygen atoms and hydroxyl groups on the C(111)-(1×1) surface. 196

References **203**

List of Figures

1.1 Schematic diagram of the top view of bulk-terminated (1×1) C(111) surface. The grey circles represent the topmost carbon atoms, while the white (open) ones represent the 2nd layer of carbon atoms from the top. 25

1.2 Cross-sectional view of a bulk terminated C(111) surface showing an adsorbed oxygen atom (yellow circle) on a single dangling bond termination (SDB), and some dangling bonds. 25

1.3 Side view of a (2×1) reconstructed (111) diamond surface. After Walter *et al.* [16] 26

1.4 Top view of a (2×1) reconstructed (111) diamond surface. The large dark circles represent carbon atoms at the upper π-bonded zigzag chains, while the smaller grey circles correspond to the lower π-bonded zigzag chains. 27

1.5 Total energy of a free carbon atom for various plane wave cutoff energies. The vertical axis is given in Hartree, where 1H=27.2116eV. 31

1.6 Lattice constant of bulk diamond for various minimum total energies. 33

1.7 Bulk properties of diamond. Panel (a) shows the total energy, panel (b) the lattice constant, panel (c) the binding energy and panel (d) the bulk modulus of diamond, all plotted with various plane wave cutoff energies. 34

1.8 Total energy versus bond length of an oxygen molecule at a plane wave cutoff energy of 70Ry. 36

1.9 Bulk properties of a free oxygen molecule. Panel (a) shows the bond length, panel (b) the binding energy and panel (c) the vibrational frequency, all plotted against various cutoff energies. . 37

1.10 Total energy of a free oxygen atom for various plane wave cutoff energies. 39
1.11 Total energy of a free oxygen molecule for various plane wave cutoff energies. 40
1.12 Total energy versus bond length of a free hydroxyl group at a plane wave cutoff energy of 50Ry. 40
1.13 Two atom unit cell used in determining the initial diamond-carbon atom positions, together with a representation of the atoms stacking in the z-axis . Note the diamond's A, B, C stacking. 44
1.14 Various oxygen monolayer coverages at the ONTOP bonding sites. 45
1.15 Initial geometry showing various oxygen adsorption sites. Note that the triangle formed by the top layer of carbon atoms is facing upwards for the HCP site, and downwards for the FCC site. . . 45
1.16 Clean super cell used for the calculations involving the full and half monolayer coverages of oxygen atoms and hydroxyl groups. The letters C_1, C_2, C_3 etc. refer to the respective carbon atom layers. **J** and **K** are different types of surface bonds. 49
1.17 A full ML of oxygen atoms adsorbed at an ONTOP site. The letters **G** and **H** refer to different types of surface bonds. The small blue spheres represent the H atoms passivating the lower end of the slab, the gold coloured ones the carbon atoms, and the red spheres the adsorbed oxygen atoms. 49
1.18 A full ML coverage of OH groups co-adsorbed initially at a hexagonal close packed (HCP) and a bridge site. Note the staggering of the OH groups after relaxation. 50
1.19 A half ML coverage of oxygen atoms adsorbed at an ONTOP site. Carbon atoms bonded to the oxygens are raised by 0.2464Å above those that are not. 50
1.20 A half ML coverage of OH groups that were initially adsorbed at a hexagonal close packed site. (see figure 1.15) 51

1.21 Unterminated super cell used for calculations involving the quarter monolayer coverages with oxygen atoms and hydroxyl groups. Numbers on the left hand side (LHS) of the side view show the z-axis values of the respective carbon and hydrogen atoms. T stands for true, meaning that the carbon atom should be relaxed, while F represents false, implying that the carbon atom should not be relaxed. 51
1.22 A quarter ML coverage of oxygen atoms adsorbed at an ONTOP site. The letters **A**, **B**, **C** and **D** represent different types of surface bonds. 52
1.23 A quarter ML coverage of OH groups that were adsorbed initially at a Hexagonal close packed site. 52
1.24 A clean slab used for calculations involving the third monolayer coverages. 53
1.25 A third ML coverage of oxygen atoms adsorbed at an ONTOP site. Letters **A** and **B** represent different types of surface bonds. 53
1.26 A third ML coverage of hydroxyl groups adsorbed at an ONTOP site. Note the alternate orientation of the OH groups in the top view after system relaxation. 54
1.27 A clean (2×1) reconstructed C(111) surface. Note the small buckling of the upper and lower π-bonded chains. 55
1.28 A full ML coverage of oxygen atoms adsorbed initially at an ONTOP site, of a (2×1) reconstructed C(111) surface. The upper π-bonded chains are buckled by 0.0083Å, and the lower ones by 0.0129Å. 56
1.29 A full ML coverage of hydroxyl groups at an ONTOP site, of a (2×1) reconstructed C(111) surface. The upper π-bonded chains are buckled by 0.0186Å, and the lower ones by 0.001Å. 56
1.30 A half ML coverage of oxygen atoms adsorbed at an ONTOP site, of a (2×1) reconstructed C(111) surface. Letters **A**, **B**, **C** and **D** represent different types of surface bonds. 57
1.31 A half ML coverage of oxygen atoms adsorbed at a bridge site, of a (2×1) reconstructed C(111) surface. 57

1.32 Workfunction for the most stable configurations of O and OH on the (1×1) surface plotted with the coverage. 102
1.33 Work function (eV) for various sites and coverages of a (2×1) reconstructed C(111) surface. The shaded symbols represent the work function for surfaces terminated with oxygen atoms, while the open ones represent the work function from the hydroxyl terminated surfaces. The half-shaded circle shows the work function of a clean surface. 109
1.34 Adsorption energy versus coverage for the most stable coverages of oxygen atoms and hydroxyl groups on C(111)-(1×1) surfaces. 117
1.35 Adsorption energy versus coverage for full and half monolayer coverages of O atoms and OH groups adsorbed initially at bridge or ONTOP sites on a 2×1 reconstructed C(111) surface. 134
1.36 Density of states (Dos) for C(111)-(1×1) surfaces terminated by a full monolayer of oxygen atoms and hydroxyl groups at ONTOP sites. 139
1.37 Density of states for C(111)-(1×1) surfaces terminated by a half monolayer of oxygen atoms and hydroxyl groups at ONTOP sites. 140
1.38 Density of states for C(111)-(1×1) surfaces terminated by a half monolayer of oxygen atoms and hydroxyl groups at hexagonal close packed (HCP) sites. 141
1.39 Density of states for C(111)-(1×1) surfaces terminated by a half monolayer of oxygen atoms and hydroxyl groups at sites whose starting geometry were bridge-bonded as shown in figures A.5 and A.6. 142
1.40 Density of states for a clean C(111)-(1×1) surface used for calculations involving the quarter monolayer coverages with oxygen atoms and hydroxyl groups. Note the strong C-2p states in the energy gap for carbon atoms in the topmost layer, and the lack of these for carbon atoms in the 2nd topmost layer or even in the bulk states. 143
1.41 Density of states from C(111)-(1×1) surfaces terminated with a quarter monolayer of oxygen atoms and hydroxyl groups at ONTOP sites. 144

1.42 Density of states from C(111)-(1×1) surfaces terminated with a quarter monolayer of oxygen atoms and hydroxyl groups at sites whose initial geometry was Hexagonal close packed. 145
1.43 Density of states from C(111)-(1×1) surfaces terminated with a third monolayer of oxygen atoms and hydroxyl groups at ONTOP sites. 146
1.44 Density of states (Dos) for bulk and surface carbon atoms from a clean (2×1) reconstructed C(111) surface. Note the close resemblance of the states for the two surface carbon atoms in the upper π-bonded chains, emphasizing the similarities of the two bonding sites, and also the difference between this and those of clean C(111)-(1×1) surface shown in figure 1.40. 159
1.45 Density of states from (2×1) reconstructed C(111) surfaces terminated with a full monolayer of oxygen atoms and hydroxyl groups at the ON-TOP sites. 160
1.46 Density of states from (2×1) reconstructed C(111) surfaces terminated with a half monolayer of oxygen atoms and hydroxyl groups at the ON-TOP sites. 161
1.47 Density of states from (2×1) reconstructed C(111) surfaces terminated with a half monolayer of oxygen atoms and hydroxyl groups. The adsorbates were originally located at bridge-bonded site. Note that there are no states in the energy gap, except for the surface C atoms from the hydroxyl termination. 162

A.1 A full ML coverage of hydroxyl groups adsorbed at an ONTOP site. 180
A.2 A full ML coverage of oxygen atoms co-adsorbed at an ONTOP and a hexagonal close packed (HCP) site. 181
A.3 A half ML coverage of OH groups adsorbed at an ONTOP site. The carbon atoms bonded to the hydroxyl groups are raised by 0.176Å above those that are not. 181
A.4 A half ML coverage of oxygen atoms which were initially adsorbed at a Hexagonal close packed site. 182
A.5 A half ML coverage of oxygen atoms adsorbed at a bridge site. . 182

A.6 A half ML coverage of OH groups that were initially adsorbed at a bridge site. Unlike the oxygen atoms (fig. A.5, the hydroxyl groups moved to new positions that were very close to the ONTOP site. 183
A.7 A half ML coverage of oxygen atoms adsorbed a face centred site. 183
A.8 A half ML coverage of OH groups adsorbed at a face centred cubic site. 184
A.9 A quarter ML coverage of OH groups adsorbed at an ONTOP site. 184
A.10 A quarter ML coverage of oxygen atoms that were initially adsorbed at a Hexagonal close packed site. 185
A.11 A quarter ML coverage of oxygen atoms adsorbed at a bridge site. Letters **A**, **B**, **C** and **D** represent different types of surface bonds. Note the disruption of the topmost bilayer of carbon atoms due to the bridge-bonded O atoms. 185
A.12 A quarter ML coverage of OH groups whose starting geometry was a bridge-bonded one. 186
A.13 A quarter ML coverage of oxygen atoms adsorbed at a face centred cubic site. 186
A.14 A quarter ML coverage of OH groups adsorbed at a face centred cubic site. 187
A.15 A third ML coverage of oxygen atoms that were initially adsorbed at a Hexagonal close packed site. 187
A.16 A third ML coverage of OH groups that were initially adsorbed at a Hexagonal close packed site. The HCP site appears quite unstable against OH adsorption. 188
A.17 A third ML coverage of oxygen atoms adsorbed at a bridge site. 188
A.18 A third ML coverage of OH groups that were initially adsorbed at a bridge site. The bridge site is also unstable against the adsorption of OH groups. 189
A.19 A third ML coverage of oxygen atoms adsorbed at a face centred cubic site. 189

A.20 A third ML coverage of OH groups that were initially adsorbed at a face centred cubic site. The carbon atoms bonded to the OH groups were raised by 0.197Å over the ones that were not, and the FCC site appears to be also unstable against the OH groups' adsorption, instead preferring the ONTOP:OH site. 190
A.21 A half ML coverage of OH groups adsorbed at a site whose starting geometry was a bridge-bonded one, on a (2×1) reconstructed C(111) surface. 191
A.22 A half ML coverage of hydroxyl groups adsorbed at an ONTOP site, of a (2×1) reconstructed C(111) surface. 192
A.23 A plot of the work function (eV) for various sites and coverages from (1×1) bulk terminated C(111) surfaces. The shaded symbols represent the work function for surfaces terminated by oxygen atoms, while the open ones show that of the hydroxyl terminated surfaces. The half shaded circles show the values of the work function for the clean surfaces. 194
A.24 Density of states (Dos) for C(111)-(1×1) surfaces terminated by a half monolayer of oxygen atoms and hydroxyl groups at face centered cubic site (FCC) sites. 197
A.25 Density of states for C(111)-(1×1) surfaces terminated with a quarter monolayer of oxygen atoms and hydroxyl groups at sites that were initially bridge-bonded. Except for the O atoms, the DOS for the carbon atoms appear very much alike. 198
A.26 Density of states from C(111)-(1×1) surfaces terminated with a quarter monolayer of oxygen atoms and hydroxyl groups at face centered cubic sites. 199
A.27 Density of states from C(111)-(1×1) surfaces terminated with a third monolayer of oxygen atoms and hydroxyl groups at sites that were initially hexagonal close packed. 200
A.28 Density of states for C(111)-(1×1) surfaces terminated with a third monolayer of oxygen atoms and hydroxyl groups at face centered cubic sites. 201

A.29 Density of states for C(111)-(1×1) surfaces terminated with a third monolayer of oxygen atoms and hydroxyl groups at sites that were originally bridge-bonded. 202

List of Tables

1.1 Calculated DFT-GGA and experimental bulk properties of diamond-carbon. Plane wave cutoff energy E_{cut} is in Rydbergs (Ry), while the lattice constant a_o, and the distances between the C atoms d_{c-c} are in Å. The binding energy E_{coh} is shown in eV/atom, while the bulk modulus is in Mbar 32

1.2 Calculated DFT-GGA and experimental properties of an oxygen molecule. The plane wave cutoff energy E_{cut} is given in Ry, the bond length a_0, in Bohrs, the binding energy E_{coh} in eV/atom, while the vibrational frequency ν, is in cm^{-1} 38

1.3 Calculated DFT-GGA adsorption energies of oxygen on diamond (111)-(1×1) surfaces for testing the optimum slab size. Tests were done for the full oxygen monolayer coverage at the ON-TOP sites. 42

1.4 Calculated C-C bond lengths (d_{C-C} as in figure 1.16 expressed in Å for the C(111)-(1×1) surface), and their % changes for the bulk and near surface carbon atoms for full and half ML coverages of O & OH. Except for the O-O bond, numbers in parentheses are the relative percentage changes to the experimental values of 1.54Å [74] for the C-C bond, 1.36Å for a single C-O bond and 1.43Å for the C-OH bond, as well as 0.98Å for the O-H bond. . 59

1.5 Calculated C-C atom bond lengths (d_{C-C} in Å for the C(111)-(1×1) surface), and their % changes for bulk and near surface carbon atoms from the quarter monolayer coverages of O & OH. The numbers in parentheses are the relative % changes to the experimental values similar to those used in Table 1.4. The resulting C-O, C-OH and O-H bond lengths are also shown. . . . 60

1.6 Calculated C-C bond lengths (d_{C-C}, in Å for the C(111)-(1×1) surface), and their % changes for bulk and near surface carbon atoms obtained from the third monolayer coverages of O & OH. These are shown together with bond lengths for the C-OH, C-O, and O-H terminations. The numbers in parentheses are the relative % changes to the experimental values similar to those shown in Table 1.4. 61

1.7 Bond lengths and their changes % within the topmost bilayer of carbon atoms from the clean slabs of the (1×1) bulk terminated C(111) surfaces. These are shown together with those obtained from surfaces terminated by a full ML of O atoms or OH groups. The bond lengths are given in Å while the numbers in parentheses are the corresponding percentage changes relative to the bulk C-C bond length of 1.54Å. 62

1.8 Bond lengths in the topmost bilayer of C(111)-(1×1) surfaces terminated with half a monolayer of O atoms and OH groups at different sites. The bond lengths are shown in Å while the figures in parentheses are the corresponding percentage changes relative to the C-C bulk bond length of 1.54Å. 63

1.9 Bond lengths and their % changes in the topmost bilayer of C(111)-(1×1) surfaces terminated with a quarter monolayer O atoms and OH groups. The bond lengths are shown in Å while the corresponding percentage changes which are shown in parentheses were obtained relative to the C-C bulk bond length of 1.54Å. 64

1.10 Bond lengths and their % changes in the topmost surface bilayer of the bulk terminated C(111)-(1×1) surfaces. The surfaces were terminated with a third monolayer of O atoms and OH groups at different sites. The bond lengths are shown in Å, while the numbers in parentheses are the corresponding percentage changes relative to the bulk C-C bond length of 1.54Å. 65

1.11 Calculated C-C atom bond lengths (d_{C-C}) and their % changes (numbers in parentheses) relative to the bulk bond length of 1.54Å, for bulk and near surface carbon atoms from a (2×1) reconstructed diamond (111) clean surface. 86
1.12 Calculated C-C atom bond lengths and their % changes, for bulk and near surface carbon atoms from a (2×1) reconstructed diamond (111) surface. The percentages changes for the C-C bonds, (numbers in parentheses) were calculated relative to the experimental bond length of 1.54Å. Also shown are the lengths for the C-OH bonds relative to the experimental value 1.43Å, the single C-O bonds relative 1.36Å, double C=O bond relative to 1.23Å and the O-H bonds which are compared to the experimental value of 0.98Å. 87
1.13 Bond lengths (in Å) within the topmost π-bonded carbon-atom chains of (2×1) reconstructed diamond (111) surfaces, together with those joining them. These are shown for a clean surface and for those that were terminated with a full and half monolayer of oxygen atoms or hydroxyl groups at an ONTOP and bridge sites. The numbers in parentheses are the percentage changes relative to the C-C bulk bond length of 1.54Å. 92
1.14 Computed buckling of the lower and upper π-bonded zigzag chains and the bond angles between the two. 96
1.15 Calculated DFT-GGA total minimum energies, adsorption energies, and work function values for various full and half monolayer coverages of oxygen atoms and hydroxyl groups at different sites on (1×1) bulk terminated (111) diamond surfaces. A plane cut-off energy of 50Ry was used, and the corresponding total energy of the oxygen atom at the same cut-off energy was 15.70077Hartree, while that of the hydroxyl group was -16.41753Hartree. The most stable configurations for each coverage with O atoms or OH groups are bolded. 114

1.16 Calculated DFT-GGA total minimum energies, adsorption energies and work function values for various quarter monolayer oxygen and hydroxyl coverages at different sites on a (1×1) bulk terminated (111) diamond surface. A similar value for the plane wave cutoff and total energy for an oxygen atom and the hydroxyl group as in Table 1.15 was used. 115
1.17 Calculated DFT-GGA total minimum energies, adsorption energies and work function values for various third monolayer oxygen and hydroxyl coverages at different sites on a (1×1) bulk terminated (111) diamond surface. A plane cut-off energy similar to that shown in Table 1.15 was used, and the values of the total energies for the oxygen atom and hydroxyl group were also the same as those shown in Table 1.15. The most stable configurations with O atoms or OH groups are bolded. 116
1.18 Adsorption energies of the lowest energy configurations per coverage for O and OH species on the bulk terminated (1×1)-C(111) surface. 118
1.19 Calculated DFT-GGA total minimum energies, adsorption energies and work function values for various full and half monolayer coverages of oxygen atoms and hydroxyl groups at different sites on a (2×1) reconstructed diamond (111) surface. A plane cut-off energy of 50Ry was used, and the corresponding total energy of the oxygen atom at the same cut-off energy was 15.70077Hartree, while that of the hydroxyl group was -16.41753Hartree. 133

A.1 Changes in the work function of (1×1)-C(111) surfaces terminated with full and half ML coverages of O atoms and OH groups compared to that of the clean surface (3.6131). 193
A.2 Changes in the work function of C(111)-(1×1) surfaces terminated with a quarter ML of O atoms and OH groups, compared to that of the clean surface (3.6322). 193
A.3 Changes in the work function of C(111)-(1×1) surfaces terminated with a third ML of O atoms and OH groups compared to that of the clean surface (3.6798). 193

A.4 Changes in the work function of C(111)-(2×1) surfaces terminated with full and half monolayers (ML) of O atoms and OH groups compared to that of the clean surface (2.3459). 195

Chapter 1

ab initio Density Functional Theory (DFT) study of the adsorption of oxygen atoms and hydroxyl groups on the (111) diamond surfaces

1.1 Outline of the Chapter

This chapter discusses the *ab initio* DFT calculations of both oxygen atoms and hydroxyl groups after adsorbing on the bulk terminated (1×1) and the (2×1) reconstructed diamond (111) surfaces. The total minimum energies of the systems terminated by either O atoms or OH hydroxyl groups are considered together with adsorption energies, in order to establish their preferred bonding sites as well as the most stable coverages. In addition, the changes occurring in the work function of the respective surfaces when the two adsorbates are bonded on to them are computed and discussed quite extensively. Density of states for the clean surfaces as well as those terminated with the adsorbates are also considered. These include the density of states for carbon atoms located within the bulk, those at the surface, as well as states from the adsorbed oxygen atoms from the O-only terminated surface, and those of oxygen atoms from the hydroxyl groups. The chapter deals initially with the theoretical background

and principles of density functional theory, followed by a description of the atomic structure of the bulk terminated (1×1) diamond surface, and then the (2×1) reconstructed (111) diamond surface. The computational procedure, as well as the testing of the pseudopotentials and the optimum plane wave cutoff energies are initially explained. These are followed by the determination of the converged properties of the free carbon and oxygen atoms, those of the free oxygen molecule and the hydroxyl group as well as the total minimum energies of the converged systems terminated with the desired adsorbates. The results obtained are then presented, their discussion made, conclusions drawn and finally some recommendations are made.

1.1.1 General introduction

The role of adsorbed oxygen atoms, as well as the OH groups and other organic groups, on "clean" diamond surfaces have been discussed in detail in the XPS chapter (presented in volume I) as well as in the references quoted in the respective literature review sections. However, in spite of the vast body of experimental findings and their associated successes, theoretical predictions still play a crucial role in complementing these results. The wide spread use of theoretical predictions in solving material science problems has become almost routine in certain industrial applications as well as in research, a feat that has been made possible by the fact that the principles governing the theoretical calculations are now very well established as is evident from the large body of literature available, making the calculations not only more reliable, but also quite accurate. In addition, the tremendous and almost exponential increase of the computational power over the recent past has made it possible to handle systems containing a large number of atoms which are truly representative of the material under investigation, within a fairly short period of time. This makes the calculations less expensive computationally, and hence attractive and

reliable say in industry, where quick results may be required.

1.1.2 Theoretical Background

On the microscopic scale, any solid can be considered to be made up of a collection of a large number of atoms which are bound together. The solid is therefore thought of as being formed by heavy positively charged nuclei and lighter negatively charged electrons. In such a scenario, all the particles interact with each other electromagnetically, and if there are N nuclei in the solid whose atomic number is Z, then there will be ZN electrons, giving rise to a total of N+ZN interacting particles. Such is a many-body problem, and owing to the fact that the particles are also light, it requires one to seek a many-body quantum mechanical solution to the problem. For such a system, the exact many-particle Hamiltonian is expressed as, viz [1, 2],

$$\hat{H} = -\frac{\hbar^2}{2}\sum_i \frac{\nabla^2_{\vec{\mathbf{R}}_i}}{M_i} - \frac{\hbar^2}{2}\sum_i \frac{\nabla^2_{\vec{\mathbf{r}}_i}}{m_e} - \frac{1}{4\pi\epsilon_0}\sum_{i,j}\frac{e^2 Z_i}{\mid \vec{\mathbf{R}}_i - \vec{\mathbf{r}}_j \mid} + \frac{1}{8\pi\epsilon_0}\sum_{i\neq j}\frac{e^2}{\mid \vec{\mathbf{r}}_i - \vec{\mathbf{r}}_j \mid} + \frac{1}{8\pi\epsilon_0}\sum_{i\neq j}\frac{e^2 Z_i Z_j}{\mid \vec{\mathbf{R}}_i - \vec{\mathbf{R}}_j \mid} \tag{1.1.1}$$

or

$$\hat{H} = -\frac{1}{2}\sum_i \frac{{P_i}^2}{M_i} - \frac{1}{2}\sum_i \frac{{p_i}^2}{m_e} - \frac{1}{4\pi\epsilon_0}\sum_{i,j}\frac{e^2 Z_i}{\mid \vec{\mathbf{R}}_i - \vec{\mathbf{r}}_j \mid} + \frac{1}{8\pi\epsilon_0}\sum_{i\neq j}\frac{e^2}{\mid \vec{\mathbf{r}}_i - \vec{\mathbf{r}}_j \mid} + \frac{1}{8\pi\epsilon_0}\sum_{i\neq j}\frac{e^2 Z_i Z_j}{\mid \vec{\mathbf{R}}_i - \vec{\mathbf{R}}_j \mid} \tag{1.1.2}$$

where M_i is the mass of the nucleus at $\vec{\mathbf{R}}_i$, m_e the mass of an electron at a position vector $\vec{\mathbf{r}}_i$, while P_i and p_i are the momentum operators of the nucleus and the electrons respectively. The Schrödinger equation for such a system is thus written as,

$$(\hat{T}_{ion} + \hat{T}_e + \hat{V}_{e-ion} + \hat{V}_{e-e} + \hat{V}_{ion-ion})\Psi = E[\Psi] \tag{1.1.3}$$

In this case, the Hamiltonian consists of the kinetic energy operators of the nucleus $\hat{T}_{ion}$ and that of the electrons $\hat{T}_e$ respectively, which are represented by the first two terms in equations 1.1.1, 1.1.2 and 1.1.3. The last three terms in the equations describe the Coulomb interaction between the electrons and nuclei $\hat{V}_{e-ion}$, between the electrons and other electrons $\hat{V}_{e-e}$ and between the nuclei and other nuclei $\hat{V}_{ion-ion}$. The electrons can further be separated into either valence and/or core level ones. The core level electrons are found in the filled orbitals, and are therefore mostly localized around the nuclei. As a result, they are often lumped together with the ion cores.

Although all the interacting particles in a solid may be considered to be in motion, the relatively heavier mass of the nuclei (ion cores) compared to the electrons allow them to be considered as being stationary within the Born-Oppenheimer approximation. Thus, by separating the electronic and nuclear motions, the nuclei are considered frozen and the electrons are assumed to be in instantaneous equilibrium with them, meaning that the electrons are the only participants in the many-body problem. The nuclei then become sources of positive charge and hence external to the electron cloud. This means that the first term of the Hamiltonian in equations 1.1.1, 1.1.2 and 1.1.3 disappears, while the last terms become constant, thus simplifying the many-body problem. With the nuclei frozen, and further assuming that the electrons are non-interacting, the electron cloud can be regarded as that of an electron gas, and the Hamiltonian reduces to,

$$\hat{H} = \hat{T}_e + \hat{V}_{e-e} + \hat{V}_{ext} \tag{1.1.4}$$

where $\hat{T}_e$ is the kinetic energy of the electron gas, $\hat{V}_{e-e}$ is the potential energy due to the electron-electron interaction and $\hat{V}_{ext}$ is the potential energy of the electrons in the external field provided by the nuclei.

Both the kinetic energy of the electrons and the electron-electron interaction

are system independent, while the only system specific information is given by the potential energy of the electrons in the external field of the nuclei.

In seeking to find solutions to various atomic and molecular systems using such Hamiltonians, the quantum mechanical calculations can be done in various ways. Some approaches are derived semi-empirically by using parameters fitted to experiment, while others solve the quantum mechanical calculations from first principles using the foundations of quantum mechanics, in an approach commonly known as the *ab-initio* method. The principles of quantum mechanics indicate that the state of a system is fully described by a wavefunction Ψ that depends on the position of the electrons and nuclei, as well as time. For such a system, the wavefunction can be determined by solving the Schrödinger equation,

$$H\Psi = E\Psi \tag{1.1.5}$$

where H is the Hamiltonian operator, and E is the eigenenergy of the corresponding wavefunction.

1.2 The Hartree-Fock (HF) Theory

Within the Hartree-Fock theory, every electron is represented by a spin orbital which is a product of an orbital wavefunction and a spin function. The electrons are also considered to move in a mean field potential produced by the nuclei as well as the electrons in the system, and in case there is only one, the mean field is produced by an external potential [3]. The spin orbitals in the HF approximation are normally obtained from the variational theory, and these in turn give the electron wavefunction that minimises the Rayleigh ratio,

$$H_{HF} = min\frac{\int \Psi^* H\Psi}{\Psi^*\Psi} \tag{1.2.1}$$

where H is the Born-Oppenheimer Hamiltonian. The lowest energy E_{HF} is the electronic energy of the system, and is referred to as the Hartree-Fock limit, which is written as,

$$E[\Psi] \geq E_0 \tag{1.2.2}$$

This means that the energy computed from a guessed wavefunction Ψ is an upper bound to the true ground state energy E_0. Full minimisation of the functional $E[\Psi]$ with respect to all the allowed N-electron wavefunctions (single-particle orbitals) will yield the true ground state Ψ_0 and energy $E[\Psi_0] = E_0$; that is,

$$E_0 = \min_{\Psi} E[\Psi] \tag{1.2.3}$$

This approach gives rise to the Hartree-Fock equations for individual spin orbitals ψ_i (where electron i is assigned to the spin orbital ψ_i), that is,

$$\hat{F}\psi_i(n) = \sum_{j=1}^{N} \epsilon_{i,j}\psi_j(n) \tag{1.2.4}$$

where $\epsilon_{i,j}$ is the orbital energy of the spin orbital and $\hat{F}$ is the Fock operator, expressed as,

$$\hat{F}_i = H_i + \sum_k J_k(i) - K_k(i) \tag{1.2.5}$$

H_i is the core Hamiltonian for electron i, and the sum is over all spin orbitals k. J is the Coulomb operator and K is the non-classical exchange operator. The two are defined as,

$$J(x_1) = \int \psi_k^2(x_2)\frac{e^2}{\mathbf{r}_{12}}\psi_k(x_2)dx_2 \tag{1.2.6}$$

$$K(x_1) = \int \psi_k^2(x_2)\frac{e^2}{\mathbf{r}_{12}}\psi_k(x_1)dx_2 \tag{1.2.7}$$

The Hartree-Fock expectation value of the energy expressed in terms of the two operators J and K, becomes,

$$E_{HF} = \langle\Psi_{HF}|\hat{H}|\Psi_{HF}\rangle = \sum_{i=1}^{N} H_i + \frac{1}{2}\sum_{i,j=1}^{N}(J_{ij} - K_{ij}) \tag{1.2.8}$$

where

$$H_i = \int \psi_i^*(x)[-\frac{1}{2}\nabla^2 + \upsilon(x)]\psi_i(x)dx \tag{1.2.9}$$

Just like in equation 1.2.5, J_{ij} in equation 1.2.8 are the Coulomb integrals and K_{ij} the exchange integrals.

Each spin orbital is then calculated by solving the Fock operator equation. Since the Fock operator $\hat{F}$ depends on the spin orbitals of all the electrons in the system, the solution must be iterated from an initial trial set of spin orbitals until a self-consistent solution is obtained.

The Hartree-Fock (HF) theory can however be divided into two different categories depending on how one incorporates the spin of the system into the calculations. If electrons with spin $\uparrow$ are considered equal to electrons with spin $\downarrow$, it is called restricted HF(RHF), and this approach cannot be used on systems with open electron shells. When different spins are considered as different spatial orbitals, it is called unrestricted HF (UHF). Treating the spins as being different gives a double set of equations, matrices and integrals to compute and hence gives better values for calculated energies since it enables one to split the energy levels for spin $\uparrow$ and spin $\downarrow$.

1.3 Density functional theory (DFT)

Although the HF theory could accurately determine the total energies of various atomic and molecular systems, some of the difficulties encountered revealed that there was still a need to establish a theory that was computationally fast and accurate. This gave rise to the now commonly used density functional theory. Since the early 1950's, first principles density functional theory calculations have developed tremendously to become one of the most powerful theoretical techniques for materials analysis, enabling one to investigate various properties

by using only the electron density. The accuracy and reliability of DFT calculations has progressively improved over time to such a level that it has become a valuable tool in various applications, thereby complementing the traditional quantum mechanical methods [4]. It deals mainly with properties of interacting many-particle systems, and its ability to predict material properties close to those obtained experimentally makes it even more attractive. This trend is likely to continue and improve even further as computational power increases almost exponentially, coupled with significant improvements and progress in the fundamental theories governing DFT [3] which have seen the errors in calculated properties decrease rather remarkably. This feature has seen the applications of DFT extending to almost all spheres of atomic and molecular studies. An important factor that endears DFT to many researchers is its ability to simplify the calculations in such a way that it permits one to replace the complicated N-electron wavefunction $\Psi(x_1, x_2, ..., x_N)$ and its associated Schrödinger equation by the much simpler electron density $\mathrm{n}(\mathbf{r})$ and its associated calculation regime. This means that all the information that one needs to know about a system composed of atoms or even molecules can be extracted from the electron density $\mathrm{n}(\mathbf{r})$ alone, which is normally expressed as a function of the position vector $\vec{\mathbf{r}}$. In other words, the electron density uniquely determines the groundstate energy of a given system.

The total energy E of the system can be expressed as a functional of the electron density, as $\mathrm{E}=\mathrm{E}[\mathrm{n}(\mathbf{r})]$.

In their 1920s pioneering work, Thomas and Fermi [5] established the energy formula for an atom in terms of the electron density, forming the foundation for DFT. Their energy functional which is commonly referred to as the Thomas-Fermi (T-F) model had the form,

$$E_{TF}[n(\mathbf{r})] = C_F \int n^{5/3}(\mathbf{r}) d\mathbf{r} - Z \int \frac{n(\mathbf{r})}{\mathbf{r}} d\mathbf{r} + \frac{1}{2} \int \int \frac{n(\mathbf{r}_1) n(\mathbf{r}_2)}{|\mathbf{r}_1 - \mathbf{r}_2|} d\mathbf{r}_1 d\mathbf{r}_2 \quad (1.3.1)$$

where C_F is a constant that arises from the total kinetic energy T_{TF}, which is expressed as,

$$T_{TF}[n(\mathbf{r})] = C_F \int n^{5/3}(\mathbf{r}) d\mathbf{r}, \qquad \text{and} \qquad C_F = \frac{3}{10}(3\pi^2)^{\frac{2}{3}}, \tag{1.3.2}$$

In deriving their formula, they assumed that electrons were distributed uniformly in the six-dimensional phase space for the motion of an electron at the rate of two for each h^3 of volume [6], where h was the length of one side of a cubic space. They also assumed that there was an effective potential field that was itself determined by the nuclear charge and the distribution of electrons. Their model therefore used the electron gas assumption for calculating the kinetic energy T_{TF} of the system as a function of the Fermi energy, ϵ_F. The model did not however include the exchange and correlation terms [7], and therefore bonding in molecules was omitted [8] and also negative ions were unstable.

To correct this anomaly, Dirac [3], [6] added an exchange term to the T-F energy functional, giving rise to the Thomas-Fermi-Dirac model of the energy functional

$$E_{TFD}[n(\mathbf{r})] = E_{TF}[n(\mathbf{r})] + E_x[n(\mathbf{r})] \tag{1.3.3}$$

but the model still did not work well. The main drawback was the assumption that the potential was uniform or varying slowly as was the case with their initial starting point of a uniform electron gas.

Various attempts to improve on the Thomas-Fermi energy functional as well as the Thomas-Fermi-Dirac energy functional were made and in fact, the initial attempts to approximate the Hohenberg-Kohn functional $F_{HK}[n(\mathbf{r})]$ used the kinetic energy term developed by Thomas and Fermi, but the use of this kinetic energy functional did not yield the desired results.

1.3.1 Hohenberg-Kohn Theorems

Although some principles about DFT such as the Hartree-Fock theory were already known by the 1920s, it was not until the 1960s theorems of Hohenberg and Kohn [9] that the utilization of DFT in various many-particle systems became a reality. They showed that the groundstate electron density n($\mathbf{r}$) was sufficient to determine the exact many-body energy. That is, n($\mathbf{r}$) could uniquely define the potential. The implication of their theorem was that all properties of a system could be determined from the electron density, since it alone determines the number of electrons and hence the wavefunction of a nondegenerate groundstate. They also showed that there exists a universal functional $F_{HK}[n(\mathbf{r})]$ (independent of $v(\mathbf{r})$) such that, for a given external potential $v(\mathbf{r})$, the actual groundstate energy E and density n($\mathbf{r}$) were obtained by minimizing the energy functional

$$E[n(\mathbf{r})] = F[n(\mathbf{r})] + \int v(\mathbf{r})n(\mathbf{r})d^3r \tag{1.3.4}$$

with respect to the variations in $n(\mathbf{r})$. This was however subject to the constraint that the particle number N within the system which is given by equation 1.3.5 should remain constant.

$$N = \int n(\mathbf{r})d^3r \tag{1.3.5}$$

The universal functional that they proposed had the form,

$$F_{HK}[n(\mathbf{r})] = T[n(\mathbf{r})] + V_{ee}[n(\mathbf{r})] \tag{1.3.6}$$

where $T[n(\mathbf{r})]$ is the kinetic energy component and $V_{ee}[n(\mathbf{r})]$ is the electron-electron interaction, which is composed of the sum of the classical repulsion and a non-classical term.

1.3.2 Kohn-Sham (K-S) Theorems

Building on the progress made in the earlier models such as the Hartree-Fock as well as the one by Hohenberg-Kohn, Kohn and Sham established a theory that was to revolutionalize the use of DFT and make it a practical tool for everyday analysis of material properties. Their theory differed from the Hartree-Fock one in the sense that the Hartree-Fock energy E_x^{HF} was replaced by the density functional $E_{xc}[n_\uparrow, n_\downarrow]$ for the exchange-correlation energy, and the nonlocal Hartree-Fock exchange potential $\upsilon_x^n(\mathbf{r}, \mathbf{r\prime})$ was replaced by local exchange-correlation potential $\upsilon_{xc}^n(\mathbf{r})$ as a component of the selfconsistent effective potential $\upsilon_{eff}^n(\mathbf{r})$. The local potential $\upsilon_{xc}^n(\mathbf{r})$ is the functional derivative $\delta E_{xc}/\delta n_{\uparrow\downarrow}(\mathbf{r})$ and hence it depends on both the spin up ($n_\uparrow$) and spin down ($n_\downarrow$) densities.

They suggested a highly nonlocal functional that was giving the major part of the kinetic energy. This was the 'single-particle'kinetic energy, $T_s[n(\mathbf{r})]$ for electrons without mutual Coulomb repulsion (i.e. independent) in their groundstate under the action of an external potential, such that their groundstate density was $n(\mathbf{r})$. This gave rise to the Kohn-Sham orbitals ϕ_i which formed a wavefunction that described exactly a system containing N non-interacting electrons. The kinetic energy term of this system was described exactly as

$$T_s[n(\mathbf{r})] = \frac{1}{2}\Sigma\langle\phi_i \mid -\nabla^2 \mid \phi_i\rangle \tag{1.3.7}$$

This approach resulted in a model that was more accurate than either the Thomas-Fermi or the Thomas-Fermi-Dirac models, but one that was also computationally expensive. The energy functional which they derived was

$$E[n(\mathbf{r})] = \int v(\mathbf{r})n(\mathbf{r}) + T_s[n(\mathbf{r})] + \frac{e^2}{2}\int \frac{n(\mathbf{r}_1)n(\mathbf{r}_2)}{|\mathbf{r}_1 - \mathbf{r}_2|}d^3\mathbf{r}_1 d^3\mathbf{r}_2 + E_{xc}[n(\mathbf{r})]$$

where $E_{xc}[n(\mathbf{r})]$ was the exchange-correlation energy, a term that contained both a kinetic and potential energy, and it was composed of the following:

◇ A negative potential energy which formed the exchange energy that tends to cancel part of the Hartree potential energy. It originated from the fact that the wavefunction antisymmetry causes electrons of like spin projection to avoid each other.

◇ A negative potential energy known as the correlation potential energy, which further reduces the Hartree potential energy. This occurs because the Coulomb potential causes electrons of either spin orientation to avoid each other.

◇ A positive correlation contribution to the kinetic energy, which arises due to the uncertainty and Pauli principles. As a result, the KE increases because mutual avoidance reduces the available space.

Minimization of the K-S energy functional with respect to the one-particle eigenfunctions, which is equivalently similar to minimising with respect to the electron density leads to the Kohn-Sham equations that give the exact ground state energy and density of a non-degenerate system. This is obtained from the self-consistent solution of the Kohn-Sham equations. The total electron density can thus be decomposed into a set of single-particle orbitals known as the Kohn-Sham orbitals which are expressed as,

$$n(\mathbf{r}) = \sum \sum \mid \phi_i(\mathbf{r}, s) \mid^2 \tag{1.3.8}$$

where s stands for spin $\uparrow$ and $\downarrow$. The above equation can further be written in a more simplified way as,

$$n(\vec{\mathbf{r}}) = \sum_{i}^{occ} \mid \phi_i(\vec{\mathbf{r}}) \mid^2 \tag{1.3.9}$$

and from these, the K-S equations can be obtained. By taking advantage of the orthonormality of the wavefunctions and also the fact that the derivative of the

energy functional should be zero for a minimum leads to the Schrödinger-like Kohn-Sham orbital equation,

$$\frac{-\hbar^2}{2m}[\nabla^2 + \upsilon_{eff}(\mathbf{r})]\phi_i(\mathbf{r}) = \epsilon_q \phi_i(\mathbf{r}) \tag{1.3.10}$$

where ϵ_q is the Lagrange multiplier for ensuring normalization. This can further be re-written in a more general way as,

$$H[n]\phi_i = \epsilon_i \phi_i \tag{1.3.11}$$

This is the DFT equivalent of the single particle Schrödinger equation in the Hartree-Fock theory. It is worth noting that, since the Kohn-Sham scheme is a ground state theory, the eigenvalues cannot be treated as transition energies to or between the interacting excited states. In equation 1.3.10, $\upsilon_{eff}(\mathbf{r})$ is the effective one-electron potential and it consists of an external potential $\upsilon(\mathbf{r})$, a Hartree term and an exchange-correlation term. That is,

$$\upsilon_{eff}(\mathbf{r}) = \upsilon(\mathbf{r}) + \frac{e^2}{4\pi\varepsilon_0}\int \frac{n\mathbf{r\prime}}{\mid \mathbf{r} - \mathbf{r\prime} \mid} d^3\mathbf{r\prime} + \upsilon_{xc}(\mathbf{r}) \tag{1.3.12}$$

where the exchange-correlation potential $\upsilon_{xc}(\mathbf{r})$ is expressed as

$$\upsilon_{xc}(\mathbf{r}) = \frac{\delta E_{xc}}{\delta n(\mathbf{r})} \tag{1.3.13}$$

The three sets of equations shown above are collectively referred to as the K-S equations, and they form the Kohn-Sham formalism which offers a simpler way of dealing with DFT. Through the K-S formalism, the scheme becomes computationally simpler than say the approximate Hartree-Fock scheme, since $\upsilon_{eff}(\mathbf{r})$ is local i.e. acts on the wavefunction at the point r. Recent developments have also seen the exchange and correlation energy functional of the Kohn-Sham equations for multicomponent systems being developed [10]. Since the DFT calculation takes place via fast fourier transform between reciprocal and real space, the Kohn-Sham equation in reciprocal space takes the form,

$$\sum_{\vec{G}\prime}[-\frac{1}{2} \mid \vec{k} + \vec{G} \mid^2 \delta_{\vec{G}\vec{G}\prime} + \upsilon_{eff}(\vec{G}, \vec{G\prime})]\psi_j(\vec{k} + \vec{G\prime}) = \epsilon_j(\vec{k})\psi_j(\vec{k} + \vec{G}) \tag{1.3.14}$$

1.3.3 Local Density Approximation (LDA) and Local Spin Density (LSDA) for the exchange-correlation energy.

Although the K-S equations offer the most ideal tool for many-body problems, the exchange-correlation term E_{xc} is still unknown.

In order to incorporate the correlation energy into their equations, Kohn and Sham split the kinetic energy functional $T[n(\mathbf{r})]$ into a part based on the independent-particle form and a remainder that adds to the unknown exchange correlation energy $E_{xc}[n(\mathbf{r})]$. They did this by considering a spin-paired (closed shell) case and a spin-unrestricted case with both approaches treating the electron density to be slowly varying, hence they approximated the density as being constant locally. This gave rise to the approach commonly referred to as the local density approximation.

In the LDA approach, the K-S orbitals are expressed as

$$-\frac{1}{2}[\nabla^2 + \upsilon(\mathbf{r}) \int \frac{n\mathbf{r\prime}}{\mid \mathbf{r} - \mathbf{r\prime} \mid} d\mathbf{r\prime} + \upsilon_{xc}^{LDA}(\mathbf{r})]\psi_q(\mathbf{r}) = \epsilon_q \psi_q(\mathbf{r}) \tag{1.3.15}$$

Since the K-S equations are non-linear, they need to be solved iteratively in a self-consistent way, and the solutions thus obtained define the K-S local density approximation (LDA).

LDA is especially applicable to systems with slowly-varying densities but cannot be formally justified for highly inhomogeneous systems such as atoms and molecules.

Often one encounters systems having electrons with spin projections either up or down, especially when the electron shells are not closed. In these cases, the electron densities can be treated separately so that those having an up spin projection will have a density $n_\uparrow$, while the density for those having a spin down is $n_\downarrow$. The two spin projections can also be combined to become,

$$n(\mathbf{r}) \equiv n_\uparrow + n_\downarrow \tag{1.3.16}$$

For systems having spin projections either up or down, the electron densities are normally generated from the spin-up and down K-S wavefunctions, that is

$$n_{\uparrow}(\mathbf{r}) = \Sigma_q \mid \psi_{q\uparrow}(\mathbf{r}) \mid^2 \tag{1.3.17}$$

and similarly for $n_{\downarrow}$.

Such an approach gives rise to the local spin density approximation (LSDA) where the exchange-correlation term is

$$E_{xc}^{LSD}[n_{\uparrow}, n_{\downarrow}] = \int d^3r n(\mathbf{r}) \epsilon_{xc}(n_{\uparrow}(\mathbf{r}), n_{\downarrow}(\mathbf{r})) \tag{1.3.18}$$

This functional utilizes the exchange-correlation energy per electron of a uniform electron gas, that is, $\epsilon_{xc}[n_{\uparrow}, n_{\downarrow}]$ which is accurately known [11]. LSD also works very well not only for odd-electron systems but also for even ones, by allowing electrons of different spin to have different densities. If the electron shells are not closed, differences in the densities between electrons with spin $\uparrow$ and spin $\downarrow$ usually occurs, and therefore the total density becomes, $(\rho^{n\uparrow} + \rho^{n\downarrow})$ while the spin density difference is $(\rho^{n\uparrow} - \rho^{n\downarrow})$. Such a system leads to a spin-polarized model which is characteristic of the LSD. LSD has been used widely in Solid State Physics to predict correct crystal structures, lattice constants, bulk moduli and vibrational frequencies, but in quantum chemistry it overestimates the atomization energies of molecules. In fact, it has already been shown that 50% or more of the energy required to atomize a molecule is the exchange-correlation energy [4]. Tong and Sham [12] also observed that this approximation tends to underestimate the exchange energy by at least 10% while overestimating the correlation energy by a factor of two or more. Such underestimation or overestimation of the energy values was attributed to the problem of self-interaction of the electrons when approximate functionals are considered. In this case, self-interaction becomes a major problem since an electron in a molecule interacts with other electrons through the coulomb potential but does not interact with

itself. Owing to its significant effects as far as the calculated total energies of a system are concerned, this problem has received a great deal of attention, starting with the earlier attempts to avoid it (in an approximate E_{xc}), as proposed by Perdew and Zunger [13], as well as by Parr and Yang [14]. Such efforts have seen the error due to the self-interaction problem in the exchange contribution being reduced to less than 3% [7] (compared to the uncorrected local spin density form) while the error in the correlation contribution (except helium) is reduced to about 30% [3].

Parr *et al.* [15] observed that the correlation energy (which is the error in the energy defined as $E_{corr}^{HF} = E - E_{HF}$) tends to remain constant for atomic and molecular changes that conserve the number and types of chemical bonds, but it can change drastically and become determinative when bonds change. Its magnitude can vary from 20 or 30 to as high as thousands of kilocalories per mole, from a few hundredths of an atomic unit on up. The exchange energies on the other hand are an order of magnitude or more larger, even when the self-exchange term is omitted.

1.3.4 Generalized Gradient Approximation (GGA) and Functionals of the electron density.

In order to improve on the accuracy and performance of the density functional theory, the fluctuation of the electron density has to the taken into account. The assumption that the electron density is constant or slowly varying as is the case with LDA and LSDA may not work well for certain systems, especially the strongly localized ones like diamond [16]. As a result, both the electron density and their gradients are normally taken into account, in an approach that is commonly known as the generalized gradient approximation (GGA), proposed by Perdew and Wang [17]. This approximation depends only on the density and its spatial derivative, making it easy to evaluate.

In the Kohn-Sham approach to the DFT, the total energy of a system can be expressed as:

$$E[n] = T_s[n] + V_{ext}[n] + J[n] + E_{xc}[n] \tag{1.3.19}$$

where $V_{ext}[n]$ is the potential energy in the field of the nuclei plus any external perturbation, $T_s[n]$ is the kinetic energy of a set of n independent (non-interacting) electrons moving in an effective one-electron potential which leads to the density $n(\mathbf{r})$, $J[n]$ is the total Coulomb interaction and $E_{xc}[n]$ is the exchange-correlation energy. The exchange-correlation energy represents the main problem in DFT, since its exact expression is unknown as mentioned previously, and approximations must be made. The simplest approach is the local spin density (LSD) in which the functional of the uniform electron gas density is integrated over the whole space, that is,

$$E_{xc}^{LSD} = \int d^3r n(\mathbf{r}) \epsilon_{xc}^{unif}(n_\uparrow(\mathbf{r}), n_\downarrow(\mathbf{r})) \tag{1.3.20}$$

where ϵ_{xc}^{unif} is the accurately known exchange-correlation energy per particle of a uniform electron gas [18]. Although the approach gives fairly accurate results [19], and was responsible for the early successes of DFT, it often provides some unsatisfactory results in chemical applications. Starting from the expression for E_{xc}^{LSD}, several corrections for the non-uniformity of atomic and molecular densities have been proposed, with those based on the gradient of the electron density receiving considerable attention in the last few years due to their simplicity. These corrections which are collectively referred to as generalized gradient approximation (GGA) are usually expressed in terms of an enhancement factor over the exchange energy of the uniform electron gas, so that the total exchange-correlation energy assumes the form,

$$E_{xc}^{GGA} = E_{xc}^{LSD} + \sum \int d^3r C_{ii}(n_\uparrow(\mathbf{r}), n_\downarrow(\mathbf{r})) \frac{\nabla n_i}{n_i^{\frac{2}{3}}} . \frac{\nabla n_{i\prime}}{n_{i\prime}^{\frac{2}{3}}} \tag{1.3.21}$$

A number of GGAs for the exchange-correlation functionals have been proposed [20], and these can be categorized in two classes. The first one deals with functionals constructed semi-empirically with parameters fitted to experiment, while the second class includes functionals which satisfy a number of theoretical physical constraints. The constraints involve derivation of the functional starting from the gradient expansion, then restoring those properties of the exchange-correlation hole that are responsible for the success of LSDA in solids, while other functionals combine the two classes. Some GGAs perform better than others and in this study, we focus on the Perdew, Burke and Enzerhoff (PBE) functional for the exchange and correlation energy [11, 21]. It's also important to add that while the Hartree-Fock approximation underbinds atoms in a molecule and LSDA overbinds them, GGAs achieve generally better accuracies with regard to binding energies [11, 21, 22, 23, 24]

1.3.5 The PBE functional

The non-empirical GGA functional developed by Perdew, Burke and Ernzerhof commonly referred to as PBE has been noted to be probably the most promising non-empirical functional [25, 17, 21, 22]. It significantly reduces the mean absolute error in the calculation of say molecular bond energies, and it is therefore among the most widely used functionals to approximate the exchange-correlation energy. Its construction ensures that it retains a number of physical features in both the correlation and exchange parts, and key among the features that it satisfies are as follows [26]:

- ▷ Fulfilment of the required uniform gas limit
- ▷ The correct upper bound of the correlation energy $E_c \leq 0$
- ▷ The correct upper bound of the exchange energy $E_x < 0$
- ▷ The exact exchange energy obeys the spin scaling relationship and uniform density scaling of E_x

▷ Satisfies the linear response of the spin-polarized uniform electron gas.

▷ Satisfaction of the Lieb-Oxford bound. [27]

The PBE exchange-correlation functional is very much like the one developed by Perdew and Wang, referred to as PW91 which was derived from a model for the exchange-correlation hole [17] and its form is expressed as,

$$E_{xc}^{PBE-GGA}[n_\uparrow, n_\downarrow] = \int d^3r n \epsilon_X^{unif} F_{XC}(r_s, \xi, s) \tag{1.3.22}$$

where F_{XC} is an enhancement factor, and ϵ_x^{unif} is expressed as,

$$\epsilon_X^{unif} = \frac{-3e^2 \mathbf{k}_F}{4\pi} \tag{1.3.23}$$

ξ is the relative spin polarization, expressed as,

$$\xi = \frac{(n_\uparrow - n_\downarrow)}{n} \tag{1.3.24}$$

and r_s is the local Seitz radius obtained from,

$$n(\mathbf{r}) = \frac{3}{4\pi r_s^3} = \frac{\mathbf{k}_F^3}{3\pi^2} \tag{1.3.25}$$

However, although the PBE exchange-correlation functional E_{xc}, is a great improvement to the application of DFT in solving many problems relating to atoms, molecules and solids, GGA functionals are still too limited to yield a fully consistent improvement over LDA and to describe binding energies with the desired chemical accuracy of better than 1kcal/mol or 50meV/atom. It is therefore envisaged that a hybrid Hartree-Fock/DFT approach has the potential to offer better numerical accuracy [28]: a model that uses a linear combination of the two, that is, a Hartree-Fock exchange with DFT exchange-correlation.

In this case, while trying to improve on the GGA's E_{xc}, Lee, Yang and Parr approximated the Colle-Salveti functional [29, 30, 31] which is an orbital functional that is automatically free from the self-interaction error and is also invariant under unitary transformation of the occupied orbitals. They obtained

the correlation energy as an explicit functional of the density, its gradient and Laplacian. The functional that they derived is now generally known as the Lee-Yang-Parr (LYP) functional [32] and it gave rise to perhaps the most widely used and popular implementation of such a hybrid model, the so-called BLYP (Becke-Lee-Yang-Parr) [33, 34]. It uses in a self-consistent way the Becke88, (E_x^B) [35] exchange functional together with the Lee-Yang-Parr correlation. The BLYP functional has the form viz [36],

$$E_{xc}^{BLYP} = (1-A)E_x^{Slater} + AE_x^{HF} + BE_x^{Becke} + CE_c^{LYP} + (1-C)E_c^{VWN}$$

where E_x^{Slater} is the Slater exchange, E_x^{HF} is the Hartree-Fock exchange, E_x^{Becke} is the gradient part of the exchange functional of Becke [35], E_c^{LYP} is the correlation functional of Lee-Yang-Parr (LYP) [32] and E_c^{VWN} is the correlation functional of Vosko-Wilk-Nuisar parametrization [37]. The three semi-empirical parameters A, B and C are often obtained by fitting the heats of formation of a standard set of molecules.

In this model, the LSD contribution to the exchange energy is actually that of a uniform spin-polarized electron gas.

With such new improvements to DFT, within either the LDA or the GGA, accuracy of geometries can now be obtained to better than 0.1Å and the calculated relative energies to better than 0.2eV and for special cases even better than 0.01eV [38]

1.4 Basis set

Both the Hartree-Fock and Kohn-Sham equations can be solved using similar mathematical techniques, where one seeks to find coefficients c_q^l to express the wavefunctions ψ_q in a given basis set ψ_l^n, where q represents a set of quantum numbers $(n, \vec{\mathbf{k}})$. This may be written as,

$$\psi_q = \sum_{l=1}^{L} c_l^q \psi_l^n \tag{1.4.1}$$

where ψ_q is a member of a function space having infinite dimensions, and hence L, which needs to be large, is also infinite in principle. However, when solving real problems, a limited set of basis functions is often needed and as such the wavefunctions ψ_q cannot be described exactly. Instead, one tries to find a basis that can generate a function that is close to ψ_q. In this case, one only needs to find a few of the basis set functions to describe the wavefunction accurately, and such a basis set is said to be efficient. Limiting L may however lead to approximate eigenfunctions that carry too many of the properties from the basis set, and such a basis is said to be biased. Therefore one needs to find a basis set that is both efficient and unbiased. Two basis sets have been used widely, and these include plane waves as well as augmented plane waves [1]. Since a basis set composed of plane waves was used in this study, it will form the main focus of this section. It was chosen for its simplicity and for being unbiased, meaning that it does not force the result in some hidden way to go in a particular way. In this approach, any eigenfunctions $\psi_{\vec{k}}^n$ of a periodic Hamiltonian can be expressed exactly in the plane wave basis set by means of an infinite set of coefficients $c_{\vec{K}}^{n,\vec{k}}$. Therefore,

$$\psi_{\vec{k}}^n(\vec{r}) = \sum_{\vec{K}} c_{\vec{K}}^{n,\vec{k}} e^{i(\vec{k}+\vec{K}).\vec{r}} \tag{1.4.2}$$

This compares with equation 1.4.1 where q represents quantum numbers $(n, \vec{k})$ and l stands for $\vec{k} + \vec{K}$. Using this representation, one basis function for $\psi_{\vec{k}}^n(\vec{r})$ or $\vec{K}$ would be,

$$\phi_{\vec{K}}^{\vec{k}}(\vec{r}) = \mid \vec{K}\rangle = e^{i(\vec{k}+\vec{K}).\vec{r}} \tag{1.4.3}$$

Since one cannot work with an infinite basis set, the limiting in the case of plane waves is achieved by limiting the set of all $\vec{K}$ with $K \leq K_{max}$, which

corresponds to a sphere with radius K_{max} centred at the origin of the reciprocal space. As such, all the reciprocal lattice vectors that are inside this sphere are taken into the basis set [1]. However, to make the basis set limiting and more practical, instead of using K_{max}, one often uses the free electron energy corresponding to K_{max}, and this is called the cut-off energy E_{cut}, which is expressed as,

$$E_{cut} = \frac{\hbar^2 K_{max}^2}{2m_e} \tag{1.4.4}$$

where m_e is the mass of an electron.

Using the reciprocal lattice vectors $\vec{G}$, the cut-off energy E_{cut} (expressed in Rydbergs) is obtained as $\mid \vec{k} + \vec{G} \mid \leq \sqrt{E_{cut}}$ and in the reciprocal lattice space, the wavefunction (plane wave) expansion of the Kohn-Sham states is,

$$\psi_{\vec{k}}(\vec{r}) = \sum_{\vec{G'}} c_{\vec{k}}(\vec{G}) e^{i(\vec{G}+\vec{k}).\vec{r}} \tag{1.4.5}$$

or

$$\psi_j(\vec{k}, \vec{r}) = \sum_{G} \psi_j(\vec{k} + \vec{G}) \frac{e^i(\vec{k} + \vec{G}).\vec{r}}{\sqrt{\Omega}} \tag{1.4.6}$$

Since plane waves are orthogonal, then

$$\langle \vec{K_1} \mid \vec{K_2} \rangle = \int e^{i(\vec{K_2} - \vec{K_1}).\vec{r}} = \delta(\vec{K_2} - \vec{K_1}) \tag{1.4.7}$$

The number of plane waves in a basis set is usually determined by the smallest length scales that are described in the real space. Depending on the value stated, the number of plane waves may turn out to be very large, thus putting the plane wave basis set's efficiency into doubt. However, this problem is overcomed by taking into account the fact that the most oscillating parts of the wavefunctions are the tails that reach out into the region close to the nucleus. Fortunately, this region of the solid is shielded from the more outer regions of the atoms where valence electron are, and hence where many chemical

processes take place. This means that the electrons in this region will not behave differently from free atom electrons. It therefore becomes possible to replace the potential in the inner regions by a pseudopotential that is designed to yield very smooth tails of wavefunctions inside the atom. When the inner regions (core - states) are removed from the spectrum, one no longer considers the all-electron potential of a system given by the expression,

$$(-\frac{1}{2}\nabla^2 + V_{eff})\psi_q = \epsilon_q \psi_q \tag{1.4.8}$$

but rather the pseudopotential (ps), so that the Schrödinger equation becomes

$$(-\frac{1}{2}\nabla^2 + V_{eff}^{(ps)})\psi_q^{ps} = \epsilon_q \psi_q^{ps} \tag{1.4.9}$$

The pseudopotential should however perform equally well as the all electron potential.

In the outer regions of the atoms, the pseudopotential continuously evolves into the true potential such that this region of the crystal behaves as if nothing had happened. As a result, it is possible to use the ultrasoft plane wave basis set for realistic cases with a given cut-off energy. The pseudopotentials constructed will need to be both soft and transferable, whereby the softness means that only a manageable number of plane waves are needed. In order to make a pseudopotential soft [39, 40, 41], it has to be tailored for a particular element in a given environment. However, one also requires a potential that can be used in many environments i.e, solids, molecules, clusters, surfaces, insulators, metals etc., of the corresponding element, and if this is realized, such a potential is said to be transferable.

1.5 The diamond (111) surface

The (111) diamond surface is not only one of the most important growth planes in CVD diamond, but it is also the natural cleavage plane, yielding a clean

surface terminated by one dangling bond parallel to the surface normal [42], and in other cases three dangling bonds forming an angle of 70.5° with the surface normal [43]. This surface also finds a lot of use in industry, especially owing to its surface atomic structure. In trying to establish the most stable dangling bond terminations between the single (SDB) and triple dangling bonds (TDB), Scholze *et al.* [43] observed in their DFT calculations that the single-dangling bond arrangement was the most favoured energetically. They found the surface energy for the TDB minimum energy configuration to be 1.35eV higher than that of the SDB surface. Such an outcome was not unexpected, since it is energetically easier to break a single bond than three, although some workers suggest that it is possible for the two terminations to coexist on the same surface [44]. A clean (111) diamond surface is normally bulk-terminated (figures 1.1 and 1.2), but it may reconstruct into (2×1) π-bonded Pandey chains [45] (figures 1.3 and 1.4) that are nearly undimerized and unbuckled under say heating conditions above 950°C [46]. Walter *et al.* [16] observed in their LEED measurements that the π-bonded chains forming the (2×1) reconstructed surface were not tilted or only negligibly tilted, which tended to differ slightly from the work of Huisman *et al.* [47] who observed some degree of buckling. A similar result to that obtained by Walter *et al.* [16] and Scholze *et al.* [43] was also obtained by Kern *et al.* [48] using DFT energy minimisation, and they further found that there was a substantial buckling in some of the inner layers.

Over and above this study looking at the O and OH adsorbates on the C(111) surfaces, it also sheds some more light on both the clean unterminated (1×1) and the (2×1) reconstructed diamond (111) surfaces, with a view to reconciling both the experimental observations and the theoretical predictions.

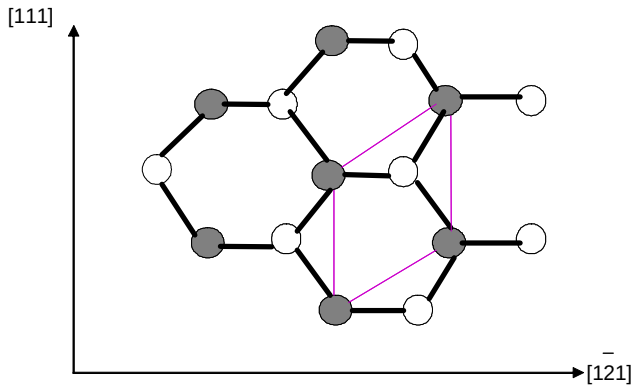


Figure 1.1: Schematic diagram of the top view of bulk-terminated (1×1) C(111) surface. The grey circles represent the topmost carbon atoms, while the white (open) ones represent the 2nd layer of carbon atoms from the top.

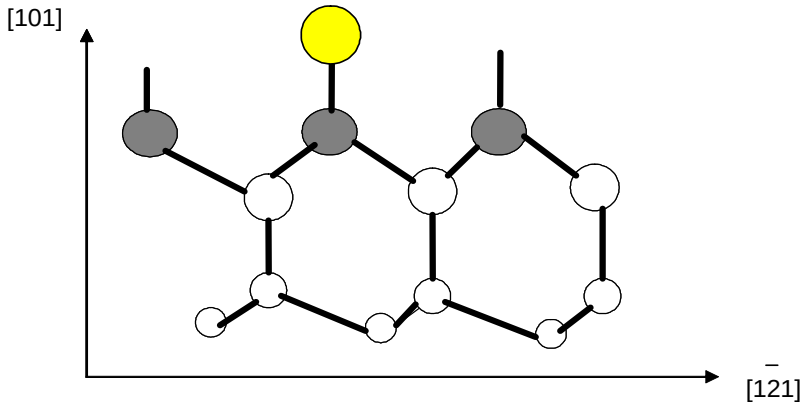


Figure 1.2: Cross-sectional view of a bulk terminated C(111) surface showing an adsorbed oxygen atom (yellow circle) on a single dangling bond termination (SDB), and some dangling bonds.

In the presence of adsorbates under various ambient conditions, the structure of diamond surfaces is found to change somewhat, while in other cases it is preserved. In this regard, Klauser *et al.* [49] observed that the C(111)-(2×1) structure of the annealed surface remains after saturation coverage of oxygen which appears to be contradictory to other works, including the findings of this study. It is not clear if the surface was exposed to oxygen while still being annealed, or if it was allowed to cool down, then exposed, since heating may provide an energy barrier to the expected 1×1 dereconstruction under these O-exposure conditions. A recovery from a $(2 \times 2)/(2 \times 1)$ reconstruction to a 1×1 bulk terminated surface is nonetheless achieved after exposure of the surfaces to hydrogen generated at a hot filament [46].

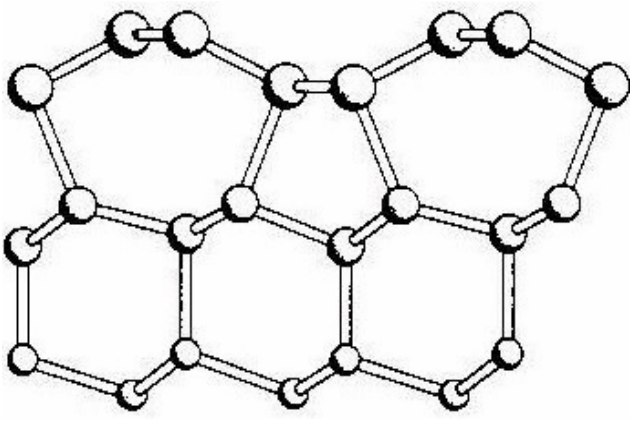


Figure 1.3: Side view of a (2×1) reconstructed (111) diamond surface. After Walter *et al.* [16]

Adsorbed oxygen atoms or hydroxyl groups have been shown to particularly alter the surface properties of diamond in a way that makes it quite attractive for various technological applications. In particular, some of the changes already observed involve modifying the chemical, mechanical and electronic properties of diamond surfaces, making them quite useful in semiconductor as well as in other high-tech applications. Apart from making the surfaces either hydrophobic or

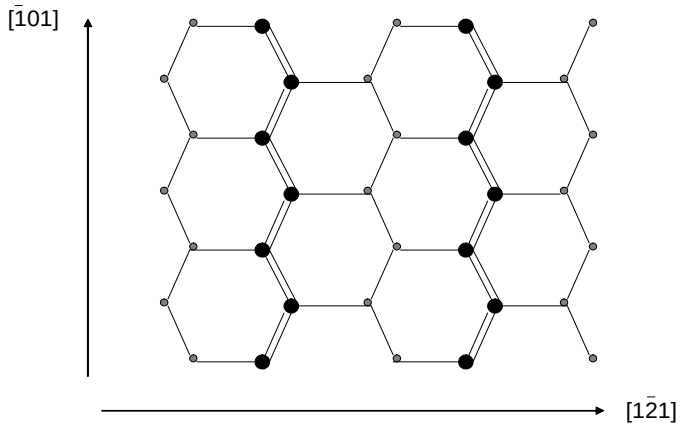


Figure 1.4: Top view of a (2×1) reconstructed (111) diamond surface. The large dark circles represent carbon atoms at the upper π-bonded zigzag chains, while the smaller grey circles correspond to the lower π-bonded zigzag chains.

hydrophilic, these adsorbates may also affect the bonds formed at the interface with other materials, either making them more useful or instead compromising the devices thus formed.

It has already been shown that adsorbed oxygen atoms result in positive electron affinities (PEA) on various diamond surfaces for different oxygen terminating groups [50, 51], while hydrogen terminated surfaces exhibit a negative electron affinity (NEA). Additionally, hydroxyl terminated diamond surfaces have been shown to yield negative electron affinities, which makes them potentially useful in for example cold cathode applications. Using *ab initio* calculations, Loh *et al.* [52, 53] have investigated several models of atomic oxygen chemisorption on the C(111) plane, where they indicate that oxygen chemisorption depends on the coverage. They further suggest that at low coverages (0.5 monolayer), epoxy-like (bridge) oxygen adsorbs while at higher coverages, the carbonyl ONTOP chemisorption dominates. Our earlier XPS findings as well as the results of Derry *et al.* [42] and Rebuli *et al.* [54] revealed that under Ultra High Vacuum (UHV) conditions, the optimum coverage of oxygen on the C(111) surface was $\frac{1}{3}$ of a monolayer, while the XPS results further showed that

the most preferred adsorption site was the On-Top one. Rebuli *et al.* [54] went ahead to show that the oxygen adsorption depends on the vacuum level, and hence the environment under which the surfaces are prepared or exposed (i.e. either in the presence of oxygen atoms or hydroxyl groups) becomes an integral part of the observed coverage. To the best of our knowledge, this possibility has however not been explored fully theoretically to establish unambiguously which terminations and sites were most favoured as the adsorbate coverage increased progressively. It has nonetheless been known for sometime that diamond surfaces used for various applications and prepared under atmospheric conditions are always terminated with oxygen atoms, hydroxyl groups and hydrogen atoms. Even then, it is still conceivable that in spite of the presence of these species at diamond surfaces, some form of surface defects may exist on real surfaces.

Oxygen has also been reported to play a significant role in CVD diamond synthesis, where it preferentially attacks the graphitic sp^2 bonds [53], and hence improves the diamond film quality as well as having an influence on its texture and morphology [55]

Establishing the optimum coverages of oxygen atoms or hydroxyl groups on clean diamond (111) surfaces when they are exposed to the environment as well as determining the preferred adsorption sites remains an important and intriguing subject of study. This is especially so due to the reasons alluded to previously, and more importantly bearing in mind the unique properties of diamond and how these can change in the presence of the two adsorbates (O & OH). The general understanding of the behaviour of such surfaces or interfaces in the presence of the adsorbates is therefore central to knowing and controlling their performance when put into use in various applications. This makes it possible to harness the accruing advantages and at the same time avoid any difficulties that may arise due to their presence, by choosing to engineer the surfaces in such a way that the undesirable adsorbates are avoided, while the

useful ones are exploited.

1.6 The Computational procedure

All the calculations reported in this study were done using the FHI98MD computer code [56, 38]. This is a molecular dynamics computer code that employs first principles pseudopotentials and a plane wave basis set. The pseudopotentials that were used for the carbon, oxygen and hydrogen atoms were all norm-conserving, and they were generated by the scheme of Troullier-Martins [57]. The norm-conserving nature of the pseudopotential ensured that they exhibited the same scattering properties (logarithmic derivatives) as the all-electron potential in the neighbourhood of the atomic eigenvalues, which is a measure of the pseudopotential's proper performance. Pseudopotentials generated by the scheme of Troulier-Martins are also both smooth and transferable, whereby their smoothness ensures that they have rapid convergence in the calculated total energy of system. This means that there is also rapid convergence of the system properties, with respect to an increase in the plane wave basis set. The fact that they are also transferable means that they work in various environments such as atoms, molecules or solids. Pseudopotentials generated through the Troullier-Martins scheme also work much better for strongly localized valence states such as in the case of diamond.

The calculations were performed using the generalized gradient approximation (GGA) for the exchange-correlation functional.

The Monkhorst-Pack [58] scheme was implemented in the start utility of the package to generate the special **k**-points and for each of the **k**-point, the accuracy of the scheme was automatically performed and checked following the procedure proposed by Chadi and Cohen [59]. The Monkhorst-Pack scheme ensures that the irreducible part of the Brillouin zone is integrated over a set

(mesh) of uniformly spaced special **k**-points.

The slab approach was used to simulate the surfaces as opposed to the cluster representation.

1.7 Calculations of the bulk parameters of the free carbon, oxygen and diamond-carbon atoms, as well as those of the oxygen molecule and the hydroxyl groups.

This study involved the calculation of the total minimum energies of relaxed geometries of the C(111) surface with and without adsorbed oxygen atoms or hydroxyl groups on them, and hence it was essential to establish initially the bulk properties of all the participating atoms, principally carbon and oxygen. This was then followed by the computation of the bulk properties of the oxygen molecules and the hydroxyl groups as well as those of bulk diamond, before embarking on the main surface or slab calculations. It was essential to compare these first, because they were a prerequisite to the determination of not only the converged energies of the relaxed structures of both diamond-carbon and the oxygen molecule, but also in establishing the interatomic spacings (bulk lattice constants) which were required in the calculation of the initial atom positions within the slabs. Their total minimum energies were also required for the determination of the adsorption energies of the oxygen atoms and the hydroxyl groups on the respective surfaces. Starting the calculations with atom positions that were not too far off from the expected relaxed locations helped quite a lot with faster system convergence.

The free carbon atom was placed at the origin of a large box measuring 20 Bohrs in size (where 1 Bohr $\cong$ 0.5291Å) when determining its bulk properties, and the plane wave cutoff energy was varied between 30 and 80Ry, where 1Ry=13.6eV. A large sized box was necessary because it ensured that the atom

properties were simulated as if it were completely free. The cutoff energy was varied between the values mentioned above in order to determine the optimum value where the total energy converged, since the cutoff energy was directly related to the number of plane waves and therefore the size of the basis set. A very large cutoff energy would nonetheless make the specific problem expensive computationally, while a smaller one would result in a total energy that may not be adequately converged. Based these arguments, the range between 30 and 80Ry for the plane wave cutoff energy was considered to be ideal. Figure 1.5 shows a plot of the total energy versus cutoff energy of a free carbon atom. A

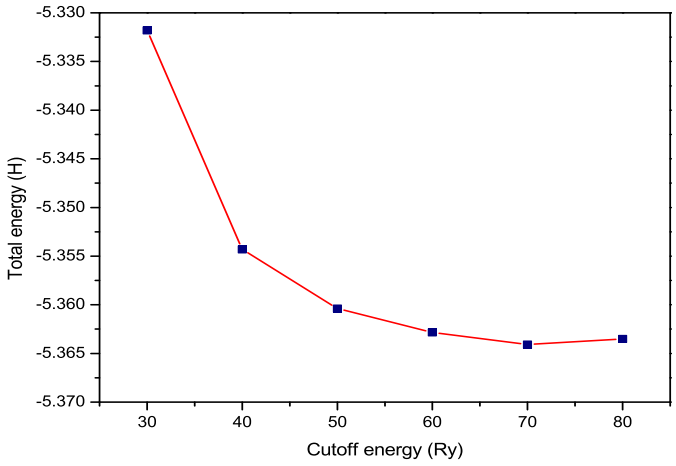


Figure 1.5: Total energy of a free carbon atom for various plane wave cutoff energies. The vertical axis is given in Hartree, where 1H=27.2116eV.

similar calculation was also done for two carbon atoms simulating the diamond lattice. These were placed within a cell whose size was appropriate for bulk diamond, with one atom being placed at the origin, while the other was placed at a distance of $(\frac{1}{4}, \frac{1}{4}, \frac{1}{4})$ of the diamond's lattice constant. The experimental value of the lattice constant of diamond (3.567Å) was used to determine the initial (guessed) atom positions and the calculated bulk properties of diamond are shown in Table 1.1

Table 1.1: Calculated DFT-GGA and experimental bulk properties of diamond-carbon. Plane wave cutoff energy E_{cut} is in Rydbergs (Ry), while the lattice constant a_o, and the distances between the C atoms d_{c-c} are in Å. The binding energy E_{coh} is shown in eV/atom, while the bulk modulus is in Mbar

	Ecut	a_o	dc-c	Ecoh	B
Exp.	-	3.567[60]	1.544[16]	7.37[61], 3.65eV per bond [62]	4.42[61, 63]
Theo.	30	3.606	1.543	7.45	3.19
	40	3.581	”	7.82	4.22
	50	3.562	”	7.90	4.18
	60	3.563	”	7.89	4.14
	70	3.563	”	7.87	4.15
	80	3.563	”	7.89	4.16

The lattice parameters of bulk diamond were reproduced to within very good agreement of the experimental values as seen from Table 1.1. Using the Murnaghan equation of state [64] which is given by equation 1.7.1, the bulk modulus of diamond was found to be about 4.14Mbars on average, compared to the experimental value of 4.42Mbars.

$$F(V) - F(V_0) = \frac{B_0 V}{'B_0}[\frac{(V_0/V)^P}{'B_0} + 1] - \frac{B_0 V_0}{'B_0 - 1} \tag{1.7.1}$$

In this equation, F = free energy (of deformation of an isotropic medium) P = uniform pressure, V_0=equillibrium (initial) volume, B_0= bulk modulus and $'B_0$=pressure derivative of the bulk modulus.

The Murnarghan equation of state was evaluated by the main computational package (FHI98MD) together with a small Fortran program known as the murn package, which performs a least squares fit to the calculated points, then extracts the equilibrium lattice constant a_0, the bulk modulus B_0 and its pressure derivative $'B_0$. The output of the Murnaghan equation of state's fit is then plotted together with the calculated lattice constant values, and the minimum value of the fitted curve as shown in figure 1.6 gives the required relaxed bulk lattice constant of diamond.

The binding energy E_{coh} of bulk diamond which is expressed as (eV/atom)

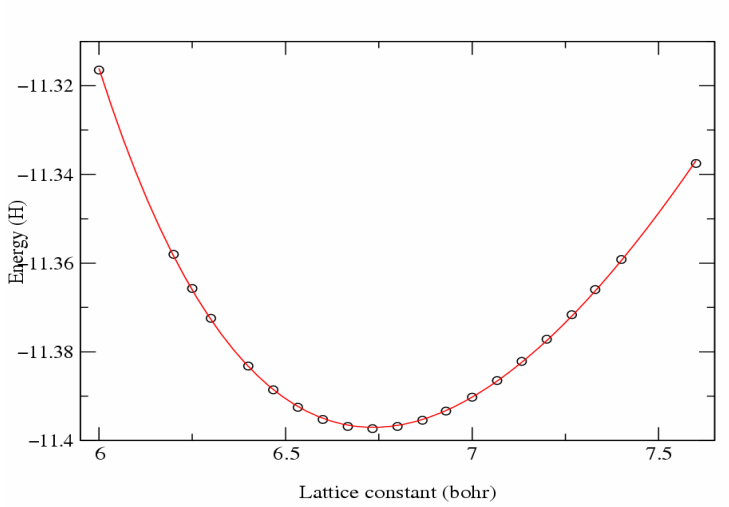


Figure 1.6: Lattice constant of bulk diamond for various minimum total energies.

was obtained by using the relation,

$$E_{coh} = \frac{1}{n}\{E_{diamond-bulk} - n \times (E_{carbon-atom} - \frac{1.24}{27.2116})\}27.2116$$
$$= \frac{1}{2}\{E_{diamond-bulk} - 2 \times (E_{carbon-atom} - \frac{1.24}{27.2116})\}27.2116 \qquad (1.7.2)$$

where $E_{diamond-bulk}$ is the total energy of bulk diamond, $E_{carbon-atom}$ is the total energy of a system containing only the carbon atom, n is the number of carbon atoms per unit surface cell in a given calculation, and the value of 1.24 eV is the correction for the spin polarization energy of the carbon atom within the GGA approach. Using the values shown in Table 1.1, the converged parameters of bulk diamond were plotted as shown in figure 1.7 for various plane wave cutoff energies.

A procedure similar to that followed for determining the bulk properties of diamond-carbon, was also applied to determine the relaxed bulk properties of the oxygen atom and molecule. For the oxygen molecule, the two oxygen atoms were placed within a large box whose dimensions were similar to those used for the calculations involving the carbon atoms. The only difference in this case

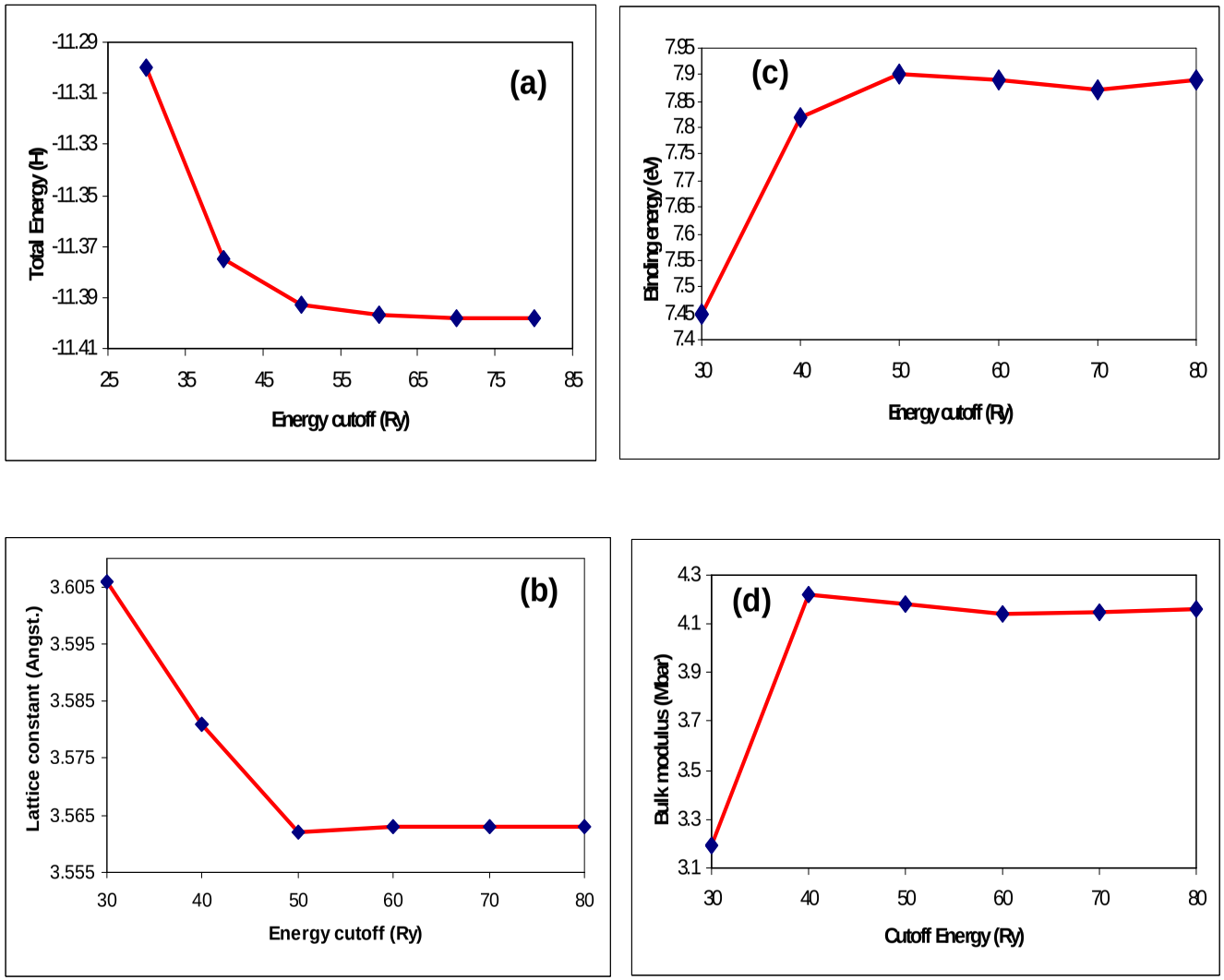


Figure 1.7: Bulk properties of diamond. Panel (a) shows the total energy, panel (b) the lattice constant, panel (c) the binding energy and panel (d) the bulk modulus of diamond, all plotted with various plane wave cutoff energies.

was the fact that the plane wave cutoff energy was varied over a wider range, (between 30 and 130Ry) because the oxygen molecule's vibrational frequency depended quite sensitively on the cutoff energy. In the case of the oxygen atom, the initial atom was placed at the origin of the large box (measuring 20 Bohrs), while the two oxygen atoms forming the oxygen molecule as well as the oxygen and hydrogen atoms constituting the hydroxyl group, were placed at half of the respective bond length values about the origin i.e. at $(-\frac{a_0}{2},0,0)$ and $(\frac{a_0}{2},0,0)$. Table 1.2 shows the calculated DFT-GGA values of the oxygen molecule together with the corresponding experimental ones for comparison purposes. Figure 1.8 shows a plot of the relaxed total energy versus the bond lengths of a free oxygen molecule at a plane wave cutoff energy of 70Ry, which yielded a converged bond length of 2.30 Bohrs for the oxygen molecule. This value was in very good agreement with other DFT studies [65] as well as the experimental value of 2.28 Bohrs [65, 66]. The total minimum energy of the oxygen molecule was found to be -31.8202H which corresponded to the global minimum of figure 1.8.

The third order polynomial equation (eqn 1.7.3) was used to determine the relaxed parameters of the oxygen molecule such as its bond length. This involved fitting the theoretical curve given by equation 1.7.3 to a plot of the calculated total energies, E(H) versus the bond lengths ($a_{lattice}$) using the computer program **Grace** (Graphing Advanced Computing and Exploration of data) [67].

$$y = a_3(x - a_1)^3 + a_2(x - a_1)^2 + a_0 \tag{1.7.3}$$

In this relation (1.7.3), a_0=calculated total energy of the system, a_1=bond length, while the equilibrium vibrational frequency was obtained from the relation

$$\nu(cm^{-1}) = \frac{1}{2\pi}\sqrt{[E''\{m^{-1}\}]} \tag{1.7.4}$$

where E'' is the second order derivative of the energy E, and m is the mass of

an oxygen atom.

Using the plot of E versus bond length ($a_{lattice}$), as shown in figure 1.8, the equilibrium vibrational frequency of the O_2 molecule was obtained after rewriting the expression (eqn. 1.7.4) as,

$$\nu(cm^{-1}) = \frac{1}{2\pi}\sqrt{[(2a_2 \times 3113.8235\{m^{-1}\})]}\frac{1}{c} \tag{1.7.5}$$

where c=speed of light and m = mass of an oxygen atom ($15.9994\times1836.15\times 9.109\times10^{-26}$)=($2.675\times10^{-26}$kg). a_2 was obtained after fitting equation 1.7.3 to the data, and then by solving equation 1.7.5, the vibrational frequencies which are shown in Table 1.2 for various plane wave cutoff energies were obtained.

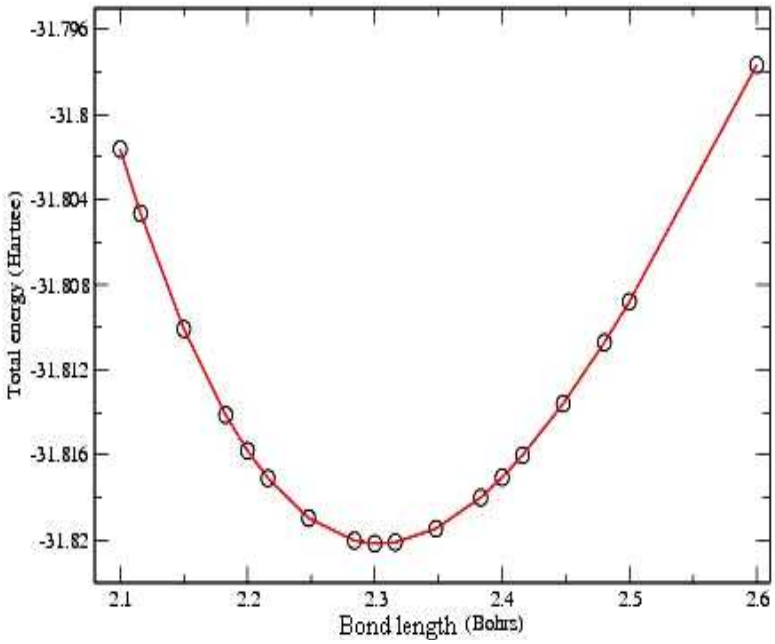


Figure 1.8: Total energy versus bond length of an oxygen molecule at a plane wave cutoff energy of 70Ry.

The various bulk properties of a free oxygen molecule shown in Table 1.2 were plotted as shown in figure 1.9, while figures 1.10 and 1.11 show the total energies of a free oxygen atom and molecule plotted against the plane wave cutoff energies respectively. Figures 1.10 and 1.11 further show that the total

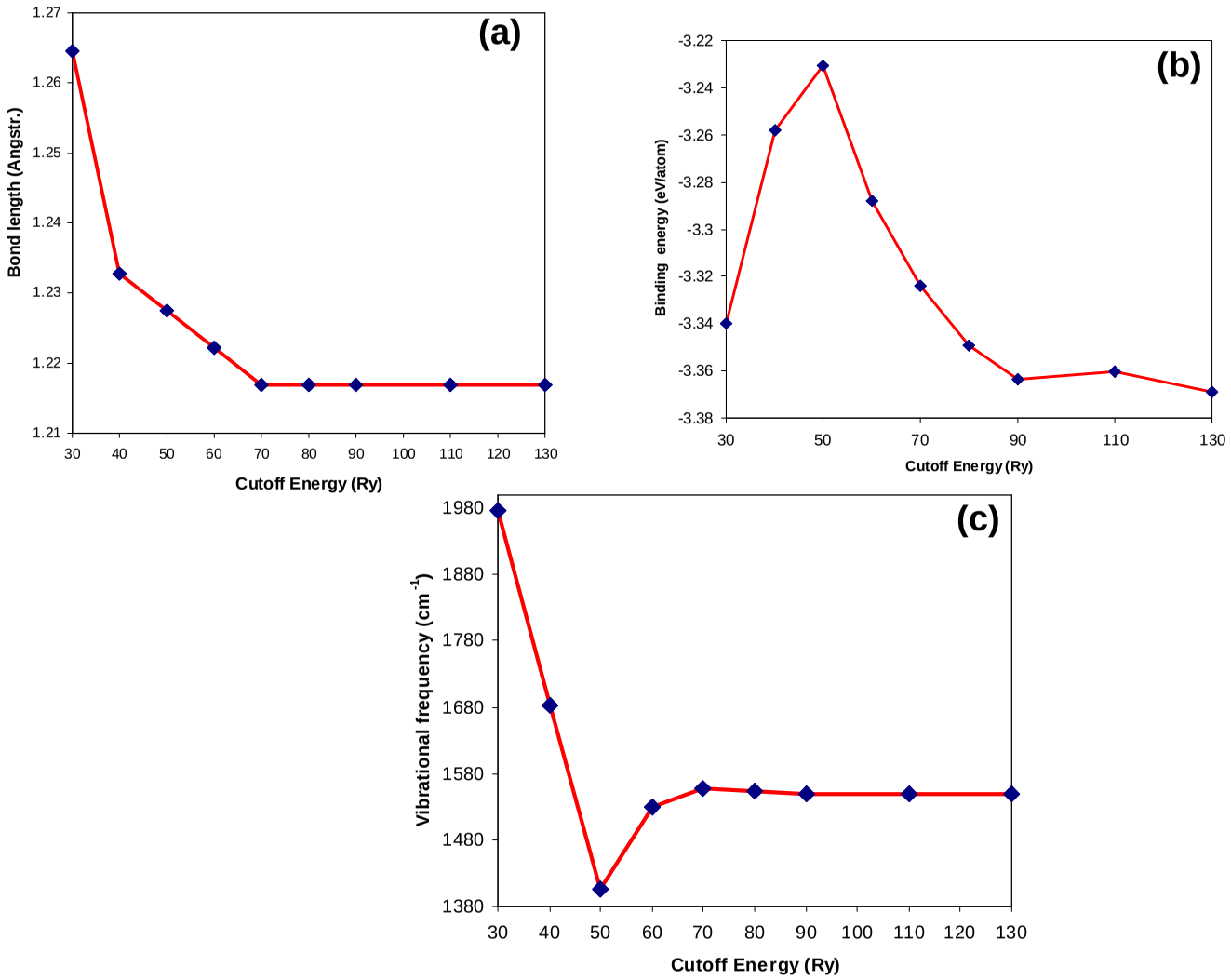


Figure 1.9: Bulk properties of a free oxygen molecule. Panel (a) shows the bond length, panel (b) the binding energy and panel (c) the vibrational frequency, all plotted against various cutoff energies.

Table 1.2: Calculated DFT-GGA and experimental properties of an oxygen molecule. The plane wave cutoff energy E_{cut} is given in Ry, the bond length a_0, in Bohrs, the binding energy E_{coh} in eV/atom, while the vibrational frequency ν, is in cm^{-1}

	E_{cut}	a_o	E_{coh}	ν
Exp.	-	2.28 [65, 66]	2.56 [65]	1586.0 [65]
Theo.	30	2.39	3.31	1977.0
	40	2.29	3.22	1683.5
	50	2.32	3.22	1406.7
	60	2.31	3.28	1530.0
	70	2.30	3.31	1556.9
	80	2.30	3.31	1552.9
	90	2.30	3.32	1549.1
	110	2.30	3.31	1550.1
	130	2.30	3.31	1550.2

energies of both the oxygen atom and molecule were almost well converged at a cutoff energy of 60Ry.

The binding energy (eV/atom) of the oxygen atoms constituting the free oxygen molecule was obtained from the relation,

$$E_{Coh} = \frac{1}{n}\{(E_{Oxy-molecule} - \frac{0.9}{27.2116}) - n(E_{Oxy-atom} - \frac{1.6}{27.2116})\}27.2116$$
$$E_{Coh} = \frac{1}{2}\{(E_{Oxy-molecule} - \frac{0.9}{27.2116}) - 2(E_{Oxy-atom} - \frac{1.6}{27.2116})\}27.2116 \quad (1.7.6)$$

where $E_{Oxy-molecule}$ was the total energy of a free oxygen molecule, $E_{Oxy-atom}$ was the total energy of a free oxygen atom, and both 0.9 and 1.6eV [65] were the spin polarization (energy) corrections for an oxygen molecule and an oxygen atom respectively, within the GGA approach. These corrections arise from the fact that the atoms have spins when they are free, but they loose it once they get bonded to the surfaces.

From the plots of the bulk properties together with the values shown in Tables 1.1 and 1.2, a value of 50Ry was taken to represent an optimum cutoff energy for all the subsequent calculations. This value was chosen on the basis of the fact that it ensured that a not-too-large plane wave basis set was used, while

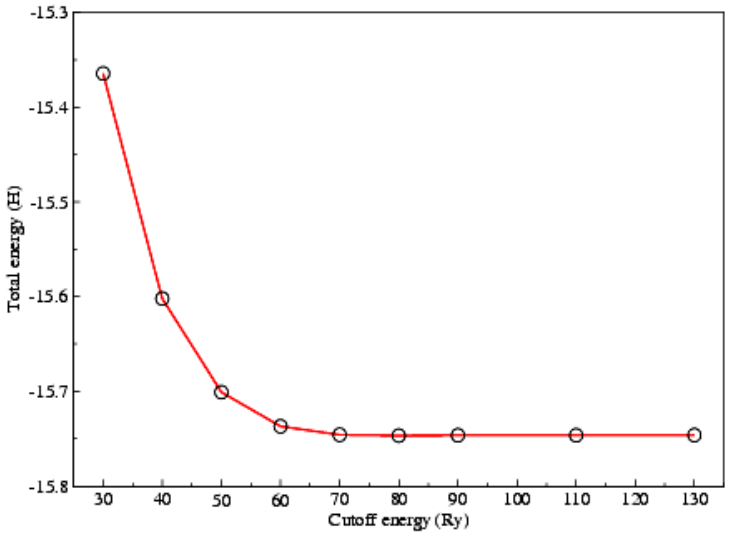


Figure 1.10: Total energy of a free oxygen atom for various plane wave cutoff energies.

at the same time it was not too small to be within the regime where convergence was not yet achieved. As such, when determining the relaxed properties of the free hydroxyl group as shown in figure 1.12, a plane wave cutoff energy of 50Ry was used unlike in the other cases whereby this was varied over a given set of values.

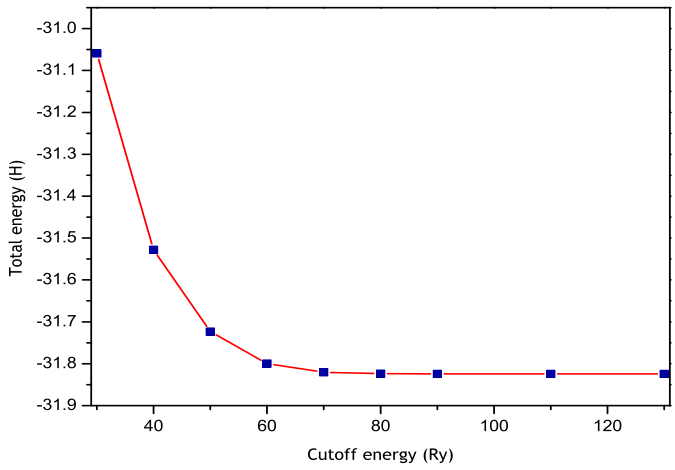


Figure 1.11: Total energy of a free oxygen molecule for various plane wave cutoff energies.

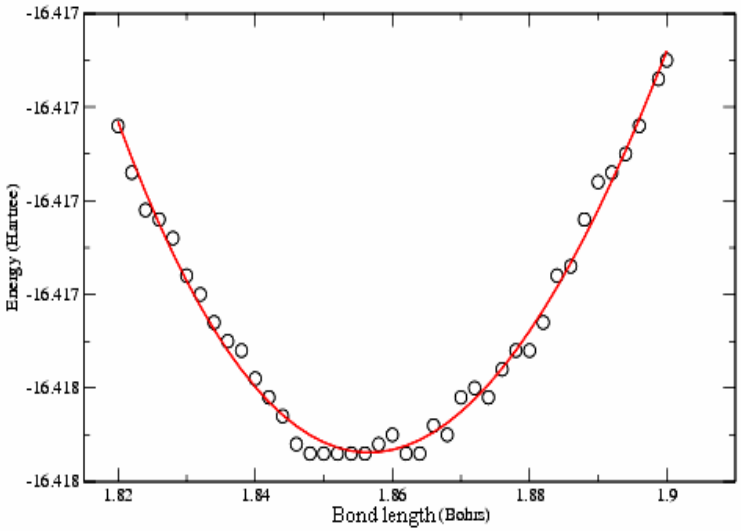


Figure 1.12: Total energy versus bond length of a free hydroxyl group at a plane wave cutoff energy of 50Ry.

The minima of the figure 1.12 gave the total energy of the hydroxyl group as well as its bond length. From these, the adsorption energy E_{ads}(OH) of the hydroxyl group, which was essentially the energy that it gains by adsorbing on to the surface was calculated from the relation,

$$E_{ads}(OH) = 1/n[E_{slab}(OH) - E_{clean-surf.} - n(E_{tot}(OH) - \frac{0.445}{27.2116})] \times 27.2116 \quad (1.7.7)$$

E_{slab}(OH)= total energy of a slab terminated with a hydroxyl group, $E_{clean-surf.}$ = total energy of the corresponding clean (unterminated) surface, E_{tot}(OH)=total minimum energy of the hydroxyl group, n=number of hydroxyl groups per surface unit cell; n=2 for full monolayer coverages and 1 for half monolayer coverage, and 0.445eV=spin polarization correction energy of the free OH group within the GGA approach [68]. This was obtained using the DMol computer program since the total energies obtained from the FHI98MD molecular dynamics computer program were not corrected for the spin polarization energy. The converged bond length of a free hydroxyl group was found to be 0.978Å, which was slightly shorter than, but almost equal to the experimental value of 0.98Å [69] by -0.2%, while the total minimum energy was found to be -16.41753Hartree.

1.8 Surface modelling

The diamond surfaces were initially modeled using carbon-atom slabs made up of five, six and seven bi-layers. This was done with a view to establishing the optimum slab size that was not too large to consume an unnecessarily large amount of computer time(i.e. expensive computationally), yet not too small that it was not representative of both the diamond's bulk and surface properties. Ruter *et al.*[50] observed previously that, although a surface can

be easily modeled by an infinite periodic sandwich of substrate and vacuum regions, care must be taken to ensure that the bulk properties can be estimated from as little bulk and vacuum regions as possible. In our case, the atoms were allowed to relax along the x, y and z directions, with the lower end of the slab being passivated with hydrogen atoms. For each of the different slab sizes, the top 7 layers of carbon atoms were allowed to relax while the rest were kept fixed at their calculated bulk positions.

Table 1.3 shows the adsorption energies of oxygen atoms at the ONTOP site of the three different slab sizes, as well as the corresponding changes in their work function compared to those of the corresponding bare (clean) slab.

Table 1.3: Calculated DFT-GGA adsorption energies of oxygen on diamond (111)-(1×1) surfaces for testing the optimum slab size. Tests were done for the full oxygen monolayer coverage at the ON-TOP sites.

Slab size	$E^{O}_{adsorption}$ (eV/atom)	$\Delta\Phi$(work function) (Clean surface) (eV)	$\Delta\Phi$(work function) (O-Terminated) (eV)
5 bi-layers	-5.0065683	3.6131	6.0756
6 bi-layers	-5.0041192	3.6040	6.07575
7 bi-layers	-5.0005817	3.5902	6.0695

The adsorption energies of the oxygen atoms $E^{O}_{adsorption}$ (eV/atom) were calculated from the relation,

$$E^{O}_{adsorption} = \frac{1}{n}\{[E^{O-term.}_{slab} - E^{bare-surf.}_{slab} - n(E^{O-atom} - \frac{1.6}{27.2116})]\} \times 27.2116$$
$$\frac{1}{2}\{[E^{O-term.}_{slab} - E^{bare-surf.}_{slab} - 2(E^{O-atom} - \frac{1.6}{27.2116})]\} \times 27.2116 \quad (1.8.1)$$

In these relations, $E^{O-term.}_{slab}$ = total energy of an oxygen-terminated surface, $E^{bare-surf.}_{slab}$= total energy of a clean surface and E^{O-atom}= relaxed total energy of an oxygen atom (-15.70077H). n=2 for a full and a third monolayer coverages, and 1 for half and quarter monolayer coverages.

The thickness of the slabs together with the vacuum spacing were thoroughly tested to ensure that they were large enough, to avoid any interaction between

replicas. In this case, a vacuum region of similar size as the z-axis component of the slab was used, totaling to a combined height of ∼44 Bohrs in the case of the 5 bilayer slab. The slab approach was especially preferred over the cluster method because of edge effects associated with the cluster method. It was also believed to produce more accurate results.

Based on the results of Table 1.3 where there was no noticeable differences between the adsorption energies of the oxygen atoms located on different slabs, the 5 bi-layer(or a 10-layer) carbon-atom slab was considered to be the optimum representation of the diamond's bulk region, surface and near surface regions. It was thus used for all the subsequent surface calculations reported in this work. This slab size was neither too small nor too large, and therefore while satisfying all the basic material requirements, it was also less expensive computationally.

The clean diamond surfaces were modeled by passivating the bottom side with hydrogen atoms, while the top side was left clean with only the dangling bonds. These were then to be terminated with either oxygen atoms or hydroxyl groups at different sites and for various coverages. The initial atom positions (i.e. starting geometries) were obtained using the two atom unit cell shown in figure 1.13. Terminating the slabs with hydrogen on one side had the unique advantage that it was considered by the computer program as if the material was of an infinite extension. This was well corroborated by the already established fact that the dangling bonds on diamond surfaces are preferentially terminated by hydrogen [70]. The slab approach had another added advantage in the sense that, both the x and y directions were also considered infinite, thereby ensuring a large-enough size of the diamond material was simulated. The only variable was therefore the number of carbon atom bilayers within the z-axis, as well as the adsorbed oxygen atoms or hydroxyl groups.

The adsorbed oxygen atoms or hydroxyl groups induces dipole moments at the surfaces, which would have a direct bearing on the work functions of the

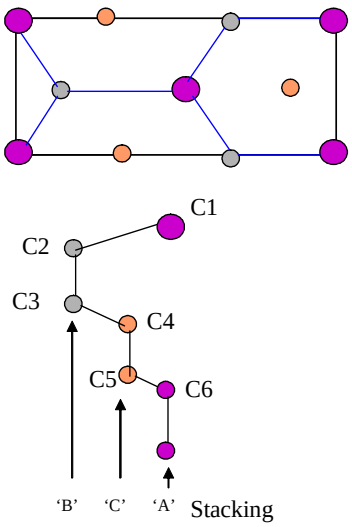


Figure 1.13: Two atom unit cell used in determining the initial diamond-carbon atom positions, together with a representation of the atoms stacking in the z-axis . Note the diamond's A, B, C stacking.

surfaces, compared to that of the clean surfaces.

The oxygen atoms and the hydroxyl groups were placed at various sites and for different coverages on the slabs as shown in figure 1.14. These included adsorbing them at a full, half, third and quarter monolayer (ML) coverages, while the adsorption sites were the ONTOP, Bridge, Hexagonal-close packed (HCP) and the Face-centred cubic (FCC) one as shown in figure 1.15.

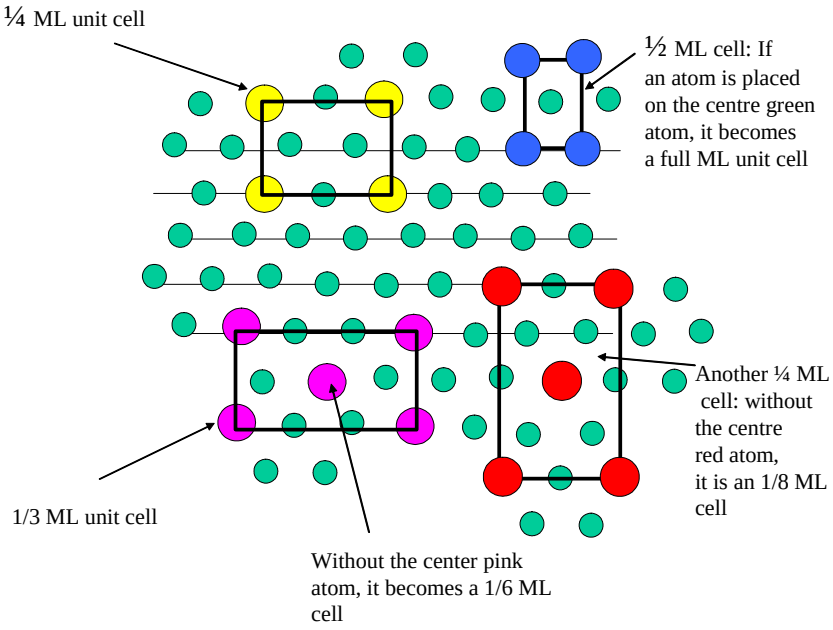


Figure 1.14: Various oxygen monolayer coverages at the ONTOP bonding sites.

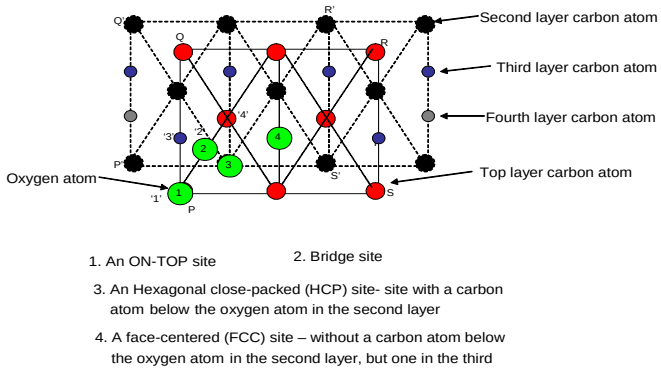


Figure 1.15: Initial geometry showing various oxygen adsorption sites. Note that the triangle formed by the top layer of carbon atoms is facing upwards for the HCP site, and downwards for the FCC site.

The convergence criteria for the system was set in such a way that the calculation terminated when the relative forces on the atoms was greatly reduced and almost equal from all sides, the K.E of the ions was less that 0.1eV, while the difference between the total energy and the Harris energy which is expressed as in equation 1.8.2 was equal to or less than 0.0005Hartree.

$$E_{tot}^{Harris}[n^{(m)}] = \sum_{i=1}^{N} \sum_{j \epsilon BZ} \varepsilon_{i,j} + \Delta E^{e-e}[n^{(m-1)}] + \Delta E_{XC}[n^{(m-1)}] + V_{R_I}^{ion-ion} \tag{1.8.2}$$

where the charge density is,

$$n^{(m)}(\mathbf{r}) = \sum_{j}^{N_j} \sum_{i}^{n_B} f_{i,j} |\varphi_{i,j}^{(m)}(\mathbf{r})|^2 \tag{1.8.3}$$

and

$$f_{i,j} = \frac{1}{exp((\varepsilon_{i,j} - \epsilon_F)/kT) - 1} \tag{1.8.4}$$

1.9 Results

The relaxed geometries of the clean surfaces as well as those terminated with oxygen atoms or hydroxyl groups at various sites and for different coverages are shown in figures 1.16 to 1.26, for the (1×1) bulk terminated diamond (111) surfaces, and figures 1.27 to 1.31 for the relaxed geometries of the (2×1) reconstructed (111) diamond surface. The structures shown here are only for the most stable configurations for each site and monolayer coverage on the (1×1) and (2×1)-C(111) surfaces, while those of the less stable configurations are shown in Appendix A. These structural diagrams were plotted using the XCRYSDEN [(X-Window) Crystalline Structures and Densities] computer program [71]. From these, the converged bond lengths, angles and the percentage (%) changes occurring within them were computed for the bulk region, surface layer and for the adsorbed species. The results obtained are shown in Tables

1.4 to 1.6. On the other hand, Tables 1.11 to 1.12 show the corresponding bond lengths and their % changes for a (2×1) reconstructed C(111) surface. Due to the relatively large bond length changes in the very topmost bilayer of carbon atoms, these were considered separately from those within the bulk and near surface regions. Results obtained from these are shown in Tables 1.7 to 1.10, for the bulk terminated (1×1) C(111) surface, and Table 1.13 for the (2×1) reconstructed C(111) surface. The % changes were computed relative to the bulk C-C bond length of 1.54Å.

The presence of the adsorbates was found to have a significant effect on the distribution of the electron clouds of the carbon atoms located within their neighbourhoods and less or no effect at all for those located within the bulk. This also tended to affect the bonding environment. These effects were investigated quite extensively, with a view to establishing how the electronic properties of the surfaces terminated with either oxygen atoms or hydroxyl groups at different sites and for various coverages compared with those of the clean surfaces. Of particular importance was the investigation of how the density of states (Dos) changed in the presence or absence of the adsorbates, for a carbon atom located within the bulk or at the surface, or even those of the adsorbed oxygen atoms themselves. Results obtained for the density of states are shown in figures 1.36 to 1.43 for the (1×1) bulk terminated surfaces and figures 1.44 to 1.47 for the (2×1) reconstructed C(111) surface. Just like in the case of the (atomic) structural diagrams, these are for the most stable configurations on the (1×1) C(111) surfaces, and those of the (2×1) reconstructed surfaces. States for other less stable configurations for the 1×1 surfaces are shown in Appendix A.

To establish the preferred bonding sites and the most stable coverages, the total minimum energies of the various systems were computed, and from these the adsorption energies. Surface dipoles due to the adsorbates were also expected to have a significant effect on the specific surfaces's work function, in a

way that would either make it easier or harder to draw electrons from them, and for this reason, changes occurring in the respective surfaces work functions were also investigated. In addition, although only coverages between the full and quarter monolayers were considered, the behaviour of those that were lower than these was to be inferred from the trends observed in the higher coverages. Results obtained for the total minimum energies, adsorption energies and the work function values for the various relaxed geometries are shown in Tables 1.15, 1.16 and 1.17 for the (1×1) bulk terminated surfaces, and in Table 1.19 for the (2×1) reconstructed surfaces. For the latter case, i.e. the (2×1) reconstructed (111) diamond surfaces, only the ONTOP and bridge sites were considered, with Oxygen atoms or hydroxyl groups occupying either a full or half ML coverages.

1.9.1 Structural diagrams of the relaxed geometries of the (1×1) bulk terminated (111) diamond surfaces.

The relaxed geometries of clean bulk terminated (111) diamond surfaces and those terminated with oxygen atoms or hydroxyl groups at different sites are shown in figures 1.16 to 1.26. These are for the most stable C(111)-1×1:O and 1×1:OH terminations for each of the coverage, while structures for other less stable configurations are presented in Appendix A. In each of the diagrams, the left hand side (LHS) panel shows the top view while the right hand side (RHS) one shows the corresponding side view.

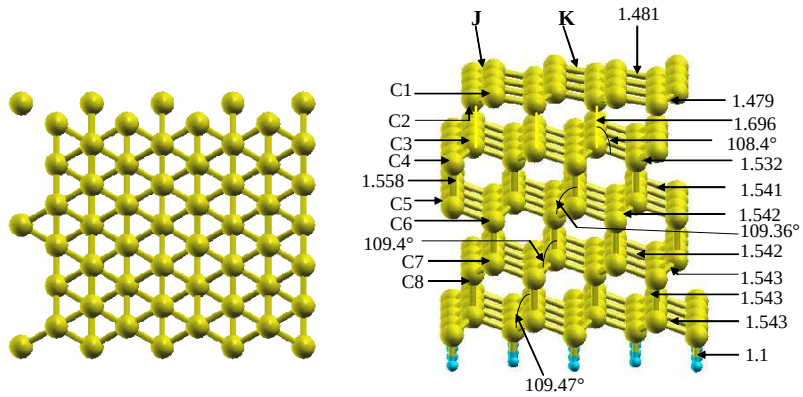


Figure 1.16: Clean super cell used for the calculations involving the full and half monolayer coverages of oxygen atoms and hydroxyl groups. The letters C_1, C_2, C_3 etc. refer to the respective carbon atom layers. **J** and **K** are different types of surface bonds.

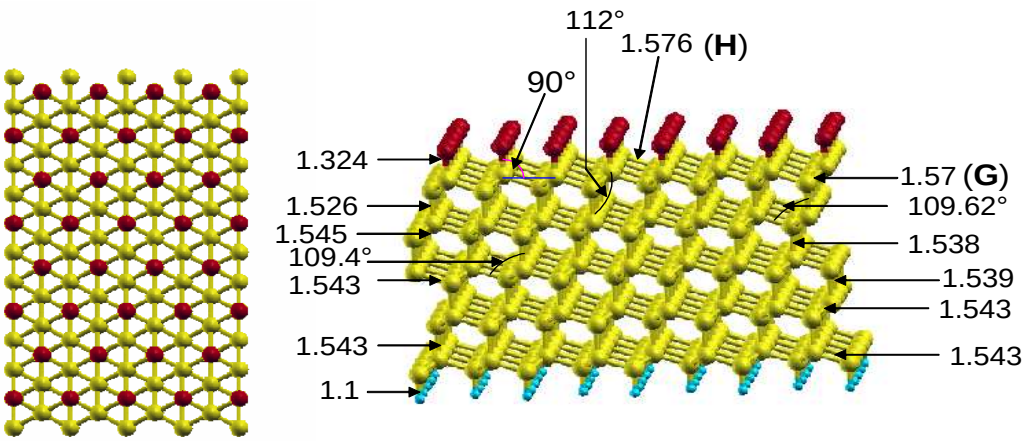


Figure 1.17: A full ML of oxygen atoms adsorbed at an ONTOP site. The letters **G** and **H** refer to different types of surface bonds. The small blue spheres represent the H atoms passivating the lower end of the slab, the gold coloured ones the carbon atoms, and the red spheres the adsorbed oxygen atoms.

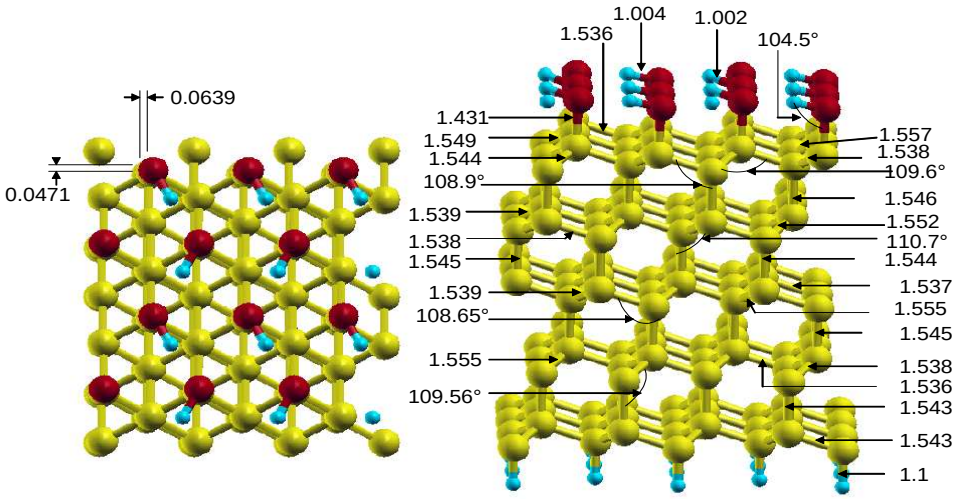


Figure 1.18: A full ML coverage of OH groups co-adsorbed initially at a hexagonal close packed (HCP) and a bridge site. Note the staggering of the OH groups after relaxation.

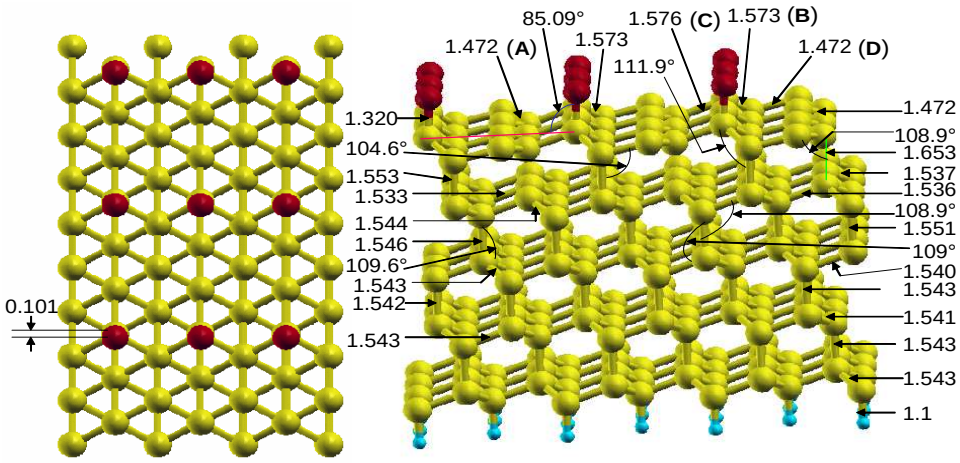


Figure 1.19: A half ML coverage of oxygen atoms adsorbed at an ONTOP site. Carbon atoms bonded to the oxygens are raised by 0.2464Å above those that are not.

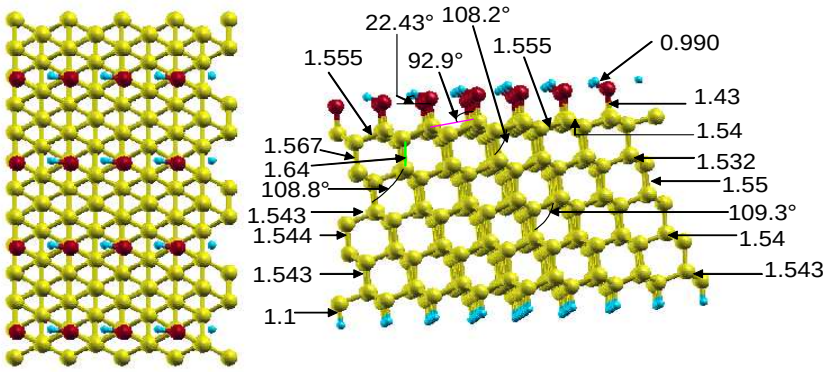


Figure 1.20: A half ML coverage of OH groups that were initially adsorbed at a hexagonal close packed site. (see figure 1.15)

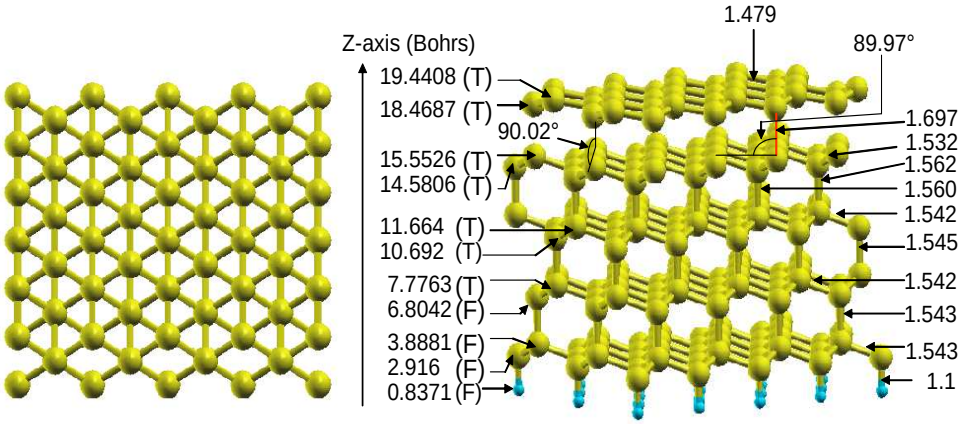


Figure 1.21: Unterminated super cell used for calculations involving the quarter monolayer coverages with oxygen atoms and hydroxyl groups. Numbers on the left hand side (LHS) of the side view show the z-axis values of the respective carbon and hydrogen atoms. T stands for true, meaning that the carbon atom should be relaxed, while F represents false, implying that the carbon atom should not be relaxed.

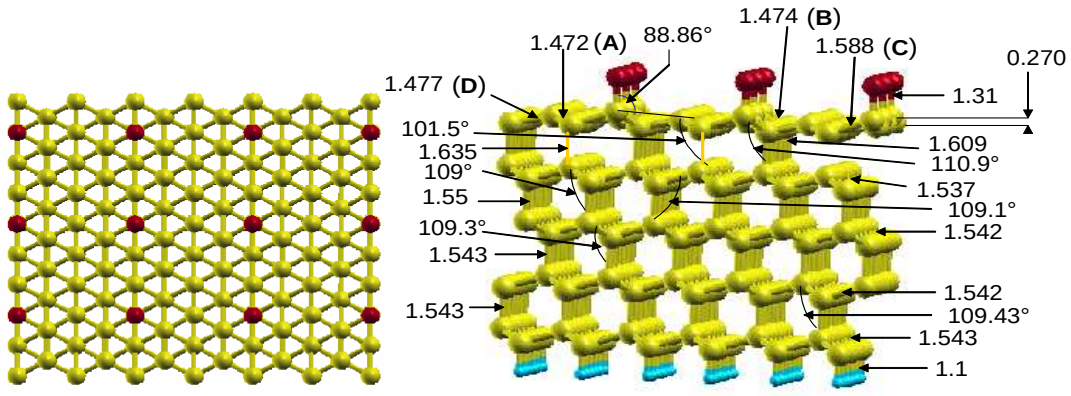


Figure 1.22: A quarter ML coverage of oxygen atoms adsorbed at an ONTOP site. The letters **A**, **B**, **C** and **D** represent different types of surface bonds.

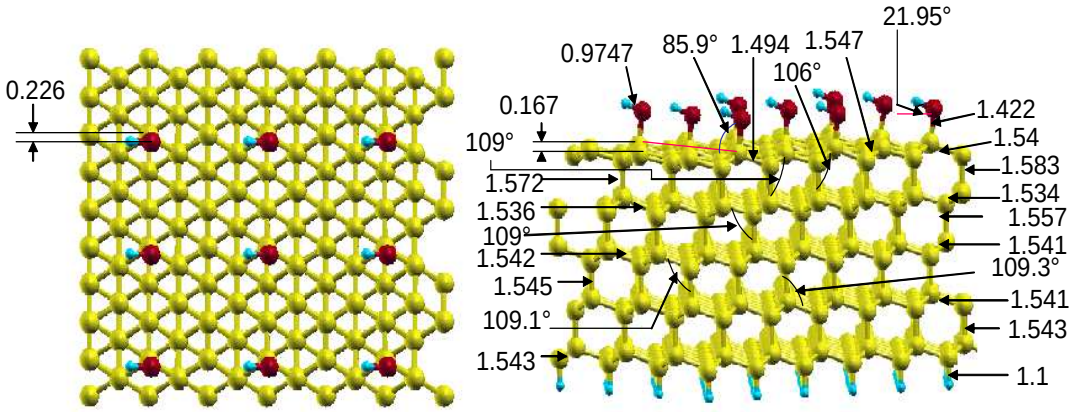


Figure 1.23: A quarter ML coverage of OH groups that were adsorbed initially at a Hexagonal close packed site.

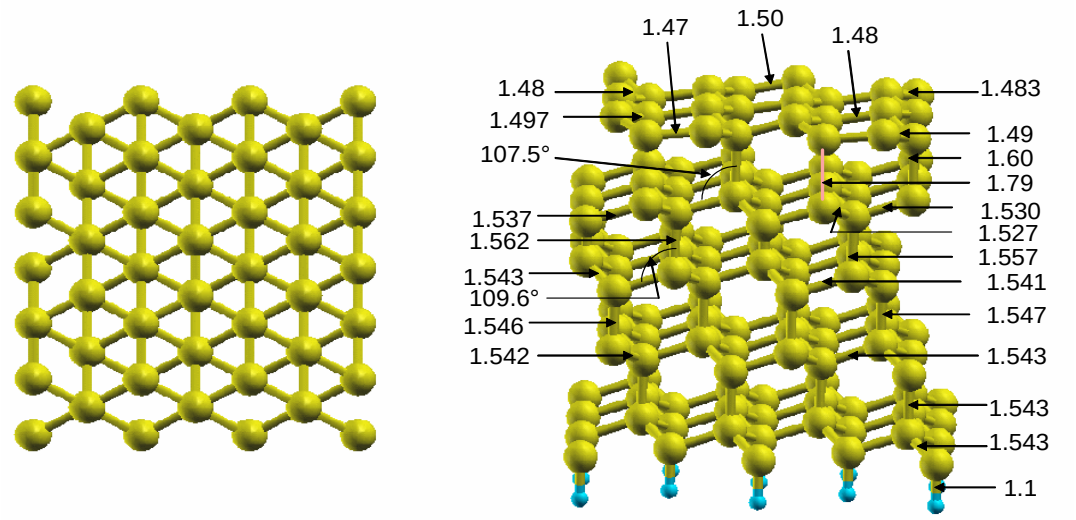


Figure 1.24: A clean slab used for calculations involving the third monolayer coverages.

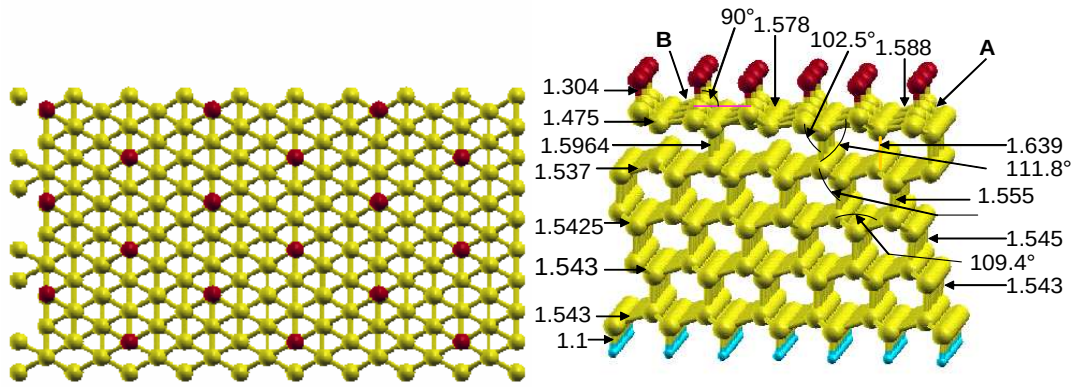


Figure 1.25: A third ML coverage of oxygen atoms adsorbed at an ONTOP site. Letters **A** and **B** represent different types of surface bonds.

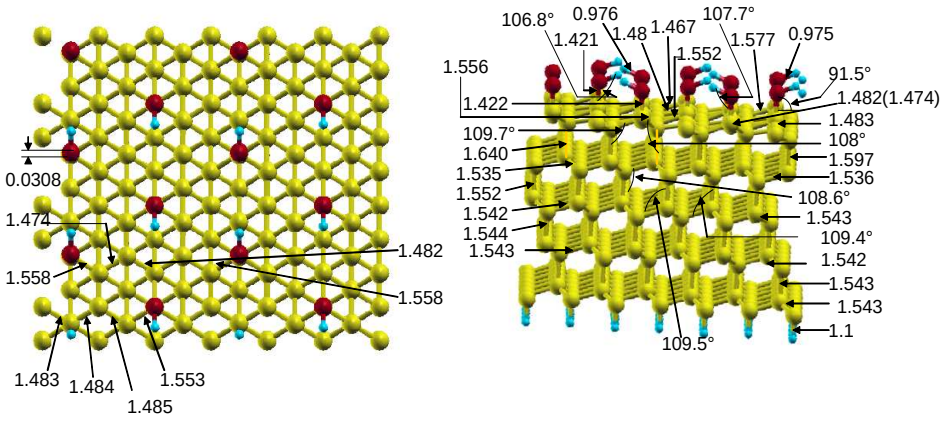


Figure 1.26: A third ML coverage of hydroxyl groups adsorbed at an ONTOP site. Note the alternate orientation of the OH groups in the top view after system relaxation.

1.9.2 Relaxed geometries for the (2×1) reconstructed (111) diamond surfaces

Following the optimization processes, the adsorbed oxygen atoms and hydroxyl groups as well as the carbon atoms located within the bulk and those at the surface regions of the (2×1) reconstructed (111) diamond surfaces were found to move to new positions that ensured maximum coordination for each, as shown in figures 1.27 to 1.31. As mentioned before, other less stable structures are shown in Appendix A. The left-hand side panel in each diagram shows the top view, while the right-hand side one is the corresponding side view.

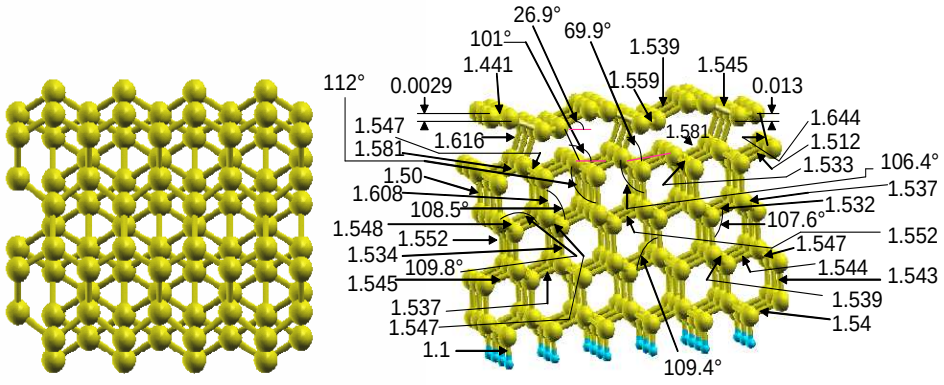


Figure 1.27: A clean (2 × 1) reconstructed C(111) surface. Note the small buckling of the upper and lower π-bonded chains.

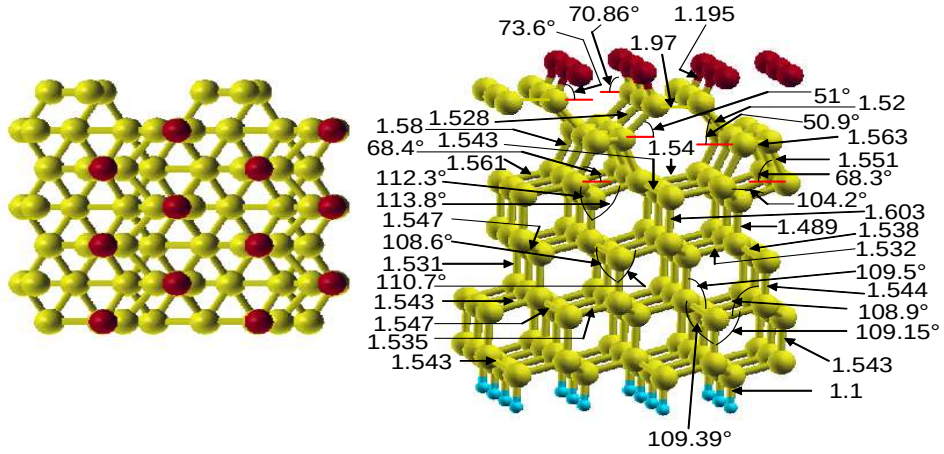


Figure 1.28: A full ML coverage of oxygen atoms adsorbed initially at an ON-TOP site, of a (2×1) reconstructed C(111) surface. The upper π-bonded chains are buckled by 0.0083Å, and the lower ones by 0.0129Å.

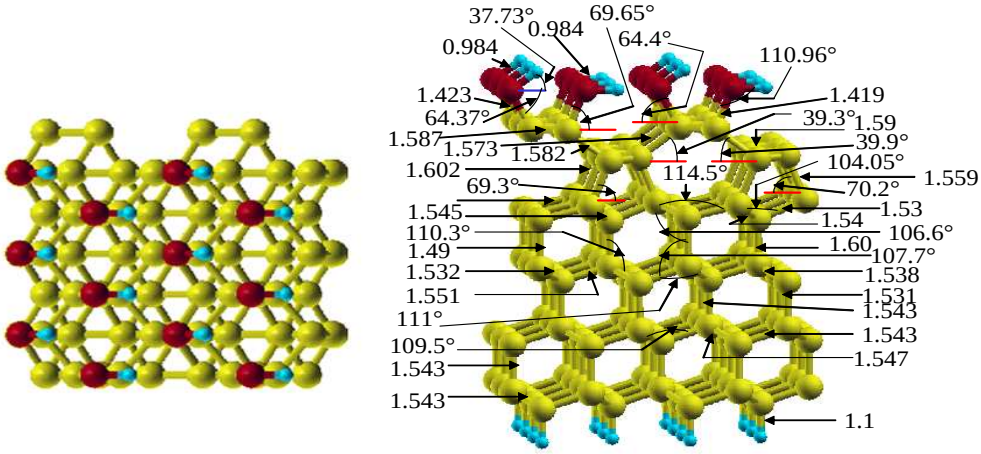


Figure 1.29: A full ML coverage of hydroxyl groups at an ONTOP site, of a (2×1) reconstructed C(111) surface. The upper π-bonded chains are buckled by 0.0186Å, and the lower ones by 0.001Å.

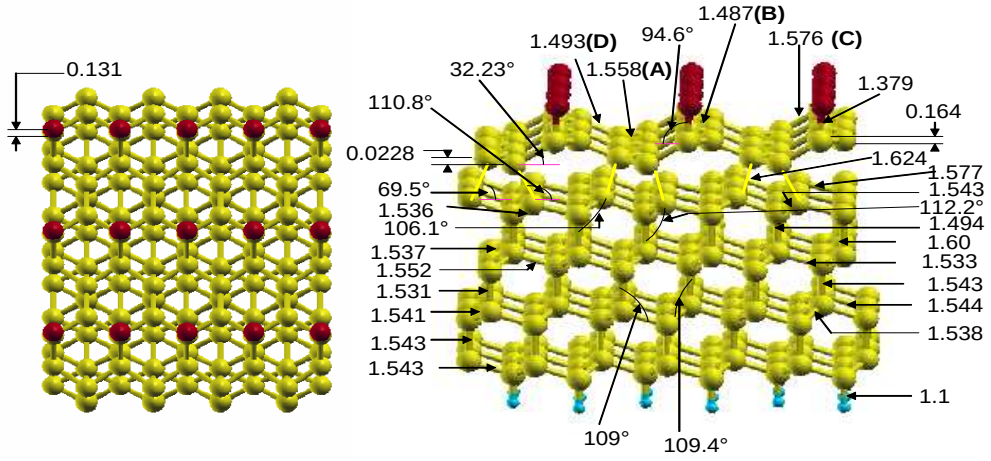


Figure 1.30: A half ML coverage of oxygen atoms adsorbed at an ONTOP site, of a (2×1) reconstructed C(111) surface. Letters **A**, **B**, **C** and **D** represent different types of surface bonds.

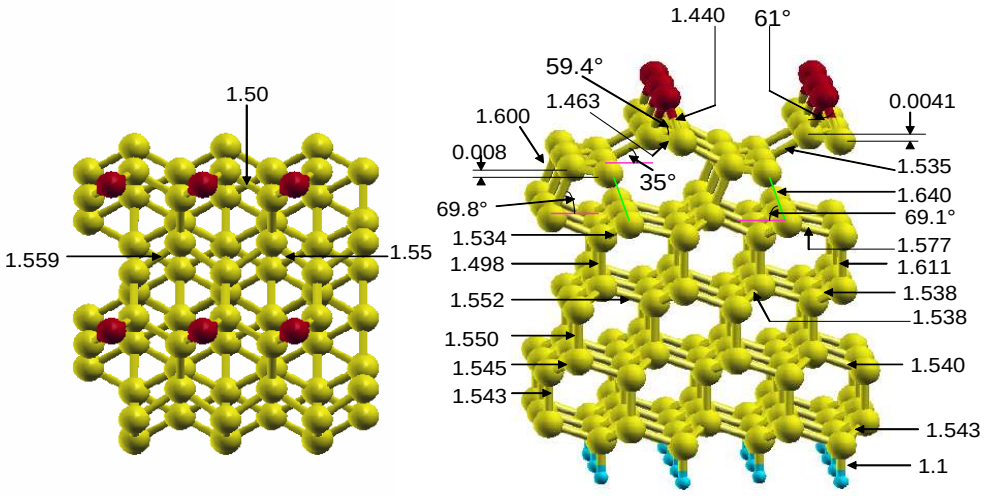


Figure 1.31: A half ML coverage of oxygen atoms adsorbed at a bridge site, of a (2×1) reconstructed C(111) surface.

1.10 Structural and bond-length changes within the bulk and near surface regions of (1×1) bulk terminated (111) diamond surfaces, together with those of the C-O, C-OH and O-H bonds.

Tables 1.4, 1.5 and 1.6 show the bond lengths and their % changes for those carbon atoms located within the bulk and near surface regions of (1×1) bulk terminated (111) diamond surfaces, while Tables 1.7 up to 1.10 show bond lengths and their % changes for the topmost bilayer of carbon atoms. The tables contain data for all the configurations considered in this study, in order to get a clear and complete picture of how these bond lengths and their % changes were related to the stabilities of the given sites or coverages. However, the most stable structures for both O & OH coverages and those of the clean slabs are bolded in the tables for easier identification from the others. As mentioned before, bond lengths in the surface layer were considered separately from those within the bulk or near surface regions, since a significant amount of bond changes were observed. The changes observed within the bond lengths are given relative to the respective experimental values, which are 1.36Å for the C-O bond obtained from paraffinic compounds [66], 1.43Å [66] for the C-OH bond, and 0.98Å [69] for O-H bond. Although the C-O bond length of 1.36Å is considered as a single bond, Lide *et al.* [66] refers to it as a partial C=O bond. From their x-ray measurements, Huisman *et al.* [72] reported a value of 1.43Å which was most likely a C-OH bond, although they appear to refer to it as a single C-O bond. Additionally, an experimental value of 0.95Å is listed by Hiroyuki *et al.* [73] for the O-H bond, which they obtained from a (100) surface, while their calculations yielded a value of 0.96Å. The C-H bond length was taken as 1.1Å which was quite close to the experimental value of 1.09Å [69].

Slab termination (Monolayers)	$d_{C_8-C_7}$ (%)	$d_{C_7-C_6}$ (%)	$d_{C_6-C_5}$ (%)	$d_{C_5-C_4}$ (%)	$d_{C_4-C_3}$ (%)	$d_{C_3-C_2}$ (%)	d_{C-O} & d_{C-OH}(%)	d_{O-H} (
Full and half clean DFT-[75]	1.543(0.195)	1.542(0.13)	1.541(0.065)	1.558(1.17)	1.532(-0.52) (2.1)	1.696(10.1)		
Full ONTOP-O DFT [53])	1.543(0.195)	1.539(-0.065)	1.543(0.195)	1.538(-0.13)	1.545(0.32) 1.538(-0.13)	1.526(-0.91) 1.518(-1.4)	1.324(-2.6) 1.326(-2.5)	
Full ONTOP-OH DFT [53] X-ray [60] X-ray [72](0.15ML)	1.542(0.13)	1.539(-0.065)	1.542(0.13)	1.539(-0.03)	1.542(0.13) 1.539(-0.065) 1.50(-2.6) 1.55(0.65)	1.54(0.0) 1.539(-0.065) 1.50(-2.6) 1.50(-2.6)	1.427(-0.21) 1.448(1.26) 1.43(0.0) 1.43(0.0)	0.985(0 0.995(1
Full ONTOP & HCP-O Co-adsorp.	1.543(0.195) 1.542(0.13)	1.542(0.13) 1.544(0.26)	1.54(0.0) 1.544(0.26)	1.544(0.26)	1.54(0.0) 1.543(0.195)	1.537(-0.195) 1.598(3.77)	1.417(-0.91)	1.412(C
Full HCP & Bridge -OH Co-adsorp.	1.538(-0.13) 1.555(0.97)	1.545(0.32)	1.55(0.97) 1.539(-0.065)	1.544(0.26) 1.545(0.32)	1.538(-0.13) 1.552(0.78)	1.546(0.39)	1.431(0.07)	1.004(2 1.002(2
Half ONTOP-O	1.543(0.195) 1.541(0.065)	1.543(0.195) 1.542(0.13)	1.54(0.0) 1.543(0.195)	1.551(0.71) 1.546(0.39)	1.544(0.26) 1.537(-0.19)	1.553(0.84) 1.653(7.3)	1.320(-2.9) -	- -
Half ONTOP-OH	1.542(0.13)	1.545(0.32)	1.542(0.13)	1.553(0.84)	1.54(0.0)	1.565(1.62) 1.644(6.75)	1.41(-1.4)	0.969(-
Half Bridge-O	1.543(0.195) 1.544(0.26)	1.537(-0.195)	1.548(0.52) 1.544(0.26)	1.536(-0.26) 1.559(1.23)	1.537(-0.195) 1.525(-0.97)	1.477(-4.09) 1.72(11.7)	-	-
Half Bridge-OH	1.534(-0.39) 1.544(0.26)	1.545(0.32)	1.534(-0.39)	1.552(0.78)	1.542(0.13) 1.535(-0.32)	1.56(1.3) 1.65(7.1)	1.428(-0.14)	0.991(1
Half HCP-O	1.541(0.065) 1.544(0.26)	1.542(0.13) 1.544(0.26)	1.543(0.195) 1.542(0.13)	1.553(0.84)	1.533(-0.45) 1.541(0.065)	1.547(0.45) 1.676(8.83)	1.330(-2.2)	-
Half HCP-OH	1.54(0.0)	1.544(0.26)	1.543(0.195)	1.555(0.97)	1.532(-0.519)	1.64(6.49) 1.567(1.75)	1.43(0.0)	0.990(1
Half FCC-O	1.544(0.26) 1.542(0.13)	1.544(0.26)	1.543(0.195)	1.55(0.65)	1.538(-0.13) 1.543(0.195)	1.568(1.8) 1.64(6.49)		
Half FCC-OH	1.542(0.13)	1.545(0.32)	1.544(0.26)	1.55(0.65)	1.543(0.195)	1.582(2.73) 1.66(7.8)		0.981(0

Table 1.4: Calculated C-C bond lengths (d_{C-C} as in figure 1.16 expressed in Å for the C(111)-(1×1) surface), and their % changes for the bulk and near surface carbon atoms for full and half ML coverages of O & OH. Except for the O-O bond, numbers in parentheses are the relative percentage changes to the experimental values of 1.54Å [74] for the C-C bond, 1.36Å for a single C-O bond and 1.43Å for the C-OH bond, as well as 0.98Å for the O-H bond.

Slab termination (Monolayers)	$d_{C_8-C_7}$ (%)	$d_{C_7-C_6}$ (%)	$d_{C_6-C_5}$ (%)	$d_{C_5-C_4}$ (%)	$d_{C_4-C_3}$ (%)	$d_{C_3-C_2}$ (%)	d_{C-O} & d_{C-OH}(%)	d_{O-H} (%)
Quarter monolayer (clean-super cell)	1.542(0.13)	1.545(0.32)	1.542(0.13)	1.562(1.43) 1.56(1.3)	1.532(-0.52)	1.697(10.2)		
Quarter ONTOP-O	1.542(0.13)	1.543(0.195)	1.542(0.13)	1.55(0.65)	1.537(-0.195)	1.609(4.5) 1.635(6.2)	1.31(-3.7)	
Quarter ONTOP-OH	1.542(0.13) 1.543(0.195)	1.544(0.26)	1.543(0.195) 1.542(0.13)	1.549(0.58)	1.537(-0.195) 1.54(0.0)	1.606(4.3) 1.74(12.9)	1.423(-0.49)	0.975(-0.51
Quarter Bridge-O	1.541(0.065) 1.543(0.195)	1.542(0.13)	1.544(0.26) 1.536(-0.26)	1.548(0.52)	1.538(-0.13) 1.559(1.23)	1.481(-3.83) 1.83(18.8)		
Quarter Bridge-OH	1.545(0.32) 1.54(0.0)	1.546(0.39)	1.542(0.13) 1.534(-0.39)	1.549(0.58) 1.557(1.1)	1.544(0.26) 1.535(-0.32)	1.592(3.38) 1.585(2.9) 1.659(7.3)	1.418(-0.84)	0.986(0.61)
Quarter HCP-O	1.542(0.13)	1.547(0.45)	1.542(0.13)	1.56(1.3)	1.537(-0.195)	1.554(0.91) 1.618(5.06)	1.34(-1.47)	
Quarter HCP-OH	1.541(0.065)	1.545(0.32)	1.542(0.13) 1.541(0.065)	1.557(1.1)	1.536(-0.26) 1.534(-0.39)	1.583(2.8) 1.572(2.08)	1.422(-0.56)	0.9747(-0.5
Quarter FCC-O	1.54(0.0) 1.543(0.195)	1.546(0.39)	1.54(0.0)	1.542(0.13) 1.575(2.3)	1.537(-0.195) 1.53(-0.65)	1.474(-4.3) 1.82(18)		
Quarter FCC-OH	1.542(0.13) 1.546(0.39)	1.544(0.26)	1.542(0.13)	1.545(0.32) 1.56(1.3)	1.54(0.0) 1.535(-0.32)	1.515(-1.62) 1.63(5.8)		1.007(2.76)

Table 1.5: Calculated C-C atom bond lengths (d_{C-C} in Å for the C(111)-(1×1) surface), and their % changes for bulk and near surface carbon atoms from the quarter monolayer coverages of O & OH. The numbers in parentheses are the relative % changes to the experimental values similar to those used in Table 1.4. The resulting C-O, C-OH and O-H bond lengths are also shown.

Slab termination (Monolayers)	$d_{C_8-C_7}$ (%)	$d_{C_7-C_6}$ (%)	$d_{C_6-C_5}$ (%)	$d_{C_5-C_4}$ (%)	$d_{C_4-C_3}$ (%)	$d_{C_3-C_2}$ (%)	d_{C-O} & d_{C-OH}(%)	d_{O-H} (%)
Third monolayer-(clean-super cell)	1.542(0.13) 1.543(0.195)	1.546(0.39) 1.547(0.45)	1.541(0.065) 1.543(0.195)	1.557(1.1) 1.562(1.4)	1.53(-0.65) 1.537(-0.195)	1.60(3.9) 1.79(16.2)		
Third ONTOP-O	1.543(0.195)	1.545(0.32)	1.542(0.13)	1.555(0.97)	1.537(-0.195)	1.60(3.9) 1.639(6.4)	1.304(-4.1)	
Third ONTOP-OH	1.543(0.195) 1.542(0.13)	1.544(0.26)	1.543(0.195) 1.542(0.13)	1.552(0.78)	1.535(-0.32) 1.536(-0.26)	1.597(3.7) 1.64(6.5)	1.422(-0.56)	0.976(-0.4 0.975(-0.5
Third Bridge-O	1.543(0.195)	1.545(0.32)	1.537(-0.195) 1.546(0.39)	1.548(0.52)	1.536(-0.26) 1.541(0.065)	1.478(-4.0) 1.673(8.6)		
Third Bridge-OH	1.54(0.0)	1.543(0.195)	1.542(0.13)	1.55(0.65)	1.54(0.0) 1.533(-0.45)	1.59(3.2) 1.595(3.57)	1.422(-0.56)	0.975(-0.5
Third HCP-O	1.538(-0.13) 1.541(0.065)	1.545(0.32)	1.543(0.195) 1.549(0.58)	1.556(1.04)	1.543(0.195) 1.547(0.45)	1.532(-0.52) 1.643(6.69)	1.38(1.47)	
Third HCP-OH	1.55(0.65) 1.539(-0.065)	1.547(0.45)	1.54(0.0) 1.55(0.65)	1.554(0.91)	1.542(0.13) 1.537(-0.195)	1.595(3.57)	1.424(-0.42)	0.973(-0.7
Third FCC-O	1.542(0.13) 1.54(0.0)	1.543(0.195)	1.547(0.45) 1.532(-0.52) 1.542(0.13)	1.555(0.97)	1.534(-0.39) 1.555(0.97) 1.525(-0.97)	1.479(-3.96) 1.678(8.96)	1.57	
Third FCC-OH	1.545(0.32) 1.54(0.0)	1.542(0.13)	1.542(0.13) 1.55(0.65) 1.539(-0.065)	1.551(0.71)	1.542(0.13) 1.538(-0.13)	1.696(10.1) 1.594(3.5)	1.422(-0.56)	0.975(-0.5

Table 1.6: Calculated C-C bond lengths (d_{C-C}, in Å for the C(111)-(1×1) surface), and their % changes for bulk and near surface carbon atoms obtained from the third monolayer coverages of O & OH. These are shown together with bond lengths for the C-OH, C-O, and O-H terminations. The numbers in parentheses are the relative % changes to the experimental values similar to those shown in Table 1.4.

Surface bonds for clean slabs (super cells)	Bonds as shown in	Bonds within the zigzag C atom chains of a clean slab. (marked as**(J)** in fig. 1.16)	Bonds joining the adjacent zigzag C atom chains of a clean slab. (marked as**(K)** in fig. 1.16)
For full & half ML coverages	Figure 1.16	1.48(-3.89)	1.481(-3.83)
For quarter ML coverages	Figure 1.21	1.48(-3.89)	1.479(-3.96)
For third ML coverages		1.48(-3.89) 1.483(-3.7) 1.497(-2.8)	1.47(-4.5) 1.48(-3.89) 1.50(-2.6)
DFT-[43] DFT-[75] DFT-[76] DFT-[77]		(-4.2) (-4.1) (-5.1)	 (-3.1)
Oxygen & hydroxyl coverages & Adsorption Site (Monolayers-ML)	Bonds as shown in	Bonds within the C atom zigzag chains bonded to O or OH (marked as**(G)** in fig. 1.17)	Bonds joining any two adjacent C atom zigzag chains. (marked as**(H)** in fig. 1.17)
Full ONTOP-O	Figure 1.17	1.57(1.9%)	1.576(2.34%)
Full ONTOP-OH X-ray [60]	Figure A.1	1.546(0.39%)	1.538(-0.13%) 1.54(0.0%)
Full ONTOP-O & HCP-O	Figure A.2	1.545(0.32%) 1.527(-0.84%)	1.533(-0.45%)
Full BRIDGE-OH & HCP-OH	Figure 1.18	1.544(0.26%) 1.549(0.58%) 1.539(-0.065%) 1.557(1.1%)	1.536(-0.26%)

Table 1.7: Bond lengths and their changes % within the topmost bilayer of carbon atoms from the clean slabs of the (1×1) bulk terminated C(111) surfaces. These are shown together with those obtained from surfaces terminated by a full ML of O atoms or OH groups. The bond lengths are given in Å while the numbers in parentheses are the corresponding percentage changes relative to the bulk C-C bond length of 1.54Å.

Oxygen & hydroxyl coverages & Adsorption Site (Monolayers-ML)	Bonds as shown in	Bonds within zigzag C-atom chains unbonded to O. (Marked as ***A*** in e.g figure 1.19)	Bonds within O-termin. zigzag C -atom chains. (Marked as ***B*** in e.g figure 1.19)	Bonds joining O-bonded C atoms to adjacent zigzag C-atom chains unbonded to O. (Marked as ***C*** in e.g fig. 1.19)	Bonds joining zigzag C-atom chains not bonded to O atoms. (Marked as ***D*** in e.g figure 1.19)
Half ONTOP-O	Figure 1.19	1.472(-4.41)	1.573(2.14)	1.576(2.34)	1.472(-4.41)
Half ONTOP-OH	Figure 1.19	1.493(-3.05)	1.548(0.519)	1.551(0.714)	1.551(0.71) 1.548(0.52)
Half Bridge-O		1.62(5.19) 1.499(-2.66)	1.561(1.36) 1.495(-2.92)	1.63(5.84)	1.506(-2.21)
Half Bridge-OH		1.47(-4.54) 1.474(-4.28)	1.549(0.58)	1.559(1.23)	1.496(-2.86)
Half HCP-O	Figure 1.22	1.471(-4.48) 1.472(-4.41)	1.567(1.75) 1.571(2.01)	1.579(2.53)	1.48(-3.9)
Half HCP-OH		1.475(-4.22) 1.474(-4.28)	1.548(0.519) 1.54(0.0)	1.555(0.974)	1.494(-2.99)
Half FCC-O		1.481(-3.83)	1.61(4.54) 1.529(-0.71)	1.53(0.65)	1.437(-6.68)
Half FCC-OH		1.481(-3.83)	1.542(-0.13)	1.487(-3.44)	1.524(-1.04)

Table 1.8: Bond lengths in the topmost bilayer of C(111)-(1×1) surfaces terminated with half a monolayer of O atoms and OH groups at different sites. The bond lengths are shown in Å while the figures in parentheses are the corresponding percentage changes relative to the C-C bulk bond length of 1.54Å.

Oxygen & hydroxyl coverages & Adsorption Site (Monolayers-ML)	Bonds as shown in	Bonds within zigzag carbon atom chains unbonded to O or OH. (Marked as ***A*** in e.g Fig. 1.22)	Bonds within the O or OH term. zigzag C-atom chains (Marked as ***B*** in e.g Fig. 1.22)	Bonds joining adjacent zigzag C-atom chains bonded to O or OH groups (Marked as ***C*** in e.g Fig. 1.22)	Bonds joining zigzag C-atom chains not bonded to O or OH groups. (Marked as ***D*** in e.g Fig. 1.22)
Quarter ONTOP-O	Figure 1.22	1.472(-4.41) 1.478(-4.02)	1.474(-4.28)	1.588(3.1) 1.465(-4.87)	1.477(-4.09)
Quarter ONTOP-OH	Figure 1.22	1.487(-3.44) 1.474(-4.28)	1.555(0.974) 1.483(-3.70)	1.551(0.714) 1.487(-3.44)	1.487(-3.44)
Quarter Bridge-O	Figure A.11	1.544(0.26) 1.498(-2.72) 1.507(-2.14)	1.532(-0.52) 1.612(4.67) 1.49(-3.24) 1.443(-6.3)	1.63(5.8) 1.469(-4.6)	1.507(-2.14) 1.489(-3.31)
Quarter Bridge-OH	Figure A.11	1.493(-3.05) 1.48(-3.89)	1.551(0.71) 1.487(-3.44) 1.489(-3.3) 1.542(0.13)	1.557(1.10) 1.463(-5.00)	1.502(-2.46) 1.489(-3.31)
Quarter HCP-O	Figure 1.22	1.474(-4.28) 1.484(-3.63) 1.468(-4.67)	1.559(1.23) 1.536(-0.26) 1.487(-3.44) 1.48(-3.89)	1.612(4.67) 1.466(-4.80)	1.500(-2.60) 1.486(-3.50)
Quarter HCP-OH	”	1.476(-4.15) 1.467(-4.74) 1.47(-4.54) 1.479(-3.96)	1.547(0.45) 1.54(0.0) 1.497(-2.79) 1.494(-2.99)	1.47(-4.54) 1.57(1.95)	1.494(-2.99) 1.495(-2.92)
Quarter FCC-O	”	1.46(-5.19) 1.495(-2.92)	1.509(-2.01) 1.622(5.32)	1.544(0.26)	1.483(-3.70) 1.481(-3.83)
Quarter FCC-OH	”	1.500(-2.6) 1.491(3.18)	1.542(0.13) 1.517(-1.49)	1.520(-1.3)	1.496(-2.86) 1.464(-4.93)
0.15 ML-ONTOP-O X-ray [72]				1.55(0.65)	

Table 1.9: Bond lengths and their % changes in the topmost bilayer of C(111)-(1×1) surfaces terminated with a quarter monolayer O atoms and OH groups. The bond lengths are shown in Å while the corresponding percentage changes which are shown in parentheses were obtained relative to the C-C bulk bond length of 1.54Å.

Oxygen & hydroxyl coverages & Adsorption Site (Monolayers-ML)	Bonds as shown e.g. in	Bonds within the C-atom zigzag chains bonded to O or OH. (Marked as **(A)** in figs. 1.25 & A.20)	Bonds joining 2 adjacent C-atom zigzag chains. (Marked as **(B)** in figs. 1.25 & A.20)
Third ONTOP-O	Figure 1.25	1.577(2.4),1.575(2.27),1.475(-4.22)	1.47(-4.54),1.578(2.46)
	”	1.478(-4.02),1.472(-4.41)	
Third ONTOP-OH	”	1.482(-3.77),1.474(-4.28),1.557(1.1)	1.577(2.40),1.48(-3.9)
	”	1.484(-3.64),1.485(-3.57),1.553(0.84)	1.476(-4.15),1.462(-5.06)
	”	1.554(0.91),1.558(1.17),1.473(-4.35)	1.467(-4.74),1.552(0.78),1.555(0.97)
Third Bridge-O	”	1.486(-3.5),1.497(-2.8),1.526(-0.91),1.645(6.8)	1.633(6),1.497(-2.8),1.486(-3.5)
	”	1.483(-3.7),1.523(-1.1),1.491(-3.18),1.52(-1.3)	1.498(-2.7)
Third Bridge-OH	”	1.554(0.91),1.545(0.32)	1.559(1.23),1.562(1.43)
	”	1.470(-4.54),1.484(-3.63),1.485(-3.57)	1.489(-3.31),1.494(-2.98)
	”		1.493(-3.05)
Third HCP-O	Figure A.20	1.502(-2.47),1.554(0.91)	1.524(1.0),1.47(4.54)
		1.487(-3.44),1.524(1.0)	1.502(-2.47),1.62(5.3)
	”	1.471(-4.48),1.48(-3.89)	1.483(-3.7)
Third HCP-OH	”	1.549(0.58),1.554(0.91)	1.549(0.58),1.560(1.29)
	”	1.481(-3.83),1.469(-4.61)	1.488(-3.38),1.489(-3.31)
	”	1.47(-4.54),1.484(-3.63)	
Third FCC-O	”	1.64(6.5),1.495(-2.92),1.518(-1.43)	1.486(-3.5),1.647(6.9)
	”	1.498(-2.73),1.635(6.17),1.485(-3.57)	1.495(-2.92),1.498(-2.73)
	”	1.527(-0.84),1.52(-1.3)	
Third FCC-OH	”	1.483(-3.7),1.554(0.91),1.553(0.84)	1.559(1.23),1.494(-2.99)
	”	1.542(0.13),1.475(-4.22),1.547(0.84)	1.491(-3.18)
		1.490(-3.24),1.486(-3.5),1.469(-4.6)	

Table 1.10: Bond lengths and their % changes in the topmost surface bilayer of the bulk terminated C(111)-(1×1) surfaces. The surfaces were terminated with a third monolayer of O atoms and OH groups at different sites. The bond lengths are shown in Å, while the numbers in parentheses are the corresponding percentage changes relative to the bulk C-C bond length of 1.54Å.

1.10.1 Bulk and near surface C-C bond lengths

The following section discusses only the changes observed within the bulk and near surface C-C bond lengths, excluding those at the topmost carbon-atom bi-layer, due the reasons mentioned before. The labelling of the carbon atom layers referred to in this section and also in the corresponding tables was similar to that shown in figures 1.16 and 1.21.

In all cases, very little changes were observed within the C-C bond lengths for those carbon atoms located within the bulk. These were in the neighbourhood of 0.2% of the bulk bond length (1.54Å), and it appeared as though on average most of the bonds tended to elongate a little bit rather than contract. This behaviour was noted mainly in the bonds that were located between the 8th and 7th carbon atom layers for all slabs and coverages, as well as between the 7th and 6th carbon atom layers, and those between the 6th and the 5th carbon atom layers. However, some rather pronounced bond length changes began to be observed between the 5th and 4th carbon atom layers, for the clean surfaces as well as those that were terminated with either oxygen atoms or hydroxyl groups. Incidentally, the clean surfaces showed a relatively larger bond length elongation than those terminated with either oxygen atoms or hydroxyl groups thus suggesting a weakening of the bonds between the 5th and 4th carbon atom layers for the clean surfaces. This also appeared to indicate that the charge distribution around the adsorbates played some role towards the observed apparent shortening of the said bond lengths. This was however not sufficient on its own to conclude if the effect of the adsorbates extended this far into the material. For the third ML coverages, changes of between 0.5 and 1% were observed within the bonds between the 5th and 4th carbon atom layers, while in the quarter ML coverages, the changes were confined between 0.13% and 1.33% of the bulk bond length (1.54Å). These were predominantly

between -0.1% and 1.2% of the bulk bond length for full and half ML coverages. As such, one can almost conclude with all certainty that on average the bond lengths between the 5th and 4th carbon atom layers changed by about 0 and 1.33% of the C-C bulk bond length, and hence they involved mainly elongation rather that contraction except only in a few cases.

Bonds between the 4th and 3rd carbon atom layers, experienced mainly lengthening, while others contracted. In particular, the clean surfaces experienced only bond contractions of between -0.19 and -0.65%, while the full and half monolayer coverages experienced both bond expansions and contractions of between 0.065 and 0.78% and between -0.519 and -0.97% of the bulk bond length respectively. Most of the bonds within this layer for surfaces terminated by a quarter ML of either oxygen atoms or hydroxyl groups experienced contractions except the quarter ML bridge site that was terminated with O atoms and OH groups. Based on the above observations, it was concluded that bonds between the 4th and 3rd carbon atom layers were just only stronger than those between the 4th and 5th layers. Incidentally, some bonds within the quarter ML coverage did not experience any contraction nor expansion at all, and therefore had similar bond lengths as the experimental bulk C-C bond length of 1.54Å. Bonds between the 4th and 3rd carbon atom layers for the third ML coverages experienced alternate contraction and expansion, except the third ML HCP site terminated with oxygen atoms where expansions of between 0.195 and 0.45% were observed, and the the third ML ONTOP site terminated with hydroxyl groups where contractions of between -0.268 and -0.32% were observed. Other bonds within the 4th and 3rd carbon atom layers associated with the third ML coverages retained bond lengths that were similar to the bulk C-C bond length of 1.54Å as shown in Table 1.6. The alternate contraction and expansion of the bonds appeared to suggest evidence of the bulk symmetry breakdown, although in a small way due to the magnitudes of the % changes. In a nutshell, most

bonds below the 4th and 3rd carbon atom layers experienced contractions or expansions that were less than ±1%, except between the 5th and 4th carbon atom layers, where these breached this value by experiencing an elongation of up to 1.3% of the bulk bond length.

The largest bond length changes were witnessed within the vertical bonds between the 3rd and 2nd carbon atom layers that were incidentally located in the near-surface region. Although most of the bonds showed some elongation, a few did exhibit some strong contractions leading to stronger bonds. The clean surfaces and the third ML FCC site terminated with OH groups showed some of the largest bond elongations of between 10 and 16%. Stumpf *et al.* [76] made a similar observation between the 3rd and 2nd carbon atom layers of clean C(111)-(1×1) surfaces, and they attributed this to the strong rehybridization of the bonding of the surface carbon atoms. Interestingly though, the adsorption of a full ML of O atoms and OH groups at the ONTOP site resulted in the least contractions between the 3rd and 2nd carbon atom layers, ranging only between -0.91 and -0.065%, while the co-adsorption of O atoms at the HCP and ONTOP sites led to fairly remarkable bond expansions of about 3.8%. However, unlike this coverage (i.e. the co-adsorption of O atoms at the HCP and ONTOP sites), a full ML of OH groups which were initially adsorbed at the bridge and HCP sites showed relatively smaller bond extensions of around 0.39% as shown in Table 1.4. The two scenarios gave strong indications that the co-adsorption of a full ML of O atoms or OH groups at different sites affected the surface structure rather differently, and one of the reasons for this was the absence of dangling bonds unlike the lower coverages.

The half monolayer coverages showed generally larger bond elongations of between 0.45 and 11.7% between the 3rd and 2nd carbon atom layers, when compared to the other coverages, with the largest elongation of 11.7% being observed in the half ML bridge site terminated with O atoms. It was also in

this coverage where the largest contraction of -4.1% was observed among all the half ML coverages. The lowest bond length expansion of 0.45% for all the half monolayer coverages was observed in the half ML HCP site terminated with O atoms, suggesting a strengthening of these bonds. These bond length changes were attributed mainly to the lack of sufficient coordination in the topmost layer of the half ML coverages.

With only 25% and 30% of the surface bonds being terminated with either oxygen atoms or hydroxyl groups, the lower coverages corresponding to a quarter and third ML showed alternate bond contraction and expansion between the 3rd and 2nd carbon atom layers, probably due to the presence of a large number of dangling bonds. In this case, only surfaces terminated by a quarter and third ML of oxygen atoms at a bridge site and those terminated with hydroxyl groups at a quarter ML FCC site, together with the third ML FCC site terminated with oxygen atoms showed some significant bond contractions. Most of the other sites had their bonds between the third and second carbon atom layers experiencing elongations, meaning that these bonds (between the 3rd and 2nd atom layers) were relatively weaker. The expansions were found to lie between 3.2 and 10% for the third ML coverages, and between 0.9 to as large as 8% for the quarter ML terminations with O atoms and OH groups. Although fairly large bond contractions were observed between the 3rd and 2nd carbon atom layers in some instances, these were confined mainly between -0.52 and -4% of the bulk bond length for both the quarter and third ML coverages.

1.10.2 Bond lengths and their % changes within the topmost C-C surface bilayer of bulk terminated (1×1) C(111) surfaces.

The topmost bilayer of carbon atoms (between the 1st and 2nd carbon atom layers) suffered quite a significant amount of bond length changes, both before

and after adsorbing the oxygen atoms or the hydroxyl groups as mentioned before, with even more changes being observed after terminating the surfaces with the O atoms or OH groups. The changes did not seem to be related to any type of adsorbate or even the coverage, and a closer look at the surface bond lengths revealed that most of these tended to be relatively large and random as shown in Tables 1.7 to 1.10. These changes were however not unexpected because the coordination of the surface atoms was different from that within the bulk and not to mention the effects of the adsorbates and the associated bonding anisotropy. It was therefore quite logical to imagine that, while the systems relaxed to the optimized atom positions that accommodated the lack of sufficient coordination at the surfaces, the bondlength changes mentioned above were certainly bound to occur, especially within the surface layer. Besides, the adsorbate atoms were different from the substrate matrix, and this could again have contributed to the observed changes. These changes are detailed in Table 1.7 which contains data for the topmost surface layer bondlengths from the clean surfaces and those terminated with a full monolayer of oxygen atoms and hydroxyl groups. Table 1.8 on the other hand details the optimized bond lengths and their % changes for surfaces terminated with a half monolayer of O atoms and OH groups, while Tables 1.9 and 1.10 show the surface bond lengths and their % changes for C(111) surfaces terminated with a quarter and third ML of O atoms and OH groups respectively.

Surface bonds within the topmost zigzag carbon atom chains of all the clean surfaces as well as those joining them experienced mainly contraction of between -2.6% and -4.5% as shown in figure 1.16, 1.21, 1.24 and Table 1.7. These findings were all in good agreement with other DFT calculations as shown in Table 1.7, where contractions of between -3.1 and -5.1% have been reported previously. Again, these contractions were clearly driven by the lack of sufficient coordination in the topmost layer, and the presence of dangling bonds on the

clean surfaces.

The full ML coverages did not show much changes within the surface carbon atom bond lengths as opposed to the lower ML coverages, probably due to the lack of dangling bonds. However, some minimal bond elongations and contractions were observed in certain cases, but the most important observation was that the changes occurring within the surface layer bonds of the full ML coverages (whether expansion or contraction) were much smaller than those observed in the clean surfaces. Adsorbing oxygen atoms up to a full ML at the ONTOP site resulted in the carbon atom zigzag chains extending by 1.9%, while only a minimal extension of 0.39% occurred in the corresponding hydroxyl termination. This meant that the presence of the hydrogen atom in the hydroxyl group played some role towards the observed bond modifications. The relative shortening of the surface C-C bonds due to the adsorption of the hydroxyl groups when compared to the lengthening of the surface C-C bonds following the adsorption of oxygen atoms meant that they became relatively stronger. These changes were also found to affect the surface bonds joining any two adjacent zigzag carbon atom chains, where alternate bond expansions and contractions were observed. In particular, fairly large bond expansions of between 0.0 and 2.3% were observed within the bonds joining the zigzag carbon-atom chains following the adsorption of a full ML of oxygen atoms at an ONTOP site, while the adsorption of the OH groups at similar sites resulted only in minimal contractions of up to -0.13% compared to the bulk bond length.

The co-adsorption of oxygen atoms at the ONTOP and the HCP sites or hydroxyl groups at a bridge and HCP sites resulted in overall contraction of the surface bonds joining the zigzag carbon atom chains by margins ranging between -0.45 and -0.26% of the bulk bond length. This led to alternate bond expansions and contractions within the surface-layer zigzag carbon atom chains as shown in Table 1.7. These were accompanied by a substantial increase in

the bond lengths of the immediate underlying carbon atom layers as seen from figures 1.18 and A.2, and also as mentioned before. The changes observed in the bond lengths appeared to suggest that the adsorbate charges modified the bond strengths in such a way that the ones located at the surface got relatively stronger due to their apparent shortening while the immediate underlying C-C bonds became relatively weaker.

With only 50% of the surface carbon-atom bonds being terminated with either of the two adsorbates in the case of the half monolayer coverage, the concentration of the adsorbates and hence the coordination was obviously varied. This led to some differences between the surface bonds within the zigzag carbon atom chains, and those joining them. This was especially more pronounced between those surface bonds that were bonded to the oxygen atoms or hydroxyl groups, and those that were not. The surface bonds within the zigzag carbon atom chains that were not bonded to either the O atoms or the OH groups were found to contract by between -2.66 and -4.54% except in the case of the half ML bridge site terminated with oxygen atoms. This contrasted with observations made in the surface bonds within the zigzag carbon atom chains terminated with either O atoms or OH groups, where a general expansion of between 0.9 and 2% as shown in Table 1.8 was observed. Nonetheless, some fairly large contractions (-2.92%) were observed in the case of the half ML bridge site terminated with oxygen atoms, as well as some minimal ones in the half ML FCC sites terminated with oxygen atoms (-0.31%) or hydroxyl groups (-0.71%). However, these were rather less stable configurations as discussed later, and for this reason their varied bond lengths were somewhat not unexpected. On average, the degree of bond extensions within the surface zigzag carbon-atoms chains that were bonded to either O atoms or OH groups was much smaller than the contraction experienced in the surfaces.

Due to the contractions and expansions experienced within the surface zigzag

carbon-atom chains of the half ML coverages, the C-C bonds joining them also suffered some bond length changes. In this case, surface bonds joining the carbon atoms bonded to either oxygen atoms or hydroxyl groups to adjacent ones that were not bonded to the oxygen atoms or hydroxyl groups (marked as **C** in Table 1.8 and figure 1.19) suffered fairly large expansions of between 0.65 and 5.84%. The only exception to this general trend was the half ML FCC site terminated with OH groups, where a large contraction of -3.44% was observed. Unlike these bonds, those within the surface layer and joining two adjacent carbon atoms that were not bonded to either oxygen atoms or OH groups (i.e. bond type **D** as shown in Table 1.8 and figure 1.19), appeared to suffer more contraction than expansion. Once again, the expansions were generally lower than the contractions, with typical values of between 0.71 and 0.52% being recorded within the half ML ONTOP site with OH groups. All the other type **D** bonds within the half ML coverages experienced bond contractions ranging between -1.0 and -6.6%, with the largest and minimum bond contractions being witnessed in the half ML FCC sites terminated with oxygen atoms and hydroxyl groups respectively, leading to major surface bond interuptions. This obviously meant that the presence of the adsorbates not only influenced the bond lengths of the carbon atoms bonded directly to them, but also the ones in their neighbourhood. As a result, some bonds got stronger while others became weaker, depending on the charge distribution within and around the respective bonds and sites, which in some way resulted in the breaking down of the expected surface symmetry.

Lack of sufficient coordination, increased number of dangling bonds and bond anisotropy again were cite as key factors towards the changes observed in the surface bond lengths for the lower coverages, such as the quarter ML. For the low coverages, it was observed that, although the surface bonds contracted or

expanded by varying degrees, in a majority of the cases, these involved contraction as shown in Table 1.9. Most of the bonds within the surface zigzag carbon atom chains that were not bonded to either oxygen atoms or hydroxyl groups contracted upon system relaxation, by values ranging between -2.6 and -5.19%. This trend was also observed in the surface carbon atom bonds within the zigzag carbon-atom chains bonded to either oxygen atoms or hydroxyl groups, although some bonds did expand. These changes were accompanied by bond contractions of between -1.3% and -5% for a majority of the surface carbon atom bonds joining the zigzag carbon atom chains that were bonded to either oxygen atoms or hydroxyl groups (i.e. bond type **C** in Table 1.9 and figure 1.22) and expansions of between 0.26 and 5.8%. These differences were attributed to the upwards displacement of the carbon atoms bonded to the oxygen atoms or hydroxyl groups, as seen in figures 1.22 and 1.23 and also in figures A.9, A.10 and A.11 (shown in Appendix A. These changes were a clear testimony of the competing forces existing at the surfaces. The only exception to this was the quarter ML bridge site terminated with oxygen atoms only, where the expansions were always less than the contractions in the respective adsorption sites and coverages. However, the surface bonds appeared to be quite significantly distorted in this particular case.

Surface carbon-atom bonds joining the zigzag carbon atom chains that were not bonded to either of the adsorbates (i.e bond type **D** as shown in Table 1.9) contracted by values that were between -2.14 and -4.9% of the bulk bond length, for all quarter ML coverages. Incidentally, these values were quite close to those observed in the surfaces terminated by the half ML coverages, in spite of the obvious differences between the two coverages. This suggested that whenever the surface bonds were not attached to any adsorbates, they always contracted just like in the case of the clean surfaces so as to accommodate the changes taking place at the surfaces. This was partly due to the fact that the adsorbates

always resulted in upwards relaxation of the carbon atoms bonded to them, thereby increasing the resulting interatomic C-C bond lengths.

With only 30% of all the surface bonds terminated with either oxygen atoms or hydroxyl groups, the very nature of the third ML coverages, ensured that all the zigzag carbon atom chains at the surface had either an oxygen atom or a hydroxyl group terminating the carbon atoms. From this atomic arrangement, some bonds within the same surface zigzag chains were found to extend by between 0.13 and 2.27%, while others contracted by -0.84 and -4.6% depending on whether the surfaces were terminated with oxygen atoms or hydroxyl groups as shown in Table 1.10. This was found to occur in both the surface bonds within the carbon atom zigzag chains bonded to the oxygen atoms or the hydroxyl groups (bond type **A** in figure 1.25) and those joining any two adjacent carbon-atom zigzag chains (bond type **B** in figure 1.25). The former showed more tendency towards either contraction or expansion of the bonds, owing to the presence of the adsorbates.

A few instance did however show relatively large bond expansions of up to 6.8% of the bulk bond length as shown in Table 1.10, resulting in a significant amount of surface structure distortion in those specific instances, leading to surface symmetry breakdown.

On the other hand, the number of surface bonds joining the zigzag carbon-atom chains (bond type B in figure 1.25 & Table 1.10) that suffered expansion was almost equal to those that contracted, with the amount of bond contraction ranging between -1.0 and -5% and expansions of between 1.23 and 2.46%, except in the third ML bridge:O, the third MLHCP:O and third ML FCC:O where instead large bond expansions of up to 6, 5.3 and 6.9% were observed respectively.

1.11 Bond angles within the bulk and near surface regions of a bulk terminated (1×1) diamond (111) surface.

Most of the bond angles within the bulk regions of diamond were found to be very close to experimental value of 109.4°. This was mostly up to the third bilayer of carbon atoms from top, a factor that was attributed to the strong covalent bonding of the diamond C-C bonds. This preservation of bond angles was supported by the lack of significant bond distortions within the bulk as discussed previously, and it also meant that the changes occurring within the surface bonds did not extend deep into the bulk. The bond angles within this regime ranged between 108.9 and 109.8°, thus exhibiting a small difference of about ±0.5° from the experimental value.

However, due to the fairly large bond distortions in the surface and near surface layers, the bond angles within and close to the surface region were also found to vary, with values of between 101 and 117° being observed. In spite of this large change, most of the bond angles differed only by 3 to 4° from the experimental value as shown in figures 1.16 to 1.26 and figure A.1 to A.20 (shown in Appendix A), with only a few bond angles lying at the two extremes. Some of the changes were attributed to the presence of the adsorbates, and especially so their effect on the topmost bilayer of carbon atoms. It was further found that whenever the bond lengths differed quite significantly from the bulk bond lengths, almost similar large changes occurred within the respective bond angles. Nonetheless, the changes occurring within the bond angles were fairly small in a majority of the cases, when compared to the experimental value, and this led us to the conclusion that the bond angles were generally preserved, just like the bond lengths were within the bulk regions. This was in line with previous experimental observations where it was established that unlike silicon, diamond tends to preserve the bond angles more than the bond lengths [47].

1.12 C-O and C-OH bond lengths and their orientations from the (1×1) bulk terminated (111) diamond surface.

The presence of the oxygen atoms or even the hydroxyl groups on the C(111) surfaces had a profound effect not only on the surface C-C bonds, but also the bonds that they formed with the surface carbon atoms. Depending on the strength of a given bonding site, the C-O bonds were either single or double (C=O) bonds, the distinction between the two being primarily their lengths in comparison with the known ones.

Our calculations revealed that the C-O bonds from surfaces terminated with either a full, half, third or quarter ML of oxygen atoms at an ONTOP site were all inclined at almost 90° to the topmost carbon atoms as shown in figures 1.17, 1.19, 1.22 and 1.25. In addition, the C-O bond from the half ML ONTOP site terminated with oxygen atoms was further inclined at 85.09° when considered between the atomic rows, leading to a displacement of 0.101Å for the O atom relative to the underlying carbon atoms. This was accompanied by some alternate shortening and lengthening of the bonds between the topmost and second-from top carbon atom bilayers (see figure 1.19). The C-O bond length from the quarter ML ONTOP site terminated with O atoms was also inclined at 88.86° when considered between the atomic rows, and as a result the O atom was slightly displaced by 0.0261Å in one (y-)direction only. In the process, some carbon atoms within the topmost layer bonded to the O atoms relaxed upwards by 0.271Å over those that were not bonded, thereby causing some unequal buckling of the surface layer. In the third ML ONTOP site with O atoms, the carbon atoms bonded to the oxygen atoms were found to be raised by 0.274Å compared to those that were not bonded to the adsorbates. This led to the shortening of some of the C-C bonds within the surface, especially those within the carbon atom zigzag chains, and the lengthening of those that were

bonded to the oxygen atoms. The optimized C-O bond lengths for the various ONTOP sites considered in this study are summarized in Tables 1.4, 1.5 and 1.6, where it was found that the third ML ONTOP terminated with O atoms had the shortest C-O bond length of 1.304Å. It was further found that all the ONTOP sites had C-O bonds that were shorter than the value of 1.36Å obtained by Lide *et al.* [66] for paraffinic compounds which they even referred to as a partial double bond. These values were also shorter than the value of 1.34Å for a single CO bond obtained by Zheng *et al.* [44] through their energy minimization calculations.

Following the adsorption of hydroxyl groups at the ONTOP sites, it was found that the C-OH bond were inclined at slightly different angles relative to the underlying carbon atoms for the various coverages, ranging between 90° to 94.5° as seen in figures 1.26, A.1, A.3 and A.9 (shown in Appendix A. The small inclination from the true 90° was attributed to the presence of the adsorbed H atoms from the OH groups, as well as their associated steric repulsion. This led to an upward relaxation of between 0.202 and 0.273Å for the OH-terminated carbon atoms relative to the unbonded ones, and it was especially more prevalent for the lower coverages. The C-OH bond in the case of a full ML coverage was 1.26% longer than the experimental one, while this varied between 0.0 and 1.4% for the half ML coverages. The quarter and third ML coverages also exhibited contractions of between -0.49 and -0.84% of the experimental value of 1.43Å, and these values were clearly much smaller than those observed in the half ML coverages. The corresponding O-H bonds varied between -1.12% and 1.53% from the experimental value of 0.98Å, thereby illustrating both contraction and expansion, with some larger expansions of up to 2.4% being observed in the case of the full ML co-adsorption of OH groups at a HCP and bridge sites, and up to 2.74% for the quarter ML FCC site terminated with OH groups. The expansions were observed only in the full, half and some of the quarter ML

coverages, while for the third ML coverages, only contractions of between -0.41 and -0.71% were observed. The inclinations of the relaxed O-H bonds to the C-O bonds varied between 106.8° and 107.7°.

The co-adsorption of a full ML of oxygen atoms at the HCP and the ONTOP sites, yielded a C-O bond that was inclined at 90° to the topmost carbon atoms for the ONTOP site, but instead of forming a bond with the carbon atoms, the oxygen atom at the HCP site formed a O-O bond with the oxygen atom located at the ONTOP site. This suggested the possible adsorption/formation of an oxygen molecule on the C(111) surface, with the resulting ∠OOC bond angle being 101.8° as shown in figure A.2. The C-O bond length was 1.417Å which was clearly longer than the experimental value quoted previously, and hence weaker. The O-O bond length was 1.412Å, which was also a bit longer than our optimized O-O bond length of 1.217Å for the free oxygen molecule, and the experimental value of 1.21Å [73, 66]. Again, the formation of the O-O bond alluded to the possibility of an oxygen molecule bonding on to a diamond (111) surface, and that the molecule was not likely to dissociate to either O atoms or detach itself as an oxygen group, unless sufficient energy was supplied to overcome the barrier. Zheng *et al.* [44] also reported an O-O bond length of 1.49Å, which was located at a bridge-bonded site on a (1×1) single dangling bond diamond (111) surface, which is fairly longer than ours which (1.412Å).

Following the co-adsorption of hydroxyl groups at the HCP and bridge sites, the resulting C-O and O-H bonds were found to be staggered at different angles with respect to the underlying carbon atoms as shown in figure 1.18. Such orientations were clearly meant to achieve mutually optimized atom positions that accommodated the adsorbed atoms at the two sites, especially in the presence of other competing effects such as (OH-OH) steric repulsions. After relaxation, the OH groups moved from their initial adsorption sites to positions that approximated the ONTOP site, and in the process resulting in C-OH bonds of

1.431Å long.

The full and half monolayer coverages had the same surface unit cell, with the only difference being the fact that, instead of having two oxygen atoms or hydroxyl groups per unit cell as was the case in the full monolayer coverage, there was only one for the half monolayer coverage. This meant that only half of the surface bonds were terminated with O atoms or OH groups in the case of the half ML coverages, while the remainder were not.

Due to the location of either the O atoms or OH groups in the bridge sites, the carbon atoms nearest to them were always displaced by a certain amount from their expected sites. In the case of the half ML bridge (epoxy) bonding site, one of the two carbon atoms bonded to the oxygen atom was displaced by 0.141 & 0.102Å in the y and x-directions respectively, and the other by 0.133 & 0.118Å from their expected lattice sites, indicating an unequal displacement and therefore some form of surface structure asymmetry. A similar observation was also made in the quarter ML O-bridge bonding, but in addition to this, a buckling of 0.109Å for those carbon atoms in close proximity to the adsorbed O atoms were also observed, resulting in the carbon atoms in the 2nd layer of the topmost bi-layer relaxing upwards by 0.232Å. The relaxed oxygen atom was located at 1.195Å above the topmost carbon atoms. Just like in the half and quarter ML coverages, the oxygen atom in the third ML coverage was not entirely centrally placed between the two nearest carbon atoms as shown in figure A.17. Instead, one of the C-O bonds was a bit longer, being 1.688Å while the other was 1.611Å, and the O atom was located at 1.185Å directly above the topmost layer of carbon atoms. The carbon atoms located close to the oxygen atoms were also found to suffer some displacements of 0.0784Å in the x-direction and 0.142Å in the y-direction, as shown in the top view of figure A.17. Due to this displacement, some bond distortion was observed within the topmost carbon-atom layer, whereby some of the carbon atoms were found to

be raised by as much as 0.198Å relative to the others within the same layer, while others were displaced vertically by 0.280Å. As a result of this surface bond disruption, the bond lengths between the first and second carbon atom bi-layers experienced both alternate contractions and expansions. This led to a significant amount of bond length changes within the topmost zigzag carbon atom chain as shown in figure A.5 and in the other bridge-bonding structures too.

All the bridge sites were found to be rather unstable against the adsorption of hydroxyl groups. In this case, although the starting geometry was the actual bridge bonding site, the hydroxyl groups always relaxed to new sites that closely resembled the ONTOP one. This was in agreement with other DFT calculations (Loh *et al.* [53]), and it was supported by our computed adsorption energies (reported later) where the resultant ONTOP:OH sites were favoured by as much as 0.3462eV (for the $\frac{1}{2}$ ML coverage) over the actual ONTOP site terminated by OH groups. This outcome wasn't however wholly unexpected since the stoichiometry of the bonding atoms (and especially the O atom) based on the available valence electrons would only allow the formation of two C-O and not three bonds on a single-dangling-bond C(111) surface as would be expected if the OH groups were to bond at the bridge sites. This would therefore exclude the adsorption of the OH groups at these sites.

Although the FCC site was also unstable against the adsorption of both the oxygen atoms and hydroxyl groups, the adsorbates did not move to new positions after relaxation like the bridge bonding where these moved to sites that were quite close to the ONTOP one, except the third ML termination with OH groups at the FCC site. Others relaxed to sites that were quite close to their initial adsorbed FCC positions.

Due to the unique FCC site, neither the O atoms nor the OH groups formed bonds with the underlying carbo atoms, except the third ML coverage. The O

atom was situated at 1.23Å directly above the topmost carbon atom layer in the half ML coverage (which was higher than for the bridge sites), while in the quarter ML coverages it was located at 1.164Å as shown in figure A.13 and in the third ML coverage at 1.19Å (which incidentally was quite close to the values observed in the bridge sites). Due to the position of the oxygen atom, the two surface carbon atoms in it neighbourhood were found to suffer some unequal displacements. These were 0.151 and 0.170Å in the x-direction for the third ML FCC coverage, and the resulting C-O bond was 1.57Å and it was inclined at an angle of 49° relative to the topmost carbon atoms as shown in figure A.19. As a result of the displacement witnessed in the topmost carbon atoms in the neighbourhood of the oxygen atoms, a fairly large amount of surface bond distortion was experienced. This tended to break the surface symmetry, a phenomenon that was also observed in the half and quarter ML FCC:O sites as shown in figures A.7 and A.13 respectively. In the quarter ML FCC:O site, the carbon atom located close to the oxygen atom was displaced vertically by 0.283Å compared to an adjacent one that was not too close to the oxygen atom. In addition, the oxygen atom was centrally positioned between the two closest carbon atoms, and the C-O bond lengths between the oxygen atom and the carbon atoms were each 1.603Å as shown in figure A.13.

The hydroxyl groups behaved in an almost similar manner as the oxygen atoms adsorbed at the FCC sites. Displacements of the topmost carbon atoms in close proximity to the OH groups were observed as seen in the respective FCC structures, accompanied by a significant amount of surface bond distortions. Whereas no measurable C-OH bonds were observed due the location of the OH (except the third ML FCC:OH), the O-H bonds showed very good agreement with the experimental ones and other DFT calculations as summarised in Tables 1.4, 1.5 and 1.6. It was felt that the presence of strong antibonding states may have compromised the stability of the FCC sites terminated with oxygen atoms

or hydroxyl groups, making them generally unattractive for bonding.

Unlike the face centered cubic site, the hexagonal close packed site was defined as a site with a carbon atom below the oxygen atom or the hydroxyl group in the second layer as shown in figures 1.13 and 1.15. Unfortunately just like the bridge sites and a majority of the FCC sites, this site was also quite unstable against the adsorption of either oxygen atoms or hydroxyl groups. In this case, in spite of the starting geometry being the ideal HCP sites, both the oxygen atoms and the hydroxyl groups drifted to positions that were quite close to the ONTOP site for the half and quarter ML coverages as shown in figures 1.20, 1.23, as well as in figures A.4, A.6 and A.10 (shown in Appendix A, with the only exception being the third ML HCP site where a small tilt was observed as shown in figure A.15.

However, while it was possible to account for the instability of the HCP:OH site in terms of the available bonding electrons on the hydroxyl group and the carbon atom matrix, it was not quite easy to do the same for the HCP:O, except to infer to the fact that the bond lengths formed may not have been stable enough to retain the structure and instead the system always relaxed to a state that was close to the ONTOP site. In fact, it was established that in the case of the half ML coverage with oxygen atoms at the HCP site, the C-O bonds were oriented at 90° to the top carbon atom layers when considered within the rows and 82.51° between the rows as shown in figure A.4. This resulted in the O atom being displacement by about 0.207Å in the x-direction and a minimal 0.00822Å in the y-direction, which in turn led to an outward relaxation of 0.253Å for the carbon atoms bonded to the O atom, compared to the unbonded ones. The C-O, C-OH and O-H bonds associated with the HCP sites (i.e. HCP:O and HCP:OH) are summarized in Tables 1.4, 1.5 and 1.6 together with those of other sites as well as in the structural diagrams shown here and others in Appendix A. In this case, the C-O bond in the half ML

HCP:O was -2.2% shorter than the experimental value of 1.36Å, while it was -1.47% shorter for the quarter ML site and longer by 1.47% in the third ML HCP:O site. As such, the C-O bond was a lot weaker for the third ML HCP:O site than either of the other two HCP coverages mentioned above. This was thought to be due to the almost ONTOP site assumed by the two HCP:O sites after relaxation together with the resulting O-O interactions. Again, the HCP position of the adsorbed O atoms resulted in the shortening and lengthening of some of the surface C-C bonds within the topmost bi-layer, as illustrated in the respective structural diagrams.

The adsorption of OH groups at various HCP sites and coverages resulted in different C-OH bond lengths. In the full ML HCP:OH site, the C-OH bond was almost equal to the the experimental value of 1.43Å, differing by only 0.07% while in the half ML HCP:OH site it contracted by -1.4%. The quarter and third ML HCP sites with OH groups had much lower margins of contractions, which were -0.56% and -0.2%. The accompanying O-H bond differed from the experimental value of 0.98Å by 2.2% for the full ML coverage, 1.02% for the half ML coverage, -0.54% for the quarter ML coverage and -0.71% for the third ML coverage. These values were also in good agreement with other DFT calculations [53], and the O-H bonds were inclined at orientations of between 107.85 and 112.43° relative to the C-O bond. While no clear pattern was established, the variations in the C-OH and O-H bonds was likely to be coverage depended, due to the OH-OH interactions. The lower coverages showed more contractions for the C-OH and O-H bonds, due to reduced repulsive effects.

In addition, the inclination of the hydroxyl group's bonds relative to the underlying oxygen atoms' horizontal plane was generally larger in the case of the half monolayer coverages than it was for the full monolayer ones, averaging at 22.3° compared to that of the full ML coverages which was 15.5° on average. This was attributed to the adsorbates interactions alluded to previously.

The fact that, in spite of starting the optimizations at different geometries the OH groups always relaxed to adsorption sites that were close to the ONTOP site suggested that the ONTOP sites were on average always preferred for bonding. The oxygen atoms were found to be capable of bonding at many other sites, although the ONTOP site was still the favoured one. The OH groups were unstable at all sites except the ONTOP one, unlike the oxygen atoms that showed stability at the ONTOP, bridge and even the FCC sites. The HCP site was found to be generally unstable for bonding of both oxygen atoms and the hydroxyl groups, with the OH groups being more unstable, and instead drifting to new sites that were close to the ONTOP one. The oxygen atoms adsorption at the HCP site sometimes resulted in an optimized structure that was lying in between the original HCP and the ONTOP sites, again emphasizing the preference and dominance of the ONTOP site for bonding over the others.

1.13 Bulk and near surface C-C bond lengths of (2×1) reconstructed diamond (111) surfaces; for clean and O or OH-terminated surfaces.

Tables 1.11 and 1.12 show the C-C bond lengths together with their % changes within the bulk and near surface regions of a (2×1) reconstructed diamond (111) surface, for clean and O or OH-terminated surfaces respectively. These were extracted from the structural diagrams shown in figures 1.27 to 1.31 and in figures A.21 & A.22 for the less stables ones (shown in Appendix A). The surfaces were terminated with either a full and half monolayer of oxygen atoms or hydroxyl groups at a bridge or an ONTOP site.

All the calculations were started from the symmetric chain model proposed by Pandey [45].

Slab termination (Monolayers)	$d_{C_8-C_7}$ (%)	$d_{C_7-C_6}$ (%)	$d_{C_6-C_5}$ (%)	$d_{C_5-C_4}$ (%)	$d_{C_4-C_3}$ (%)	$d_{C_3-C_2}$ (%)
Full/Half ML	1.539(-0.065)	1.534(-0.39)	1.537(-0.19)	1.608(4.4)	1.547(0.45)	1.616(4.93)
clean slab	1.544(0.26)	1.552(0.78)	1.532(-0.52)	1.50(-2.6)	1.581(2.6)	1.644(6.75)
	1.545(0.32)		1.547(0.45)		1.533(-0.45)	
	1.547(0.45)		1.552(0.78)		1.512(-1.82)	
	1.537(-0.19)					
LEED-[16]				1.49(-3.5)		1.62(4.9)
				1.61(4.3)		1.64(6.2)
X-ray-[78]				1.45(-6.0)		1.56(1.0)
				1.6212(5.0)		
DFT-[48]				1.49(-3.5)	1.52(-1.6)	1.60(3.6)
				1.60(3.6)	1.57(1.7)	1.63(5.6)
DFT-[48]					1.51(-2.2)	1.60(3.6)
					1.53(-0.91)	1.63(5.6)
DFT-[43]				(-2.8)	(2.6)	(6.6)
				(4.3)		(4.5)
DFT-[75]					(0.7)	(8.1)

Table 1.11: Calculated C-C atom bond lengths (d_{C-C}) and their % changes (numbers in parentheses) relative to the bulk bond length of 1.54Å, for bulk and near surface carbon atoms from a (2×1) reconstructed diamond (111) clean surface.

Slab termination (Monolayers)	$d_{C_8-C_7}$ (%)	$d_{C_7-C_6}$ (%)	$d_{C_6-C_5}$ (%)	$d_{C_5-C_4}$ (%)	$d_{C_4-C_3}$ (%)	$d_{C_3-C_2}$ (%)	d_{C-O} & d_{C-OH}(%)	d_{O-H} (%)
Full ML ONTOP-O	1.543(0.195) 1.535(-0.32) 1.547(0.45)	1.531(0.58) 1.544(0.26)	1.532(-0.52) 1.55(0.65) 1.547(0.45)	1.603(4.1) 1.489(-3.3)	1.561(1.36) 1.54(0.0)	1.58(2.6) 1.551(0.71)	1.196(-2.76) -	- -
Full ML ONTOP-OH	1.535(-0.32) 1.543(0.195)	1.531(-0.58) 1.543(0.195)	1.551(0.71) 1.532(-0.52) 1.538(-0.13)	1.60(3.89) 1.49(-3.2)	1.572(2.1) 1.545(0.32) 1.54(0.0) 1.53(-0.65)	1.602(4.0) 1.559(1.23)	1.419(-0.77) 1.423(-0.49)	0.984(0.41) 0.984(0.41)
Half ML ONTOP-O	1.538(-0.13) 1.541(0.065) 1.544(0.26)	1.543(0.195) 1.531(-0.58)	1.533(-0.45) 1.552(0.78) 1.537(-0.195)	1.494(-2.99) 1.60(3.9)	1.545(0.32) 1.536(-0.26) 1.577(2.4)	1.624(5.45)	1.379(1.4)	-
Half ML ONTOP-OH	1.534(-0.39) 1.548(0.52)	1.547(0.45) 1.536(-0.26)	1.547(0.45) 1.551(0.71) 1.539(-0.06)	1.497(-2.79) 1.609(4.48)	1.54(0.0) 1.543(0.19) 1.577(2.4)	1.612(4.7) 1.615(4.9)	1.45(1.4)	0.972(-0.82)
Half ML Bridge-O DFT-[53] ”	1.54(0.0) 1.545(0.32)	1.55(0.65)	1.538(-0.13) 1.552(0.78)	1.611(4.6) 1.498(-2.73)	1.577(2.4) 1.534(-0.39) 1.544(0.26) 1.576(2.3)	1.64(6.5) 1.60(3.89) 1.592(2.37) 1.634(6.1)	1.44(0.69)	-
Half ML site with initial geometry as bridge-bonded-OH	1.54(0.0) 1.533(-0.45) 1.55(0.65)	1.549(0.58) 1.538(-0.13)	1.53(-0.65) 1.546(0.39)	1.499(-2.7) 1.611(4.6)	1.577(2.4) 1.52(-1.29) 1.545(0.32) 1.539(-0.06)	1.61(4.5) 1.62(5.2)	1.459(2.03)	0.994(1.43)

Table 1.12: Calculated C-C atom bond lengths and their % changes, for bulk and near surface carbon atoms from a (2×1) reconstructed diamond (111) surface. The percentages changes for the C-C bonds, (numbers in parentheses) were calculated relative to the experimental bond length of 1.54Å. Also shown are the lengths for the C-OH bonds relative to the experimental value 1.43Å, the single C-O bonds relative 1.36Å, double C=O bond relative to 1.23Å and the O-H bonds which are compared to the experimental value of 0.98Å.

The tables together with the structural diagrams showed that the bulk bond lengths for the (2×1) reconstructed diamond (111) surface did not experience much changes from the experimental bulk bond length of 1.54Å, except some minimal changes in certain instances of ±1% of the bulk bond lengths. This appears to suggest that the effects of surface reconstruction was only confined only to the top two bilayers of carbon.

Our calculations revealed that bond contractions and expansions were generally less than ±1% of the bulk bond length between the 8th and 7th, 7th and 6th as well as 6th and the 5th layers of the clean (2×1) reconstructed diamond (111) surface.

However, large bond relaxations within the range observed by Scholze *et al.* [43] were found between the 5th and 4th carbon atom layers, a phenomenon that was found to traverse through all the surfaces terminated with oxygen atoms or hydroxyl groups as well as the clean ones. Some bonds got shorter by as much as -6 and -2.6%, while others became longer by 3.6 and 5% of the bulk bond length, and these changes did not appear to depend on the type of adsorbate or whether the surface was terminated or not. This alternate expansion and contraction of bonds tended to distort the structure and therefore break the existing symmetry, which in turn would have had an effect on the observed density of states. Such large bond length changes, implied that certain bonds were relatively weaker than the others. The DFT calculations of Scholze *et al.* [43] found bond length expansions and contractions of 4.3 and -2.8% respectively between the 4th and 5th carbon atom layers, while the LEED measurements of Walter *et al.* [16] showed the same bonds contracting and expanding by -3.5 and 4.4% respectively, values which were in approximate agreement with our DFT calculations. In addition, our findings were also in good agreement with the X-ray measurements of Huisman *et al.* [47] who found bond contractions and expansions of -6 and 5% respectively. The DFT work of Kern *et al.* [48],

on the other hand established bond length expansions of 3.6% (1.60Å) and contractions of -3.6% (1.49Å) for the clean surface, which were again in good agreement with our observations, where the bonds contracted predominantly by -2.6% and expanded by 4.6% of the bulk C-C bond length. These bond lengths led to a rather strong buckling of the bond between the fourth and fifth layers (by Δz=0.17 and Δz=0.06Å) respectively according to Kern *et al* [48]. The buckling then led to a reduction (increase) of the interatomic distances between these layers as indicated above.

Bonds between the 4th and 3rd carbon atom layers experienced minimal expansions and contractions, especially when compared to those occurring between the 5th and 4th carbon atom layers, although still larger than those observed between the 8th and 7th or even the 7th and 6th layers. This applied to all the sites and terminations as well as the clean surface. In this case, whereas bond expansions of 4.7% were observed between the 5th and 4th carbon atom layers, only modest expansions of around 2.6% were observed between the 4th and 3rd carbon atom layers of the clean surface. Similarly, maximum bond length contractions of -1.30% were found between the 4th and 3rd carbon atom layers for surfaces terminated with the adsorbates, accompanied by expansions of between 0.45 & 2.6%. From their DFT calculations, Kern *et al.* [48] observed that these bonds contracted and expanded by margins that were between -0.9 and 1.7% of the bulk bond length (1.54Å) respectively, while Scholze *et al.* [43] observed some bonds expanding by 2.6%, and van der Bilt *et al.* [39] established only bond contractions of -8.1% which were fairly large for the clean slab.

Based on these findings, our results showed more agreement with the observations of Kern *et al.* [48] and Scholze *et al.* [43], yet they differ quite significantly from those of van der Bilt *et al.* [39]. Loh *et al.* [53] on the other hand found that the bonds between the 3rd and 4th layers for a surface terminated with oxygen atoms at a bridge site expanded by 0.26 and 2.3%, which

agreed quite well with our computed values of between -0.39 and 2.4%.

The 3rd and 2nd carbon atom layers presented even larger bond length changes than all the other cases, mainly because this is where the effect of the surface reconstruction was greatly felt. In this case, the bonds expanded by margins that were between 3.89 and 6.7%, suggesting the inevitability of correspondingly large bond length distortions and bond angle changes. Most of the bonds within this layer were elongated, with none of them contracting. Kern *et al.* [48] observed that the distances between the atoms in the second and third layers of a clean surface increased by +3.6% and +5% respectively, while all other interatomic distances changed only slightly. The LEED measurements of Walter *et al.* [16] showed these bonds expanded by 6.2 and 4.9% for a clean surface, while the X-ray measurements of Huisman *et al.* [47] for the clean slab also, only yielded an expansion of 1.0% for the said bonds. The DFT calculations of Scholze *et al.* [43] for the clean surface showed the same bonds expanding by 4.5 and 6.6% of the bulk bond length, while VanderBilt *et al.* [75, 39] found only large expansions of ∼8.1% for the same bonds within a clean surface. Our results were therefore quite close to the experimental findings mentioned previously, than those of most of the other workers. Up on the adsorption of oxygen atoms at a half ML bridge site, Loh *et al.* [53] found the bond lengths between the 3rd and 2nd layers expanded by 3.37 and 6.1%. From our DFT calculations, all the terminations (with the adsorbates) showed relatively large bond expansions between the 2nd and 3rd carbon atom layers, which were very close to those of the clean slab. Only marginal reductions in the values of the expansions were observed, implying that the presence of the adsorbates did not have a major effect on the respective bulk and near surface bond lengths. No clear pattern was established within the bond lengths expansions or contractions for those surfaces terminated with oxygen atoms or hydroxyl groups, to conclude if any had a higher or lower effect on the

bond lengths between the 3rd and 2nd carbon atom layers than the other. This appeared to suggest that the bond lengths were independent of the two adsorbates.

1.14 C-C bond lengths and their % changes in the lower and upper π-bonded chains of (2×1) reconstructed diamond (111) surfaces.

One of the main objectives of this study was to investigate how the π-bonded zigzag C-C atom chains changed in the presence or absence of O atoms or hydroxyl groups at different sites. These changes are summarized in Table 1.13 for the topmost π-bonded bilayers of carbon atoms, and they are also shown together with those of the clean surfaces for comparison purposes.

In this case, some notable changes were observed in the surface bond lengths just like in the bulk terminated C(111) surfaces, and a majority of these were attributed to the presence of the adsorbates, which in addition contributed towards the observed surface layer bond distortions, leading to the breakdown of the surface reconstruction in certain cases. The lower π-bonded zigzag carbon atom chains that were not bonded to either oxygen atoms or hydroxyl groups experienced mainly expansion of between 0.63 and 3.2% of the bulk bond length, both in the presence and absence of the adsorbates as shown in Table 1.13. The largest expansions were associated mainly with the OH terminations. On the contrary, bonds within the upper π-bonded zigzag chains experienced varying degrees of expansion and contraction. Those within the clean surface suffered more contractions of about -6.7%, but upon adsorption of either a half ML of O atoms or OH groups, the contraction reduced to between -1.62 and -5% which showed good agreement with other DFT calculations [53]. The largest contraction of -5% was observed in the bonds within the most stable half ML

Oxygen & hydroxyl coverage & Adsorption Site (Monolayers-ML)	Bonds as shown in e.g. figures	Bonds within the lower π-bonded zigzag C-atom chains unbonded to O. (Marked as ***A***)	Bonds within the upper π-bonded O-termin. zigzag C -atom chains. (Marked as ***B***)	Bonds joining O- or OH-terminated C atoms in upper π-bonded zigzag chains to C atoms in lower π-bonded zigzag chains. (Marked as ***C***)	Bonds joining C atom in upper & lower π-bonded chains not bonded to O atoms. (Marked as ***D***)
Half ML clean DFT-[43] DFT-[75] X-ray-[47] DFT-[48] DFT-[53] DFT-[45]	Figure 1.30	1.59(1.23) (0.9) (0.7) (1) 1.53(-0.65) 1.525(-0.97) 1.54(0)	1.441(-6.4) 1.43(-7.1) (-3.1) (-5) 1.43(-7.1) -1.423(-7.6),1.420(-7.8) 1.42(-7.8)	1.539(-0.065) (-3) 1.54(0)	1.545(0.32) (2)
Full ONTOP-O	1.30	1.563(1.5)	1.974(28.2)	1.52(-1.3)	1.528(-0.78)
Full ONTOP-OH	1.30	1.59(3.2)	1.587(3.05)	1.573(2.14)	1.582(1.77)
Half ONTOP-O		1.558(1.17)	1.487(-3.44)	1.576(2.3)	1.493(-3.0)
Half ONTOP-OH	Figure 1.30	1.574(2.21)	1.515(-1.62)	1.506(-2.2)	1.624(5.45)
Half Bridge-O DFT-[53]	” ” ”	1.559(1.23) 1.55(0.65) 1.525(-0.97),1.527(-0.84)	1.463(-5) 1.55(0.65) 1.50(-2.6) -1.457(-5.3),1.498(-2.7)	1.535(-0.32)	-
Half ML site with starting geometry as bridge-bonded with -OH groups.		1.577(2.4)	1.515(-1.62)	1.661(7.86)	1.50(-2.6)

Table 1.13: Bond lengths (in Å) within the topmost π-bonded carbon-atom chains of (2×1) reconstructed diamond (111) surfaces, together with those joining them. These are shown for a clean surface and for those that were terminated with a full and half monolayer of oxygen atoms or hydroxyl groups at an ONTOP and bridge sites. The numbers in parentheses are the percentage changes relative to the C-C bulk bond length of 1.54Å.

bridge-bonded site with oxygens atom on a 2×1 reconstructed surface (i.e. the C-C bond length between the bridge-bonded oxygen atom), while the least (-1.62%) was seen within the surface terminated by a half ML of hydroxyl groups at the ONTOP site (i.e. the least stable configuration on a 2×1 reconstructed C(111) surface). The full ML coverages of OH groups or O atoms at the ONTOP sites, resulted in quite large expansions of between 3.05 and 28.2% of the bulk bond length, for bonds in the upper π-bonded chains, which certainly had the potential of disrupting the 2×1 reconstruction of the surface.

Our computed values for the C-C bond lengths of 1.441Å within the upper π-bonded zigzag chains of the clean surface were in good agreement with the corresponding experimental value of 1.45Å obtained from the LEED experiments of Sowa *et al.* [79]. The results of this study further showed that very small buckling and no dimerization of the surface carbon-atom bonds occurred on a clean (2×1) reconstructed C(111) surface, which agrees to a large extent with the findings of Kern *et al.* [48] and the LEED measurements of Walter et al [16]. This stems from the well known definition of the degree of dimerization which is expressed as $\Delta = (d - d')/d + d')$ with d and d' being the two bonds within the upper π-bonded chain. Based on this, our findings showed that this value was actually 0, since d'=d=1.441Å, implying that the structure of the clean (2×1) reconstructed C(111) surface was symmetric. A buckling of 0.0029Å was established in the upper π-bonded chain and 0.013Å for the lower π-bonded chain of a clean surface. Scholze *et al.* [43] reported finding a symmetric structure with vanishing buckling δ<0.01Å and almost no dimerization, which was in excellent agreement with our findings. Our calculated bond angles were also in good agreement with those obtained in these works as shown in all the optimized structural diagrams of the (2×1) reconstructed diamond (111) surfaces, with and without the adsorbates. Kern *et al.* [48] observed from their DFT calculations that the bond angles varied between 93.6 and 125.3°, meaning

that the distortions from the ideal tetrahedral bond-angle were smaller than in the ideal Pandey geometry, where the smallest and largest bond angles were 84.7 and 134.2°.

Our study further revealed that all the bonds within the lower π-bonded zigzag chains experienced some degree of expansion, but overall, not as large as the contractions observed in the upper π-bonded zigzag chains. The oxygen terminations tended to lead to contraction of the bonds within the upper π-bonded zigzag chains by fairly large amounts, although the observed expansions were still relatively lower than those of the clean surface, as shown in Table 1.13. Except for the bridge site terminated with oxygen atoms and the half ML ONTOP site with OH groups, all the other bonds joining the upper π-bonded zigzag carbon atom chains bonded to either O atoms or OH groups to the lower π-bonded zigzag carbon-atom chains experienced expansions which were much larger than the marginal contractions suffered by similar bonds in the clean surface. These expansions ranged between 2.3 and 7.8%, while those of the clean surfaces were only a mere 0.52% of the bulk bond length. Such expansions implied that the electron's cloud distributions within the adsorbate-carbon atom bonds tended to give rise to the stretching of the respective bonds, thereby leading to the breaking of the surface bond's symmetry.

Surface bonds joining the upper and lower π-bonded zigzag carbon atom chains that were not bonded to either oxygen atoms or hydroxyl groups experienced mostly contractions, except in the case of the half and full ML ONTOP sites terminated with OH groups. The contractions were relatively large, ranging between -0.78 and -3.0% of the bulk bond length. This alternate expansion and contraction of the surface bonds was again attributed mainly to the presence of the adsorbates, (since it wasn't so large for the clean surface) as the topmost carbon-atom layer relaxed either inwards or outwards in order to achieve optimum coordination that would suitably accommodate all of the

competing factors onto the surfaces. In the process, the bond angles as well as the orientations of the adsorbates themselves relative to the underlying carbon atoms changed quite significantly as shown in the various structural diagrams.

1.15 C-O, C=O, C-OH and O-H bonds on the (2×1) reconstructed diamond (111) surfaces.

Only the ONTOP sites of the full ML coverage with oxygen atoms and hydroxyl groups were considered, together with the ONTOP and bridge sites for the half monolayer coverages with oxygen atoms and hydroxyl groups. The ONTOP and bridge sites were chosen on the basis of previous studies that indicated these to be the most stable bonding sites on a (2×1) reconstructed diamond (111) surface.

The adsorption of oxygen atoms at the ONTOP site up to a full ML coverage resulted in C-O bond lengths of 1.195Å which clearly indicated that they were strong C=O bonds, when compared to the experimental value of 1.23Å, and these were inclined at 73.6° and 70.86° relative to the horizontal plane formed by the top π-bonded zigzag carbon atom layer. This was attributed possibly to the small buckling observed in the topmost carbon atom layer as shown in Table 1.14, which was related to the stretching of the surface bonds joining the upper and lower π-bonded chains of up to 1.58Å, compared to those of a clean surface which were 1.54Å and 1.545Å as summarized in Table 1.13. In addition, bonds joining the upper and lower π-bonded zigzag chains for surface terminated with O atoms were inclined at 51°, while those from the clean surface were inclined at 27°.

The adsorption of hydroxyl groups up to a full ML at the ONTOP site resulted in C-OH bonds that were 1.423 and 1.42Å as seen in figure 1.29 and summarized in Table 1.12. The two C-OH bonds were inclined at 69.65° and

	System	Buckling of lower π-bonds	Buckling of upper π-bonds	$\angle$between upper &lower π-bonded chains
This work	Clean	0.013	0.0029	26.9°
LEED-[16]	Clean	0.01	0.01	
X-ray-[47]	Clean	-0.10 [80]	0.3	
DFT-[48]	Clean	0.01	0.01	
This work	Full ML ONTOP:O	0.0129	0.0083	51°
	Full ML ONTOP:OH	0.001	0.0186	39.9/39.3°
	Half ML ONTOP:O	0.0228	0.164	32.2°
	Half ML ONTOP:OH	0.0238	0.200	29.9°
	Half ML bridge:O	0.008	0.0041	35°
	Half ML bridge:OH	0.0273	0.219	

Table 1.14: Computed buckling of the lower and upper π-bonded zigzag chains and the bond angles between the two.

64.4° to the horizontal plane formed by the carbon atoms within the upper π-bonded chains respectively, in order to optimize the OH-OH interactions due to such a high coverage. The corresponding O-H bonds were each 0.984Å and these were inclined at 111° to the C-OH bond. The adsorption of the OH groups resulted in the extension of the C-C bonds within the upper π-bonded zigzag carbon atom chains to 1.587Å, compared to those of the clean surface which were 1.44Å leading to a breakdown of the (2×1) reconstruction. Bonds within the lower π-bonded zigzag carbon atom chains were also extended slightly up to 1.59Å compared to those of the clean (2×1) reconstructed surface which were 1.56Å. The C-C bonds joining the upper and lower π-bonded zigzag carbon atom chains were 1.573Å and 1.582Å, with their respective inclinations to the lower π-bonded zigzag carbon atom chains being 39.3° and 39.9°. Those from the clean surface were 1.54Å and 1.545Å, with equal orientations of ∼27° to the lower π-bonded zigzag carbon atom chains, which again illustrated the effect of the adsorbates to the (2×1) reconstructed diamond's surface layers. Based on these findings, the (2×1) reconstruction was found to be disrupted after adsorbing a full ML of oxygen atom or hydroxyl groups at the ONTOP site. In

spite of this, the surface did not appear to have reverted completely to the true (1×1) bulk termination, and very small buckling of the upper π-bonded zigzag carbon atom chains was observed with the two adsorbates as shown in Table 1.14.

Following the adsorption of oxygen atoms up to a half ML at the ONTOP site of a (2×1) reconstructed surface, it was found that carbon atoms in the upper π-bonded zigzag chains, that were bonded to the oxygen atom were raised by a relatively large amount of 0.164Å while those within the lower π-bonded zigzag chains only suffered a negligible buckling of 0.0228Å. The resultant C-O bonds were perpendicular to the topmost carbon atoms within the rows, and 94.6° when considered in respect to the carbon atoms between the rows, yielding a small displacement of 0.131Å for the oxygen atom relative to the underlying C atom bonded to it, as shown in figure 1.30. With a bond length of 1.38Å, the C-O bond was much closer to the experimental value of a single C-O bond which is 1.36Å than the experimental double C=O bond of 1.23Å. The bond lengths observed were all in good agreement with those of other experimental and theoretical predictions such the findings of Loh *et al.* [53]. A summary of the inclinations angles of the bonds joining the upper and lower π-bonded zigzag carbon atom chains are shown in Table 1.14.

Up on terminating the ONTOP site with a half ML of hydroxyl groups, it was found that the C-O bonds were inclined at 112.2° to the topmost carbon atoms when considered between the atomic rows and 90° to the surface carbon atoms within the C-OH rows (see figure A.22 in Appendix A). This meant that the hydroxyl groups relaxed to new positions that were only slightly off those of the corresponding half ML ONTOP:OH site. A possible contributing factor to this movement could have been the orientation of the OH group arising from the OH-OH interactions, though the coverage was still lower than that of a full ML where this effect was expected to be strongly felt. The true (2×1) surface

reconstruction was not preserved after adsorbing a half monolayer of hydroxyl groups at the ONTOP site. In particular, the bonds within the topmost zigzag chains that were bonded to the hydroxyl groups were found to extend to 1.516Å compared to those of the clean slab with no adsorbates, which are 1.441Å. The bonds within the lower π-bonded zigzag chains did not experience much change, only differing by 0.019Å from those of the clean slab as shown in figures 1.27 and A.22. The optimized C-OH bond length was 1.45Å, showing a great deal of closeness to the experimental value of 1.43Å, and also the one obtained from the DFT calculations of Theije *et al.* [60]. The final optimized structure of the OH groups that were initially adsorbed at a half ML ONTOP site was one where the topmost π-bonded carbon-atom chains were buckled by 0.2Å while the lower ones only experienced a small buckling of 0.0233Å possibly due to the lack of the adsorbates influence, in spite of their close proximity. As a result of the upwards relaxation of the topmost carbon atoms that were bonded to the hydroxyl groups, the surface bonds joining them to the carbon atoms within the lower π-bonded zigzag chains also suffered some significant elongation. This resulted in these bonds extending to 1.624Å, as opposed to those of the clean surfaces which were 1.548Å, indicating some degree of bond weakening and possible breakdown of the (2×1) surface symmetry. Such bonds were inclined at 30° relative to the lower π-bonded zigzag chains compared to $\sim$27° for the clean surface, while others are summarized in Table 1.14. Based on the optimized bond lengths, the adsorption of oxygen atoms at the half ML bridge site of a (2×1) reconstructed surface did not result in the lifting of the (2×1) reconstruction. Instead, the bond lengths within the upper π-bonded zigzag chains between the adsorbed oxygen atom extended by a small value to 1.463Å, compared to 1.441Å for the clean surface. Nonetheless, the C-C atom bonds within the upper π-bonded zigzag carbon-atom chains that were not bonded to the oxygen atoms became longer, extending upto 1.50Å as shown in figure 1.31

compared to a value of 1.441Å for the clean surface. The optimized C-O bonds were 1.44Å, and these were inclined at 59.4° to the underlying carbon-carbon atom bonds, while the angle at the apex between the carbon-oxygen-carbon (∠COC) angle was 61° as seen from figure 1.31. This was in good agreement with the observations of Loh *et al.*[52] who obtained a C-O bond length of 1.434Å and a ∠COC angle of 61.1°. Very minimal upwards displacement was observed within the carbon atoms in the two topmost π-bonded zigzag chains, mainly because all the dangling bonds were already terminated with oxygen atoms in this coverage. These differed by negligible values of 0.008 and 0.0041Å for the lower and upper π-bonded chains respectively, meaning that the adsorption of the oxygen atoms at the bridge site quenches the buckling witnessed in other cases, especially when there are no dangling bonds.

1.15.1 Changes in the work function of the bulk terminated (1×1) diamond (111) surface due to the adsorbed O atoms and/or OH groups.

In their work on diamond surfaces, Himpsel *et al.* [81] and Baumann *et al.* [51] found that surfaces of wide band gap semiconductors like diamond posses the potential to exhibit negative electron affinity(NEA) because their conduction band minimum is very close to the vacuum level. This means that electrons present in the conduction band have sufficient energy to overcome the work function of a NEA surface and be emitted into the vacuum. They further state that different surface terminations and adsorbates have the ability to shift the position of the bands with respect to the vacuum level and hence induce NEA or remove it all together. For this to happen, the adsorbates cause changes in the surface dipole, leading to an increase or decrease of the surface's electron affinity. It has already been shown that hydrogen induces NEA on diamond (111) and (110) surfaces, while oxygen on the other hand gives a dipole that

results in positive electron affinity (PEA) on the two surfaces [50]. Rutter *et al.* [50] observed that surfaces terminated by hydroxyl groups exhibited a negative electron affinity, in spite of the presence of the oxygen atoms. Clean diamond (111) surfaces terminated by single dangling bonds have also been said to posses PEA, owing to the orientation of the surface dipole. All these changes in the electron affinities have a direct bearing on the work function of such surfaces. This section investigates the role of O atoms and OH groups on the work function of C(111) surfaces when these are adsorbed at different sites and for various coverages, in relation to that of the clean surface. This is motivated by the need to establish how the work function changes with respect to the two parameters.

Previous studies have tended to concentrate mainly on the role of the oxygen atoms and hydroxyl groups, in relation to the surface properties for higher monolayer coverages above say 0.5ML. No efforts have so far been made to extend this to lower coverages, meaning that certain surface properties such as electron affinities or even work functions for those surfaces with generally much lower adsorbate coverages than 0.5ML have not been adequately probed. A major part of this study seeks to establish among other things the relationship between the work function and the coverages due to the adsorbed oxygen atoms as well as the hydroxyl groups, starting with a layer of a full ML coverage of each, up to a quarter ML. The sites investigated included the ONTOP, bridge, hexagonal close packed and the face centred cubic one. The initial investigations are focussed on the bulk terminated (1×1) surface and then extensions are made to the (2×1) reconstructed (111) diamond surface.

The dipoles observed on diamond surfaces have been attributed variously to the presence or absence of the adsorbates, which leads to the observed electronegativity due to specific adsorbing species, as well as the symmetry of the charge distribution at a given site. Both hydrogen and oxygen terminated sites

on diamond surfaces have been shown to be asymmetric [82], leading to additional dipole effects, which in turn affects the electron affinity. In particular, the lone pair orbitals of oxygen extending from the surface are expected to increase the work function, and similarly, an adsorbate free surface would exhibit dangling bonds resulting in dipole of the same polarity as that of an oxygen terminated surface, while hydrogen adsorption results in a dipole that lowers the work function.

Initial calculations involving three different sizes of clean slabs showed that there wasn't much differences in the values of their work function as seen in Table 1.3, probably due to the fact that they all exhibited the same number of dangling bonds per surface carbon atom, except some minor differences that could be attributed to the changes within the bond lengths, symmetry etc. These small differences were found to vary in such a way that the super cell for the third monolayer clean surface had a marginally higher value of the work function, followed quite closely by those used for calculations involving the quarter monolayer coverage, and finally those associated with the full/half monolayer clean surfaces. The differences from each other were rather small and almost negligible, with a value of 0.0476eV being established between the work function of the clean surfaces associated with the third and quarter monolayer coverages, and 0.0668eV between that of the third and full or half monolayer coverages. These differences were additionally much smaller than those found between the clean surfaces and those terminated with oxygen atoms. Tables 1.15 to 1.17 show the values of the work function for (1×1) bulk terminated surfaces terminated with different adsorbates together with those of the clean surfaces, while Table 1.19 shows similar results for the (2×1) reconstructed C(111) surface. These values were then plotted against the respective coverages as shown in figures 1.32 for the most stable configurations, and A.23 (shown in

Appendix A) for all the sites and coverages considered in this study. These values are for the workfunction of the (1×1) bulk terminated C(111) surface, while figure 1.33 shows the changes in the workfunction for the (2×1) reconstructed C(111) surfaces. Based on the computed values of the work function and fig-

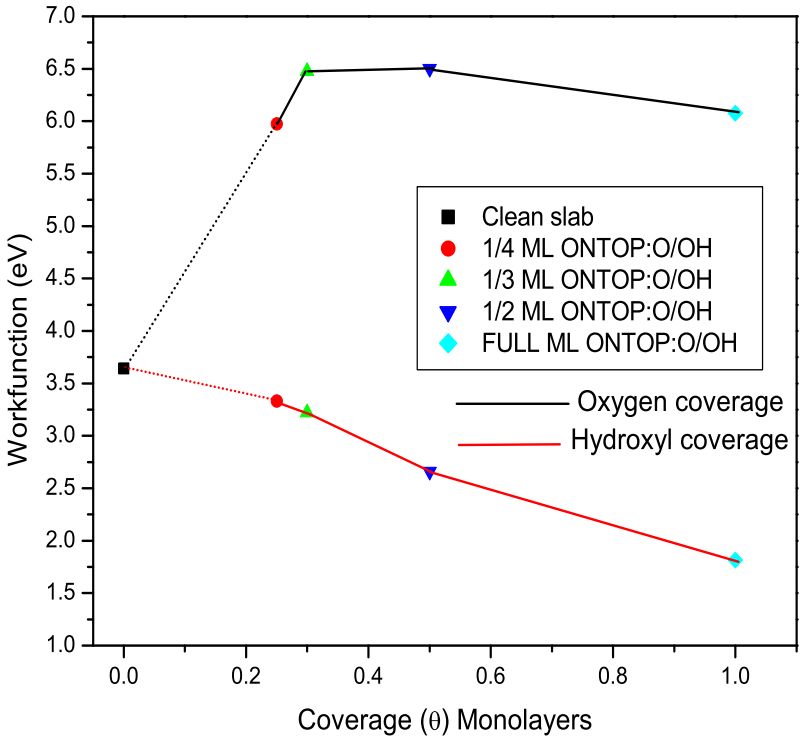


Figure 1.32: Workfunction for the most stable configurations of O and OH on the (1×1) surface plotted with the coverage.

ures 1.32 and A.23, it was concluded that both oxygen atoms and hydroxyl groups had a remarkable effect on the work function of the surfaces, in relation to that of the clean surfaces. It was further found that, while the adsorption of hydroxyl groups lowered the work function compared to that of the clean surfaces, adsorption of oxygen atoms on the other hand did the opposite by increasing it as shown in figures 1.32 and A.23 for the (1×1)-C(111) surfaces. The highest and least changes in the work function were observed in the half

monolayer ONTOP site terminated with oxygen atoms, and the full monolayer ONTOP site terminated with hydroxyl groups respectively.

Some general decrease in the work function was further established in the case of the full monolayer co-adsorptions, especially in the case of the adsorption of the hydroxyl groups at the hexagonal close packed and bridge sites. This implied that co-adsorption of different groups at various sites contributed to the lowering of the workfunction, although this may not necessarily be the case always as seen in the co-adsorption of oxygen atoms at the ONTOP and HCP sites. A reason for this was the resultant surface dipoles in the two cases and it suggested that the adsorption of the same species, be it atoms or a group of atoms at different sites may actually result in some relatively marginal decrease of the overall work function, even when this involves oxygen termination, which is ironically known to contribute towards its increment, and hence the reported PEA of such surfaces. This means that other factors may be acting and hence, while the adsorption of oxygen atoms increases the work function and the hydroxyl groups decreases it, the co-adsorption of both oxygen and/or hydroxyl groups at different sites would contribute towards the overall lowering of the work function, when compared to a situation where the surface was only terminated by a single species such as oxygen atoms. Clearly, the surface dipoles, and any other effects acting together with the corresponding charge distributions around the different sites would vary, leading to the observed changes in the work function. Adsorbing hydroxyl groups at an ONTOP site in the case of the full monolayer coverage resulted in relatively large reductions of the work function, when compared to that observed in the case of a full monolayer coverage with oxygen atoms at an ONTOP site as shown in Table 1.15.

The situation changes quite a lot in the case of the half monolayer coverages at different sites, probably due to the presence of the dangling bonds and the resultant C-O, C-OH, O-H or even the relaxed surface C-C bonds. Adsorbing

oxygen atoms at an HCP and an ONTOP site was found to increase the work function slightly above that observed in the case of full monolayer coverage. As a result, the highest change in the work function for the half monolayer coverages with oxygen atoms was established in the adsorption of oxygen atoms at an ONTOP site, followed quite closely by the hexagonal close packed site, then the face centred cubic site, and finally the bridge site. A significant amount of change in the surface symmetry of some of the surface bonds occurred, which obviously in turn contributed to the observed changes in the work function as observed before. Comparing all the four half monolayer coverages terminated with oxygen atoms, a difference of about 2.33eV was found between the highest (half ML ONTOP:O) and lowest (half ML bridge:O) values of the work function. This was incidentally twice the difference of 1.165eV found in the case of the full monolayer oxygen adsorptions.

All the half monolayer sites terminated with hydroxyl groups showed a general decrease in their values of work functions when compared to those of the corresponding oxygen adsorption sites. The values were even lower than those of the clean surface, suggesting a clear possibility of the surfaces possessing NEA. Table 1.15 shows that, the half monolayer ONTOP site terminated with hydroxyl groups had the least value of the work function, followed by the bridge site, then the hexagonal close packed site, and the highest value was established in the case of the face centred cubic site. In spite of this difference though, all the OH terminated surfaces had much lower values of work function than their corresponding half ML oxygen terminated surfaces. A possible explanation for this order of change in the work function was again due to the asymmetry of the charges about the various bonding sites as mentioned before, as well as some bond distortions as witnessed in the surface layers (structural diagrams).

A replica of almost what was observed in the half monolayer coverages was found in the quarter monolayer coverages, although the values obtained for the

work function were generally much lower than those observed in the case of the full monolayer coverages. Here, all the oxygen terminated surfaces had higher work function values compared to those of the corresponding ones from the surfaces terminated with hydroxyl groups. As such, it was found that the work function in the case of the quarter ML coverages with oxygen atoms decreased, following the order; quarter ML ONTOP:O >quarter ML HCP:O>quarter ML FCC:O>quarter ML Bridge:O. Out of the four bonding sites, the work function for surfaces terminated by a quarter monolayer of oxygen atoms at the ONTOP and HCP sites were relatively higher than those of the FCC or bridge sites. The work function of the former two was very close to each other, with a difference of only 0.1223eV being established while for the latter two it was quite close, with a difference of 0.1489eV being found between their respective values of work functions. One may therefore conclude that the surface dipoles developed in each of the two cases had almost similar character, and hence the observed similarities. This was again not too surprising since the structural diagram shown in figure A.10 (in Appendix A) for the quarter ML site terminated with oxygen atoms at the HCP site shows that up on relaxation, the adsorbed oxygen atoms moved quite a lot, and finally settled at positions that were quite close to those of the ONTOP site as seen in figure 1.22, except for the minimal tilt of the C-O bond of 14° from the surface normal.

The values of the work function in the case of the quarter ML hydroxyl terminations were not very different from each other and therefore showed little scatter unlike the oxygen terminations. Except in the case of the bridge site, all the other quarter monolayer(ML) hydroxyl terminations had their work function values being generally lower than those of the clean unterminated surface. These differed by a value of 0.9415eV between the highest and lowest values. As such, comparing the change observed in the work function values for all the quarter ML hydroxyl terminations, it was found that they increased from the quarter

ML FCC:OH site, to the quarter ML ONTOP:OH site, then the quarter ML HCP:OH, and the highest value was registered in the quarter monolayer bridge site terminated with hydroxyl groups. This order was completely different from that of the quarter ML O terminations. In addition, the results appeared to suggest that the work function was somehow tied to the suitability of a given bonding site, since among other factors, the strong bonds would tend to offer more resistance to the extraction of electrons from there, and vice versa for the unfavourable bonding sites.

The third monolayer oxygen terminations at the ONTOP and hexagonal close packed sites showed values of their work functions being relatively higher than those of the other third ML sites. These were the sites with the highest values of adsorption energies (discussed later in section 1.16) in the case of the third monolayer coverages (and hence most stable), just like in the case of the quarter and half ML coverages. The values of the work function were also quite close to some of those observed in the half and full monolayer coverages. Incidentally, the changes observed in the values of the work function for the two sites (ONTOP and HCP) were very close to each other, which again confirmed that the surface dipoles in the two cases were almost quite similar in character and/or alternatively had properties that made them behave in the same way. On the contrary, although the values of the work function for the face centred cubic and bridge sites were also quite close to each other, they were generally much lower than those of the hexagonal close packed and the ONTOP sites, and their values incidentally almost approached those of the clean surface. As such, the order of the increase in the work function of the third ML coverages with oxygen atoms was, the Third ML ONTOP:O >Third ML HCP:O>Third ML FCC:O>Third ML Bridge:O site.

Just like in the case of half and quarter monolayer coverages, the work function was also lowered by the adsorption of hydroxyl groups at different sites in

the case of third monolayer coverage. However, unlike the quarter monolayer coverage where one value of the work function for an hydroxyl termination was higher than that of the clean surface, in the case of third monolayer coverage, all the hydroxyl groups lowered the work function values below those of the clean surfaces. This meant that the resultant surface dipole due to the adsorbed hydroxyl groups behaved more or less like that of the hydrogen atom as mentioned earlier. The difference between the highest and the lowest values of the work function in the case of third monolayer hydroxyl termination was not as large as that between the surfaces terminated with oxygen. For the third ML hydroxyl terminations, the work function was least in the case of a third monolayer HCP site terminated with hydroxyl, followed by the bridge site, then the face centred cubic site, and finally the ONTOP site. A detailed plot of the work function versus coverage/site is given in figure A.23 which is shown in Appendix A. What was interesting in this case though was the fact that the decrease in the work function did not necessarily imply a weak bonding site as seen from Table 1.17 as far as the adsorption of hydroxyl groups on diamond surfaces was concerned. The adsorption energies of the third ML sites terminated with OH groups for the four sites were surprisingly very close to each other, differing by only 0.316eV between the highest and lowest values, while the changes in the work function between the highest and lowest values differed by 0.4073.

By lowering the work function, it became evident that the adsorption of the hydroxyl groups created a surface dipole that modified the electronic structure around the surface atoms, thereby making it easier to extract electrons from these sites. In addition, depending on the surface dipoles, changes reported earlier in the bond lengths of the adsorbed hydroxyl groups, and the corresponding C-OH bonds as well as the C-C bonds joining the surface carbon atoms could all have easily contributed towards the aligning of the surface dipoles in a way that favoured the lowering of the work function.

There was therefore no doubt that, the surface dipoles developed as shown in the structural diagrams of figures 1.16 to 1.26 and in figures A.1 to A.20 (shown in Appendix A for C(111)-(1×1) surfaces) together with the asymmetry of the bonds and their various lengths (especially the surface ones) played a major role, with regard to the changes observed in the work function values, as well as the resultant electron affinities. The inclinations of the adsorbed hydrogen atoms from the OH groups changed the orientation of the C-O bond, and therefore influenced the charge distribution within its vicinity and by extension the surface dipole, which was effectively responsible for the observed changes in the work function.

1.15.2 Changes in the work function of (2×1) reconstructed diamond (111) surfaces terminated with O and OH adsorbates compared to that of a clean one.

Figure 1.33 shows a plot of the work function for a (2×1) reconstructed C(111) surfaces terminated with either a full or half ML of oxygen atoms and hydroxyl groups at a bridge or an ONTOP site. Both the oxygen atoms and hydroxyl groups affected the work function of the reconstructed surface in a manner that was similar to that observed on the (1×1) bulk terminated surface, with regard to the specific roles played by each of the two adsorbates. In this case, the oxygen atoms contributed towards the raising of the work function, thereby making the surfaces to exhibit a positive electron affinity, while those terminated with hydroxyl groups had lower values of the work function, which gave rise to the possibility of such surfaces having a negative electron affinity. The changes observed in the work function were referenced to that of the clean surface, which is known to posses positive electron affinity [48]. Although few sites and coverages were considered here as opposed to the bulk terminated cases, out of these only the full and half ML ONTOP sites terminated with OH groups

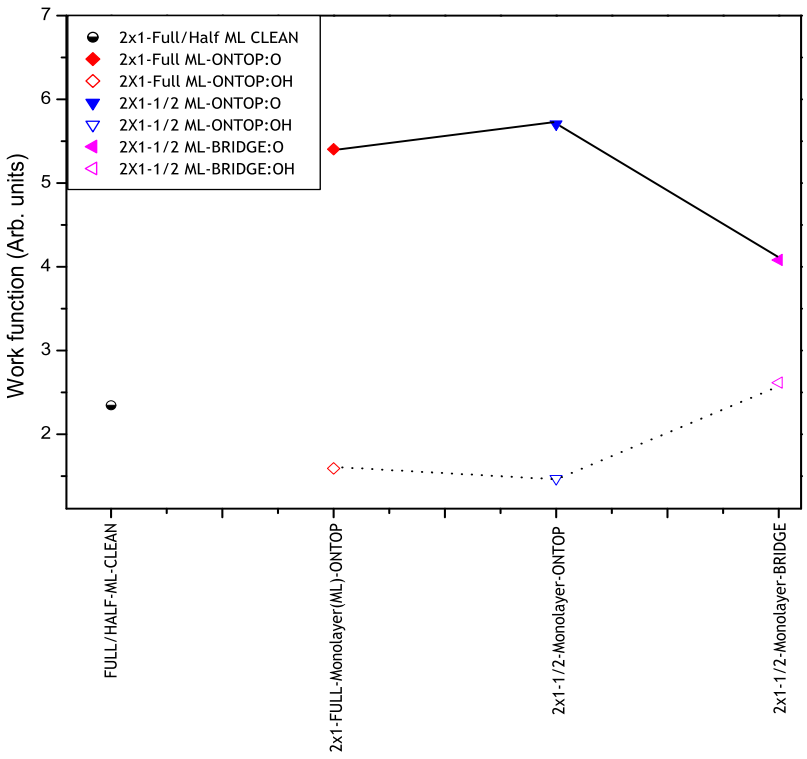


Figure 1.33: Work function (eV) for various sites and coverages of a (2×1) reconstructed C(111) surface. The shaded symbols represent the work function for surfaces terminated with oxygen atoms, while the open ones represent the work function from the hydroxyl terminated surfaces. The half-shaded circle shows the work function of a clean surface.

resulted in work function values that were lower than that of the clean surface. For the adsorbed oxygen atoms, the increase in the work function was much lower in the case of the half monolayer (2×1):O terminated surface compared to that of the corresponding (1×1):O terminated surface. It was also found that the work function values were relatively much lower than those of the corresponding half monolayer coverages associated with the bulk terminated (1×1):OH diamond surfaces, especially the one from the ONTOP site. The largest difference between the work function of any two given corresponding sites terminated alternately with oxygen atoms and hydroxyl groups was found

in the case of the half monolayer (2×1) reconstructed ONTOP sites (4.2354eV), while the half monolayer bridge site presented the lowest value for the difference (i.e. $\Delta\Phi$:O-$\Delta\Phi$:OH) of 1.465eV (see Table 1.19 and figure 1.33).

By comparing the values of the work function of the (2×1) reconstructed surfaces terminated with various half ML oxygen atoms or hydroxyl groups at the ONTOP or bridge sites with those of the (1×1) bulk terminated surface, it was found that the work function decreased from the half monolayer (1×1):O ONTOP site> half monolayer (2×1):O ONTOP site >half monolayer (1×1):O bridge site> half monolayer (2×1):O bridge site>half monolayer (1×1):OH bridge site>half monolayer (2×1):OH bridge site>half monolayer (1×1):OH ONTOP site> half monolayer (2×1):OH ONTOP site. This clearly demonstrates the fact that the work function of the surfaces due to the adsorbed O atoms was always higher than that of surfaces terminated with OH groups in any given situation. This again was attributed mostly to the resultant surface dipoles. The influence of other factors such as steric hindrance, bonds asymmetry, lack of sufficient coordination in the half ML coverages and also the presence of the adsorbates themselves and the reconstructed nature of the (2×1) also contributed somewhat towards the changes observed in the values of the work function. In particular, the effect of the steric hindrance was possibly stronger for higher coverages such as the full and half monolayers, and then got less and as the coverage was decreased to third and quarter monolayers (for the (1×1) terminations).

Pickett [83] investigated previously the negative electron affinity and low work function of a surface due to Cesium on oxygenated diamond (100) surface, where he showed that addition of Cesium on an full monolayer of ether bonded oxygen resulted in an effective negative electron affinity. His finding led to the conclusion that lowering the work function which was due to the shifting of the surface dipole did indirectly or directly lead to the the observed negative electron

affinity . At the same time, van der Weide *et al.*[70] indicates quite explicitly that lowering of the work function causes the diamond (111) surfaces to exhibit a negative electron affinity which gives more credence to our earlier assertions on the relationship between the surfaces's electron affinity and the work function. When a surface attains a NEA (which in this case is closely related to low work function), the secondary electrons which are thermalized to the conduction band minimum get emitted, and then appear as sharp peaks in the photoemission spectra. Based on these arguments, we were able to conclude from our findings that the lowering of the surfaces's work function with different terminations indicated that such surfaces probably possessed NEA, while the opposite was true for those cases where the work function increased, which would induce a PEA, though marginally. It was further found that both the oxygen atoms and the hydroxyl groups terminations on the (1×1) surfaces resulted in higher values of work function than their corresponding sites and coverages on the (2×1) reconstructed surfaces. Just like in the bulk terminated (1×1) surface, the two different electron affinities were again speculated (not tested here) to be quite closely intertwined to the changes observed in the work function, and hence the corresponding sites, configurations, and monolayer (ML) coverages. This study therefore shows that devices utilizing different but suitable electron affinities can easily be fabricated by taking advantage of the various values of work function and hence the corresponding electron affinities associated with each species, site or coverage as established in this study.

1.16 Total and adsorption energies of oxygen atoms and hydroxyl groups, adsorbed at different sites and coverages on bulk terminated C(111) surface.

In order to establish the preferred bonding sites and optimum coverages for oxygen atoms and hydroxyl groups on C(111)-(1×1) surfaces, the systems's total minimum energy and adsorption energies of the two adsorbates were computed, thus giving us the systems ground state conditions. As mentioned before, the sites considered were the ONTOP, bridge, hexagonal close packed, and the face centered cubic sites, while the coverages were full, half, third and quarter monolayers of each of the two adsorbates at the respective sites. Results obtained are shown in Tables 1.15, 1.16 and 1.17 which include the computed total minimum energies, the adsorption energies, and the changes in the work function of the clean surfaces as well as those terminated with oxygen atoms or hydroxyl groups. We considered both the bulk terminated (1×1)-C(111) surfaces as well as those of the (2×1) reconstructed surface, but in this sections only the results of the bulk terminated surfaces are reported while those of the (2×1) reconstructed C(111) surfaces are reported later in section 1.16.1. By comparing the total energies and the adsorption energies of different systems, we were able to deduce the most stable configurations, and hence suitable for bonding. In this case, a comparison of the total and adsorption energies showed that, with an adsorption energy of $\sim$ -5.58eV/atom and a total energy of -376.84H, the third monolayer ONTOP site terminated with oxygen atoms was the most preferred bonding site in the all cases that were investigated in this study for the bulk terminated (1×1):O or (1×1):OH configurations. This agreed quite well with our earlier XPS findings that are reported in the XPS chapter of this thesis. The least favoured bonding site for both O atoms and OH groups on the (1×1) bulk terminated surfaces was the half monolayer face centered cubic

(FCC) site terminated with hydroxyl groups, whose adsorption energy was only -1.8718eV/atom.

Coverage & Adsorption Site (Monolayers)	Total Energy E_{tot}(Hartree)	$E^{O}_{adsorption}$ (eV/atom)	$\Delta\Phi$(work function) (clean surface) (eV)	$\Delta\Phi$(work function) -O or OH term. (eV)
clean super cell for- Full and half	-114.97412		3.6131	
Full ONTOP-O	-146.86123	-5.0066	3.6131	6.07575
" " DFT [53]		-4.24		
Full ONTOP-OH	-148.15987	-4.3264	3.6131	1.8155
" " DFT ([53]		-4.34		
Full ONTOP and HCP-O	-146.81416	-4.366	3.6131	4.9971
Full HCP and Bridge-OH	-148.16410	-4.384	3.6131	2.0253
Half ONTOP-O	-130.92857	-5.3030	3.6131	6.5030
Half ONTOP-OH	-131.56773	-4.3462	"	2.5239
Half Bridge-O	-130.90745	-4.7283	"	4.1725
Half Bridge-OH	-131.58045	-4.6924	"	2.6339
Half HCP-O	-130.92762	-5.2772	"	6.3887
Half HCP-OH	-131.58202	-4.7351	"	2.6603
Half FCC-O	-130.83325	-2.7092	"	5.9765
Half FCC-OH	-131.47685	-1.8718	"	3.3925

Table 1.15: Calculated DFT-GGA total minimum energies, adsorption energies, and work function values for various full and half monolayer coverages of oxygen atoms and hydroxyl groups at different sites on (1×1) bulk terminated (111) diamond surfaces. A plane cut-off energy of 50Ry was used, and the corresponding total energy of the oxygen atom at the same cut-off energy was 15.70077Hartree, while that of the hydroxyl group was -16.41753Hartree. The most stable configurations for each coverage with O atoms or OH groups are bolded.

Coverage & Adsorption Site (Monolayers)	Total Energy E_{tot}(Hartree)	$E^{O}_{adsorption}$ (eV/atom)	$\Delta\Phi$(work function) (Clean surface)	$\Delta\Phi$(work function) -O or OH term.
Quarter clean-super cell	-229.94554		3.6322	
Quarter ONTOP-O	-245.90988	-5.5722		5.9740
Quarter ONTOP-OH	-246.55216	-4.7003		3.2912
Quarter Bridge-O	-245.8846	-4.8843		4.0147
Quarter Bridge-OH	-246.55018	-4.6464		3.7847
Quarter HCP-O	-245.90515	-5.4434		5.8517
Quarter HCP-OH	-246.55222	-4.7019		3.3320
Quarter FCC-O	-245.8912	-5.0638		4.1636
Quarter FCC-OH	-246.47514	-2.6044		2.9332

Table 1.16: Calculated DFT-GGA total minimum energies, adsorption energies and work function values for various quarter monolayer oxygen and hydroxyl coverages at different sites on a (1×1) bulk terminated (111) diamond surface. A similar value for the plane wave cutoff and total energy for an oxygen atom and the hydroxyl group as in Table 1.15 was used.

Coverage & Adsorptio Site (Monolayers)	Total Energy E_{tot}(Hartree)	$E^{O}_{adsorption}$ (eV)	$\Delta\Phi$(work function) (Clean surface)	$\Delta\Phi$(work function) -O or OH term.
Third Cov. clean-super cell	-344.91152		3.6798	
Third ONTOP-O	-376.84083	-5.580733		6.4777
Third ONTOP-OH	-378.12874	-4.7546		3.2200
X-ray meas. [42]		4.2±0.8		
Experit. [66]		-4.5		
Third Bridge-O	-376.7839	-4.806155		3.9705
Third Bridge-OH	-378.12781	-4.742		2.9474
Third HCP-O	-376.81624	-5.24617		6.0714
Third HCP-OH	-378.12520	-4.706		2.8127
Third FCC-O	-376.78301	-4.794016		3.9803
Third FCC-OH	-378.11905	-4.623		3.2026

Table 1.17: Calculated DFT-GGA total minimum energies, adsorption energies and work function values for various third monolayer oxygen and hydroxyl coverages at different sites on a (1×1) bulk terminated (111) diamond surface. A plane cut-off energy similar to that shown in Table 1.15 was used, and the values of the total energies for the oxygen atom and hydroxyl group were also the same as those shown in Table 1.15. The most stable configurations with O atoms or OH groups are bolded.

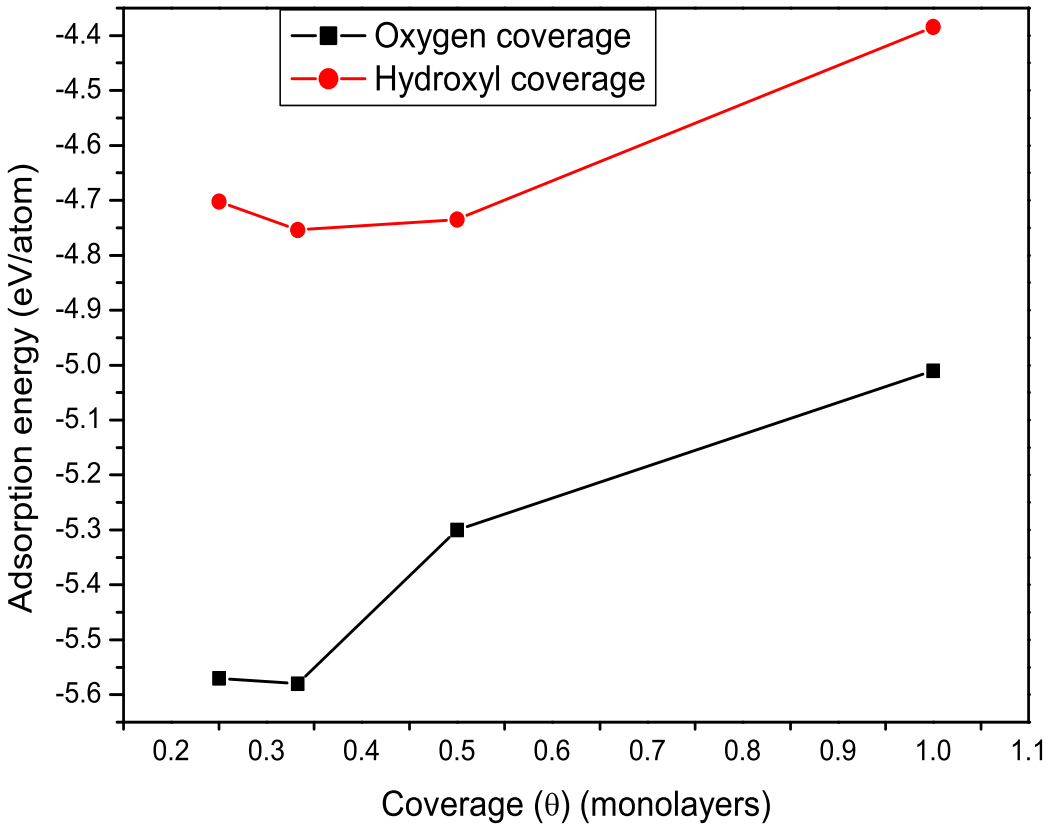


Figure 1.34: Adsorption energy versus coverage for the most stable coverages of oxygen atoms and hydroxyl groups on C(111)-(1×1) surfaces.

From the theory of bonding, it well known that the process is greatly enhanced when partially occupied orbitals of similar energy interact. Based on this premise, it would appear as though the unsuitability for bonding of certain sites, and especially the FCC ones may have arisen from the fact that the anti-bonding states somehow dominated over the bonding ones, and therefore making the sites generally unstable.

The most stable configurations on the C(111)-(1×1) surfaces for each coverage with O atoms or OH groups were extracted and summarized as shown in Table 1.18 for easier assimilation of the results, and then plotted in figure 1.34

in order to get a clearer picture of how the stability of the sites varied with the coverage of the two adsorbates.

Coverage (Monolayers)	Adsorption energy O-termination(eV/atom)	Adsorption energy OH-termination(eV/atom)
0.25	-5.57	-4.702
0.33	-5.58	-4.754
0.5	-5.30	-4.735
1.0	-5.01	-4.384

Table 1.18: Adsorption energies of the lowest energy configurations per coverage for O and OH species on the bulk terminated (1×1)-C(111) surface.

Both the two representations (figure 1.34 and Table 1.18) showed that a repulsion between the oxygen adsorbates on the bulk terminated (1×1)-C(111) surface started at coverages greater the 0.33ML, while for the hydroxyl termination, it was not until coverages greater than 0.5ML that the system got less stable due to the OH-OH interactions.

In terms of the respective coverages, it was found that in the case of the full monolayer coverage, the ONTOP site with oxygen atoms was the most favoured bonding site, followed quite closely by the co-adsorption of hydroxyl groups at an (initial) HCP and bridge sites (whereby the OH groups drifted up on system relaxation to almost ONTOP sites as shown in figure 1.18). This was followed by the co-adsorption of oxygen atoms at the ONTOP and HCP sites, and the least likely bonding site for the full ML coverage was the adsorption of a full monolayer (ML) of hydroxyl groups at the ONTOP site. This was quite an interesting result because the co-adsorption of OH groups at the HCP and Bridge sites was found to result in them relaxing to positions that approximated the ONTOP ones, which were incidentally quite stable for the OH groups. The only difference between this and the adsorption of the OH groups at the actual ONTOP site was the orientation of the H atoms after the system relaxation. These oriented themselves in a staggered way that led to the sites being quite stable. Other than the adsorption of oxygen atoms at the ONTOP site, the

adsorption energies of the other full ML sites and coverages were found to be very close to each other, as shown in Table 1.15, differing by a mere 0.0596eV between the most and least stable sites.

Since the ONTOP site terminated with oxygen atoms was the most preferred bonding site in the case of the full ML coverages while the hydroxyl group termination was the least favoured one, it was quite clear that the hydrogen atom bonded to the oxygen atom from the hydroxyl group played a key role towards the making of this site unstable for OH bonding. In particular, the C-OH bond was found to be longer than the C-O one, and therefore weaker especially with the many adsorbate atoms repelling each other. The closeness of the adsorption energies that was observed in all the other full ML sites, except the ONTOP:O site suggested that in the presence of either oxygen atoms or hydroxyl groups, any of these adsorption sites was suitable for bonding, and therefore the different terminations may actually coexist on the same surface as we have demonstrated. These observations were not only in good agreement with our earlier XPS studies where we showed the possibility of co-adsorption of O atoms and OH groups, but also with other experimental and theoretical findings [60] such as those of Zheng *et al's* [44].

More adsorption sites were considered in the case of the half ML coverages than the full ML since it was felt that the lower coverages may have been favoured over the higher ones, on account of our previous experimental work. Unlike the full ML coverages, almost all the half ML sites, except the FCC one were found to be suitable for bonding by the oxygen atoms or hydroxyl groups, with most sites exhibiting high adsorption energies. The ONTOP site terminated with oxygen atoms was found to be the most likely bonding site with an adsorption energy of -5.303eV/atom, followed by the hexagonal close packed site terminated with oxygen atoms or hydroxyl groups, then the bridge site terminated with oxygen atoms or hydroxyl groups respectively, the half ONTOP

site terminated with hydroxyl groups, and finally the FCC site terminated with oxygen atoms and hydroxyl groups respectively. It is nonetheless important to note that, atoms adsorbed at the half ML HCP sites moved up on system relaxation to new sites that were quite close to the ONTOP site. A similar trend was also observed in the half ML bridge bonding sites with hydroxyl groups, and therefore it was not surprising that the adsorption energies for these sites were quite close, since all were practically almost the same (structurally) after relaxation.

For the much lower coverages such as quarter ML sites, it was observed that in the presence of environments containing oxygen atoms or hydroxyl groups, the oxygen atoms would prefer to bond at a quarter ML ONTOP site, while the hydroxyl groups would most likely bond at an HCP or the ONTOP sites without much preference or energy barrier between the two. Again, this was due to the fact that the adsorbates at the HCP site moved to new sites after relaxation, that resembled those of the ONTOP one as shown in figures 1.23 and A.9, with the only difference being the orientation of the hydrogen atom relative to the underlying oxygen atom. In fact, the C-OH bond for the new 'HCP'site was only inclined at 85.9° to the vertical plane, while that of the ONTOP site was inclined at 88.2° to the vertical axis, illustrating some important resemblance between the two sites after relaxation. Furthermore, both the total energies and the adsorption energies for these two sites were so close as seen from Table 1.16 that it was extremely difficult choosing which among the two would be preferred by the OH groups over the other. However, since the OH groups drifted towards the ONTOP and not the HCP site, it was evident that the ONTOP site was more stable.

The oxygen atoms were found to least prefer bonding at the quarter ML bridge site, while the hydroxyl groups at the FCC site. This was attributed to

the stoichiometry of the respective bonding sites and species, which was associated with the number of available bonding electrons on each atom. The order of preference in bonding of the oxygen atoms within the quarter ML coverage was, the ONTOP:O site, the HCP:O site, the FCC:O site, and finally the bridge:O site. Incidentally, unlike in the case of the full and half ML coverages, the FCC site was actually a preferred bonding site for the oxygen atoms in the case of the quarter ML coverage, where it resembled very much the bridge site in its relaxed state, but unfortunately not so for the OH groups. The C-OH bond in the quarter ML FCC site were much elongated compared to the C-O bonds from the surface terminated by oxygen atoms only. However, the position of both the O atoms and the OH groups relative to the underlying carbon atoms was almost identical as seen from figures A.13 and A.14.

Unlike the oxygen atoms, the hydroxyl groups preferred bonding at the quarter ML HCP:OH site, followed by the ONTOP:OH site, then the bridge:OH site, and least of all, the FCC:OH site. In fact, the adsorption energy for the FCC:OH site was so low compared to that of the other sites that it may actually be exempted as a likely bonding site.

Terminations with oxygen atoms were generally more preferred over those of the hydroxyl groups in all cases involving the quarter ML coverages. This could have been due to the reduced density of the adsorbates on the respective surfaces, which in turn led to lowering of the repulsive O-O interactions.

The bonding preference in the case of the third ML coverage was slightly different from that of the other cases in the sense that there was a good measure of preference for most of the bonding sites, judging from the closeness of the adsorption energies. In spite of this, it was quite evident from the values shown in Table 1.17 that the ONTOP site terminated with oxygen atoms was the most preferred bonding site, while the least likely site was the third ML FCC site terminated with hydroxyl groups. However, although the FCC site was the

least preferred bonding site in the case of the third ML coverage, it was still the most likely bonding site for the hydroxyl groups in all the FCC sites that were considered, including the half and quarter ML coverages.

The order of preference for the oxygen atoms' bonding in the third ML coverages was the ONTOP site, followed by the HCP site, then the bridge site, and finally the FCC site. However, the adsorption energies for the bridge and the FCC sites were very much close to each other, suggesting that in the presence of oxygen, any of the two may result, or they could also exist simultaneously. What was however curious though about these two sites was the fact that the adsorbates were positioned quite differently relative to the underlying carbon atoms as shown in figures A.17 and A.19, and yet they exhibited almost similar adsorption energies. Clearly, this would suggest among other things that the bonding environment was almost similar.

The hydroxyl groups at a third ML coverage showed almost equal preference for most of the sites. Nevertheless, the ONTOP site was the most preferred bonding site over the others, with an adsorption energy of -4.7546eV/atom, followed by the site whose initial geometry was a bridge-bonded one, then the HCP site, and finally the FCC site. From their experiments, Derry *et al.* [42] established that the adsorption energy of the OH group at a third ML ONTOP site was 4.2±0.8eV/atom, which compared favourably well to the values obtained in this study as shown in Table 1.17, but certainly the third ML ONTOP:OH site was not the most stable one in this case.

In general, it was established that there was a greater likelihood of oxygen atoms bonding in the case of the third ML coverage as opposed to the adsorption of hydroxyl groups. Judging from the closeness of the adsorption energies, one could not rule out the possibility whereby in real situations co-adsorption was very much the norm here, just like in the other coverages considered previously in this study. As a result, different functional groups would co-exist on the same

surface, probably at different sites and even occupying different fractional ML coverages.

Comparing the various adsorption sites, one establishes quite clearly that the lower coverages starting from 0.5ML and below were the most stable, as opposed to the higher ones. Various reasons could be responsible for this, and key among them was the effect of steric hindrance as mentioned previously, which may exclude the higher coverages as well as the existence of bonding and antibonding states. Another factor that excludes a full ML coverage, (unless the adsorbates-O or OH are literally forced onto the surfaces) could be the size of the atoms. With a large van der Waals diameter of 2.8Å, which is much greater than the adjacent carbon surface bonds on a (111) diamond surface, Derry *et al.* [42] argue that the expected maximum coverage would be one third of a monolayer, assuming a perfectly regular array which can easily be realized in theoretical modeling. Our calculations show that this condition was well satisfied, making the third ML ONTOP site terminated with oxygen atoms as the most stable coverage in a single-dangling-bond C(111)-(1×1) surface. However, based on their DFT calculations, Zheng *et al.* [44] seem to discount this, by proposing a full ML coverage instead of the third ML obtained previously by Derry *et al.* [42] and further confirmed by Rebuli *et al.* [84, 54] and also our recent XPS studies reported earlier. Zheng *et al.* [44] did not however consider coverages lower than 0.5ML, so as to be able to conclusively exclude others, neither did they offer any explanation to suggest the van der Waals concept was inappropriate. Based on the size of an oxygen atom which was generally larger than that of a carbon atom and also due to the O-O interactions, it seems quite logical that accommodating lower coverages may be more stable than higher ones. Zheng *et al.* [44] indicate that their calculations for atomic oxygen chemisorption led them to conclude that the steric hindrance proposed by Derry *et al.* [42] which restricts oxygen adsorption on diamond surfaces to less than a monolayer was invalid. This

they state was further supported by observations of 0.75 monolayers of fluorine atoms on diamond (100) surface by Freedman *et al.* [85] instead of the 0.5ML of O atoms on the C(100) surfaces, in spite of the fact that the fluorine atoms had a larger van der Waals radius than oxygen. However, again no evidence of testing for lower coverages is indicated in their work, and their surfaces were further deliberately and forcibly fluorinated at various temperatures where the surface thermodynamics may have favoured higher coverages, and in any case some fluorine atoms may bond on top of others and not necessarily the diamond surface as observed earlier in the literature review section of the chapter dealing with atom transfer from the polishing medium (oil) to the surfaces. Freedman *et al.* [85] do not indicate if they investigated this possibility in their work, especially in view of the size of the fluorine atoms relative to that of the carbon atoms forming the diamond matrix, which cannot simply be wished away. We have addressed these in detail in this work, since we can control precisely the monolayer coverages of the adsorbates and the positions that they bond to, and hence no ambiguities regarding whether some atoms were bonding on top of each other instead of the diamond existed, and therefore questioning the findings of Freedman *et al.* [85]. Their diamond surface was also rather rough, exhibiting roughnesses of just below 400Å, while the samples used by Derry *et al.* [42], and also those used in the experimental chapters of this study were carefully polished and hence quite smooth, with absolute roughnesses of below 8nm according the Atomic force microscopy results. It was observed in the XPS chapter that roughness features on polished diamond surfaces which essentially increases the overall surface area can act as sites with more dangling bonds (for adsorbates bonding), and hence increase the total coverage of the adsorbates as opposed to a smoother surface. Freedman *et al.* [85] surfaces appears to be possessing more of this character. We would also like to add that Rebuli *et al.* [84, 54] have in fact shown that the coverage of oxygen atoms or hydroxyl

groups on polished diamond surfaces, depends quite strongly on the ambient pressure, with even higher coverages of up to a full ML being observed. In this case, some of the adsorbates were believed to be bonded on top of each other, and not necessarily on the diamond surface. It is therefore quite normal to observe these higher ML coverages experimentally as reported by Freedman *et al.* [85], without necessarily implying that the third ML coverages observed in this study or even by the experiments of Derry *et al.* [42] was invalid, depending on the nature of the surface and/or the conditions for the experiment. In fact, Pickett *et al.* [62] reported that steric effects coupled with the coulomb repulsion between adsorbed fluorine atoms due to their charging precluded a ML coverage of fluorine atoms on the C(100) surface. It was therefore inconceivable to think that a full ML or even higher coverages of fluorine atoms would be the most stable configurations on the C(111) surface either, which ties in quite well with the observations made by Derry *et al.* [42] and other workers as mentioned before.

Diamond surfaces have a very high affinity for hydrogen adsorption, and therefore oxygen atoms, hydroxyl groups and hydrogen atoms compete for the available dangling bonds. Combining the twin issues of affinity for certain species on one hand and the van der Waals radius which is 1.4Å for oxygen [50, 42] on the other, it would be very unlikely for oxygen atoms to occupy all the surface bonds in the presence of hydroxyl groups and/or hydrogen atoms, with neither of the two getting adsorbed to the surfaces. In real environments (atmospheres), all the three adsorbates are always present and therefore the dangling bonds would be saturated by any of them, following the existing equilibrium thermodynamic processes and other factors such as those already alluded to previously. Though not exactly related, Zheng *et al.* [86] reported observing submonolayer coverages of oxygen ranging from 0.25 to 0.56 from their RHEED measurements on monohydride-terminated (2×1)-C(100) surfaces exposed to

O-plasma at substrate temperatures ranging from 25 to 500°C. This suggested that not all the surface bonds would be terminated with O atoms even under conditions that encourage this to happen like the elevated temperatures, and hence its unlikely to have a full ML coverage of oxygen atoms only on diamond surfaces, unless these are literally forced onto the surfaces, and hence the full ML coverage isn't the most stable configuration as alluded to by Zheng *et al.* [44].

Besides, various studies have shown that hydrogen can displace preadsorbed oxygen, but oxygen cannot displace preadsorbed hydrogen on diamond surfaces [49]. This appears to suggest that oxygen would preferably exist as a submonolayer on diamond surfaces, while the remainder of the surface bonds would be saturated preferentially by hydrogen atoms, and sometimes by hydroxyl groups. This is what we established in our detailed XPS work [87], and it agrees quite well with the findings of Derry *et al.* [42] and other workers too. Our DFT calculations now confirm the earlier experimental observations as well as the work of Derry *et al.* [42] and Rebuli *et al.* [84, 54] which all agree that the third ML coverage with oxygen atoms or hydroxyl groups at the ONTOP site as the most stable configurations on a single-dangling-bond diamond (111) surface for oxygen atoms and hydroxyl groups respectively, at low temperatures. These results together with the arguments presented earlier therefore puts into question some of Zheng *et al's* [44] findings regarding oxygen adsorption of up to a full ML coverage as the most stable one on real surfaces. This could only be possible under conditions similar to those discussed by Rebuli *et al.* [84] in relation to the vacuum level.

From our energy minimisation studies, the ONTOP site was found to be the most favourable bonding site in all cases involving the adsorption of both the oxygen atoms and hydroxyl groups, except in the case of the half ML coverage where the hydroxyl groups preferred the HCP site, which was incidentally quite

close to the ONTOP site.

While the third ML ONTOP site was the overall preferred bonding site by the oxygen atoms, the closeness of its adsorption energy to that of the quarter ML ONTOP site showed that the two sites and coverages were arguably the most likely bonding configurations for the oxygen atoms. This implied that if the oxygen atoms did not bond at the ONTOP site in the third ML coverage, they would certainly bond at the quarter ML ONTOP site or both.

From their energy minimization calculations also, Zheng *et al.* [44] found that the lowest energy configuration on the C(111) single bond cleavage surface was the molecular oxygen peroxy bridge site. This has however been questioned by Thieje *et al.* [60] where they indicate that the C-O-O-C structure was not likely since the CO-CO bond was weaker than the C-OH bond [38 vs 105 kcal/mol]. This they argued was due to presence of hydrogen atoms which coincidentally is a common adsorbate on polished diamond surfaces as mentioned before, and therefore a prominent feature for the sort of surfaces on which Derry *et al's* [42] work as well as our XPS [87] studies were based. The hydrogen atoms make the C-O-O-C bonds to convert rapidly to -OH terminations. Our calculations involving the full ML coverage of oxygen atoms at the ONTOP and HCP sites (see figure A.2 which was close to the peroxide structure of the peroxide structure of Zheng *et al.* [44]showed that the total minimum energy of the relaxed surface was relatively higher than that of the full ML coverage with OH groups (see Table 1.15), indicating that it was not the lowest energy configuration. This showed good agreement with the findings of Thieje *et al.* [60], and in the process contradicting Zheng *et al's* [44] hypothesis. In fact, it was Thieje *et al.* [60] who ought to have have established the existence of higher oxygen-containing groups suggested by Zheng *et al.* [44] since they did their calculations using a surface that was in contact with water,

but they did not. The relatively high adsorption energy observed in the calculation involving the co-adsorption of oxygen atoms at the ONTOP and HCP sites nonetheless confirmed the stability of the site, and therefore the adsorption of oxygen molecules on the C(111) diamond surface was indeed possible, a view shared by Zheng *et al.* [44]. They observed an O-O bond length of 1.49Å at a (1×1) bridge-bonded site and 1.48Å at a (2×1) reconstructed π-bonded site.

Zheng *et al.* [44] further stated that the presence of the peroxide structure explains the experimental observations that the main desorption product from an oxygen covered diamond powder was CO_2. However, this does not agree with other studies [55] that show the main desorption product is actually CO and not CO_2. Beerling *et al.* [88] in particular found that the main desorption product was CO, and very little CO_2. The desorption of the small amounts of CO_2 may partly confirm the existence of the peroxy structure or O-O molecule on diamond surfaces as shown by one of our systems, but based on the arguments presented, it was certainly not the most stable configuration. Our earlier XPS studies done under UHV conditions (i.e. pressures of better that 10^{-11}Torr) did not establish species with large components of oxygen either, such as the C-O-O-C as proposed by Zheng *et al.* [44], an observation that is ruled invalid by Thieje *et al.* [60].

Loh *et al.* [53] concurred with Thieje *et al.* [60] when they noted that the CO-OC bond would be weak. They calculated its value to be 1.565Å, compared to our calculated CO-OC bond length of 1.412Å, while one of their C-O bond length agreed with ours of 1.417Å.

The fact that previous studies on oxygen desorption from diamond surfaces have shown that it detaches from the surface as C-O and not as CO_2, or O_2 or even as O atoms [55, 53] suggests that certain bonds close to the surface of diamond got weaker either upon the adsorption of oxygen or hydroxyl groups than others (within the bulk), and thats why some carbon atoms got detached

easily from the diamond, instead of the adsorbates dissociating themselves and then leaving the diamond surface intact. The findings of this study established that the bonds between the 2nd and 3rd carbon atom layers were generally longer, and therefore weaker than most of the other bonds. The situation was not improved by adsorbing oxygen atoms or hydroxyl groups. As a result, we speculate that when the adsorbed oxygen dissociates from the diamond surface, some of the vertical bonds between the 2nd and 3rd topmost carbon atoms layers as well as some weaker surface C-C bonds were likely to be broken easily than the much stronger C-O or C-OH bonds. This argument is supported by the large changes observed in the surface bond lengths especially within the topmost surface layer, therefore making some bonds within the topmost surface bilayer weaker and hence vulnerable to breaking up when sufficient energy is supplied. These observations could thus explain why the observed desorption products from diamond surfaces are often predominantly C-O components and not CO_2, or O_2 or even as O atoms.

However for a clean surface devoid of either oxygen atoms or hydroxyl groups but possibly terminated with hydrogen atoms, organic groups of the form C_nH_x would preferentially be desorbed, again due to the weaker C-C bond between the 2nd and 3rd carbon atom layers as opposed to the short and most likely stronger C-H bonds. This arises from the fact that diamond surfaces have a high affinity for hydrogen adsorption as mentioned previously. Loh *et al.*[53] indicates that the adsorption energy per hydrogen atom on a (1×1) surface was 4.89eV while that of oxygen was 4.24eV, indicating the preference of H over O on diamond surfaces.

Since the submonolayer coverages were found to be more preferred in this study over the full monolayer coverages, it was to be expected that upon desorption of the oxygen or hydroxyl groups, only a fraction of the surface bonds would be etched out, while others would transform into graphite, which was

similar to the argument presented by Loh *et al.*[53].

In environments containing oxygen atoms or molecules only, the preference in bonding starting from the lower intake would therefore be, quarter ML ONTOP:O (-5.5722eV), third ML ONTOP:O (-5.58073eV), half ML ONTOP:O (-5.3030eV), and full ML ONTOP:O (-5.0066eV).

However, when the environment contains hydroxyl groups only or possibly water like the calculations of Thieje *et al.* [60], the likely intake of the OH groups starting from the lower coverages would be the quarter ML HCP:OH (-4.7019eV) or ONTOP:OH (-4.7003eV), the third ML ONTOP:OH (-4.754eV), Half ML HCP:OH (-4.7351eV) and finally a full ML co-adsorption of OH groups at HCP and ONTOP sites, i.e. 0.5ML HCP:OH and 0.5ML ONTOP:OH (-4.384eV) [which essentially relaxed to the full ML ONTOP:OH site - see figure 1.18].

When both oxygen and hydroxyl groups are present in the vicinity of the diamond surfaces, the situation does not change much. In this case, the uptake starting from the lower doses would be the quarter ML ONTOP:O, Third ML ONTOP:O, Half ML ONTOP:O, and then the full ML ONTOP:O, meaning that the oxygen adsorption would clearly dominate the OH adsorptions.

Zheng *et al.* [44] reported that LEED measurements on both C(111) and C(100) diamond surfaces with sufficient amounts of oxygen did not yield any patterns, an observation that they attributed to the adsorbed oxygen not producing long range surface order, although they indicated that their explanation was only speculative. This again seems to be in conflict with the LEED measurements of Derry *et al.* [46] who found nice LEED patterns on polished diamond surfaces containing oxygen even at low electron energies, down to 14eV. As such, if Zheng *et al's* arguments of higher ML coverages were to hold, then such nice LEED patterns would not have been observed on the polished diamond surfaces, and hence the lower coverages predicted in this work were more likely

since they appear to fit in quite well with the LEED measurements, or at least explain them without inconsistencies.

Furthermore, Wang *et al.* [89] and Sergei *et al.* [90] observed that as-polished or acid treated diamond (100) surfaces showed a (1×1) LEED pattern, an observation that renders Zheng *et al's* [44] suggestion on the LEED patterns invalid too, since the acid would tend to deposit more oxygen-containing groups, possibly through the bonding of their polar -OH groups on the surfaces, or even through the reaction between the surface bonded H atoms together with the active sites of the acid on the polished diamond surfaces. The bonding would probably be promoted by the fact that oxygenated diamond surfaces are hydrophilic while hydrogenated ones are hydrophobic [49]. This means that by applying Zheng *et al's* arguments [44], no LEED pattern would be observed at all in such heavily oxidized acid-treated surfaces, of which the arguments presented above seems to discount. Some Atomic force microscopy images obtained in this study from our polished diamond surfaces and cleaned with isopropanol instead of "Contrad" as we normally do (not shown here), showed that the cleaning medium left a thin film on top of the surfaces, thereby covering the surface roughnesses, and in the process making them to appear much smoother than they actually were in reality. This tended to even mask the polishing lines that were expected to be seen at such high spatial resolutions. After thorough cleaning and rinsing, the film was removed, and the polishing lines were visible again. This therefore means that the surface cleaning process plays a key role towards the nature and properties of such as-polished surfaces, and if not properly done may actually result in misleading experimental observations, such as higher ML coverages and other vital conclusions as discussed before.

The stability of the ONTOP:O site over all the others was supported by our observations of the C-O bond length being the shortest amongst all of the C-O bonds. In the full ML ONTOP:O site, it was 1.324Å, 1.32Å for the

half ML ONTOP site, 1.31Å for the quarter ML ONTOP site, and 1.304Å for the third ML ONTOP site. In addition to the bond lengths, the adsorption energies for the ONTOP sites listed above were always higher than all the other configurations considered in this study.

1.16.1 Adsorption energies of O atoms and OH groups on a (2×1) reconstructed diamond (111) surface: the most and least preferred bonding sites.

Only two adsorption sites were considered in the case of the full ML coverages, and four for the half monolayer coverages on the (2×1) reconstructed C(111) surface as shown in figures 1.28 to 1.31 and figures A.21 to A.22 (shown in Appendix A.

These were the ONTOP and bridge bonded sites, each terminated with oxygen atoms and hydroxyl groups, while only the ONTOP site was considered in the case of the full ML coverage. Just as expected from the stoichiometry of the bridge-bonding site with OH groups, the bridge bonding was broken following the adsorption of the hydroxyl groups, resulting in adsorption sites that were quite close to those achieved by the relaxed half ML ONTOP ones, as shown in figure A.21 and A.22. The only difference between the two sites was the orientation of the adsorbed OH groups relative to the diamond matrix as seen from the top view of each corresponding diagram. The most favoured bonding site on the (2×1) reconstructed diamond (111) surface was the half ML bridge site terminated with oxygen atoms, with an adsorption energy of ∼-4.6eV/atom as shown in figure 1.30. The least preferred bonding site was the half ML coverage with hydroxyl groups at the ONTOP site, with a a very low adsorption energy of only -1.965eV/atom. Figure 1.35 shows the adsorption energies versus coverage for O atoms and OH groups adsorbed at either an ONTOP or a bridge site on the (2×1) reconstructed C(111) surface. Comparing

Coverage & Adsor. Site ((2×1) reconstructed) (Monolayers)	Total Energy E_{tot}(Hartree)	$E^{O}_{adsorption}$ (eV/atom)	$\Delta\Phi$(work function) (Clean surface)	$\Delta\Phi$-O or OH term. (work function)
Full/Half - clean	-115.02591		2.3459	
Full ONTOP-O	-146.84587	-4.0993	”	5.4054
Full ONTOP-OH	-148.12078	-3.090	”	1.59019
Half ONTOP-clean	-115.02591		2.3459	
Half ONTOP-O	-130.90318	-3.203	”	5.7029
Half ONTOP-OH	-131.53202	-1.965	”	1.4675
Half Bridge-O	-130.95469	-4.6045	”	4.0813
DFT [53]		-5.23		
Half ML site with initial geometry as bridge-bonded-OH	-131.54245	-2.249	”	2.6163

Table 1.19: Calculated DFT-GGA total minimum energies, adsorption energies and work function values for various full and half monolayer coverages of oxygen atoms and hydroxyl groups at different sites on a (2×1) reconstructed diamond (111) surface. A plane cut-off energy of 50Ry was used, and the corresponding total energy of the oxygen atom at the same cut-off energy was 15.70077Hartree, while that of the hydroxyl group was -16.41753Hartree.

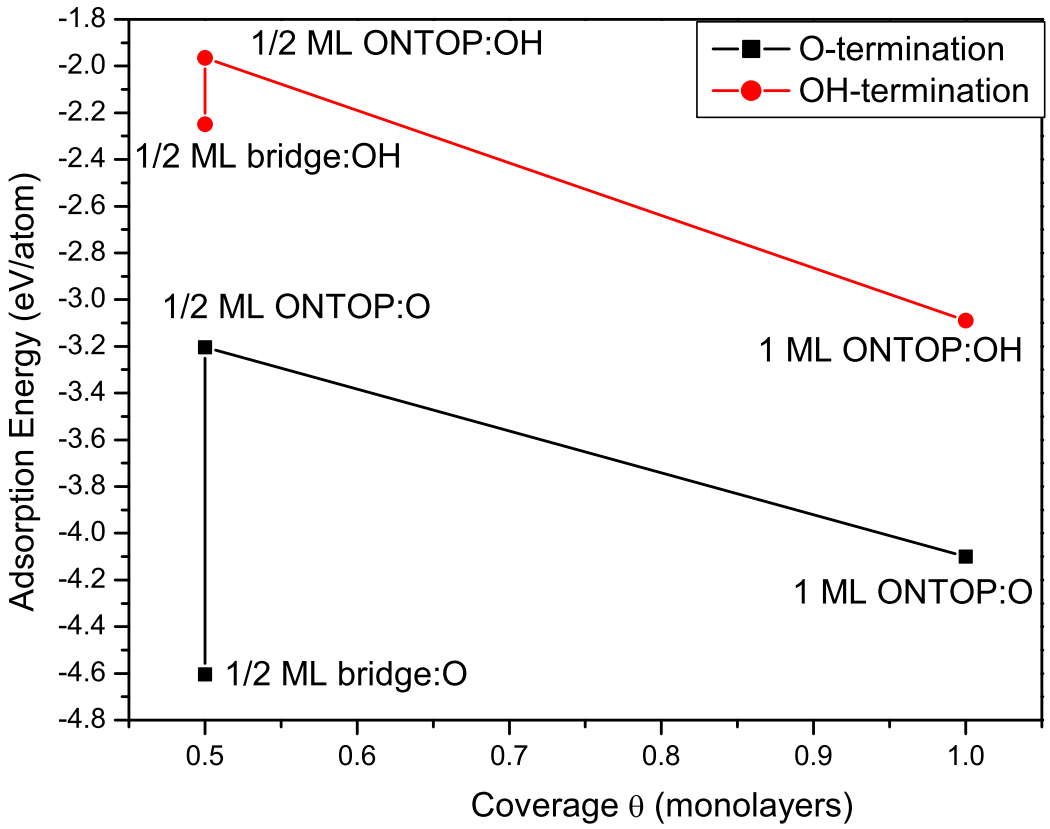


Figure 1.35: Adsorption energy versus coverage for full and half monolayer coverages of O atoms and OH groups adsorbed initially at bridge or ONTOP sites on a 2×1 reconstructed C(111) surface.

the suitability of the four half ML sites for the adsorption of oxygen atoms or hydroxyl groups, it was found that the most favoured bonding site was the half ML bridge (2×1):O as mentioned before, followed by the half ML ONTOP (2×1):O, then the half ML coverage whose initial geometry was bridge bonded (2×1):OH, and finally the half ML ONTOP (2×1):OH. This again suggested that the adsorption of oxygen atoms was generally more favoured on a (2×1) reconstructed diamond (111) surface over the hydroxyl groups just like in the C(111)-(1×1) surfaces. The hydroxyl groups did not seem to favour any of the

two half ML bonding sites (either ONTOP or bridge) that were considered, with the adsorption energies of the hydroxyl groups at the two sites beig generally low (-1.965 and -2.249eV/atom) and relatively close to each other, differing by only 0.284eV. This contrasted with the adsorption energies of the oxygen atoms at a bridge or an ONTOP site which was relatively higher (-4.6045eV and -3.203eV), although the difference between the adsorption energies for oxygen atoms at the two half ML sites was a bit higher, with a value of 1.4015eV being observed. This indicated that there was a significant energy barrier between the two bonding sites, and even so when moving from the O- to the OH-termination, but in spite of this, co-adsorption may be still be possible, especially in view of the closeness between the various adsorption energies.

On a (2×1) reconstructed diamond (111) surface, Loh *et al.*[53] found that the adsorption energy per hydrogen atom was 4.44eV while that of oxygen was 4.85 for a carbonyl site and 5.23eV for an epoxy site. In the presence of atomic H, they suggest that the oxygen-chemisorbed surface may convert to a more stable hydroxyl terminated C(111)-(1×1) surface. These findings are in good agreement with our computations of a full ML of OH groups at the ONTOP site of a C(111)-(2×1) surface. Klauser *et al.*[49] also agrees with this view where they observed that the O-exposed (2×1) reconstructed C(111) surface reacts strongly with hydrogen, but they do not explore the possibility that the H can actually bond on top of the O atoms instead of displacing it all together as suggested by the adsorption energies computed by Loh *et al.*[53]. At higher H exposures, this leads to the lifting of the surface reconstruction from a (2×1) structure to a characteristic (1×1) H-terminated surface, while atomic oxygen cannot replace the preadsorbed hydrogen.

The adsorption energies of oxygen atoms at an ONTOP site indicated that they were more favoured than the hydroxyl groups on a (2×1) reconstructed diamond (111) surface. In spite of this though, it was established that the OH

groups were more stable at the full ML ONTOP site than they were at the half ML ONTOP site or even the corresponding bridge site. This is further confirmed by the findings of Zheng *et al.* [44], who found that in spite of starting at other sites with hydroxyl groups, a configuration that was close to the ONTOP site was always achieved up on system relaxation. The stability of oxygen atoms at the half ML bridge site over the other sites and that of a full ML of OH groups against the half ML OH coverages was in good agreement with the DFT calculations of Loh *et al.* [53].

Klauser *et al.*[49] suggested that surface reconstruction is not lifted by oxygen adsorption under their exposure conditions of 0.5ML and any other coverage less than the saturation level of 1ML. However, Loh *et al.*[53] established that a full monolayer adsorption of oxygen atoms on a (2×1) reconstructed (111) diamond surface results in the lifting of the reconstruction.

Naturally, from the stoichiometry of the bonding sites, the OH groups would not bond elsewhere except at the ONTOP site, but this does not necessarily mean that the ONTOP site with OH groups was always the most stable, since to some extent the stability seems to be coverage dependent instead.

In terms of the energetics between the (1×1) and the (2×1) reconstructed C(111) surfaces, it was found that although the adsorption energy of the oxygen atom at a half ML ONTOP site of a (1×1) bulk terminated surface was larger (-5.30eV/atom) than that of the bridge site from a (2×1) reconstructed surface (-4.6eV/atom), the total minimum energies of the systems show that oxygen on the (2×1) reconstructed C(111) surface was lower in energy (-130.95469H compared to -130.92857H for the (1×1) surface) and therefore favoured due to the (2×1) reconstructed nature of the surface. This coverage (0.5ML) was also not sufficient to lift the reconstruction. On the other hand, the adsorption energy of OH groups at a half ML coverage on the (1×1) surface was -4.7351eV/atom (for 0.5ML HCP:O, that was almost close to the ONTOP:O) which was notably

larger than that obtained in the case of the (2×1) reconstructed C(111) surface of -2.2eV/atom (for 0.5ML bridge:OH). Additionally, the total energy of a half ML of OH groups on a (1×1) surface was lower (E_{total}=-131.5820H), than that of a half Ml of OH groups on a (2×1) reconstructed surface (E_{total}=-131.54245H), showing that the OH group would clearly prefer the unreconstructed surface. This was however not the case with the full monolayer coverages. With a total energy of -146.86123H and an adsorption energy of -5.00eV/atom for an oxygen-terminated (1×1:O) surface at the ONTOP site, and a total energy of -146.84587H and an adsorption energy of -4.099eV/atom for a (2×1:O) reconstructed C(111) surface terminated with a full ML oxygen atoms at the ONTOP site, it was obvious that the O atoms preferred the unreconstructed surface. Similarly, with a total energy of -148.15987H for OH-terminated surface at the ONTOP site of a (1×1:OH) (for full ML HCP/bridge:OH) and an adsorption energy of -4.384eV compared to a total energy of -148.12078eV for the (2×1:OH) reconstructed surface terminated with OH groups (for full ML ONTOP:OH) and an adsorption energy of -3.09eV, it was also quite clear that the hydroxyl groups preferred to bond on the (1×1) bulk terminated surface as opposed to the (2×1) reconstructed one. As such, 1ML would lift the (2×1) reconstruction, and the resultant (1×1) state was more stable. This was probably due to the activation barrier to go from O or OH termination on a (1×1) surface to a (2×1) reconstructed surface with the same adsorbates. Comparing the behaviour of both O atoms and OH groups with regard to the surface reconstruction, it was found that the adsorption energies of a full ML of O atoms at the ONTOP site on the (2×1) surface was -4.099eV, which was notably less than that of the (1×1) surface (-5.0066eV). At the same time, we note that the clean C(111)-(2×1) surface was lower in energy than the (1×1) surface per unit cell by 1.408eV. As such, on both the 1ML and 0.5ML, the OH groups had the highest adsorption energies and lowest total energies on the (1×1) surface, and

hence they would prefer to bond on this surface compared to the reconstructed surface.

1.17 Density of states(Dos) for bulk and surface carbon atoms of (1×1) bulk terminated C(111) surfaces, as well as those of the adsorbed oxygen atoms.

Figures 1.36 to 1.43 show the density of states for carbon atoms located within the bulk, at the surface, and for the adsorbed oxygen atoms on (1×1) bulk terminated (111) diamond surfaces. The spectra shown here are only for the most stable structures in any give coverage with O atoms or OH groups, while those of the less stable configurations are shown in figures A.24 to A.29 in Appendix A. The density of states for the O atoms were obtained from the oxygen atoms associated with the oxygen-only terminations, as well as those from the adsorbed hydroxyl groups. In each of the figures, the set of graphs shown on the left-hand side were obtained from surfaces terminated with oxygen atoms only, while those on the right-hand side were obtained from surfaces terminated with hydroxyl groups. Reference to the locations of the carbon atoms along the z-axis is given relative to figures 1.16 and 1.21. The density of states were generated using the Gaussian function, and a broadening parameter of 0.4. This value was generally large enough, and therefore ensured the production of smooth and less "peaky"distributions.

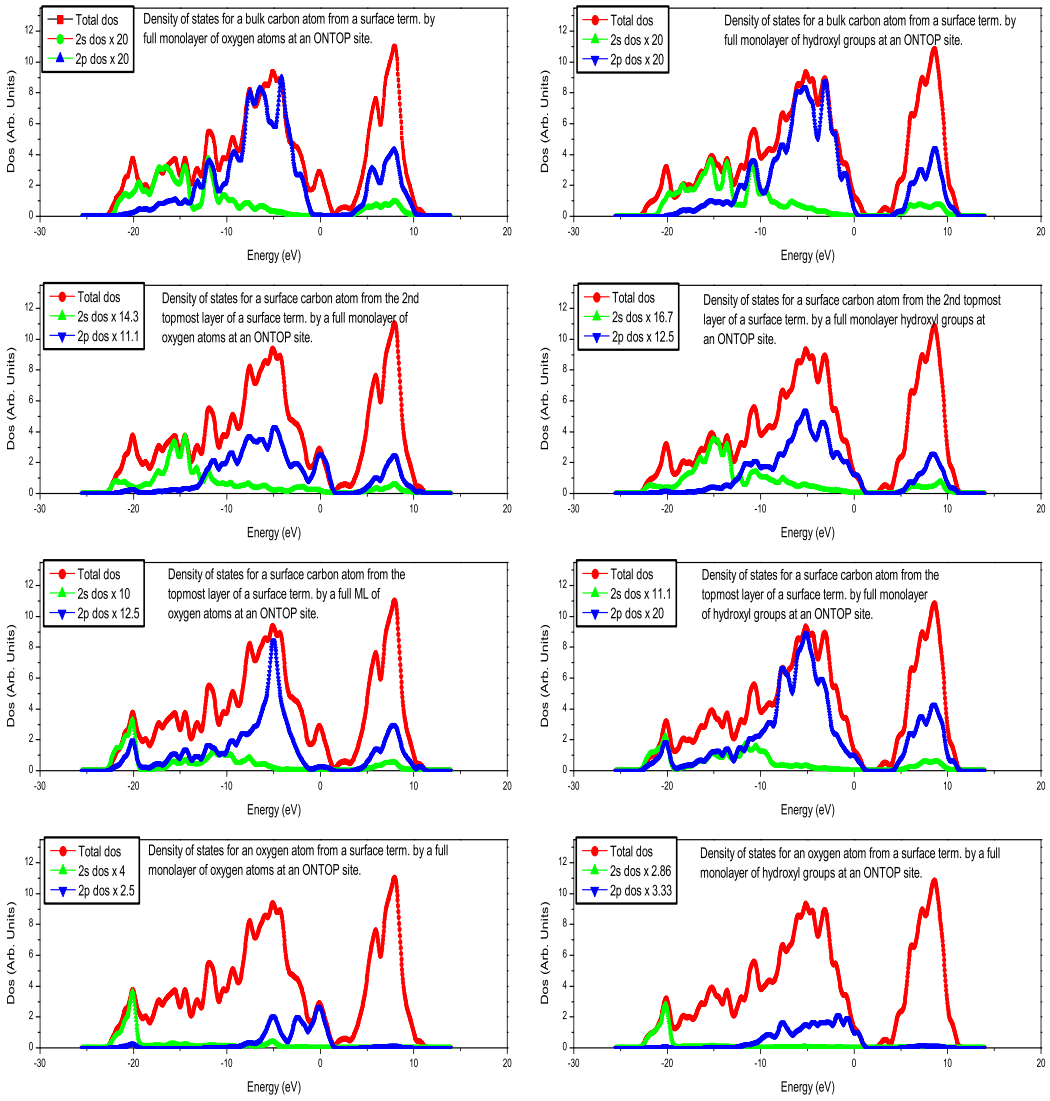


Figure 1.36: Density of states (Dos) for C(111)-(1×1) surfaces terminated by a full monolayer of oxygen atoms and hydroxyl groups at ONTOP sites.

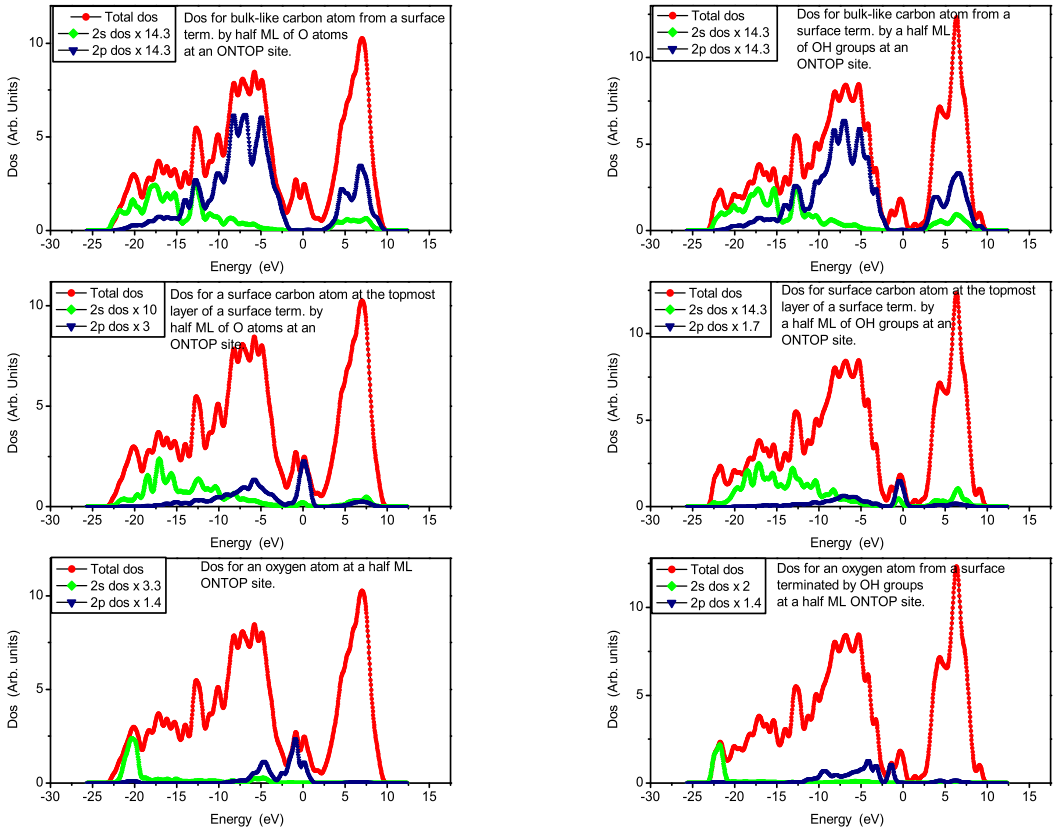


Figure 1.37: Density of states for C(111)-(1×1) surfaces terminated by a half monolayer of oxygen atoms and hydroxyl groups at ONTOP sites.

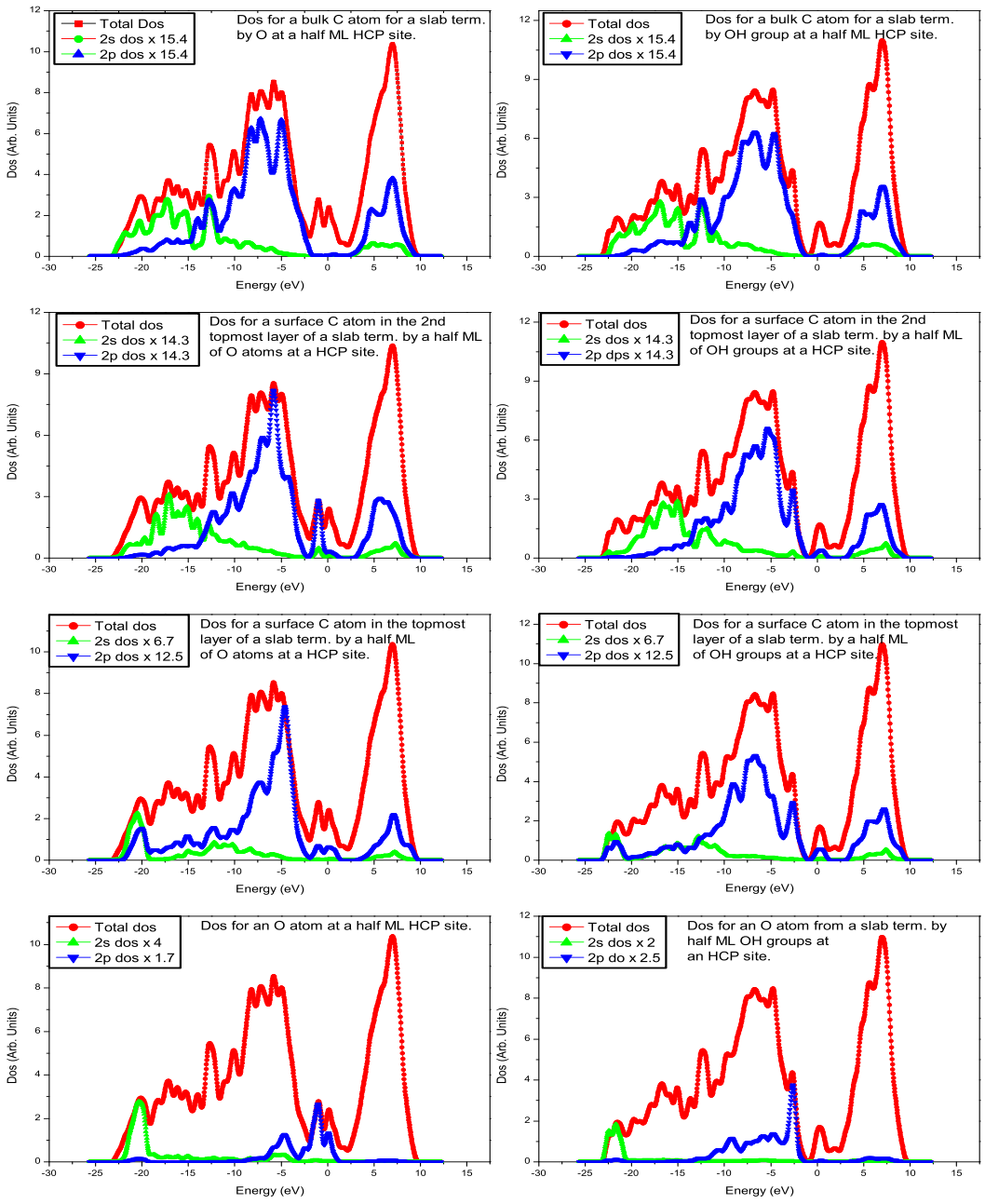


Figure 1.38: Density of states for C(111)-(1×1) surfaces terminated by a half monolayer of oxygen atoms and hydroxyl groups at hexagonal close packed (HCP) sites.

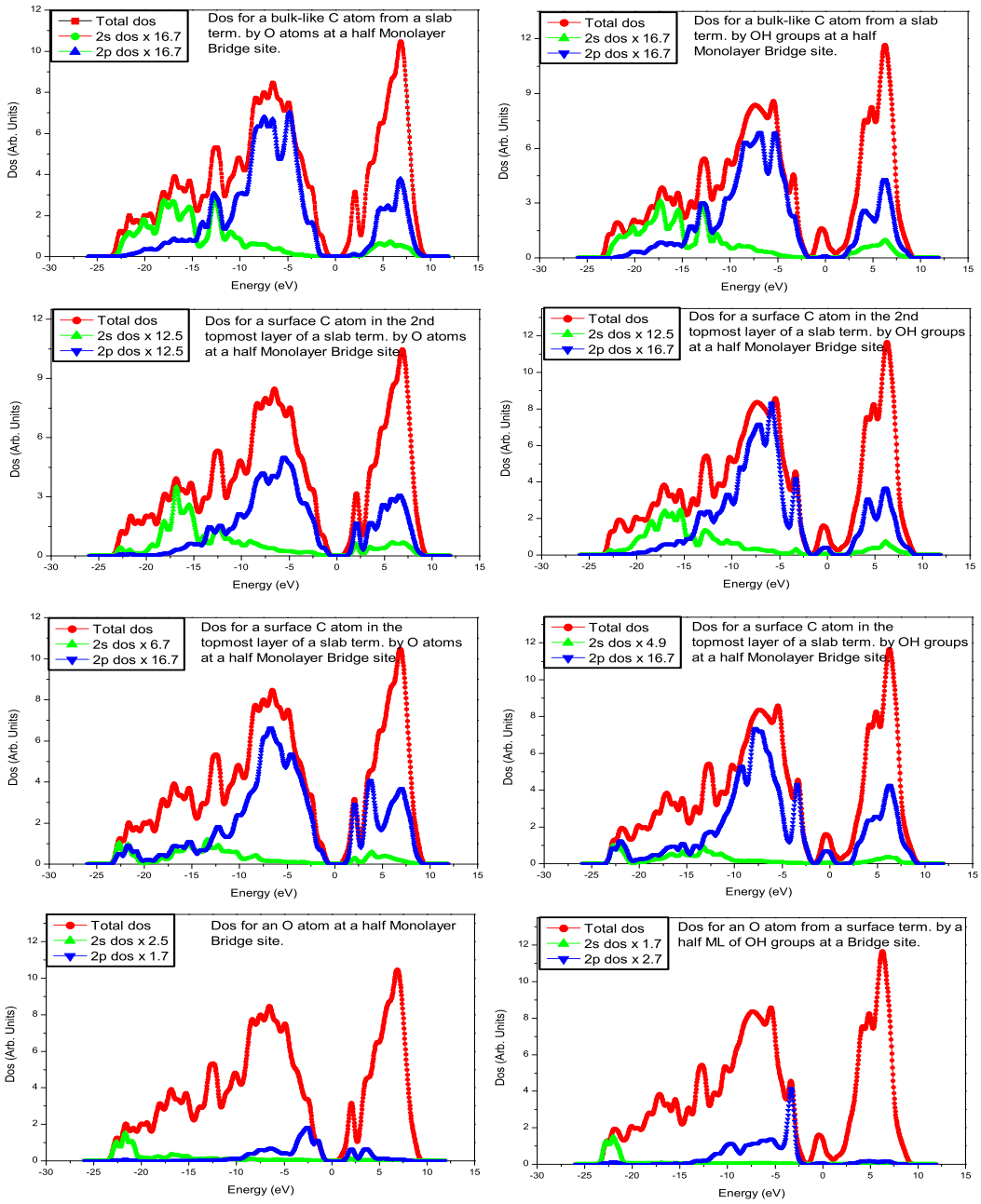


Figure 1.39: Density of states for C(111)-(1×1) surfaces terminated by a half monolayer of oxygen atoms and hydroxyl groups at sites whose starting geometry were bridge-bonded as shown in figures A.5 and A.6.

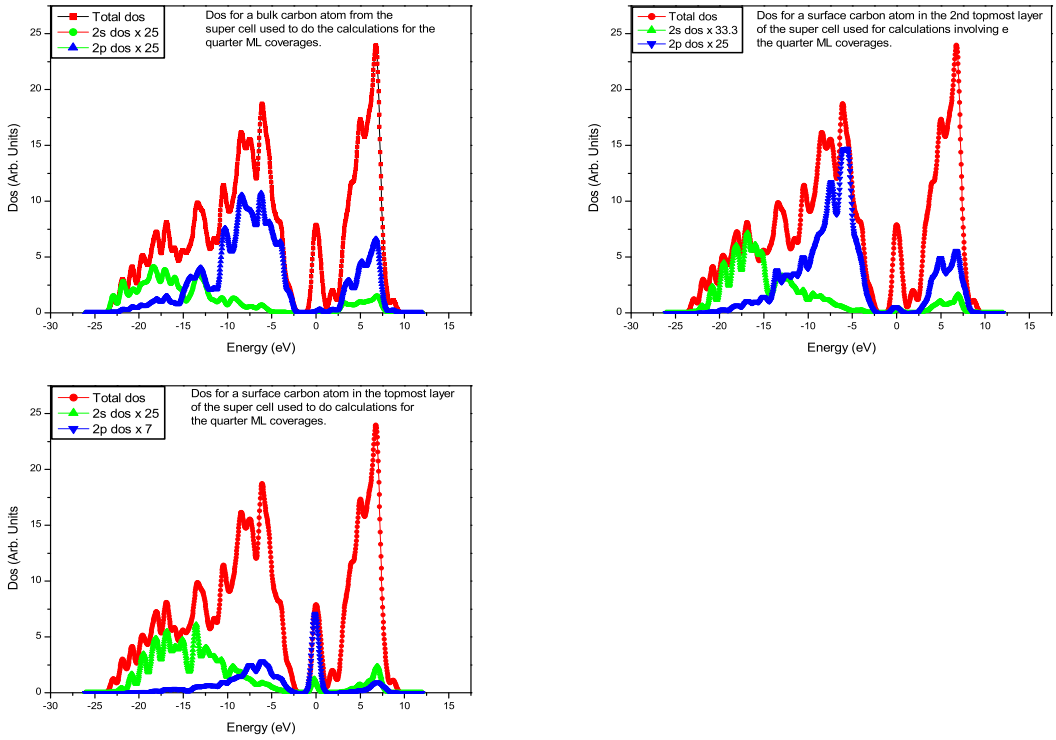


Figure 1.40: Density of states for a clean C(111)-(1×1) surface used for calculations involving the quarter monolayer coverages with oxygen atoms and hydroxyl groups. Note the strong C-2p states in the energy gap for carbon atoms in the topmost layer, and the lack of these for carbon atoms in the 2nd topmost layer or even in the bulk states.

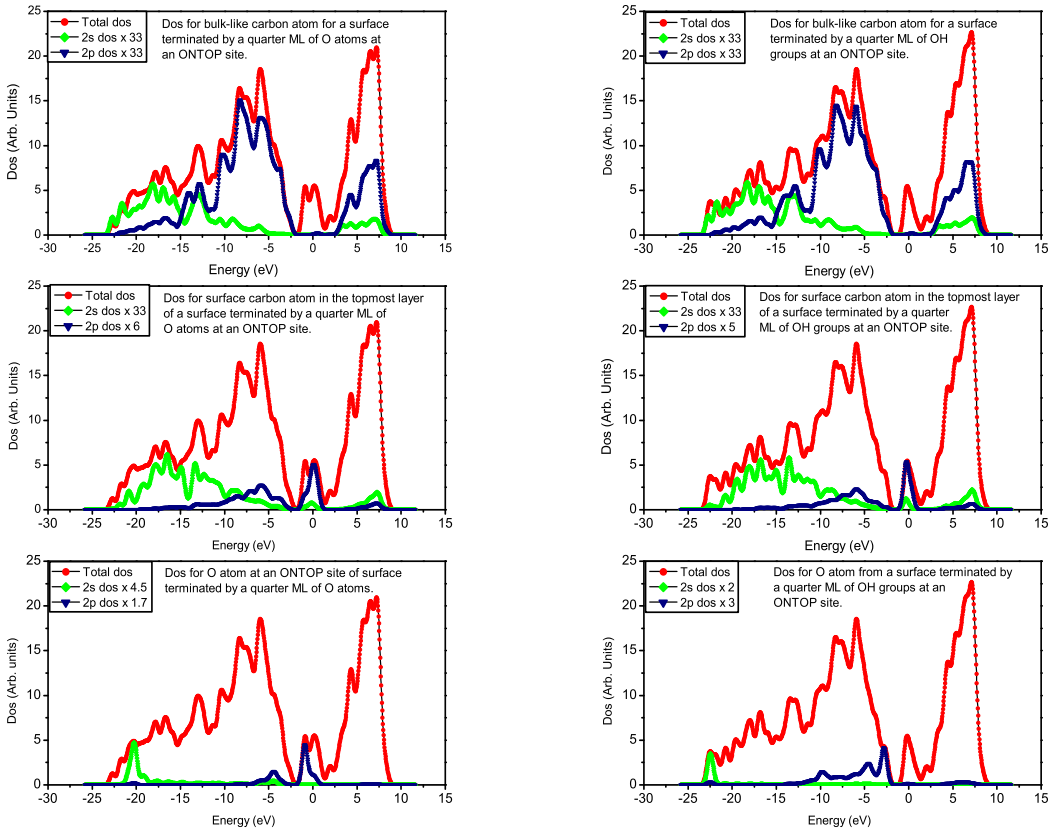


Figure 1.41: Density of states from C(111)-(1×1) surfaces terminated with a quarter monolayer of oxygen atoms and hydroxyl groups at ONTOP sites.

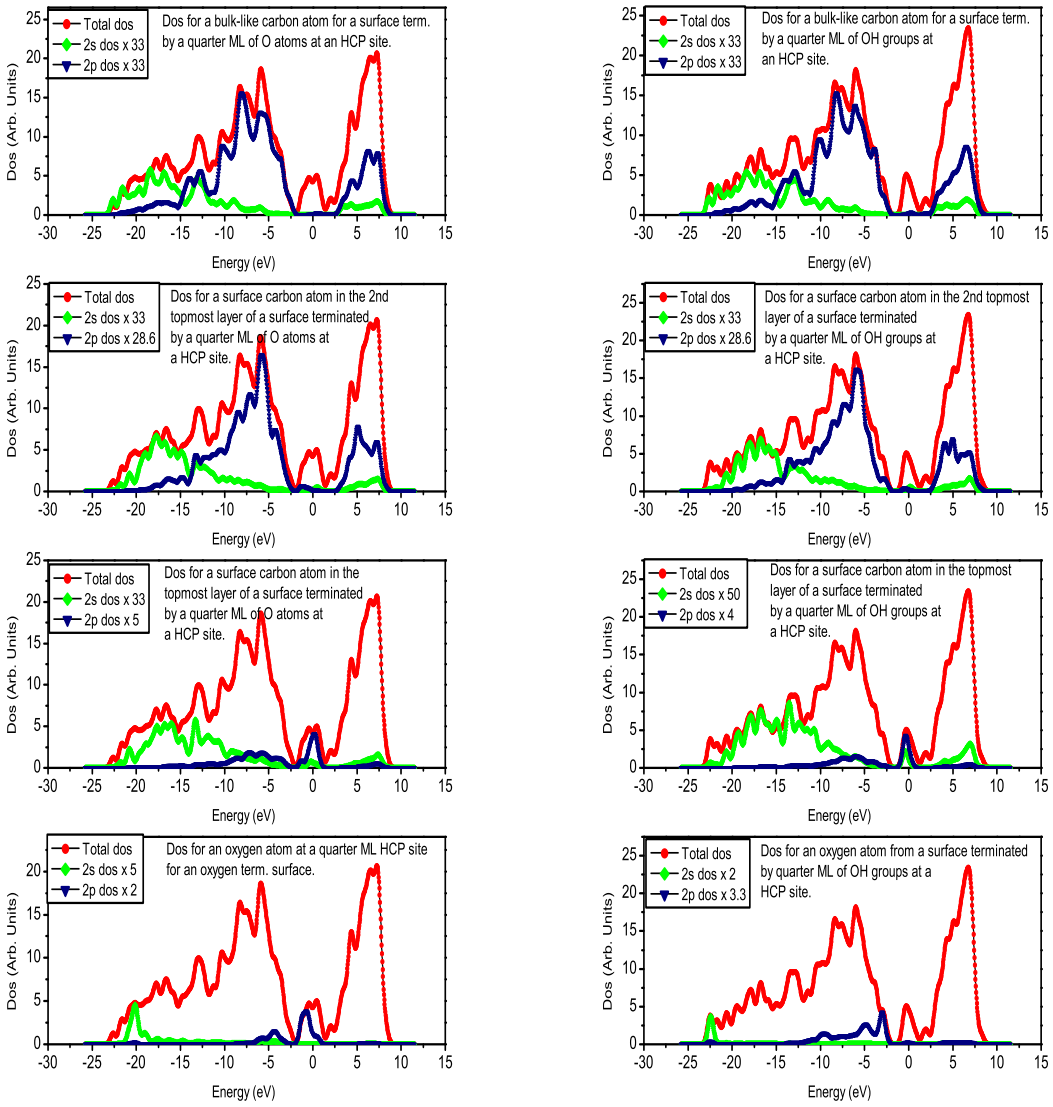


Figure 1.42: Density of states from C(111)-(1×1) surfaces terminated with a quarter monolayer of oxygen atoms and hydroxyl groups at sites whose initial geometry was Hexagonal close packed.

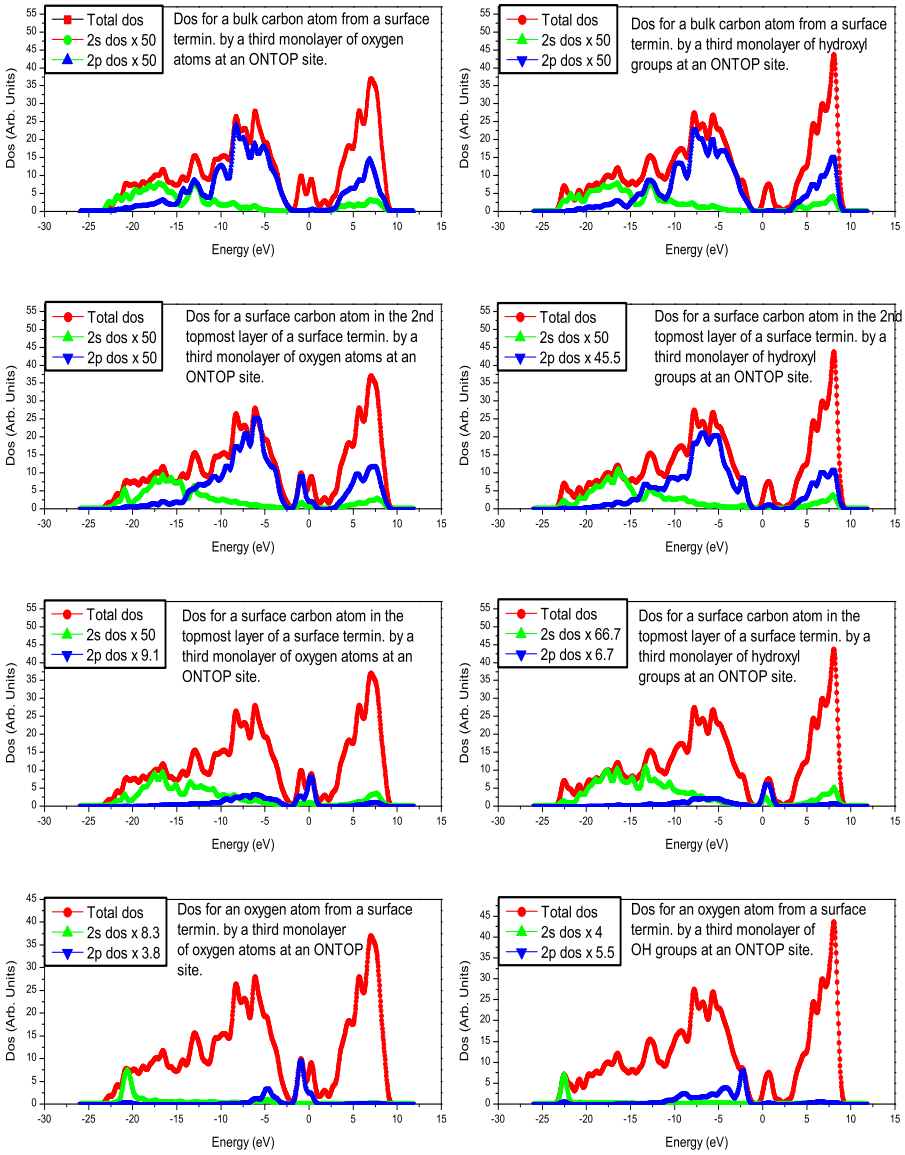


Figure 1.43: Density of states from C(111)-(1×1) surfaces terminated with a third monolayer of oxygen atoms and hydroxyl groups at ONTOP sites.

The energies of the density of states, were measured relative to the Fermi energy, which in this case was taken to correspond to 0eV. The importance of density of states regarding the electronic properties and especially the interfacial electronic structure of materials cannot be overemphasized. In relation to this, Pepper [91] alludes to the fact that the interfacial strength is indeed affected quite strongly by the interfacial chemical bonds that may be formed, especially between a diamond-metal interface. Based on these observations, the distribution of the Dos with respect to the electronic orbitals would be key towards the understanding of why certain bonds are stronger than others, and also in explaining the observed electronic properties. By terminating the diamond surfaces with species that alter their electronic structure, the properties of the material can be tailored quite easily for specific applications.

1.17.1 Dos for the bulk-like carbon atoms

The density of states from all the bulk carbon atoms associated with either the clean surfaces or those terminated with oxygen atoms or hydroxyl groups appeared almost quite similar structurally. This was nonetheless not too surprising since the preceding sections have already shown that there was minimal bond distortions ($\sim\pm1\%$) of the bulk bond lengths, and hence the electronic structure (charge distribution) was not altered much.

They all had similar features that consisted of broad valence bands that were made up of both 2s and 2p states which extended from about -22.5eV to around -2.5eV for the 2s states, and -23eV to about -2.5eV, for the 2p states while others extended up to -1eV. These yielded an average valence band width of about 21eV, which was consistent with earlier DFT calculations, where a valence band width of about 21.75eV was obtained by Kern *et al.* [48] and 21.71eV obtained by Zheng *et al.*[86] on a (100) diamond surface. They observed that their value (21.71eV) was in good agreement with the value of 21.63eV

calculated from the linearized augmented plane wave method(LAPW) by Fong *et al.*[92]. Our computed value of the valence band width was also in excellent agreement with the photo-emission results of Himpsel *et al.*[93] where they obtained a value of 21.0±1.0eV. The 2s states were centred at about -15eV in almost all cases, and their maxima was located at about -17.5eV. Our XPS valence band spectra (reported in the XPS chapter) showed a bulk state at ∼18eV, which corresponded to the one we calculated here at around -17.5eV, and in other cases at around -15eV for the 2s bulk states. The maxima for the 2s valence states occurred quite close to the valence band minimum, and the intensity of the 2s states was much lower and gently sloping towards the valence band maxima. In contrast, the 2p valence states were mainly centred at about -10eV, and these were found to be gently rising from the valence band minima, and increasing quite strongly between -12eV and -1.8eV. They yielded their maximum intensity towards the valence band maxima. A hybrid 2s/2p state was observed at slightly above -12.5eV, and this has been established elsewhere at 12eV [86] as being characteristic of diamond, while Reinke *et al.* [94] obtained this state at 13.2eV from their experiments. Our XPS valence band spectra found a similar state at around 14eV, but due shifting of the peak as a result of sample charging, this was likely to be closer to the energies reported above. No evidence of states within the energy band gap was observed for all the bulk carbon atom states. In addition, the conduction band states which were much narrower and less intense than the valence states were constituted of both the 2s and 2p orbitals, and they were located above the energy band gap. They occurred between 2.5eV and 9eV, yielding a conduction band width of about 6.5eV. They were often dominated by the unoccupied 2p states, with some contribution from the 2s states being observed too. Further, we generally found no effect of the surface states extending into the bulk carbon atom states, implying that the bulk structure of diamond was preserved, for the case of deep

lying (bulk) carbon atoms. It was also established that the 2s and 2p states were strongly delocalized within the valence band, a fact that could explain the strong covalent bonding observed in diamond. There was also no evidence of effects due to the adsorbed oxygen atoms or hydroxyl groups extending in to the states of the bulk carbon atoms. An average band gap value that was close to those of other first principle calculations such as 4.25eV obtained by Hafner *et al.* [95] and 4.2eV obtained by Zheng *et al.* [86] was expected. This was not computed in this work, but was nonetheless expected to be much narrower than the experimental band gap for diamond of 5.5eV, due to the fact that diamond is a material having an indirect band gap, and also the local density approximations (LDA) or (GGA) tend to underestimate the fundamental gap.

1.17.2 Dos for surface carbon atoms from C(111)-(1×1) surfaces.

Following system relaxations, it was found that there was a significant amount of movement in the surface carbon atoms as opposed to those located within the bulk as witnessed from the structural diagrams shown in figures 1.16 to 1.26 and in figures A.1 to A.20 shown in Appendix A, and this in a way tended to affect the associated density of states in various ways. Both the surface carbon atoms within the topmost bilayer of carbon atoms, i.e. the topmost and the second topmost layers of carbon atoms as shown in figure 1.21 were considered. Depending on the coverages under investigation, sometimes alternate density of states for the very top surface carbon atoms located in the same layer were considered. This was occasioned by the fact that, while all the topmost carbon atoms would be terminated by either oxygen atoms or hydroxyl groups in the case of full monolayer coverages (e.g. in figures 1.17 and A.1), this was not always the case, in say the lower coverages such as the half, quarter or third

monolayers where some carbon atoms at the very topmost layer would be terminated by either oxygen atoms or hydroxyl groups, while others were not. This made it necessary to consider each of the two cases separately depending on the coverage, since the electron cloud's distribution would most likely be different in the two bonding scenarios.

The computed density of states for surface carbon atoms showed that these were generally different from those of the bulk carbon atoms, and especially so for the topmost layer. Such differences were attributed mainly to the reduced symmetry and coordination of the surface carbon atom-bonds relative to the bulk ones, as observed in a number of the structural diagrams and also as detailed in Tables 1.4 to 1.10. This was also attributed sometimes to the presence of dangling bonds for the clean surfaces as shown in figures 1.2 and 1.40 and those with lower coverages of O atoms & OH groups. The covalent bonding of the adsorbed oxygen atoms or hydroxyl groups to the substrate carbon atoms also contributed towards the observed changes between the Dos of the bulk carbon atoms and those located at the surfaces. Again, the differences between the Dos for bulk and surface carbons atom were even more explicitly clear for the surface carbon atoms located in the topmost layer, while these were only just visible for the surface carbon atoms in the 2nd topmost layer. Such a result was partly due to the fact that the topmost carbon atoms had a smaller coordination than that of carbon atoms in the 2nd topmost layer, in addition to the factors already alluded to previously.

In the case of the full ML coverages, the density of states from a surface carbon atom located in the 2nd topmost layer exhibited 2s valence states that were rather broad just like those of the bulk carbon atoms. These extended from around -22.5 to -2.5eV, while those of the 2p orbitals extended from around -22eV to around -1.25eV. This range also applied to all carbon atoms located in the 2nd topmost layer for all coverages considered in this study, yielding an

average valence band width of about 21eV, just like in the bulk states. However, unlike the bulk states, those from the surface carbon atom from the full ML ONTOP site terminated with O atoms or OH groups appeared to be split into two, with two new tiny states developing at around -21.25eV for the 2s states, and -20eV for the 2p ones. This was accompanied by a general reduction in the intensity of both the 2s and 2p states, irrespective of whether the surfaces were terminated with oxygen atoms or hydroxyl groups, when compared to the bulk states. In addition, the strong hybrid 2s/2p state that was previously established in the bulk states at around -12.5eV to -11eV for the bulk carbon atoms was not present, except in the half ML FCC O and OH terminated surface, the half ML HCP sites terminated with OH groups, the half ML bridge site terminated with O atoms, as well as in all the quarter and third ML coverages with O atoms and OH groups. This state was nevertheless quite weak in all these cases. A new but relatively weak 2p surface state was also established at around -2.5eV and another at 0eV for the oxygen terminated surfaces, meaning that there were states existing within the energy band gap, unlike the case of bulk carbon states. This was observed in all coverages, except in the half ML FCC site terminated with O atoms and OH groups, the third ML ONTOP site terminated with O atoms and the third ML HCP site terminated with oxygen atoms. This made the 2p valence states to extend past the Fermi level in some cases. The prominence in terms of the intensity of the surface states at -2.5eV or 0eV alternated between the hydroxyl terminated surfaces and the oxygen terminated ones. These appeared as prominent and at times as weak shoulders, and in other cases as nice and well defined peaks.

In addition, the intensity of the conduction band states for carbon atoms within the 2nd topmost layer was somewhat reduced when compared to that of the bulk carbon atoms. It was also established that, although the conduction band states were constituted of both the 2s and 2p states which ranged from

around 3.75eV to 10 or at times 11eV, the 2p states always dominated the two, in all cases.

The valence states for the surface carbon atoms located in the topmost layer contrasted with those of the surface carbon atoms located in the 2nd topmost layer, and those of the bulk states in a number of ways. They appeared relatively modified in both their intensity, shape and features, compared to the two previous cases. These showed a maxima in their peak intensity at between -5eV and -7.5eV for both the two terminations (O and OH), and although the states from the oxygen terminated surfaces were at times a bit sharper at -5eV, both were generally broad, extending from around -22eV to around -1eV for the oxygen terminated surface and -22.5 to around -1.25eV for the hydroxyl terminated one. This also yielded an average valence band width of about 21eV, which was in good agreement with previous observations. The intensity of both the 2s and 2p valence states for the half ML ONTOP site terminated with oxygen atoms and hydroxyl groups was small due to the new states that developed within the band gap. A similar behaviour was also observed in the case of the half ML FCC site terminated with hydroxyl groups only (figure A.24), and all the quarter (figures 1.41 & 1.42 and A.25 & A.26) and third ML coverages (figures 1.43 and A.27 to A.29), especially the 2p states and occasionally the 2s states. This meant that charge was being removed from one state, resulting in bonding elsewhere.

In all the cases that were investigated, it was only the full ML ONTOP site that did not show any significant states within the energy gap. The clean surfaces had states within the energy band gap (figure 1.40) for the topmost carbon atoms, which were accompanied by a significant reduction in the intensity of the valence band's density of states for these carbon atoms. Unlike the states for the surface carbon atoms in the 2nd topmost layer, the 2p surface state appearing at -2.5eV for a surface carbon atom in the topmost layer disappeared

after the adsorption of oxygen atoms, and only appeared as a diminishing shoulder for the hydroxyl terminated surface, and a new but fairly prominent state developed at the higher binding energies, close to -20eV. The only exception to this was the half ML ONTOP site terminated with O atoms and OH groups, the half, quarter and third ML FCC sites terminated with OH groups, as well as the quarter ML ONTOP and third ML ONTOP, HCP and bridge sites terminated with O atoms and OH groups. For the half ML HCP site terminated with OH groups, the surface state at -2.5eV was quite prominent, while that of the corresponding oxygen terminated site, was barely visible. The half ML bridge site terminated with OH groups, showed a shifted surface state located between -4 and -3.75eV below the Fermi level.

It will be recalled that most of the bridge sites on the bulk terminated C(111) surface were unstable against the adsorption of OH groups, just like most of the HCP sites. They all relaxed to new positions that were close to the ONTOP:OH site. The new state that was found in a number of cases to develop at higher binding energies (between -22.5eV and -21eV in figures 1.36, 1.38, 1.39, A.26 [O termination], and A.28 [O termination]) was constituted of both the 2s and 2p states, and it was much narrower than the remaining part of the valence band states and hence weak. The remaining states were generally broad valence peaks ranging from around -19 to -1.25 and -21 to 1.25eV for the O and OH terminated surfaces respectively. Between -19 and -11eV, both the 2s and 2p valence states followed each other in their intensity and also shape, but it was quite apparent that the hybrid 2s/2p state that was previously found at around -12.5eV for the bulk carbon atoms' states was not present any more, probably due to the previously observed bond distortions at the surfaces. This phenomena was observed mainly at the full ML ONTOP and the half ML HCP sites, as well as all the bridge sites terminated with O atoms and OH groups. A similar behaviour was also observed in the density of states for the quarter and

third ML FCC sites terminated with oxygen atoms. Furthermore, it was only the full ML ONTOP site terminated with O atoms and OH groups that did not have any states within the energy band gap for the surface carbon atoms in the topmost layer, as opposed to those of the carbon atoms located in the 2nd topmost layer. This appeared to suggest that the presence of the adsorbates and the lack of dangling bonds contributed immensely towards the removal of such states.

1.17.3 Density of states for the adsorbed oxygen atoms on a (1×1) bulk terminated diamond (111) surface.

Clear differences were established between the density of states from the adsorbed oxygen atoms terminating the various surfaces and those of the underlying carbon atoms. It was therefore not possible to draw any comparisons between the density of states for the two different atom species (C and O), except possibly the obvious reduction in their intensity, and may be establishing the states that occurred at similar energies, thus encouraging stronger bonding states. As opposed to those of the carbon atoms where only one atom species was participating in the bonding process, the ones associated with the adsorbed oxygen atoms were generally related to the covalent bonding states between the oxygen and carbon atom's 2p states and sometimes the hydrogen atom's 1s states in the case of the OH bonding. Such differences in the bonding environment were thought to have had an effect on the overall variations observed in the density of states.

In all the cases involving the adsorbed oxygen atoms and the hydroxyl groups, it was found that neither the 2s nor the 2p density of states for the oxygen atom were continuous and broad over the entire valence band width, as was the case with a majority of the states involving the carbon atoms. Instead,

they often split into two, with one part located at the higher binding energies, and the other at the lower energies. Incidentally, the states at the higher binding energies were mainly dominated by the 2s states, while the 2p valence states dominated the lower energies. Additionally, the states at the higher binding energies ($\approx$ -21eV) were also very narrow and low in intensity, with a typical width of about 3eV. These coincided with similarly located narrow 2s/2p states observed previously for the carbon atom located in the topmost layer, except for the half ML ONTOP site, Quarter ML ONTOP, HCP and Bridge sites, as well as the third ML ONTOP and HCP sites, all of which were terminated with either oxygen atoms or hydroxyl groups. This was also observed in the case of the third ML FCC and bridge sites terminated with OH groups. The remaining 2p valence states occurred between -10eV and 1.25eV for most of the cases, thus presenting relatively wider band widths than those at the higher binding energies. These had significantly diminished intensities, especially the third ML HCP and ONTOP sites terminated with O atoms, as well as the quarter ML ONTOP site and the half ML ONTOP site all terminated with O atoms. This was accompanied by the development of some states within the energy band gap. The lack of states at higher binding energies could explain in part the suitability of such sites as the third ML ONTOP site for oxygen bonding. The 2p valence states from the oxygen terminated surfaces appeared to be split into three smaller peaks centred at between -5 and -4eV and at around -2.5eV and another at the Fermi level (0eV), except for the half ML bridge site terminated with oxygen atoms, as well as all the quarter and third ML bridge sites terminated with oxygen atoms. Those from the oxygen atom associated with the hydroxyl group were continuous and broad, with some smaller peaks/features riding on the overall states (envelop) being established at between -9 & -8eV, -5 & -4eV and at around -2.5eV, except for those from the less stable quarter ML FCC site terminated with OH groups.

The state located at 0eV tended to push the top of the valence band to much lower energies, thus extending the valence band maxima even beyond the Fermi level, and as a result contributing towards the narrowing of the energy band gap. This state also coincided with others already established at 0eV for the surface carbon atoms terminated with the oxygen atoms. It was also matched with some tiny 2p states that appeared as diminishing shoulders, from the two surface carbon atoms in the topmost layer from the hydroxyl terminated surface.

The O-2p surface states at -2.5eV were more intense for the half, quarter and third ML bridge and FCC sites terminated with oxygen atoms, as well as the full ML ONTOP site terminated with oxygen atoms. Strong 2p states for the oxygen atom were also found in the band gap, for sites terminated with oxygen atoms at a full, half, quarter and third ML ONTOP sites, as well as the half, quarter and third ML HCP sites, together with the half ML FCC site. The corresponding oxygen atoms from the OH group did not show many states within the energy band gap, except for the half and quarter ML FCC sites and the half ML ONTOP site too. This would therefore suggest that whereas states were observed in the band gap for most if not all the adsorbed oxygen atoms, the hydroxyl adsorption appeared to remove these in a majority of the cases.

No conduction band states were observed for the O atoms from either of the two terminations (O & OH), except in the half, quarter and third ML FCC and bridge sites terminated with oxygen atoms, unlike in the case of the carbon atoms. These were nonetheless quite narrow and extremely low in intensity.

Due to the differences observed in the states for the adsorbed oxygen atoms and those of the oxygen atoms from the hydroxyl groups, it appeared that the adsorbed hydrogen atom had some influence with regard to the overall surface states for the two adsorbates (O and OH). This was quite understandable from the point of view that its own electron cloud was bound to affect the electron

distribution of the neighbouring oxygen atom while forming the covalent bonds, and therefore the resultant density of states. We are therefore of the view that the relatively broad 2p valence states associated with the oxygen atom from the hydroxyl terminated surface may have been responsible for the stronger bonding observed in the OH group, while the states at -5 and -4eV were responsible for the strong bonding of the adsorbed oxygen atoms from the surfaces terminated by oxygen atoms only. Loh *et al.* [53] reported observing surface state features associated with O 2p centred at ∼4 and 8.5eV, while in our case these were found at between -9 & -8eV and between -5 & -4eV and at -2.5eV for those surfaces terminated with the OH groups, and between -5 and -6.25eV as well as around -2.5 and -1.25eV for surfaces terminated with oxygen atoms only.

It may therefore be concluded that in a majority of the cases, the adsorbed oxygen atoms on a (1×1) bulk terminated C(111) surface included states within the energy gap, while on the other hand, the adsorbed hydrogen atom from the hydroxyl group appeared to remove these states. The result would be the C-OH bond behaving like a C-H bond, an observation made by other workers, especially the resulting surface dipole. The change in the electronic properties of diamond surfaces terminated with either oxygen atoms or hydroxyl groups appears to be intricately related to the effects of the respective adsorbates as discussed previously. This argument is further bolstered partly by the observation that the hydroxyl terminated surfaces had generally lower work functions as opposed to those terminated with oxygen atoms, thus behaving like those terminated with H atoms. As such, the surface properties of diamond such as the strength of its bonds, stability of the bonding sites, and electronic properties among many others were also found to be somewhat intertwined to the observed density of states.

1.17.4 Density of states for the bulk and surface carbon atoms of (2×1) reconstructed diamond (111) surfaces as well as those of the adsorbed oxygen atoms.

The density of states for the (2×1) reconstructed diamond (111) surfaces are shown in figures 1.44 to 1.47. These include states for the bulk and surface carbon atoms, as well as those of the adsorbed oxygen atoms from an oxygen-only terminated surface and one that was terminated with hydroxyl groups. The same approach followed in the case of the (1×1) surface also applied here. Density of states from the bulk and surface carbon atoms of a clean surface are also shown, for comparison purposes. In each of the diagrams, the panel on the left hand side shows the density of states from the oxygen-only terminated surfaces, while that on the right hand side shows states obtained from the surfaces terminated with hydroxyl groups.

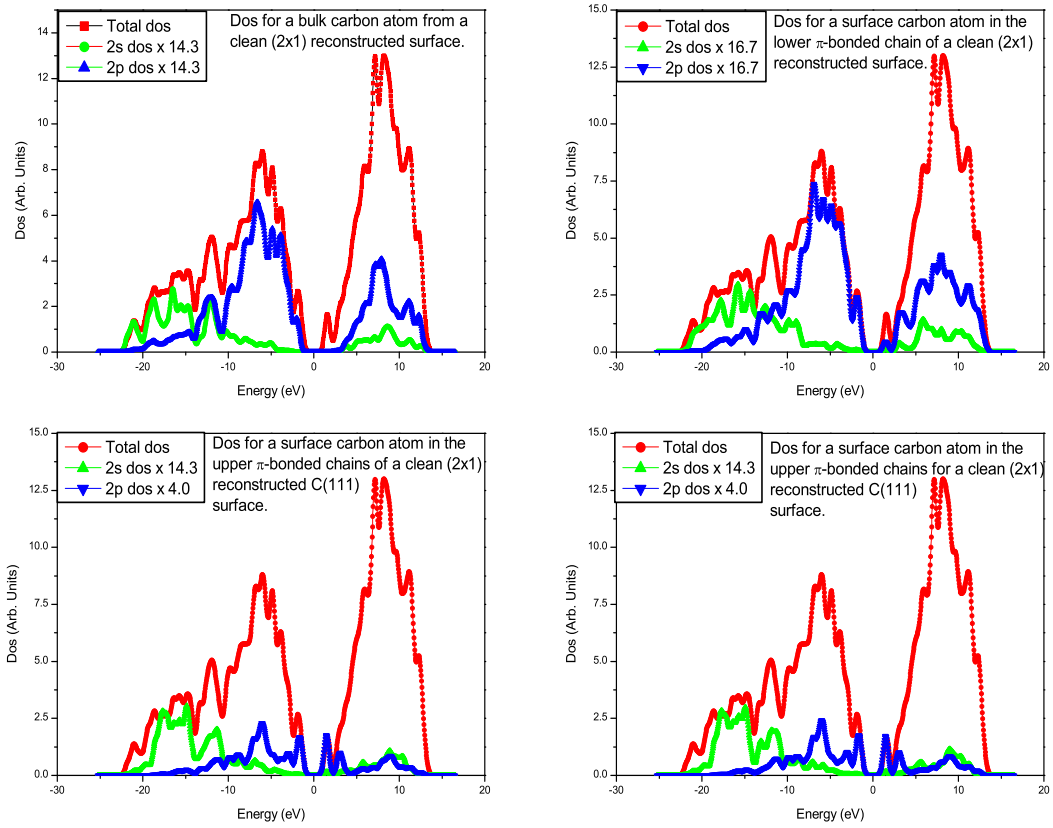


Figure 1.44: Density of states (Dos) for bulk and surface carbon atoms from a clean (2×1) reconstructed C(111) surface. Note the close resemblance of the states for the two surface carbon atoms in the upper π-bonded chains, emphasizing the similarities of the two bonding sites, and also the difference between this and those of clean C(111)-(1×1) surface shown in figure 1.40.

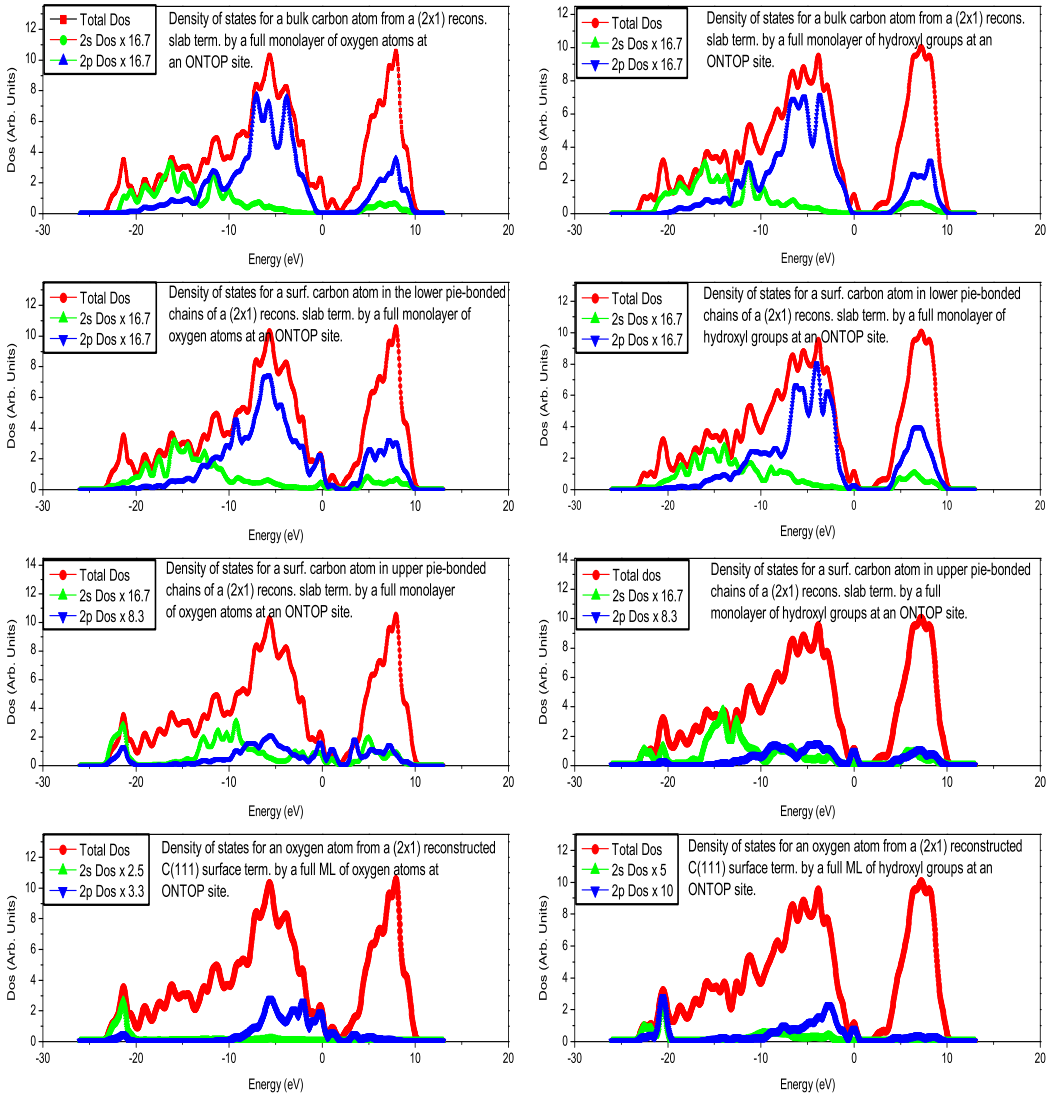


Figure 1.45: Density of states from (2×1) reconstructed C(111) surfaces terminated with a full monolayer of oxygen atoms and hydroxyl groups at the ON-TOP sites.

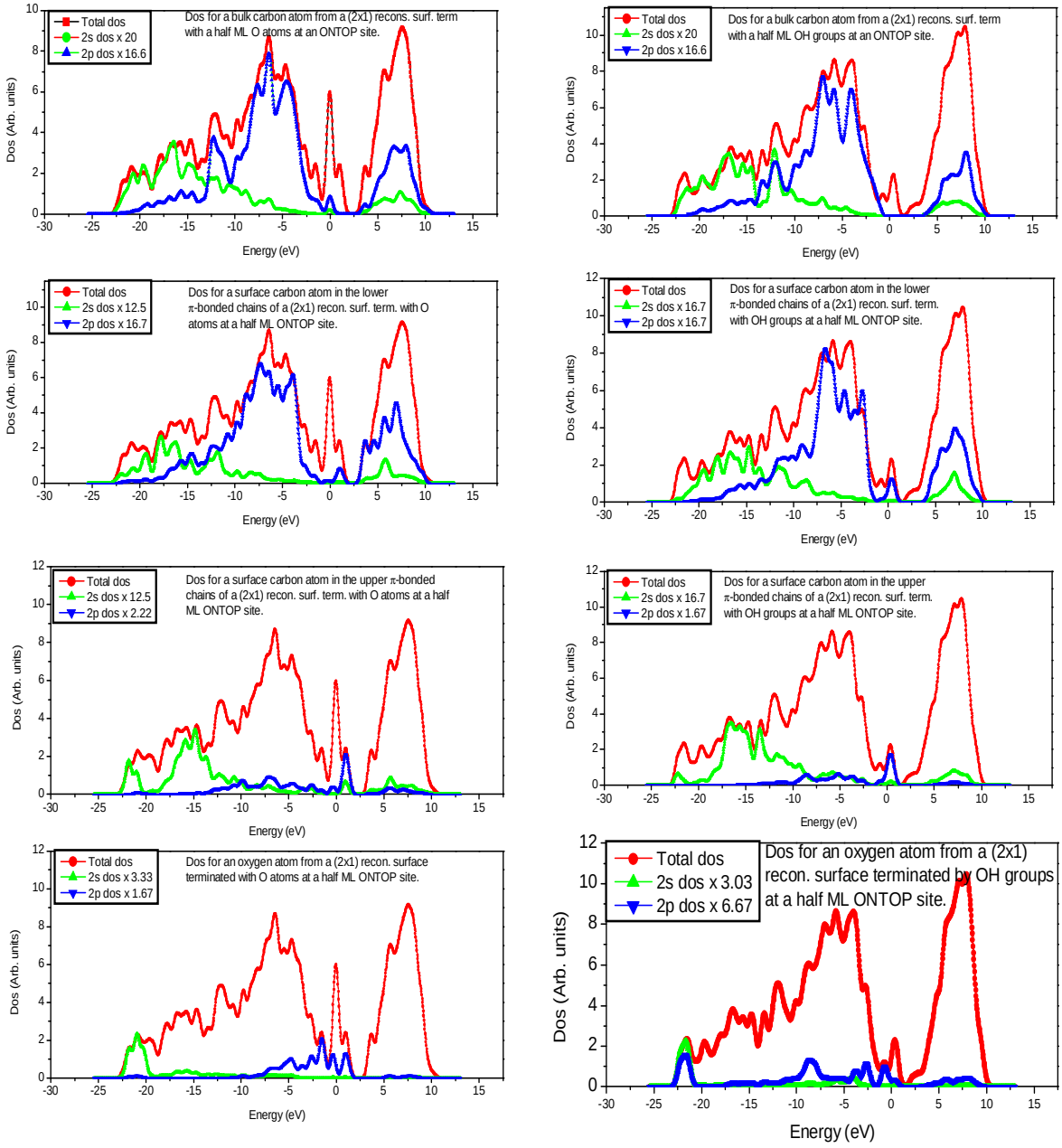


Figure 1.46: Density of states from (2×1) reconstructed C(111) surfaces terminated with a half monolayer of oxygen atoms and hydroxyl groups at the ON-TOP sites.

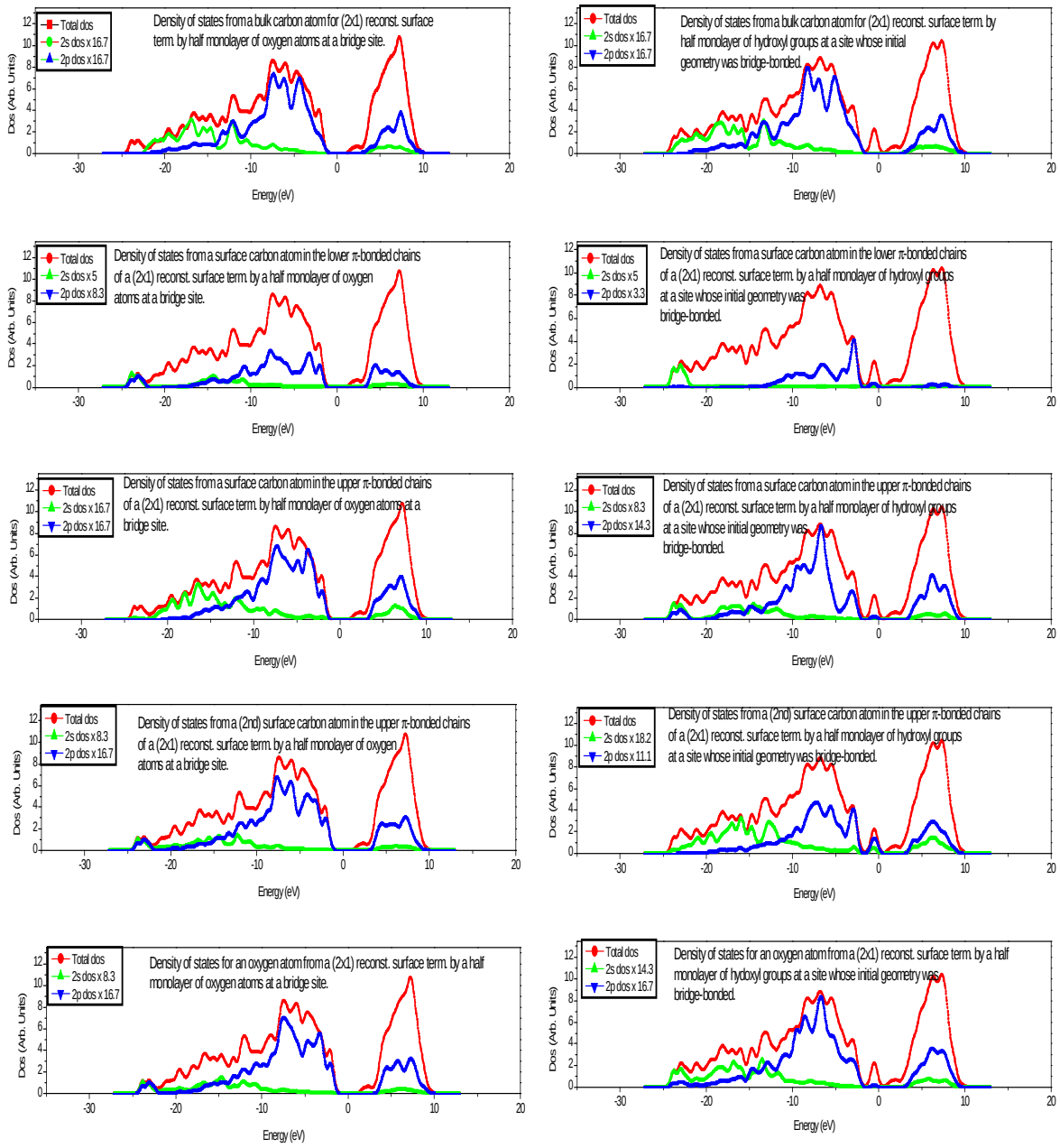


Figure 1.47: Density of states from (2×1) reconstructed C(111) surfaces terminated with a half monolayer of oxygen atoms and hydroxyl groups. The adsorbates were originally located at bridge-bonded site. Note that there are no states in the energy gap, except for the surface C atoms from the hydroxyl termination.

We started the optimization of our geometries from a (2×1) reconstructed diamond (111) surface which was terminated by a full and half ML of oxygen atoms or hydroxyl groups and from these the density of states were obtained. A common feature for the density of states for the bulk carbon atoms from the (2×1) reconstructed C(111) surface was that they were all almost similar to those of any other bulk carbon atoms from the (1×1) terminated surfaces. This similarity in the states was attributed to the fact that the effect of the surface reconstruction was not extended far in to the bulk states, but was only localized to the surface and near surface regions, which covered regions above the 5th carbon atom layer. For this surface, the bulk states were obtained from the 7th carbon atom layer (from top), since our calculations revealed that there was a significantly deeper bond relaxation within the bulk regions of a (2×1) reconstructed C(111) surface (bonds between the 5th and 4th layer), which was in excellent agreement with the findings of Kern *et al.* [48], who also established similarly deep lying bond distortions. The 2s valence states for the bulk carbon atoms ranged from around -22.5eV to -1.25eV with their center being at around -15eV, while the 2p valence states also occurred within the same range, but their highest intensity was established at approximately -7.25eV. Such a range indicated that both the 2s and 2p valence states were generally broad, leading to the observed strong C-C bonding. The hybrid 2s/2p state that was previously seen in other (1×1) bulk terminated surfaces at slightly above -12.5eV was also found here, at the same energy. Very small states from the 2p orbitals were found located at the Fermi level, only in the case of the half ML ONTOP site with oxygen termination. In all cases, the conduction band states were narrower and also low in intensity compared to those of the valence band states, and they were all constituted mainly of the 2p orbitals with some minimal contributions from the 2s states. These lay between 3.75 to 10eV, and their center was located at around 6.25eV above the Fermi level.

Density of states from the carbon atoms located in the lower π-bonded chains were almost similar to those of the bulk carbon atom in a number of cases, except that there was some slight reduction in their intensity. The only coverage that did not exhibit this behaviour was the half ML bridge site terminated with OH groups. This site was found previously to have been quite unstable against the adsorption of OH groups, and instead a structure that was very close to the ONTOP site was obtained after relaxation. Both the 2s and 2p states for carbon atoms in the lower π-bonded chains were established between -22.5eV and -1.25eV, with the center of the 2s states being at around -15eV, while the most intense peak for the 2p states was found at around -6.75eV. This indicated that all the valence states were broad peaks, just like in the bulk states. The hybrid 2s/2p state that was observed in other cases at slightly above -12.5eV was not very clearly defined, mainly due to the changes occurring in the 2p states and also the bonding environment. In addition, some 2p surface states were established at around -2.5eV, in both the oxygen and hydroxyl terminated surfaces. These were more prominent in the density of states for clean surfaces and also the hydroxyl terminated ones, especially the full ML ONTOP:O, the half ML ONTOP:OH and the half ML bridge:OH sites. The surface state at -2.5eV was also observed in the carbon atoms within the lower π-bonded chains, but its intensity was much lower, only appearing as a diminishing shoulder in most cases except the half ML bridge sites. For the full and half ML ONTOP sites with O atoms, these extended right into the energy band gap, with a fairly strong state at around -1eV for the full ML coverage and a weak one for the half ML coverage. The apparent differences between the Dos for carbon atoms within the same zigzag carbon atom chains only helped in amplifying the differences around those respective carbon atoms. Small 2p states were found within the energy band gap for the oxygen and hydroxyl terminated half ML ONTOP site, at approximately 1.0eV above the Fermi level unlike in other

cases. Just like in the bulk states, the conduction band states were constituted mainly of both the 2p and 2s states but the 2p state had a higher intensity in most cases except in the half ML bridge site terminated with hydroxyl groups. These occurred between 2.5 and 10eV for the oxygen terminated surfaces and between 3.73 to 10eV for the hydroxyl terminated surfaces, with their centers being approximately at 6.25 and 6.8eV respectively above the Fermi level.

As alluded to earlier, surfaces terminated with half monolayer of oxygen atoms or hydroxyl groups had only 50% of their surface bonds being terminated (except the most stable half ML bridge:O site), which meant that some carbon atoms located at the upper π-bonded zigzag C-C chains, were terminated with either oxygen atoms or hydroxyl groups, while others were not. This obviously meant that the density of states for a carbon atom bonded to either of the two adsorbates and one that was not terminated were bound to be different.

For a carbon atom that was not terminated with O atoms or OH groups, it was established that the intensity of the states did not decrease as much as they did for one that was terminated, except in the case of the half ML bridge site terminated with OH groups. It also turned out that for an unterminated carbon atom in the upper π-bonded chains, both the 2s and 2p valence states split in to two, forming a narrow 2s/2p state at the higher binding energy and the remainder of the states being fairly broad. The narrow state was located at around -21.25eV while the other part of the broad 2s valence states was centred at around -12.5eV and the ones for the 2p states at approximately -7.5eV. Although the overall intensities of both the 2s and 2p states were reduced, those of the 2s states was found to be the most affected. Other than the clean surface, the 2p surface state at -2.5eV was barely visible except in the case of the half ML bridge site terminated with OH groups. The energy gap for the bulk states of a clean (2×1) surface appeared quite narrow, when compared to those of carbon atoms in the π-bonded surface chains. The conduction band

states were still narrower than the valence band states and these were once more dominated by the 2p states, and their center was at around 7.25eV.

On the other hand, density of states from a surface carbon atom located in the upper π-bonded C-C chains and also bonded to either oxygen atoms or hydroxyl groups were found to vary slightly from those of the corresponding unbonded carbon atom in the upper π-bonded chains, due to the presence of the adsorbates. In this case, the 2p valence states were greatly reduced, while the corresponding 2s states experienced only minor reductions in their overall intensity. The 2s valence states were found to split into a narrow state located at the higher binding energies ($\approx$-21.25eV) for the oxygen terminated surfaces and at $\approx$ -22eV for all the hydroxyl terminated ones, except the half ML bridge site terminated with OH groups, and this was also lacking for the clean surface. The other part of the valence states was generally broad, with its center at around -15eV where a majority of the states (prominent peak) were concentrated. The broader states appeared to encourage bonding. The narrow states at the higher binding energies were constituted mainly of the 2s states except in the case of the two most stable configurations, i.e. full ML ONTOP:O and half ML bridge:O sites, and these had a relatively higher intensity for the oxygen terminated surfaces compared to that of the hydroxyl terminated ones. Furthermore, although the 2p states were significantly reduced, they were also broad in both the two terminations, and their centers coincided at about -6.75eV. The states associated with the oxygen termination were broader than those from the hydroxyl terminated surface, probably giving rise to the strong bonding observed for oxygen adsorption.

Fairly weak 2s and 2p states for the upper π-bonded carbon-atom chains which extended into the energy gap were observed in all cases except the half ML bridge:O site.

The intensity of the conduction band states was extremely small in all cases,

extending from around 2.5 to 10eV, with their center at around 6.25eV. The reduction in the overall density of states for the carbon atoms bonded to either the oxygen atoms or the hydroxyl groups when compared to those of the carbon atoms that were not terminated with any of the adsorbates suggested that the adsorbates removed some states, leading to bonding elsewhere.

In the case of the adsorbed oxygen atoms, a narrow 2s state located at around -21.25eV was observed in all cases, and the intensity of the states for the O atoms was generally much lower. A similar state at higher binding energies (23eV) has also been observed experimentally by Francz *et al.* [96], and they attributed this to O 2s core electrons. This state was constituted of both 2s and 2p states except the full and half ML ONTOP:O and the half ML bridge:OH sites where the 2s states appeared to dominate. The remaining part of the 2s states was barely visible, except in the full ML ONTOP site terminated with OH groups, the half ML ONTOP site terminated with oxygen atoms, and the half ML bridge site terminated with both O atoms and OH groups.

The 2p valence states for the adsorbed oxygen atoms (from the oxygen-only terminated surfaces) on the other hand were mainly concentrated towards the top of the valence band in both of the two terminations. These extended right into the energy band gap for most of the cases. For the oxygen-only terminated surface, a not-so-prominent 2p state's peak was found between -4 and -5eV for full and half ML ONTOP:O and at around -2.5eV for only the O terminated surfaces, and another extremely weak one at about 1eV above the Fermi level (except the half ML bridge:O). Another weak state was also observed between 0 and -2eV (except the half ML bridge:O) and instead of this, rather strong 2p states/features were observed between -6 and -9eV with its maxima at just in the neighbourhood of -7.5eV below the Fermi level. All the adsorbed O atoms had states in the energy gap except the stable half ML bridge:O.

The 2p valence states for the oxygen atoms from the adsorbed hydroxyl

groups had their maximum intensities at around -8.75eV, and they all had a surface state at -2.5eV. These values showed some agreement with those found by Klauser *et al.*[49], who found emission bands for these surfaces between -3.5 and -5eV, with their center at -4.2eV and another between -7.5 and -9.5, which was centred at -8.5eV. They attributed the two to the CO-like molecular orbitals, and therefore a signature to the presence of oxygen, and also the positions of the corresponding emission peaks on a (2×1) reconstructed diamond (111) surface. We also observed a surface state peak at slightly above -2.5eV which is related to the (2×1) reconstruction of diamond (111) surface and this has also been observed by other workers at 2.7eV. Loh *et al.*[52] further reported observing strong valence emission features on a (2×1) reconstructed diamond (111) surface at 4.2eV which they attributed to CO bonding orbital and another state at 8eV. In our case, the CO bonding states appeared at around -8.75eV and at slightly above -2.5eV, which is also related to the (2×1) reconstruction of diamond (111) surface, while the one observed by other workers at 4.2eV is only remotely discernible between ∼-3 and ∼-5eV, except in the half ML ONTOP:O site and the half ML bridge:O, while the evidence was somewhat ambiguous for the half ML bridge:OH site.

It was further found that there were no significant oxygen related conduction band states in either of the two terminations (i.e. with O or OH groups) for the (2×1) reconstructed diamond (111) surface, except in the half ML bridge site terminated with O atoms and OH groups. A major disruption of the surface bonds was also observed in this coverage with OH groups, resulting in a significant departure from the expected (2×1) reconstruction, and hence affecting the overall Dos for the O and carbon atoms, depending on their location relative to the surface.

1.18 Conclusions

A wide range of adsorption sites and coverages were considered in this study. The results obtained showed that the two adsorbates (O atoms and OH groups) played a significant role in changing the mechanical, chemical and electrical properties of diamond (111) surfaces. The computed properties of the adsorbates such the oxygen molecule, the hydroxyl groups and the bulk properties of diamond were all in good agreement with other DFT calculations as well as experiments.

The electronic density of states for bulk and surface carbon atoms were found to differ, a fact that was attributed not only to the effects of the presence of the adsorbates but also the atomic coordination, symmetry and the presence of dangling bonds at the respective environments. In particular, the surface carbon atoms showed differences in their electronic structure, depending on their location, or whether they were terminated with either oxygen atoms or hydroxyl groups, or even whether they were unterminated. The distribution of the respective density of states for the carbon or oxygen atoms was found to have a direct bearing on the stability of a given site for bonding. In most instances, broad and intense 2s core states and 2p valence states that promoted bonding were observed, especially for the bulk carbon atoms. The wider and intense Dos indicated localized electrons, which in turn favoured the bonding process. An average valence band width of $\sim$21eV was obtained, which showed good agreement with other DFT calculations as mentioned previously. A 2s/2p hybrid peak characteristic of the strong diamond covalent bonding was observed at slightly above -12.5eV below the Fermi level. This was mainly seen in the bulk carbon atoms of both the (1$\times$1) and (2$\times$1)-C(111) reconstructed surfaces, and the state was diminished or completely lacking in the surface carbon atoms, due to a combination of factors such as the breakdown of the three

dimensional symmetry, bond distortion and lack of sufficient coordination as mentioned before. Bulk carbon atom states were observed at around -17.5eV, which corresponded to similarly located bulk states observed in the XPS work, as well as by other workers. A surface state associated with the carbon atoms 2p states was observed at around -2.5eV while the O 2p states were observed at ∼-8.75eV and between -4 & -5eV among other energies as mentioned previously. In addition, a surface state that was related to the (2×1) reconstruction was found at slightly above -2.5eV below the Fermi level, which agreed quite well with the observations of Pate [97] who also established a similar state associated with the (2×2)/(2×1) surface at 2.5eV below the Fermi level. A state due to the core level O 2s states was observed at higher binding energies, precisely at around -21eV. This corresponded to the one observed experimentally at around 23eV by Francz *et al.* [96]. While states were observed in the energy gap for a number of O-terminated surfaces, these were removed by the OH terminations, especially those associated with the adsorbed oxygen atoms.

Regarding the stability of the respective sites for O or OH bonding on the bulk terminated C(111)-(1×1) surface, the third ML ONTOP site terminated with oxygen atoms was found to be the most stable bonding configuration, while the half ML FCC site with hydroxyl groups was the least stable. In addition, the ONTOP site was found to be generally the most preferred bonding site compared to all the others. However, in terms of the respective coverages, it was established that in the case of the full ML coverage, the ONTOP site with oxygen atoms was the most stable, followed by the co-adsorption of hydroxyl groups at the HCP and bridge sites, then the co-adsorption of oxygen atoms at the HCP and ONTOP sites, and the least stable site was the full ML ONTOP site terminated with hydroxyl groups. We speculate that this may have been caused by the steric repulsions due to the high concentrations (full ML) of the adsorbed OH groups among other factors.

For the half ML coverages on (1×1) surfaces, the most stable configuration was the half ML ONTOP site terminated with oxygen atoms, which was closely followed by the half ML site whose initial geometry was a HCP one terminated with oxygen atoms and hydroxyl groups respectively. It will nonetheless be recalled that these two sites resembled almost each structurally after system relaxations, and its therefore not too suprising that their stabilities were quite close. These were followed by the bridge site terminated with oxygen atoms and hydroxyl groups respectively, then the half ML ONTOP site terminated with hydroxyl groups, and finally the half ML FCC site terminated with oxygen atoms and hydroxyl groups respectively.

For the lower coverages, the quarter ML ONTOP site with oxygen atoms was the most stable, followed by the quarter ML site whose initial geometry was the HCP one terminated with oxygen atoms, then the quarter ML FCC site terminated with oxygen atoms, the quarter ML bridge site terminated with oxygen atoms, the quarter ML HCP site terminated with hydroxyl groups, the quarter ML ONTOP site terminated with hydroxyl groups, the quarter ML bridge site terminated with hydroxyl groups, and the least stable among all the quarter ML coverages was the FCC site terminated with hydroxyl groups.

A more or less similar trend for the most and least stable configurations was followed by the third ML coverages as was the case with the quarter ML ones. Here, the most stable configuration was the third ML ONTOP site terminated with oxygen atoms, followed by the site whose initial geometry was a HCP one terminated with oxygen atoms, the third monolayer bridge site with oxygen atoms, the third ML FCC site terminated with oxygen atoms, the third ML ONTOP site terminated with hydroxyl groups, the third ML site whose starting geometry was a bridge-bonded one with OH groups, then the third ML site whose initial geometry was a HCP one with hydroxyl groups, and the least stable was the third ML FCC site terminated with hydroxyl groups. Curiously,

by comparing the adsorption energies, one establishes that the FCC site became a bit stable with lower coverages, especially those below 0.5ML.

The stabilities of the various sites and coverages against the adsorption of the O atoms or OH groups suggested that if the diamond (111) surfaces were exposed to environments containing either oxygen atoms or hydroxyl groups, the intake/adsorption starting from the lower coverages would follow the order, quarter ML ONTOP site with oxygen atoms, then the third ML ONTOP site with oxygen atoms, the half ML ONTOP site with oxygen atoms, and finally the full monolayer ONTOP site with oxygen atoms too. If the environment contains water or hydroxyl groups only, the uptake/adsorption starting from the lower coverages would be, the quarter ML ONTOP site with hydroxyl groups (whose preference for OH bonding was quite close to that of the site whose starting geometry was a HCP one), then the third ML ONTOP site with hydroxyl groups, the half ML site whose starting geometry was a HCP one with hydroxyl groups (which had a lot of resemblance to the ONTOP site after optimization), and finally the full ML co-adsorption of hydroxyl groups at the HCP and bridge sites which apparently looked more or less like the ONTOP:OH coverage after relaxation.

On the (2×1) reconstructed C(111) surface, the half bridge site terminated with oxygen atoms was found to be the most stable configuration, and the least stable was the half ML ONTOP site with hydroxyl groups.

In terms of the energetics between the (1×1) and the (2×1) reconstructed C(111) surfaces, it was found that although the adsorption energy of the oxygen atoms at a half ML ONTOP sites of a (1×1) bulk terminated surface was larger (-5.30eV/atom) than that of the bridge site from a (2×1) reconstructed surface (-4.6eV/atom), the total minimum energy of the (2×1) reconstructed surface was lower (-130.95469H) than that of the (1×1) surface (-130.92857H) and therefore favoured due to the reconstructed (2×1) surface. On the other hand,

the adsorption energy of OH groups at the half ML ONTOP site (or previously a HCP site as shown in figure 1.20) on the (1×1) surface was -4.7eV/atom, notably larger than that obtained in the case of the half ML coverage of OH groups on a (2×1) reconstructed C(111) surface, which was -2.2eV/atom. In addition, the total energy of a (1×1) surface was lower (-131.58202H) compared to -131.54245H for the (2×1) reconstructed C(111) surface, showing that the OH groups would prefer the unreconstructed surface. This was perhaps due to the activation barrier to go from O or OH termination on a (1×1) surface to a (2×1) reconstructed surface. This was however not the case with the full monolayer coverages. With total energies of -146.86123H for an oxygen-terminated (1×1) surface at the ONTOP site and an adsorption energy of -5.006eV against a total energy of -146.84587H for a surface terminated with oxygen atoms at the ONTOP site of a (2×1) reconstructed surface and an adsorption energy of -4.0993eV/atom, the oxygen atoms clearly preferred the unreconstructed surface. At the same time, the total energy of the OH groups bonded up to a full ML at the ONTOP site of a bulk terminated surface was -148.15987H, while that of the OH groups adsorbed up to a full ML on the (2×1) reconstructed surface was -148.12078H. The corresponding adsorption energies were -4.33eV/atom (for full ML ONTOP:OH on a (1×1) surface) and -3.09eV/atom (for full ML ONTOP:OH on a (2×1) reconstructed surface) respectively, implying that the OH groups preferred to bond up to a full ML on the bulk terminated (1×1) surface. As a result, it was only the adsorption of O atoms at the half ML bridge and ONTOP sites that did not lift the (2×1) reconstruction, since the coverage wasn't sufficient to do this, unlike the full ML coverages. At the same time, the OH groups were all unstable at the bridge sites, an observation that is supported by the stoichiometry of the bonding species at these sites.

A plot of the adsorption energy vs coverage for the most stable configurations of O atoms or OH groups on the (1×1) surface showed that a repulsion between

the O adsorbates started at coverages greater than 0.33ML, while for the OH termination, it was not until coverages greater than 0.5ML that the systems got less stable due to the OH-OH repulsion.

The work function of both the (1×1) and (2×1)-C(111) surfaces was found to be changed quite remarkably by the adsorption of either oxygen atoms or hydroxyl groups. Adsorption of oxygen atoms led to increased work function of the surfaces, and with it the surface's electron affinity to become positive, even sometimes well above that of the clean surfaces. On the other hand, the adsorption of hydroxyl groups resulted in the lowering of the work function, therefore resulting in negative electron affinity of such surfaces, as alluded to by other researchers referred to previously in the text. The work function of the clean (1×1) surface was found to be higher than that of the (2×1) reconstructed surface, and in relation to the respective clean surfaces, the full and half ML ONTOP sites with oxygen atoms on the (2×1) reconstructed surfaces suffered greater increases in their work function compared to that of the corresponding full and half ML coverages with oxygen atoms on the (1×1) surfaces (see Tables A.1, A.2, A.3 and A.4 shown in Appendix A). However, the full and half ML ONTOP sites terminated with OH groups on the (1×1) surfaces experienced greater decrease in their work function values relative to the clean surfaces, compared to that of the corresponding full and half ML sites terminated with OH groups on the (2×1) surfaces. The most stable half ML bridge:O site on the (2×1) surface experienced almost a three times increase in its work function relative to that of the clean (2×1) surface, compared to that of the half ML bridge:O site on the (1×1) surface.

The C-C atom bond lengths were found to change depending on the location of the respective carbon atoms i.e. whether they were located within the bulk or at the surface. Those within the bulk regions appeared to preserve the bond lengths close to the experimental value of 1.54Å, with expansions or contractions

occurring between ± 0.39% or more broadly, less than ±1%. As such, these bonds suffered only minimal changes from their expected bulk values.

However, as one approached the surface region, significant bond relaxations were observed, leading to some pronounced expansion or contractions as one got closer to the surface. Some of the changes observed near the surface region have been attributed to the rehybridization of the bond orbitals [76]. Bond length changes of between 10 and 4% of the bulk bond length were routinely observed within the surface regions, specifically between the first and second carbon atom bilayers of the (1×1) bulk terminated C(111) surfaces prompting the speculation that these were generally weak and hence prone to easy erosion by heating. The bond angles were also found to change, with larger changes being recorded closer to the surface regions, which corresponded to the similarly large bond length changes within these regions. Those within the bulk were seldom changed from the expected value of ∼109.4°. Up to the third and in some cases the second bilayer of carbon atoms, the bond angles were very much close to the experimental value. They varied between 106 and 111°, while those at the surface varied between 100 and 117°, probably due to the observed bond relaxations and distortions, and also the effects of the presence of the adsorbates or their lack thereof.

Changes within the bond lengths and angles between the adsorbates and the underlying carbon atom matrix were also recorded. The C-O bond length was found to range between 1.304Å for the third ML ONTOP site terminated with O atoms on a (1×1) bulk terminated surface and 1.38Å for the third ML site whose starting geometry was a HCP one, still on the (1×1) surface. These values were all within the range of the experimental value of the single C-O bond, which was 1.36Å, and they were also in good agreement with other DFT calculations as discussed previously. The C-OH bond length varied between 1.41Å for the half ML ONTOP site to 1.431Å for the co-adsorption of hydroxyl

groups at the HCP and bridge sites on a (1×1) bulk terminated C(111) surface. Again, these values were in good agreement with the experimental C-OH bond length of 1.43Å as well as other *ab initio* calculations quoted previously.

The O-H bond length was found to vary between 0.969Å for the half ML ONTOP site terminated with hydroxyl groups and 1.004Å for the co-adsorption of a full monolayer of hydroxyl groups at the HCP and bridge sites. The longer length of the O-H bond observed in the latter case was probably due to the repulsive forces arising from the higher density of the adsorbates, as the systems relaxed to achieve optimum bonding configurations, in the presence of many competing surface and thermodynamic processes. These values were nonetheless all quite close to the experimental value of 0.98Å, and they were also in excellent agreement with other first principle calculations. The orientations of the O-H bonds lay between ∼104 and 112°, which fitted quite well with those observed in other theoretical calculations and also in experiment.

For the clean (2×1) reconstructed diamond (111) surface, no dimerization of the upper and lower π-bonded zigzag carbon atom chains were established, while a very small value of buckling of 0.0029Å was observed within the upper π-bonded chains, and 0.013Å for the lower π-bonded zigzag chain. The adsorption of the oxygen atoms or hydroxyl groups resulted in relatively higher values of buckling as discussed previously.

When oxygen atoms were adsorbed at the ONTOP site up to a half ML of the available bonding sites, the topmost π-bonded zigzag carbon-atom chains were found to suffer a buckling of 0.164Å, while the lower ones experienced only a marginal buckling of 0.0228Å. This forced the bonds joining the upper and lower π-bonded zigzag chains to contract and expand alternately, depending on whether the carbon atom bonded to it was terminated with the adsorbate or not. This was found to occur in all the other lower coverages on the (2×1) reconstructed C(111) surface, except the most stable half ML bridge:O since all

of its surface bonds were terminated with the O atoms. The largest buckling of the upper π-bonded zigzag chains of 0.219Å was observed in the half ML site whose initial geometry was a bridge bonded one with OH groups, which also happened to be among the least stable configurations on the (2×1) reconstructed surface. Overall, the upper π-bonded zigzag chains suffered a fairly large amount of buckling for the half ML coverages with oxygen atoms or hydroxyl groups than the lower π-bonded zigzag chains. The full ML coverages did not result in any buckling of either of the lower or upper π-bonded chains, probably due to lack of dangling bonds in the upper π-bonded chains unlike the lower coverages. C-C bonds between the 4th and 5th carbon atom layers were found to suffer significant distortions, resulting in alternate contractions of -3.3% (1.489Å) and expansions of 4.6% (1.611Å). Whereas this behaviour was observed in all the 2×1 reconstructed surfaces even those terminated with the adsorbates, Kern *et al.* [48] also observed it for the clean surface, where they stated this to be a good measure of converged optimization with respect to the thickness of the slab. They further observed that the previous calculations that were predicting strong dimerization of the (2×1) surface such as the slab-MINDO calculations of Zheng *et al.* [44] and the *ab initio* calculations of Iarlori *et al.* [98] were all based on rather thin slabs (six and eight layers respectively), and hence they couldn't observe the bond distortion in deeper layers and as such their calculations were not well converged with respect to the thickness of the slab. In addition, Iarlori *et al.* [98] used a plane wave cut off energy of 35Ry, which we showed in our calculations that the systems would not be well converged at this energy (see figures 1.5 and 1.7), again highlighting the reasons why they were unable to predict correct results as far as the surface dimerization of the clean (2×1) surface was concerned.

Bond angles within the third bilayer of carbon atoms for the (2×1) reconstructed C(111) surface varied between 104 and 113°, while those in the lower

layers were between 107 and 109.9°, indicating that they were very close to the experimental value, and therefore bond angles within the bulk regions were generally preserved even on the (2×1) reconstructed C(111) surface. Although the third or fourth layers were very close to the surface, the strong covalent nature of diamond bonds ensured that any changes were mainly localized at the surface regions.

The large extensions suffered by the C-C bonds between the 2nd and 3rd carbon atom layers and also those at the surface bilayer were thought to be responsible for the large proportion of the desorption products being CO and not CO_2. By virtue of their large lengths and hence reduced strengths, it was easier to break these than the shorter and strong C-O bonds.

Based on these observations, it was quite evident that the adsorption of both oxygen atoms and hydroxyl groups on diamond (111) surfaces had a remarkable effect on them, not only in their structure, but also on their electronic, optical, mechanical, chemical and physical properties among others. Establishing the preferred bonding sites for each species and their optimum coverages as was clearly established in this study was therefore immensely important regarding their eventual use in various technological fields. This has the singular advantage that one is able to control better and harness the useful processes and the resulting (surface or even bulk) phenomena, while eliminating the undesirable ones, therefore expanding quite immensely the scope of the applications of such surfaces.

1.19 Recommendation

It would be quite interesting to carry out chemical potential calculations for O atoms and OH groups on the C(111)-1×1 surfaces under various conditions, in order to establish how these compare with the findings of this study, and where

necessary complement these theoretical predictions, as well as the already reported experimental findings. Regard the optimum coverages, clarity on the experimental findings can be obtained by conducting LEED measurements to determine the register of the surface bonded O atoms or OH groups, and thus be able to resolve some of the existing conflicting predictions. Calculations involving smaller coverage steps such as 0.1ML for the intermediate coverages between 1ML down to 0.1ML would be vital in extrapolating and further understanding the properties of the C(111) surfaces (and even other non-diamond, but structurally related surfaces) at much lower coverages.

Appendix A

This section gives extra structural diagrams for the less stable configurations of O atoms & OH groups, as well as their associated density of states on C(111) surfaces.

A.1 Less stable structures for oxygen atoms and hydroxyl groups on the C(111)-(1×1) surface.

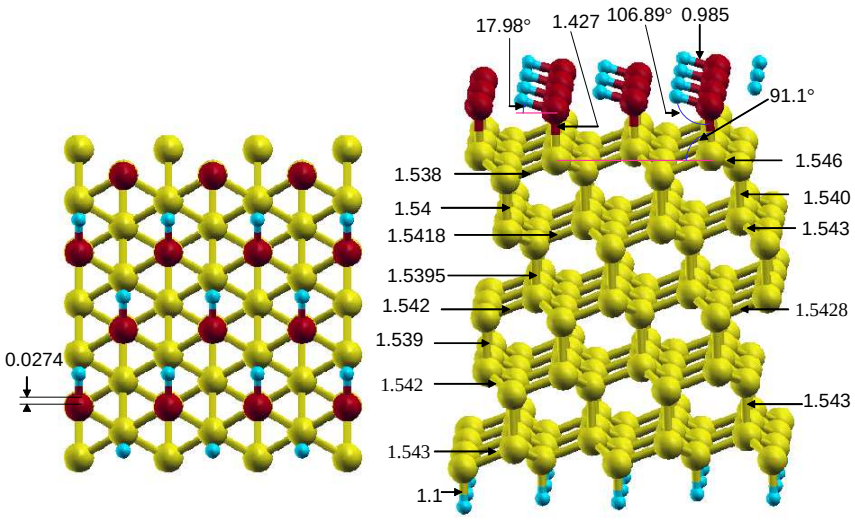


Figure A.1: A full ML coverage of hydroxyl groups adsorbed at an ONTOP site.

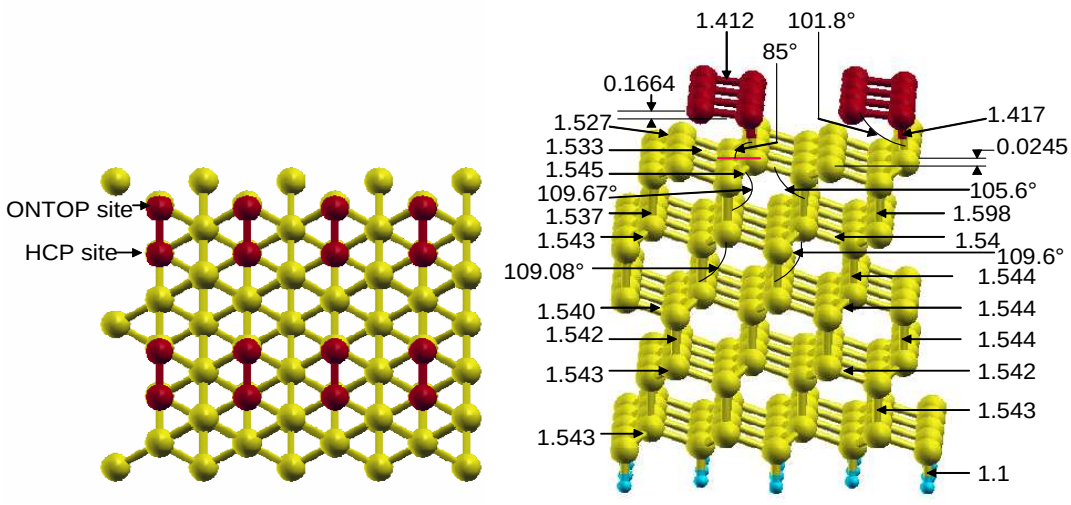


Figure A.2: A full ML coverage of oxygen atoms co-adsorbed at an ONTOP and a hexagonal close packed (HCP) site.

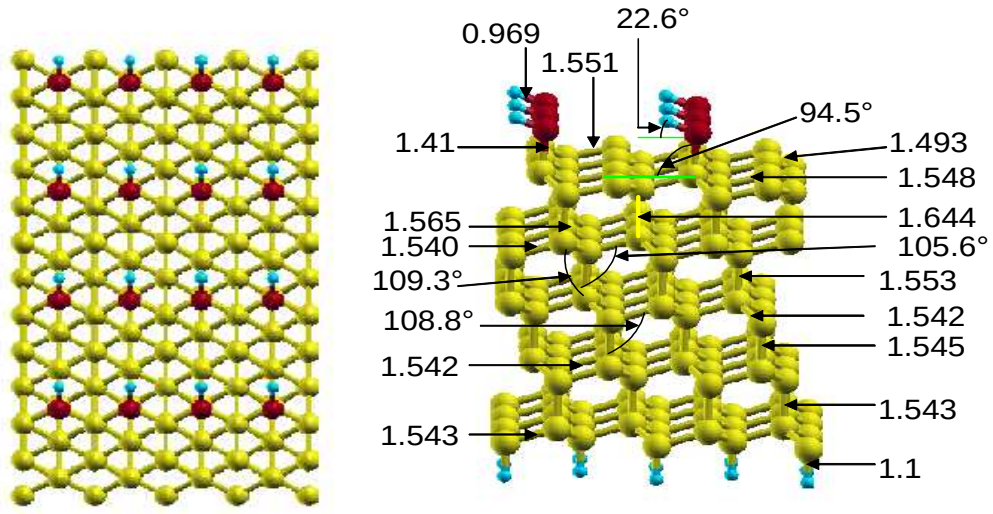


Figure A.3: A half ML coverage of OH groups adsorbed at an ONTOP site. The carbon atoms bonded to the hydroxyl groups are raised by 0.176Å above those that are not.

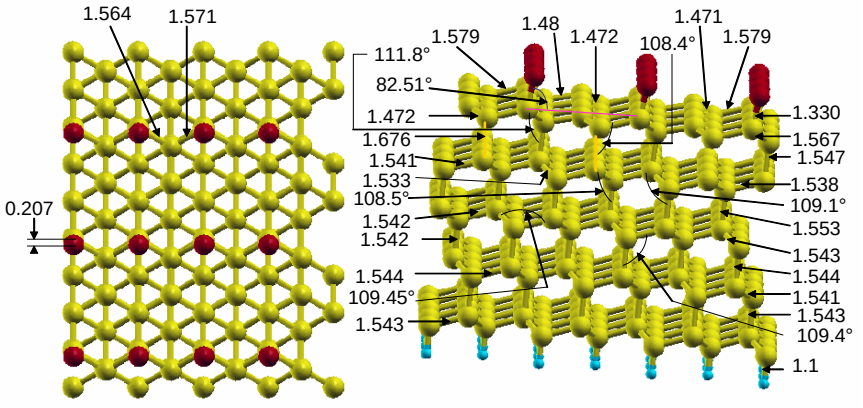


Figure A.4: A half ML coverage of oxygen atoms which were initially adsorbed at a Hexagonal close packed site.

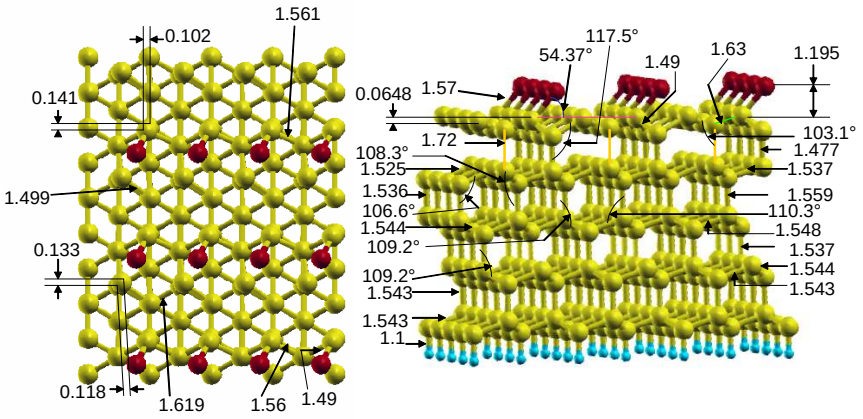


Figure A.5: A half ML coverage of oxygen atoms adsorbed at a bridge site.

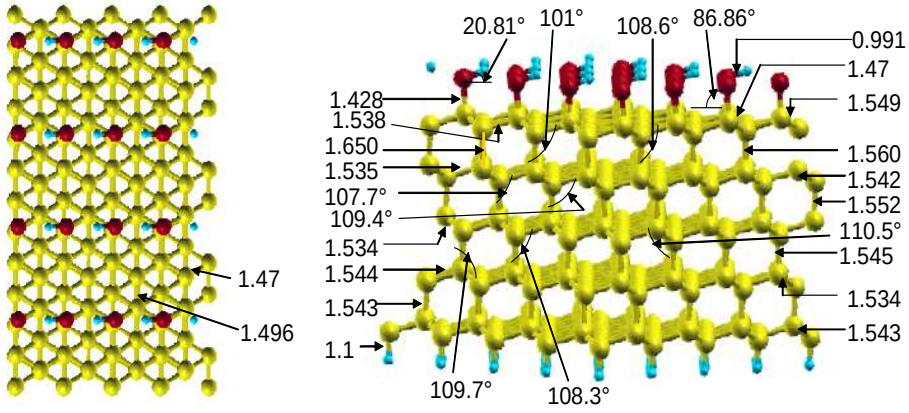


Figure A.6: A half ML coverage of OH groups that were initially adsorbed at a bridge site. Unlike the oxygen atoms (fig. A.5, the hydroxyl groups moved to new positions that were very close to the ONTOP site.

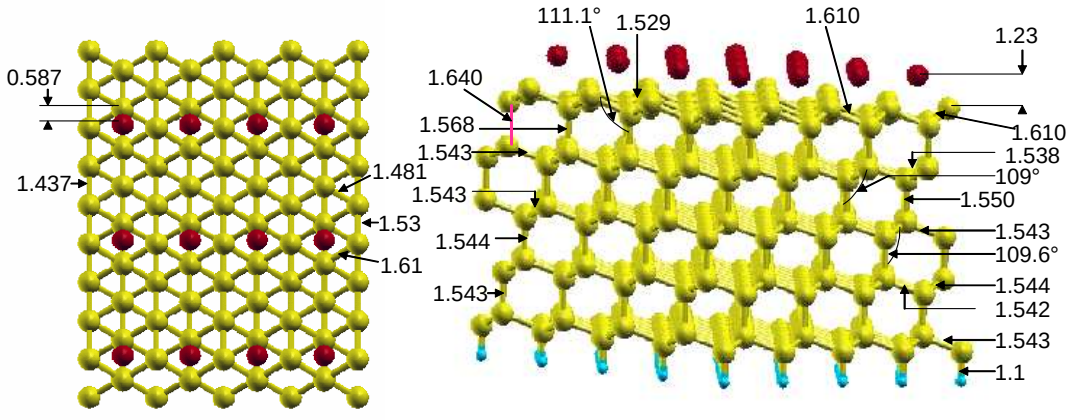


Figure A.7: A half ML coverage of oxygen atoms adsorbed a face centred site.

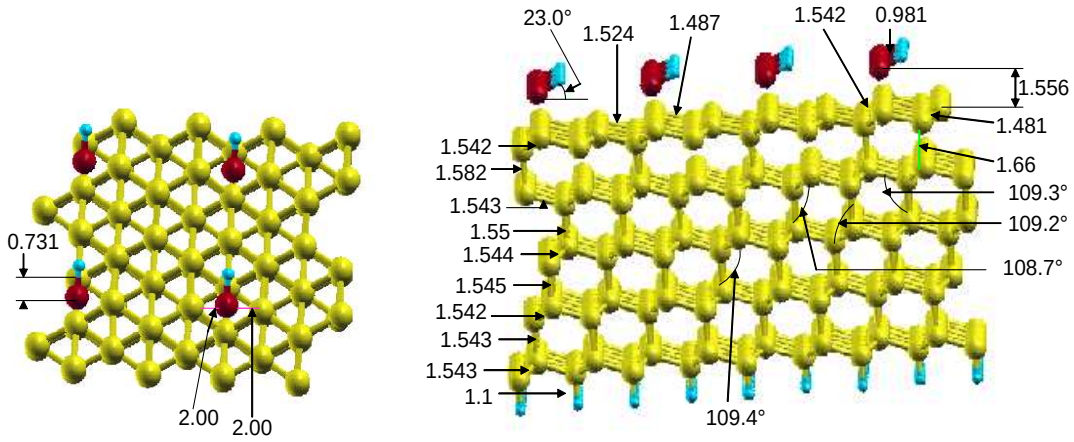


Figure A.8: A half ML coverage of OH groups adsorbed at a face centred cubic site.

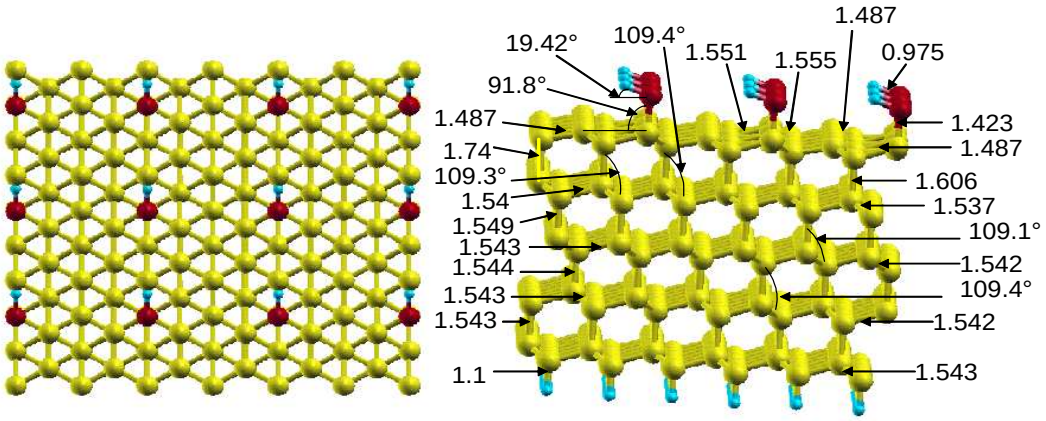


Figure A.9: A quarter ML coverage of OH groups adsorbed at an ONTOP site.

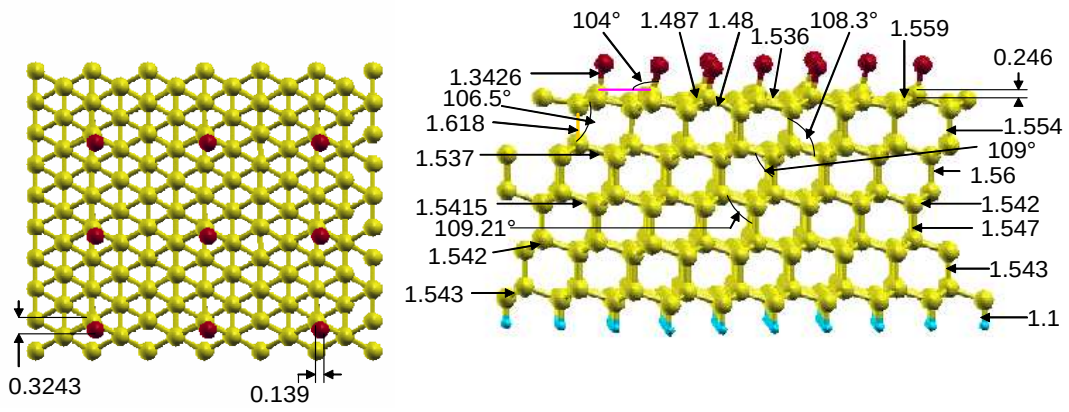


Figure A.10: A quarter ML coverage of oxygen atoms that were initially adsorbed at a Hexagonal close packed site.

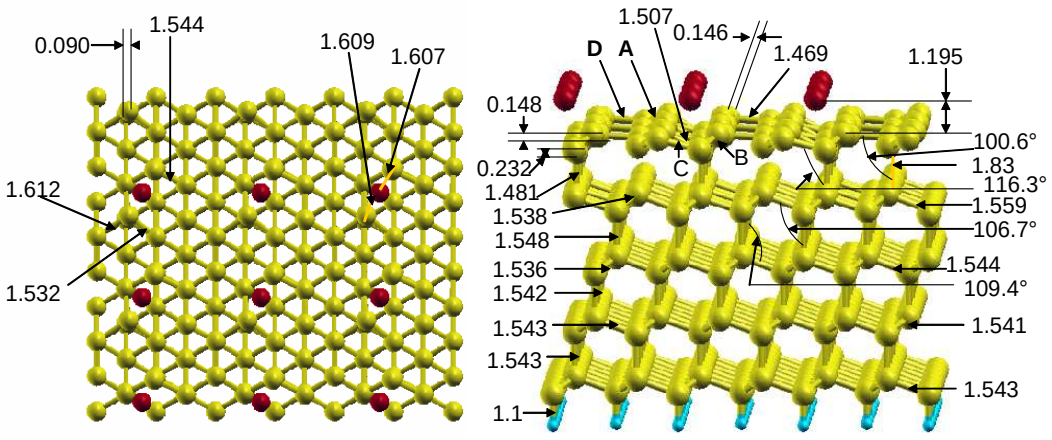


Figure A.11: A quarter ML coverage of oxygen atoms adsorbed at a bridge site. Letters **A**, **B**, **C** and **D** represent different types of surface bonds. Note the disruption of the topmost bilayer of carbon atoms due to the bridge-bonded O atoms.

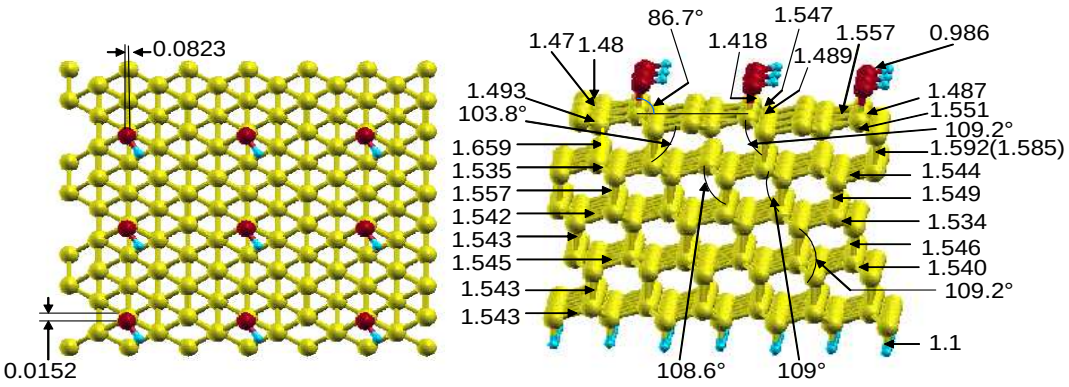


Figure A.12: A quarter ML coverage of OH groups whose starting geometry was a bridge-bonded one.

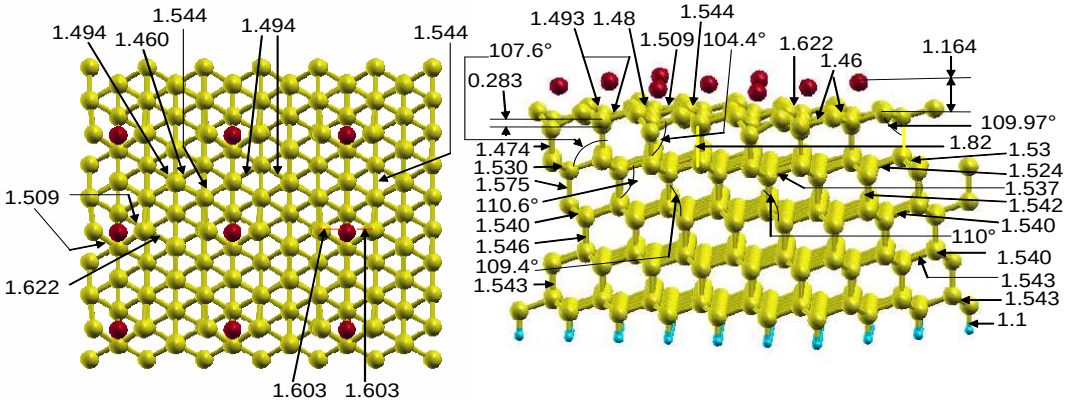


Figure A.13: A quarter ML coverage of oxygen atoms adsorbed at a face centred cubic site.

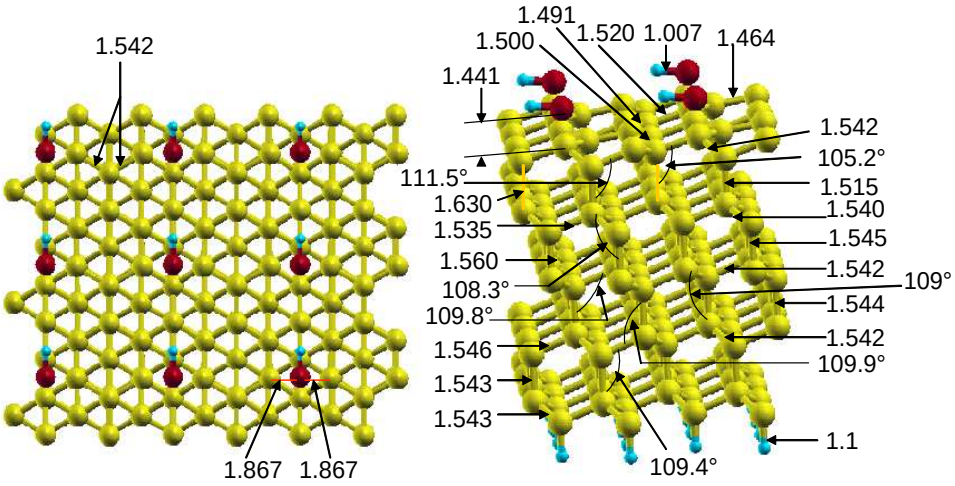


Figure A.14: A quarter ML coverage of OH groups adsorbed at a face centred cubic site.

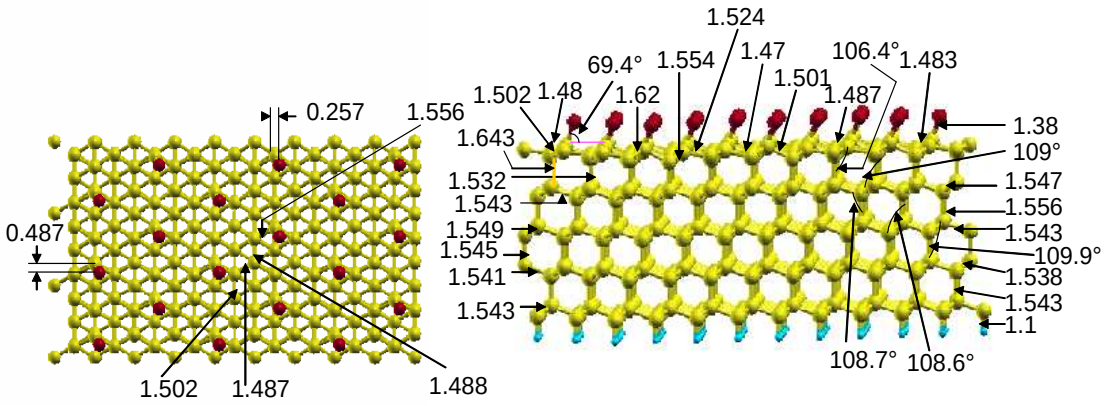


Figure A.15: A third ML coverage of oxygen atoms that were initially adsorbed at a Hexagonal close packed site.

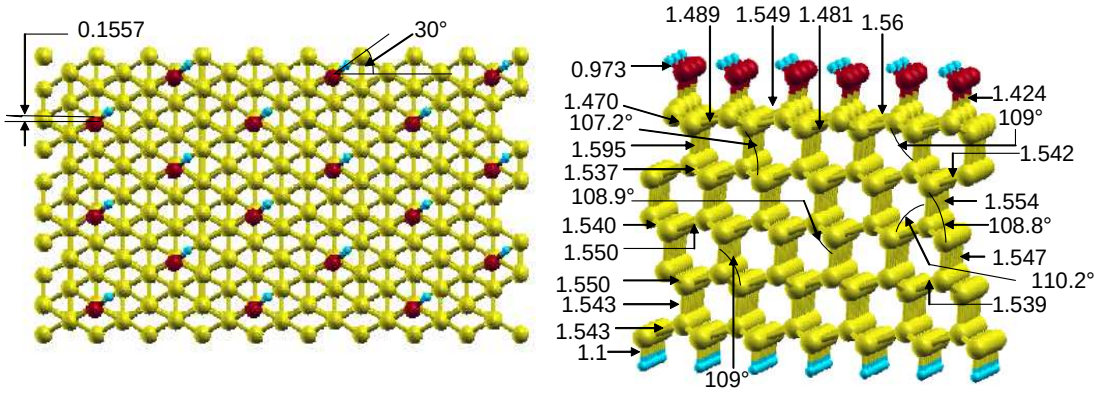


Figure A.16: A third ML coverage of OH groups that were initially adsorbed at a Hexagonal close packed site. The HCP site appears quite unstable against OH adsorption.

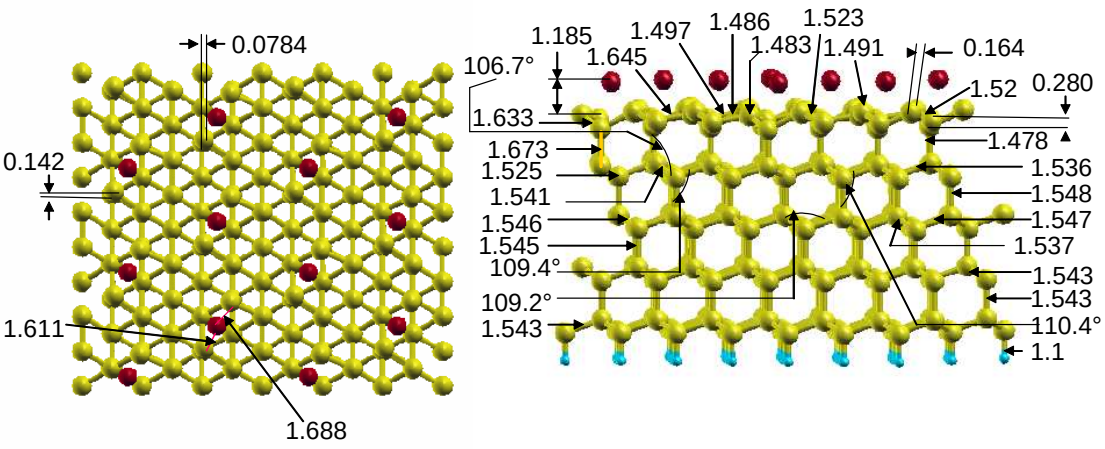


Figure A.17: A third ML coverage of oxygen atoms adsorbed at a bridge site.

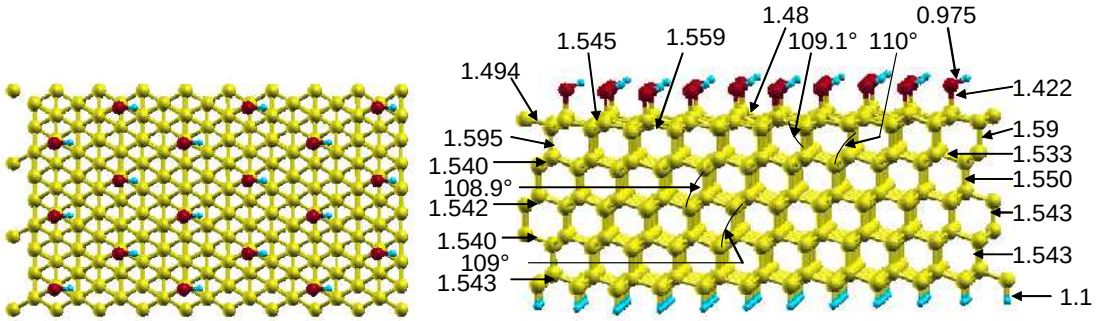


Figure A.18: A third ML coverage of OH groups that were initially adsorbed at a bridge site. The bridge site is also unstable against the adsorption of OH groups.

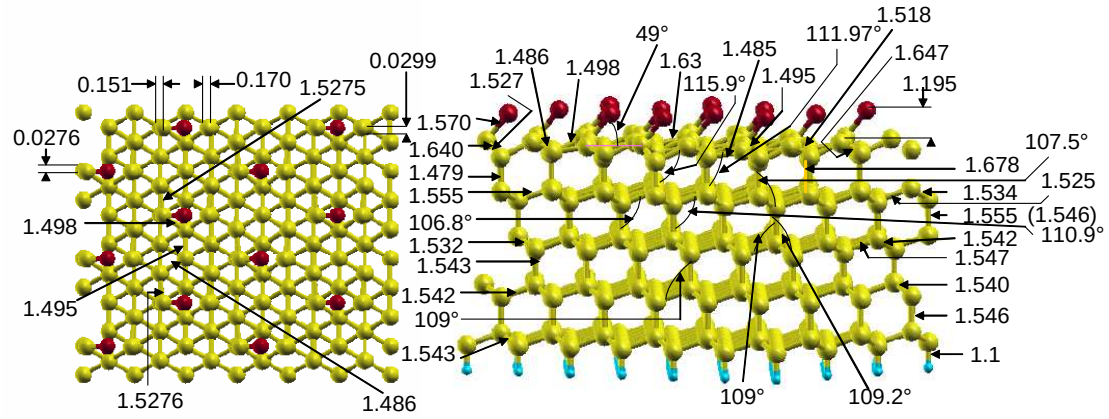


Figure A.19: A third ML coverage of oxygen atoms adsorbed at a face centred cubic site.

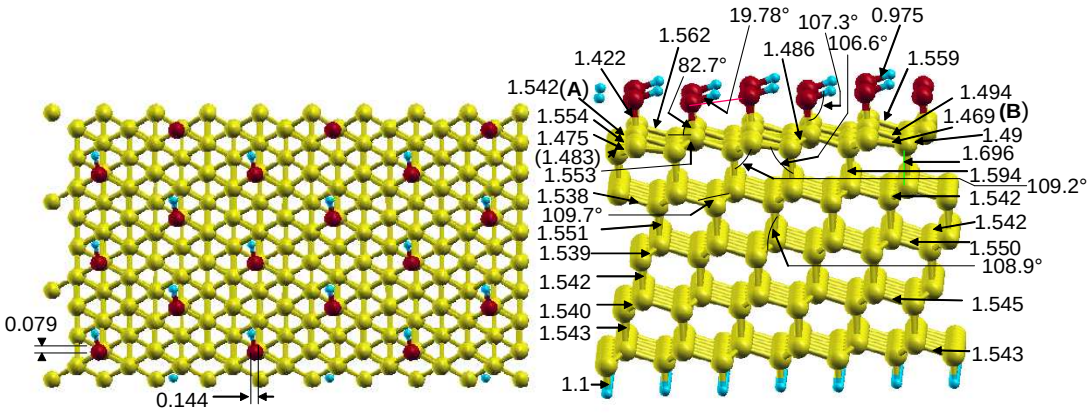


Figure A.20: A third ML coverage of OH groups that were initially adsorbed at a face centred cubic site. The carbon atoms bonded to the OH groups were raised by 0.197Å over the ones that were not, and the FCC site appears to be also unstable against the OH groups' adsorption, instead preferring the ONTOP:OH site.

A.2 Less stable structures for oxygen atoms and hydroxyl groups on the C(111)-(2×1) surface.

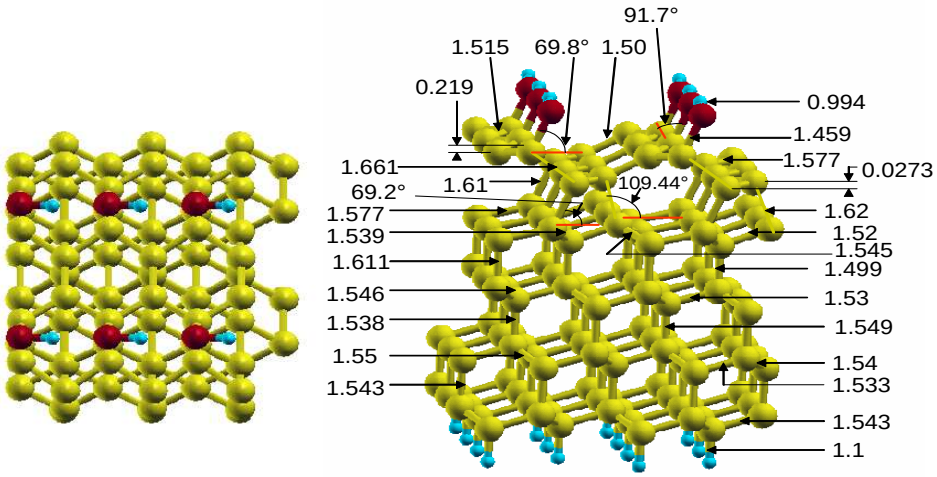


Figure A.21: A half ML coverage of OH groups adsorbed at a site whose starting geometry was a bridge-bonded one, on a (2×1) reconstructed C(111) surface.

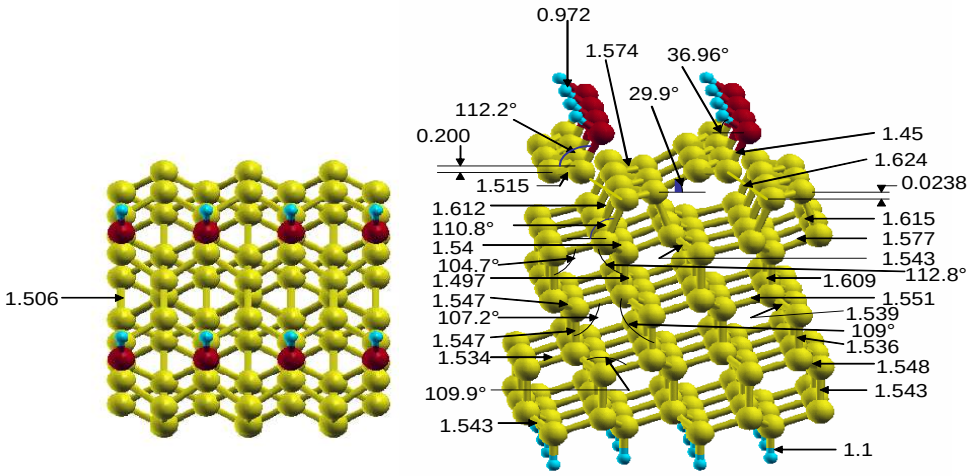


Figure A.22: A half ML coverage of hydroxyl groups adsorbed at an ONTOP site, of a (2×1) reconstructed C(111) surface.

Coverage	$\Delta\Phi$(O)-$\Delta\Phi$(clean surf)	$\Delta\Phi$(OH)-$\Delta\Phi$(clean surf.)
Full ML ONTOP	2.46265	-1.7976
Full ML co-adsorption	1.384	-1.5878
Half ML ONTOP	2.8899	-1.0892
Half ML HCP	2.7756	-0.9528
Half ML FCC	2.3634	-0.2206
Half ML site with initial geometry as bridge-bonded	0.5594	-0.9792

Table A.1: Changes in the work function of (1×1)-C(111) surfaces terminated with full and half ML coverages of O atoms and OH groups compared to that of the clean surface (3.6131).

Coverage	$\Delta\Phi$:O-$\Delta\Phi$:clean surf.	$\Delta\Phi$:OH-$\Delta\Phi$:clean surf.
Quarter ML ONTOP	2.3418	-0.341
Quarter ML Bridge	0.3825	0.1525
Qurater ML HCP	2.2195	-0.3002
Quarter ML FCC	0.5314	-0.699

Table A.2: Changes in the work function of C(111)-(1×1) surfaces terminated with a quarter ML of O atoms and OH groups, compared to that of the clean surface (3.6322).

A.3 Work function for C(111) surfaces terminated with oxygen atoms and hydroxyl groups on the C(111)-(1×1) surface.

Coverage	$\Delta\Phi$:O-$\Delta\Phi$:clean surf.	$\Delta\Phi$:OH-$\Delta\Phi$:clean surf.
Third ML ONTOP	2.7979	-0.4598
Third ML Bridge	0.2907	-0.7324
Third ML HCP	2.3916	-0.8671
Third ML FCC	0.3005	-0.4772

Table A.3: Changes in the work function of C(111)-(1×1) surfaces terminated with a third ML of O atoms and OH groups compared to that of the clean surface (3.6798).

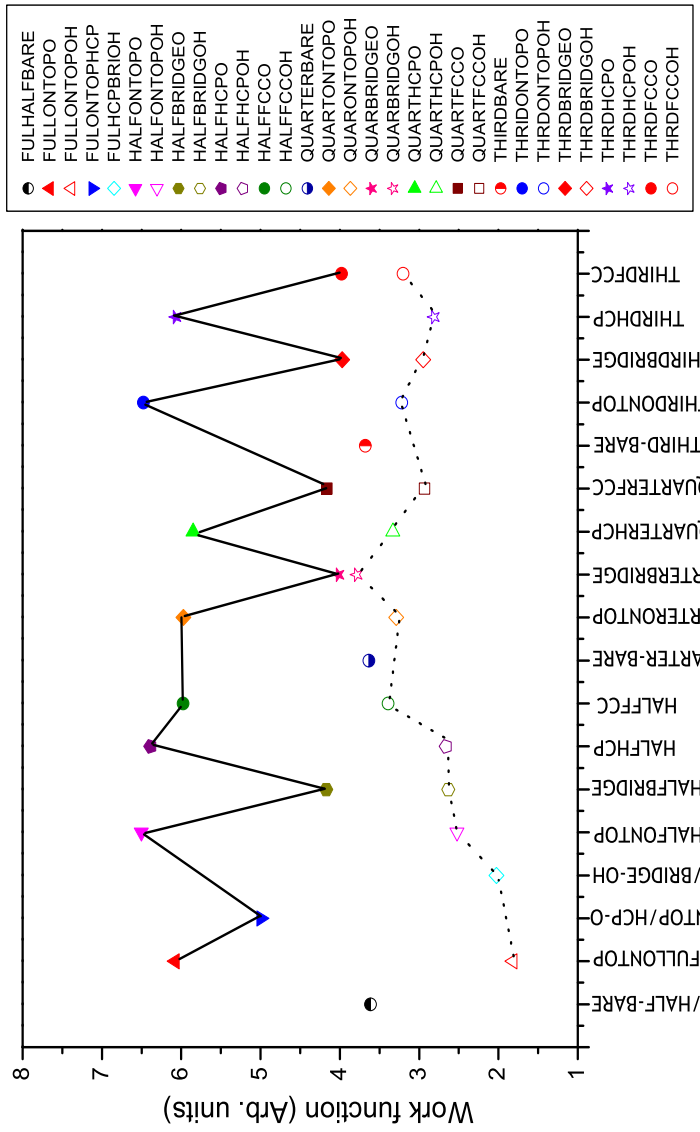


Figure A.23: A plot of the work function (eV) for various sites and coverages from (1×1) bulk terminated C(111) surfaces. The shaded symbols represent the work function for surfaces terminated by oxygen atoms, while the open ones show that of the hydroxyl terminated surfaces. The half shaded circles show the values of the work function for the clean surfaces.

Coverage	$\Delta\Phi$:O-$\Delta\Phi$:clean surf.	$\Delta\Phi$:OH-$\Delta\Phi$:clean surf.
Full ML ONTOP	3.0595	-0.75571
Half ML ONTOP	3.357	-0.8784
Half ML bridge	1.7354	0.2704

Table A.4: Changes in the work function of C(111)-(2×1) surfaces terminated with full and half monolayers (ML) of O atoms and OH groups compared to that of the clean surface (2.3459).

A.4 Density of states for the less stable structures for oxygen atoms and hydroxyl groups on the C(111)-(1×1) surface.

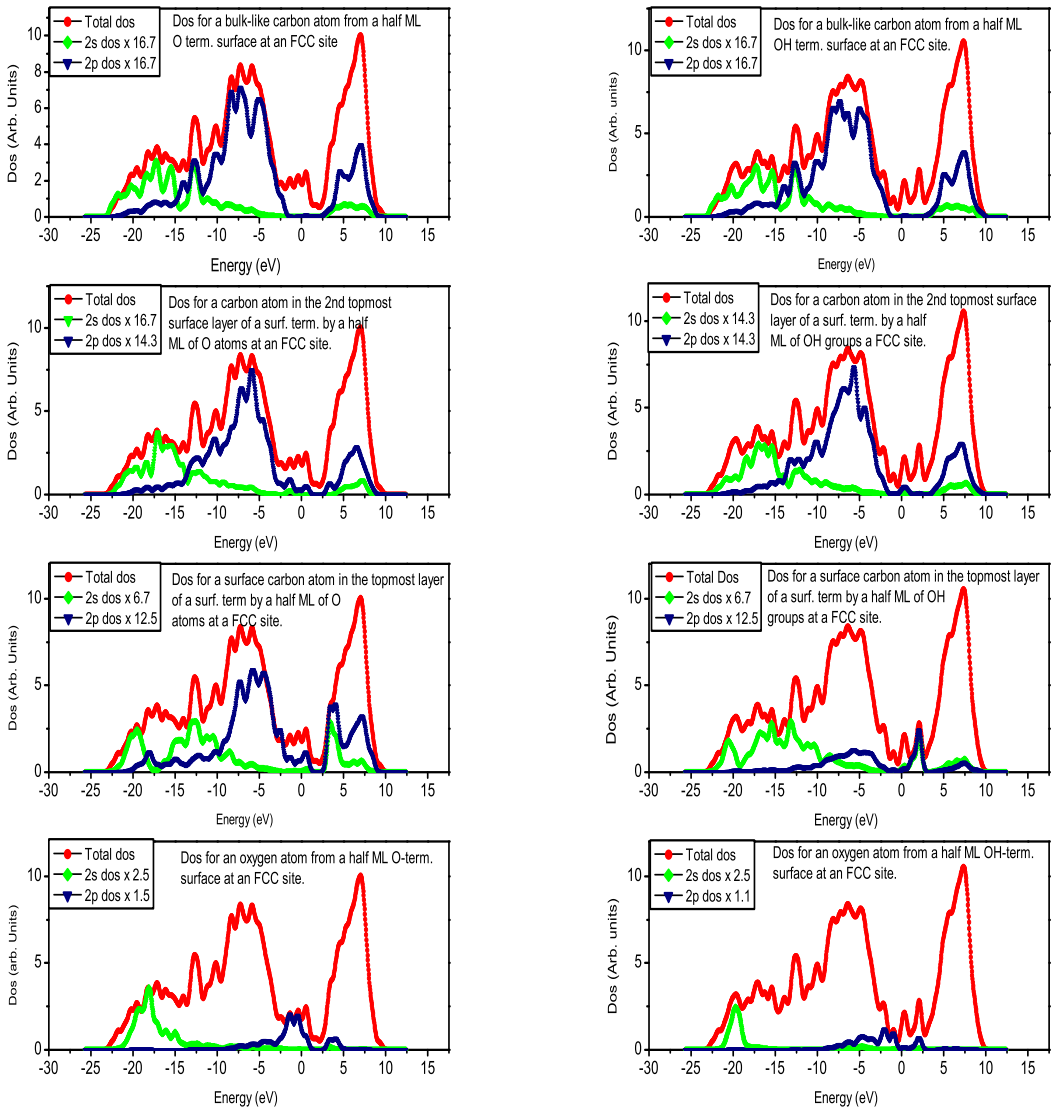


Figure A.24: Density of states (Dos) for C(111)-(1×1) surfaces terminated by a half monolayer of oxygen atoms and hydroxyl groups at face centered cubic site (FCC) sites.

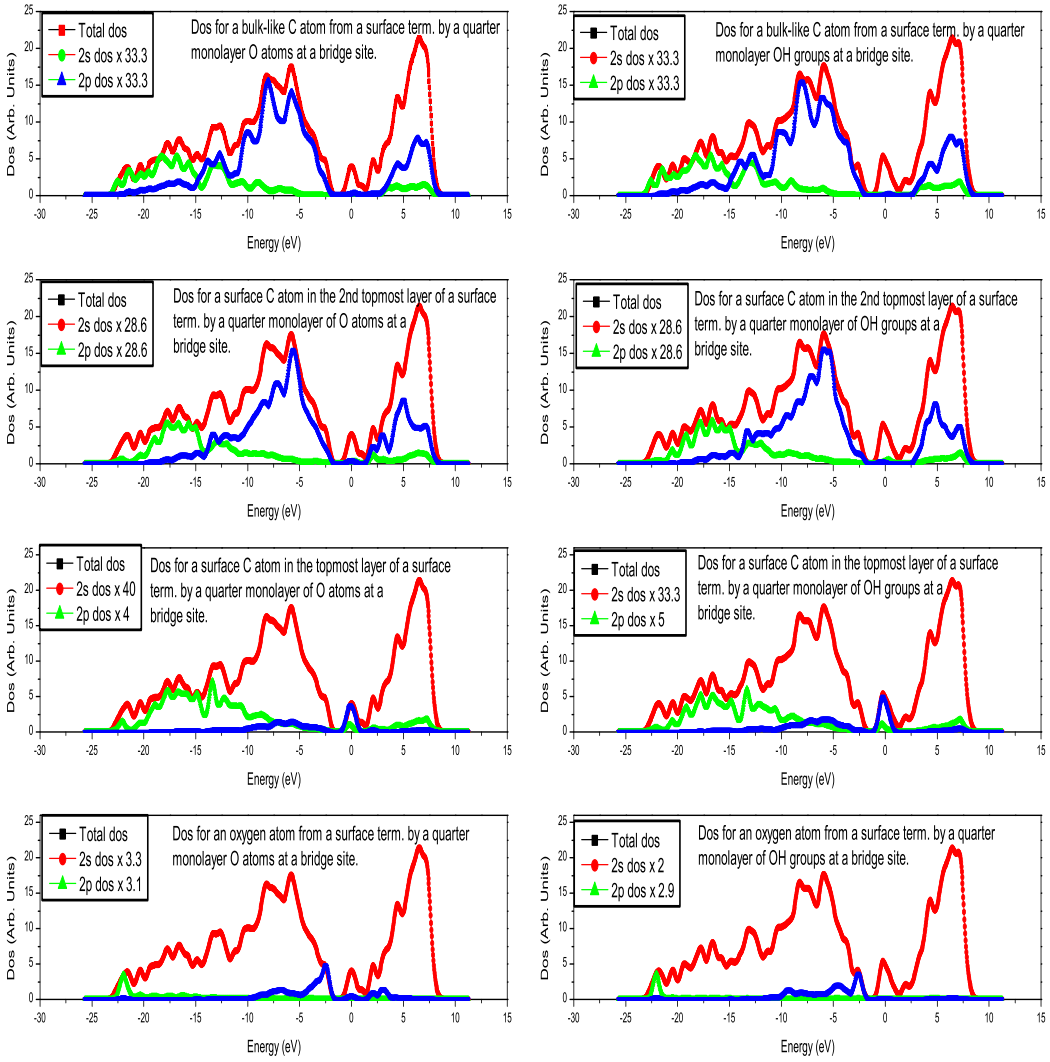


Figure A.25: Density of states for C(111)-(1×1) surfaces terminated with a quarter monolayer of oxygen atoms and hydroxyl groups at sites that were initially bridge-bonded. Except for the O atoms, the DOS for the carbon atoms appear very much alike.

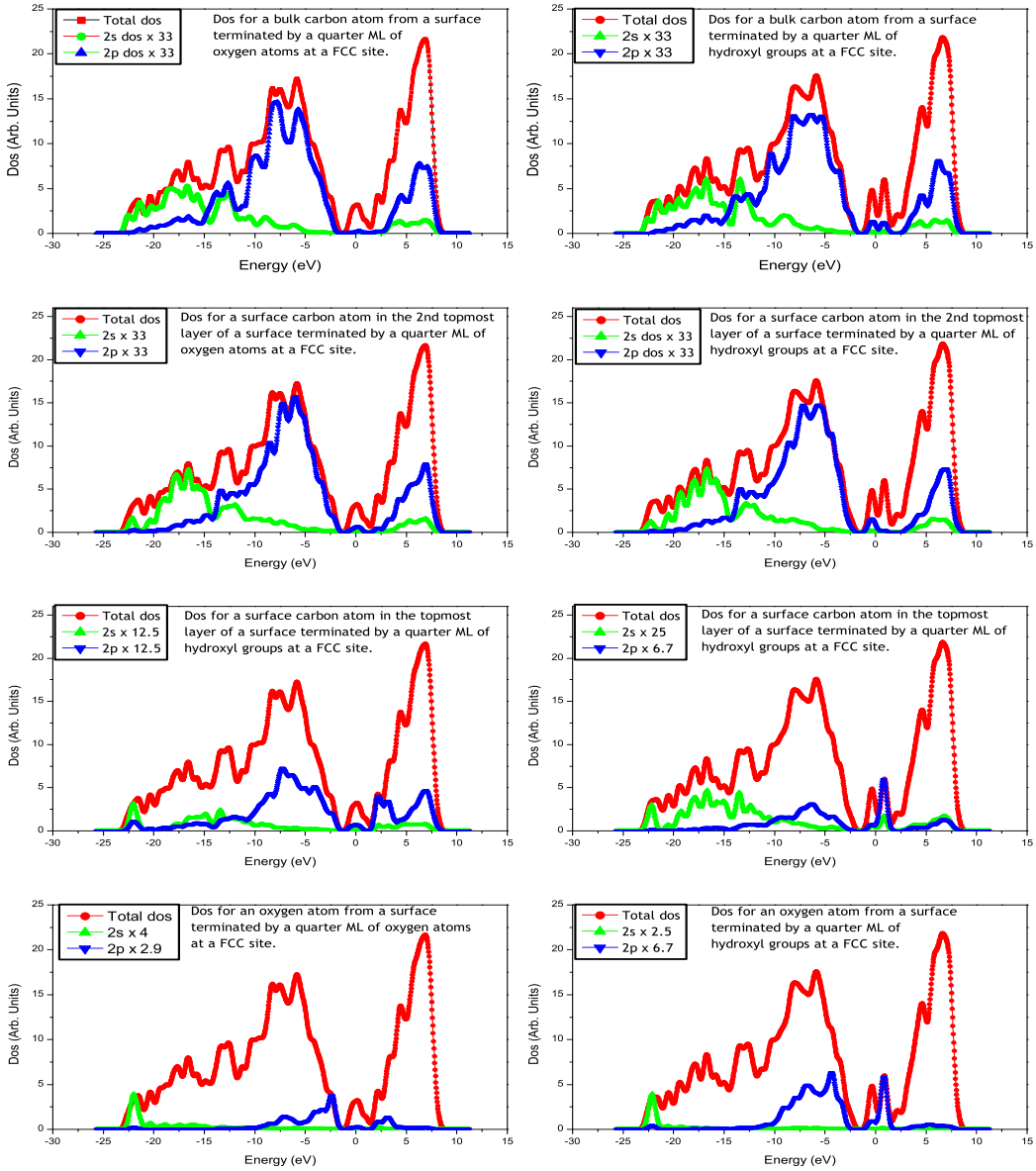


Figure A.26: Density of states from C(111)-(1×1) surfaces terminated with a quarter monolayer of oxygen atoms and hydroxyl groups at face centered cubic sites.

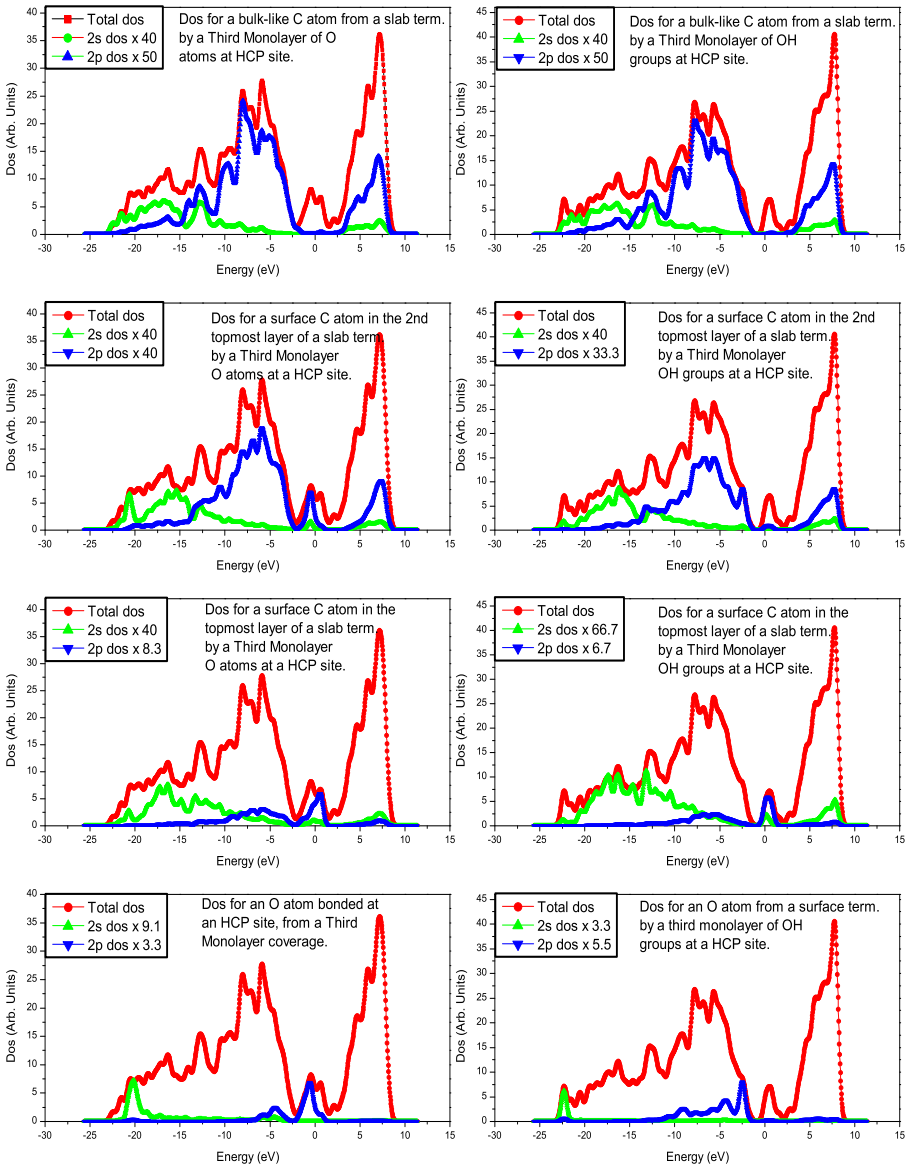


Figure A.27: Density of states from C(111)-(1×1) surfaces terminated with a third monolayer of oxygen atoms and hydroxyl groups at sites that were initially hexagonal close packed.

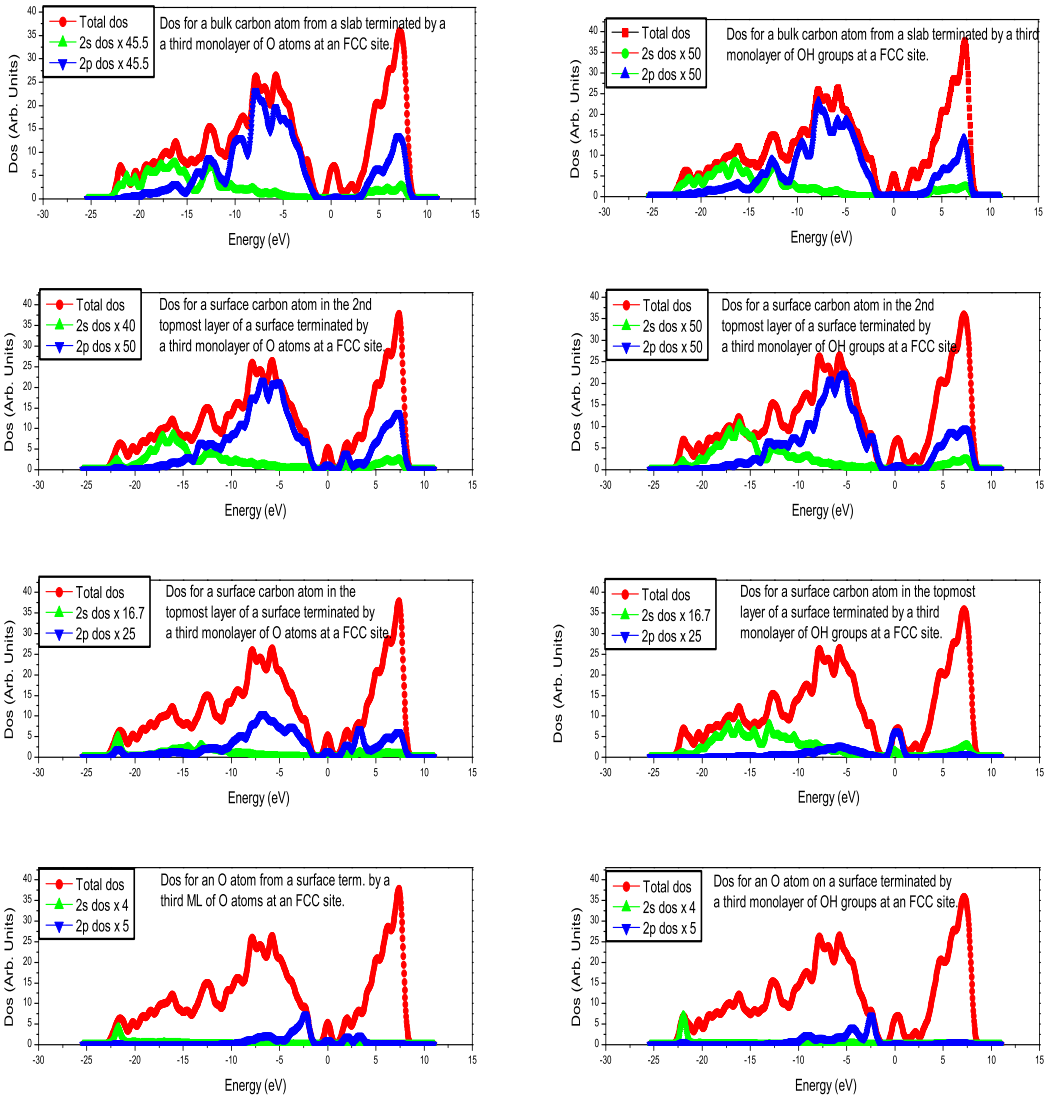


Figure A.28: Density of states for C(111)-(1×1) surfaces terminated with a third monolayer of oxygen atoms and hydroxyl groups at face centered cubic sites.

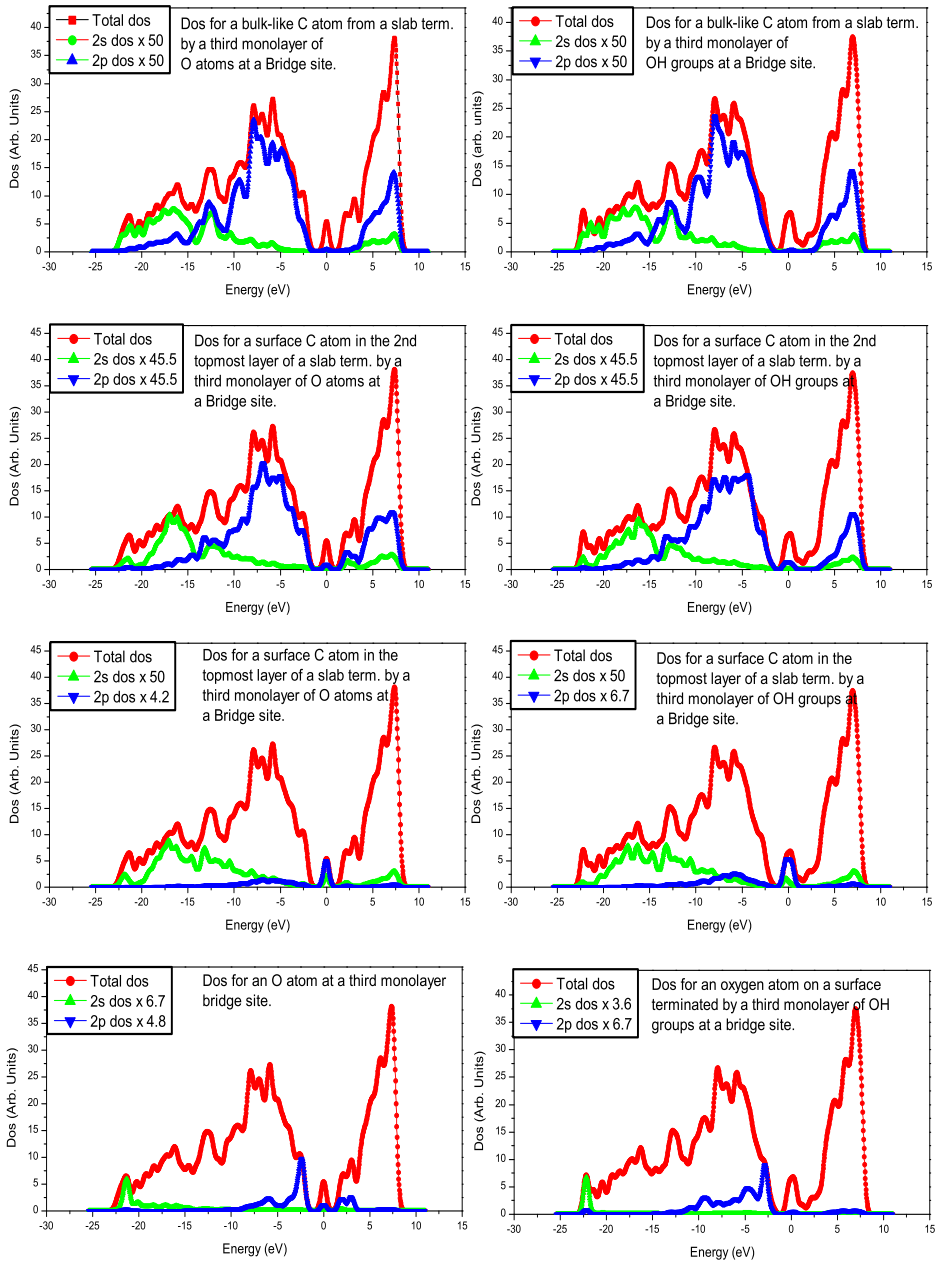


Figure A.29: Density of states for C(111)-(1×1) surfaces terminated with a third monolayer of oxygen atoms and hydroxyl groups at sites that were originally bridge-bonded.

References

[1] S. Cottenier, *Density Functional Theory and the family of (L)APW-methods: a step-by-step introduction*, Instituut voor Kern-en Stralingsfysica, K.U.Leuven, 2002, pp. 1–11.

[2] P.Y.YU and M. Cardona (Edts.), *Fundamentals of Semiconductor Physics and Material Properties.*, Springer, Berlin, 3rd edition, 2003, p. 18.

[3] R.M.Dreizler and E.K.U. Gross (Edts.), *Density Funtional Theory: An Approach to the Quantum Many-Body Problem.*, Springer-Verlag, Berlin, 1990, pp. 1,51 and 124.

[4] M.Ernzerhof, K.Burke, and J.P.Perdew. *Density functional theory, the exchange hole, and the molecular bond.* In J.M.Seminario, editor, *Recent Developments in Density Functional Theory, Theoretical and Computational Chemistry*, pp. 1–2. Elsevier, Amsterdam, 1997.

[5] R.G.Parr and W.Yang (Edts.), *Density-Funtional Theory of Atoms And Molecules.*, Oxford Universty Press, New York, 1989, pp. 47–68.

[6] R.G.Parr and W.Yang (Edts.), *Density-Funtional Theory of Atoms And Molecules.*, Oxford Universty Press, New York, 1989, pp. 105–141.

[7] J.P.Perdew and M. Ernzerhof. *Driving out the self-intraction error.* In J.F. Dobson, Giovani Vignale, and M.P.Das, editors, *Electronic Density Functional Theory: Recent Progress and New Directions*, pp. 31–37. Plenum Press, New York, 1998.

[8] E.Teller, Rev. Mod. Phys., **34** pp. 627–631, 1962.

[9] J.F.Dobson and M.P.Das (Edts.), *Electronic Density Funtional Theory:Recent Progress and New Directions.*, Plenum Press, New York, 1998, pp. 3–18.

[10] Nikitas Godopoulos, Phys. Rev. B., **57** pp. 2146–2152, 1998.

[11] J.Perdew and Y. Wang, Phys. Rev. B., **45** p. 13244, 1992.

[12] B.Y.Tong and L.J.Sham, Phys. Rev., **144** pp. 1–4, 1966.

[13] J.Perdew and A.Zunger, Phys. Rev. B., **23** pp. 5048–5079, 1981.

[14] R.G.Parr and W.Yang (Edts.), *Density-Funtional Theory of Atoms And Molecules.*, Oxford Universty Press, New York, 1989, pp. 180–183.

[15] R.G.Parr and W.Yang (Edts.), *Density-Funtional Theory of Atoms And Molecules.*, Oxford Universty Press, New York, 1989, p. 14.

[16] S Walter, J.Bernhardt, U. Starke, K.Heinz, F.Maier, J.Ristein, and L.Ley, J.Phys.: Condens. Matter, **14** pp. 3085–3092, 2002.

[17] J.P.Perdew (Edt.), *Electronic Structure of Solids*, Akademie Verlag, Berlin, 1991.

[18] D.M.Ceperley and B.J.Alder, Phys. Rev. Lett., **45** p. 566, 1980.

[19] Kieron Burke. *Digging into the exchange-correlation energy:the exchange-correlation hole.* In J.F. Dobson, Giovani Vignale, and M.P.Das, editors, *Electronic Density Functional Theory: Recent Progress and New Directions*, pp. 19–29. Plenum Press, New York, 1998.

[20] J.A.White and D.M.Bird, Phys. Rev. B, **50** p. 4954, 1994.

[21] J.P.Perdew, J.A.Chevary, S.H.Vosko, K.A.Jackson, M.R.Pederson, D.J.Singh, and C.Fiolhais, Phys. Rev. B, **48** p. 4978, 1993.

[22] A.D.Becke, J. Chem. Phys., **97** p. 9173, 1992.

[23] B.G.Johnson, P.M.W.Gill, and J.A.Pople, J. Chem. Phys., **98** p. 5612, 1993.

[24] J.M.Seminario, Chem. Phys. Lett., **206** p. 547, 1993.

[25] J.Perdew and Y. Wang, Phys. Rev. B, **33** p. 8800, 1986.

[26] J.Perdew, K.Burke, and M.Ernzerhof, Phys. Rev. Lett., **77** p. 3865, 1996.

[27] K.Burke, J.P.Perdew, and Y.Wang, *Derivation of a Generalized Gradient Approximation: The PW91 Density Functional.*, Plenum Press., New York, 1999, pp. 81–111.

[28] L.J.Sham. *Computational methods in band theory.* Plenum, New York, 1971.

[29] R.Colle and O.Salvetti, Theor. Chim. Acta, **37** p. 329, 1975.

[30] R.Colle and O.Salvetti. In R.M.Erdahl and V.H.Smith Jr., editors, *Density Matrices and Density Functionals*, pp. 545–552. D. Riedel Publ. Company, Dordrecht, Holland, 1987.

[31] E.K.U.Gross, M.Petersilka, and T.Grabo. In R.B.Ross B.B.Laird and T. Zeigler, editors, *Chemical applications of Density-Functional Theory.* ACS Books, Washington, 1996.

[32] C.Lee, W.Yang, and R.G.Parr, Phys. Rev. B, **37** p. 785, 1988.

[33] L.A.Curtiss, K.Raghavachari, P.C.Redfern, and J.A.Pople, J. Chem. Phys., **106** p. 1063, 1997.

[34] G*á*bor I., K. Csonka, *É*li*á*s, and I.M. Csizmadia, Chem. Phys. Lett., **257** pp. 49–60, 1996.

[35] A.D.Becke, Phys. Rev. A, **38** pp. 3098–3100, 1988.

[36] R.A.B. Margareta and Per.E.M Siegbahn, Theor. Chem. Acc., **97** pp. 72–80, 1997.

[37] S.J.Vosko, L.Wilk, and M.Nusair, Can. J. Phys., **58** pp. 1200–1211, 1980.

[38] M.Sheffler. *Workshop on Density Functional Theory.* Berlin, 2002. URL `http://www.fhi-berlin.mpg.de/th/fhi98md`.

[39] David Vanderbilt, Phys. Rev. B, **41** p. 7892, 1990.

[40] K. Laasnonen, A. Pasquarello, R. Car, Changyol Lee, and D. Vanderbilt, Phys. Rev. B, **47** p. 10142, 1993.

[41] W. Dong, Phys. Rev. B, **57** p. 4304, 1998.

[42] T.E.Derry, J.O.Hansen, P.E.Harris, R.G.Copperthwaite, and J.P.F.Sellschop, *In The Structure of Surfaces II: Proc. of 2nd Intern. Conf. on the Structure of Surfaces (ICSOSII), Amsterdam, June 1987; (Edts.) J.F.Van der Veen and H.A. Van Hove*, Springer Series in Surface Sciences 11, Berlin, 1988, p. 384.

[43] A. Scholze, W.G.Schimdt, and F. Bechstedt, Phys. Rev. B, **53** p. 13725, 1996.

[44] X.M.Zheng and P.W.Smith, Surf. Scie., **262** p. 219, 1992.

[45] K.C.Pandey, Phys. Rev. B, **25** p. 4338, 1982.

[46] L.Smit, T.E.Derry, and J.F.van der Veen, Surf. Scie., **167** pp. 502–518, 1986.

[47] Willem Jan Huisman, J.F.Peters, and J.F.van der Veen, Surf. Scie., **396** pp. 253–259, 1998.

[48] G.Kern, J.Hafner, and G.Kresse, Surf. Scie., **366** pp. 445–463, 1996.

[49] R. Klauser, Jin-Ming Chen, T.J. Chuang, L.M. Chem, M.C. Smith, and J.C-. Lin, Surf. Scie., **356** pp. L410–416, 1996.

[50] M.J.Rutter and J.Robertson, Phys. Rev. B, **57** pp. 9241–9245, 1998.

[51] P.K.Baumann and R.J.Nemanich, Surf. Scie., **409** pp. 320–335, 1998.

[52] Kian Ping Loh, X.N.Xie, S.W.Wang, J.S.Pan, and P.Wu, Diam. & Relatd. Mater., **11** pp. 1379–1384, 2002.

[53] Kian Ping Loh, X.N.Xie, S.W.Wang, and J.C.Zheng, J. Phys. Chem. B, **106** pp. 5230–5240, 2002.

[54] D. B. Rebuli, T. E. Derry, E. Sideras-Haddad, B. P Doyle, R. D. Maclear, S. H. Connell, and J. P. F. Sellschop., Diam. & Relatd. Matr., **8** p. 1620, 1999.

[55] K.Bobrov, H.Shechter, A.Hoffman, and M.Folman, Appli. Surf. Scie., **196** pp. 173–180, 2002.

[56] M. Fuchs and M. Scheffler, Comput. Phys. Commun., **119** pp. 67–98, 1999.

[57] N. Troullier and José Luís Martins, Phys. Rev. B., **43** pp. 1993–2005, 1991.

[58] H.J.Monkhorst and J.D.Pack, Phys. Rev. B., **13** p. 5188, 1976.

[59] D.J.Chadi and M.Cohen, Phys. Rev. B., **8** p. 5747, 1973.

[60] F.K. de Theije, M.F.Reedijk, J.Arsic, W.J.P. van Enckevort, and E.Vlieg, Phys. Rev. B., **64** pp. 085403–1, 2001.

[61] Eunja Kim and Chang Feng Chen, Physics Letts., **A 326** pp. 442–448, 2004.

[62] W.E. Pickett, M.R. Pederson, and B.N. Davidson, Nanotechnology, **5** pp. 172–178, 1994.

[63] J.E.Field (Edt.), *The Properties of Natural and Synthetic Diamond.*, Academic Press, Harcourt Brace Jovanovich, London, 1992, pp. 677–684.

[64] Andreia L da Rosa, Seung Mi Lee, and Evgeni Penev (Edts.), *The FHIMD Toolkit: User's Manual*, Berlin, 2002.

[65] Wei-Xue Li, Catherine Stampfl, and Matthias Scheffler, Phys. Rev. B., **65** p. 075407, 2002, and refs. therein.

[66] *CRC Handbook of Chemistry and Physics, 71st edition, (Edt.) D.R. Lide*, CRC Press, Boston, USA., 1992, pp. 9–1,9–2,11–34,11–37.

[67] Evgeny Stambulchik and The Grace Development team, *The Grace (Graphing Advanced Computing and Exploration of data) Software,V.5.1.10: Users Guide Manual*, 2002.

[68] C.Stampfl. *Private Communication.* 2005. URL `http://www.physics.usyd.edu.au/ stampfl/`.

[69] K.H.Wedepohl (Edt.), *HandBook of Geochemistry.*, Springer-Verlag., Berlin, 1969, pp. 1–A–2.

[70] J.van der Weide and R.J.Nemanich, Phys. Rev. B., **49** p. 13629, 1994.

[71] Antony Kolkalj, Computational Mater. Scie., **28** p. 155, 2003. URL `http://www.xcrysden.org`.

[72] Willem Jan Huisman, J.F.Peters, S.A.de Vries, E. Vlieg, W.S.Yang, T.E.Derry, and J.F.van der Veen, Surf. Scie., **387** p. 342, 1997.

[73] Hiroyuki Tamura, Hui Zhou, Kiyoshi Sugisako, Yasuto Yokoi, Seiichi Takamaki, Momoji Kubo, Kazuo Teraishi, Akira Miyamoto, Akira Imamura, Mikka N.-Gamo, and Toshihiro Ando, Phys. Rev. B., **61** p. 11025, 2000.

[74] K.H.Wedepohl (Edt.), *HandBook of Geochemistry.*, Springer-Verlag., Berlin, 1969, pp. 6–A–1.

[75] D. Vanderbilt and S.G.Louie, Phys. Rev. B, **29** p. 7099, 1984.

[76] R.Stumpf and P.M.Marcus, Phys. Rev. B., **47** p. 16016, 1993.

[77] D.R.Alfonso, D.A.Drabold, and S.E.Ulloa, Phys. Rev. B., **51** p. 14669, 1995.

[78] Willem Jan Huisman, M.Lohmeier, H.A. van der Vegt, J.F.Peters, S.A.de Vries, E. Vlieg, V.H.Etgens, T.E.Derry, and J.F.van der Veen, Surf. Scie., **396** p. 241, 1998.

[79] E.C.Sowa, G.D. Kubiak, R.H. Stulen, and M.A. Van Hove, J. Vac. Sci. Technol., **A 6** p. 832, 1988.

[80] Willem Jan Huisman, M.Lohmeier, H.A. van der Vegt, J.F.Peters, S.A.de Vries, E. Vlieg, V.H.Etgens, T.E.Derry, and J.F.van der Veen, Surf. Scie., **396** pp. 253–259, 1998.

[81] F.J.Himpsel, J.A.Knapp, J.A. van Vechten, and D.E.Eastman, Phys. Rev. B., **20** p. 624, 1979.

[82] J. Robertson, Diam. & Relatd. Mater., **5** p. 797, 1996.

[83] Warren E. pickett, Phys. Rev. Letts., **73** pp. 1664–1667, 1994.

[84] D.B. Rebuli, *MSc. Thesis*, University of the Witwatersrand, Johannesburg, South Africa, 1999, pp. 26–27.

[85] Andrew Freedman and Charter D. Stinesspring, Appl. Phys. Lett., **57** pp. 1194–1197, 1990.

[86] J.C.Zheng, X.N.Xie, A.T.S.Wee, and Kian Ping Loh, Diam. & Reltd. Mater., **10** pp. 500–505, 2001, and refs. therein.

[87] N. W. Makau and T. E. Derry, Surf. Revie. and Lett., **10 Nos. 2&3** pp. 295–301, 2003.

[88] T.E. Beerling and C.R. Helms, Appl. Phy. Lett., **65** pp. 1912–1914, 1994.

[89] Y.M. Wang, K.W. Wong, S.T. Lee, M. Nishitani-Gamo, I. Sakaguchi, K.P. Loh, and T. Ando, Diam. & Relatd. Mater., **9** p. 1582, 2000.

[90] S. Skokov, B. Weiner, and M. Frenklach, Phys. Rev. B., **49** p. 16 11374, 1994.

[91] Stephen V. Pepper, J.Vac. Sci. Technol., **20** p. 643, 1982.

[92] C.Y.Fong and B.M.Klein, *Electronic and vibrational properties of bulk diamond in Diamond: Electronic Properties and Applications. (Edts.) L.S.Pan and D.R.Kania*, Kluwer., Dordrecht, 1995.

[93] F.J.Himpsel, J.F. van der Veen, and D.E.Eastman, Phys. Rev. B., **22** p. 1967, 1980.

[94] P. Reinke, G. Francz, and P. Oelhafen, Phys. Rev. B, **54** pp. 7067–7073, 1996.

[95] J.Furthmuller, J.Hafner, and G.Kresse, Phys. Rev. B., **50** p. 15506, 1994.

[96] G.Francz and P.Oelhafen, Diam. & Reltd. Mater., **4** pp. 539–543, 1995.

[97] B.B. Pate, Surf. Sci., **165** pp. 83–142, 1986.

[98] S. Iarlori, G. Gall, F. Gygi, M. Parrinello, and E. Tosatti, Phys. Rev. Lett., **69** p. 2947, 1992.